NOAA Technical Memorandum ERL ESG-29

DUPLICATE
WITHDRAWN

AIR CHEMISTRY STUDIES OVER THE GULF OF MEXICO

A Bilateral Scientific Cooperative Project Between the
United States of America and the United States of Mexico

Edited by
Farn Parungo and John Miller

Environmental Sciences Group
Boulder, Colorado
February 1988

noaa NATIONAL OCEANIC AND ATMOSPHERIC ADMINISTRATION / Environmental Research Laboratories

NOAA Technical Memorandum ERL ESG-29

AIR CHEMISTRY STUDIES OVER THE GULF OF MEXICO

A Bilateral Scientific Cooperative Project Between the
United States of America and the United States of Mexico

Sponsored by

National Oceanic and Atmospheric Administration (U.S.A.)
Center for Atmospheric Sciences, National University of Mexico (U.S.M.)
General Direction of Naval Oceanography, Secretary of the Navy (U.S.M.)

Edited by

Farn Parungo
Environmental Sciences Group

and

John Miller
Air Resources Laboratory
Silver Spring, Maryland

Environmental Sciences Group
Boulder, Colorado
February 1988

UNITED STATES DEPARTMENT OF COMMERCE

C.William Verity
Secretary

NATIONAL OCEANIC AND ATMOSPHERIC ADMINISTRATION

Environmental Research Laboratories

Vernon E. Derr,
Director

NOTICE

Mention of a commercial company or product does not constitute an endorsement by NOAA Environmental Research Laboratories. Use for publicity or advertising purposes of information from this publication concerning proprietary products or the tests of such products is not authorized.

For sale by the National Technical Information Service, 5285 Port Royal Road
Springfield, VA 22161

CONTENTS

Preface

In the last decade, we have come to realize how important it is to understand the chemistry of the atmosphere on a global scale. Already, such questions as ozone depletion in the stratosphere, the long-range transport of acidic materials, and the influence of trace substances on the climate are day-to-day topics of conversation. The problem requires that global atmospheric chemistry measurements be made at either permanent measuring sites in remote locations or by expeditions by ship or aircraft. It is not only important to reach these locations but to also make high quality measurements under sometimes adverse conditions.

The bilateral project to measure air chemistry over the Gulf of Mexico is a good example of measuring the chemistry of the atmosphere on a regional and global basis. The cooperative research project between Mexico and the United States described in this report shows what can be achieved by such a joint program. Both sides put considerable energy into assuring that all aspects of the expedition were a success. It is hoped that this will be the first step to further cooperation in investigating our common environment.

John M. Miller

CHIEF SCIENTISTS

Dr. Humberto Bravo, A.
Seccion de Contaminacion Ambiental
Centro de Ciencias de la Atmosfera,
Universidat Nacional Antónoma de México.

Dr. Farn P. Parungo
NOAA/ERL/ESG, Boulder, CO

Rear Admiral Luis D. Salastorrea
Direcccion General de Oceanografia, Secretaria
de Marina, Col. Roma, Mexico

CONTRIBUTING AUTHORS

Ms. Evelyn Ackerman
Storage Technology Corp.
Louisville, CO.

Mr. Rosaura Camacho, C.
Seccion de Contaminacion Ambiental
Centro de Ciencias de la Atmosfera,
Universidat Nacional Antônoma de México.

Mr. Thomas J. Conway
NOAA/ERL/ARL/GMCC, Boulder, CO

Dr. Cecilia G. Griffith
NOAA/ERL/ESG/WRP, Boulder, CO

Dr. Phillip L. Haagenson
NCAR, Boulder, CO

Ms. Joyce Harris
NOAA/ERL/ARL/GMCC, Boulder, CO

Dr. James N. Galloway
University of Virginia
Charlottesville, VA.

Ms. Lisa H. Hoyt
Environmental Analytical Service, San Luis Obispo, CA

Dr. Steven Hoyt
Environmental Analytical Service, San Luis Obispo, CA

Dr. William C. Keene
University of Virginia, Charlottesville, VA

Ms. Robin E. Madel
NOAA/ERL/ESG, Boulder, CO

Dr. John M. Miller
NOAA/ERL/ARL, Silver Spring, MD

Mr. Clarence T. Nagamoto
NOAA/ERL/ESG, Boulder, CO

Dr. Everett C. Nickerson
NOAA/ERL/ESG/PROF, Boulder, CO

Mr. Francois Perrin G.
Seccion de Contaminacion Ambiental
Centro de Ciencias de la Atmosfera,
Universidat Nacional Autónoma de México

Ms. Barbara A. Quintana
NOAA/ERL/ESG, Boulder, CO

Dr. Jan Rosinski
NCAR, Boulder, CO

Ms. Ma Isabel Saavedra R.
Seccion de Contaminacion Ambiental
Centro de Ciencias de la Atmosfera,
Universidat National Autónoma de México

Mr. Rodolfo Sosa E.
Seccion de Contaminacion Ambiental
Centro de Ciencias de la Atmosfera,
Universidat National Antónoma de México.

Dr. L. Paul Steele
CIRES, University of Colorado, Boulder, CO

Ms. Lois P. Stearns
NOAA/ERL/ARL/GMCC, Boulder, CO

Mr. Guillerno Torres J.
Seccion de Contaminacion Ambiental
Centro de Ciencias de la Atmosfera,
Universidat National Autónoma de México

Mr. Ricardo Torres J.
Seccion de Contaminacion Ambiental
Centro de Ciencias de la Atmosfera,
Universidat National Autónoma de México

Mr. Diego Lopez Veneroni
Direccion de Investigaciones Oceanograficas
Piso, Mexico.

ACKNOWLEDGMENTS

The organizers of the project express deepest appreciation to Admiral Miguel Angel Gomez Ortega, Secretary of the Navy (U.S.M.) for providing Mexico Naval Oceanographic Research Ship H-02 for this research, and to Vice-Admiral Gilberto Lopez Lira, The Director General of Naval Oceanography, whose guidance made this cruise possible. We thank Dr. William Hooke, Director of the Environmental Sciences Group, NOAA/ERL, for his encouragement and support and Dr. James Buizer and Dr. R. Lawrence Swanson, International Activities Office, NOAA, for their assistance. Dr. J. Gross and Dr. M. Zimmer of the National Hurricane Center provided NHC archival GOES images. The Estacion de Investigacion Oceanografica de Veracruz is appreciated for providing XBT data and figures. Thanks are due to Luis Pimentel Dominguez and Juan Sainz Rojas for collection of bibliographies. The services of the technical staff at Environmental Pollution Section, The Center of Atmospheric Sciences, National University of Mexico, are much appreciated. Dr. Frank Kelly and Mr. Dean E. Letzring and the staff at the Department of Oceanography, Texas A&M University at Galveston provided the decking facility and greatly appreciated assistance. We are very grateful to Captain Carlos Castro Trujillo and his crew for their assistance and hospitality during the cruise.

ABSTRACT

This report documents the scientific research of a bilateral cooperative project between the United States of America and The United States of Mexico. In 1986 scientists from both nations joined a research cruise in the Gulf of Mexico to investigate the air chemistry over the water that the two nations share. Emphases were placed on natural air quality, anthropogenic air pollution, acid rain, air-sea-land exchanges of gases and aerosols. The investigation included in-situ measurements and post-cruise laboratory analyses. Chemical, physical, meteorological, and oceanographic analyses were conducted to survey temporal and spatial variations of diverse parameters throughout the Gulf. The data sets were analyzed, interpreted, and intercorrelated. The results show that during the cruise (20 July-22 August), the large-scale air trajectories were easterly from the Caribbean Sea at all levels; however, the Gulf air measured was highly polluted in general. This is probably due to the oscillation of land breeze and sea breeze, and local shifting winds that brought continental air masses into the Gulf. The aerosol mass concentrations ranged from 5 to 78 with an average of 25 $\mu g/m^3$, and the number concentrations ranged from 5×10^2 to 10^5 with an average $2 \times 10^3/cm^3$. The maxima were found near the ports and petroleum refineries; the minima were in the open sea where the concentrations were still an order of magnitude greater than measurement over the South Pacific Ocean. Concentrations of gases (O_3, CO_2, CH_4, H_2S and total hydrocarbons) generally followed a similar distribution pattern except gases decreased more rapidly than aerosols when moving away from the sources. The life cycle of dimethyl sulfide (DMS) produced by marine biotic processes was studied. Its measured concentrations in seawater ranged from 22 to 244 with an average of 130 ng/L. The maximum concentrations were found in Campeche Bay where the highest concentrations of biomass in surface seawater were measured. The anticyclonic gyres observed in the western Gulf might cause upwelling of nutrient-rich deep-sea water to support bio-activities. The total sea-to-air flux of DMS in the Gulf was calculated as 2.3×10^9 g S each day or 0.84 Tg S per year. However, the concentrations of DMS in the atmosphere were <20 ng/m^3. The result suggests that DMS has a very short lifetime ($\leq$1.6 h) in the Gulf air. It is probably oxidized rapidly and converted to other sulfur gases or aerosols. The Gulf water is also a vast sink for atmospheric aerosols and gases. The dry deposition flux of aerosols was estimated at ~120 Tg/yr including 60% of water-insoluble particles containing Si, Al, Fe, etc., and 40% of water-soluble salts containing Na^+, Cl^-, $SO_4^=$, NO_3^-, Mg^{++}, Ca^{++} K^+, etc. The anthropogenic sulfate and nitrate particles, in addition to seasalt particles, are active cloud condensation nuclei and thus have the potential to increase cloud coverage and precipitation. The rain samples collected near ports were mostly acidic (pH, 4 to 5). The major ion concentrations were $Cl^- > Na^+ > SO_4^= > NO_3^-$. Approximately 80% of the $SO_4^=$ and NO_3^- in the rain were incorporated through the aerosol phase, either by condensation nucleation at cloud base or by below-cloud scavenging; only <20% were incorporated through in-cloud adsorption of precursor gases followed by liquid-phase oxidation. (The mechanisms are different from polluted continental precipitation in which in-cloud gas-phase incorporation was observed to be more important.) Based on the data set of rainwater chemistry and the annual precipitation rate in the region (~110 cm), wet deposition of atmospheric aerosols was estimated to be much more important than dry deposition to the Gulf.

AIR CHEMISTRY STUDIES OVER THE GULF OF MEXICO

A Bilateral Scientific Cooperative Project Between the United States of America and the United States of Mexico

INTRODUCTION

Farn P. Parungo

In the summer of 1986, a scientific research cruise was conducted to investigate air chemistry over the Gulf of Mexico. It was a bilateral collaboration between scientists of the United States of America (U.S.A.) and the United States of Mexico (U.S.M.) The purposes of the expedition were (1) to investigate anthropogenic air pollution, its source, strength, physical transport, chemical transformation, and deposition over the Gulf; (2) to investigate the natural contribution of gases and aerosols from Gulf waters; (3) to determine temporal and spatial variations of gases and aerosols as affected by meteorological variables and air-sea-land interactions; (4) to study acid rain formation in the region as incorporation of air pollution into the precipitation system, from cloud formation to in-cloud scavenging, and to below-cloud washout.

The Gulf of Mexico is semi-enclosed (area ~ 1.5×10^7 km^2), surrounded by the U.S.A., the U.S.M., and Cuba. The nations share economic, ecological, and scientific interests of the Gulf. However, international cooperation to investigate this common environment has been limited. To the best of our knowledge, our project is the first U.S.A.-U.S.M. collaboration to study air pollution and acid rain problems over the Gulf. Since the development of offshore petroleum exploration, the Gulf has been a recipient of pollution products. In addition, the large cities, oil refineries, and other industries along the shore can transport anthropogenic pollution into the Gulf. It is important for both nations to know the concentration distributions of various pollutants and to assess the environmental impact of the increasing air pollution in the region.

In our cruise we measured various atmospheric gases and aerosols to study their physical interactions and chemical transformations. We also collected

rainwater samples to analyze the chemical compositions for acid rain investigation.

Because gases and aerosols are also released from sea surface into the atmosphere, it is important to know these natural backgrounds in order to appraise the anthropogenic contribution. The most prominent natural marine aerosol is seasalt particles whose chemical compositions have been thoroughly investigated (e.g., Woodcock, 1953; Blanchard and Woodcock, 1957; Parungo et al., 1986). The most important marine gas is dimethyl sulfide (DMS) which is believed to be a metabolism product of algae (Andreae et al., 1983; Andreae and Raemdonck, 1983). The Gulf of Mexico has historically been one of the most prolific fishing regions in the world for both finfish and shellfish, which live on a food network beginning with microorganisms. One would presume that primary productivity of microorganisms such as algae must also be high in the region. However, the concentrations of algae that depend on nutrients in the water and grazing rate of zooplanktons are highly variable with time and with location (El-Sayed et al., 1972). Numerous investigations of hydrology, hydrochemistry, and hydrobiology in the Gulf have been reported (e.g., Parr, 1935; Conover, 1958; Taylor, 1972; Jones et al., 1973). In 1964-1965 a joint marine expedition of U.S.S.R. and Cuba was conducted in the Gulf of Mexico and the Caribbean Sea (Dumka, 1966). Many new findings were reported, including the existence of previously unknown upwelling zones (e.g., southwestern Campeche Bay) where the nutrient-rich deep water brought to the surface enhances photosynthesis and thus supports a chain of biological activities. Since our research was aimed at the atmosphere, we measured only the hydroparameters that were directly relevant to air chemistry. We measured the temperature, pH, suspended particles, and DMS in the surface water. We studied the relationships among upwelling, concentrations of nutrients, suspended particles, or microorganisms, and DMS in the water and in the air. We assessed the natural contribution to air pollution.

To investigate the transport of air pollution or the chemical transformation of various trace species, one needs to know the wind speed and wind direction, atmospheric pressure and temperature, humidity, and solar radiation; these meteorological parameters were measured onboard. In addition, a long-range air trajectory program was used to calculate back trajec-

tories for selected locations along the cruise track. Also a land-air-sea interaction model was used to estimate the strength of land breeze and sea breeze. For rain chemistry study, satellite image analysis was used to measure cloud characteristics.

Direccion General de Oceanografica, Mexico Navy, provided oceanographic Research Vessel H-02 for this project. The ship is 57.5 m (184.5 ft) long; maximum weight is 777 tons and maximum speed is 12 knots. The research cruise began at Galveston, Texas, on 20 July 1986 and ended at Verucruz, Mexico, on 23 August 1986. The cruise track and itinerary are shown in Fig. 1.

This report summarizes the investigation results. It describes the objectives and scope of the investigation, the methods and instruments we used, the in-situ measurements, the post-cruise analyses, and data interpretation. Each section has been developed independently and should be considered an independent statement by its author or authors.

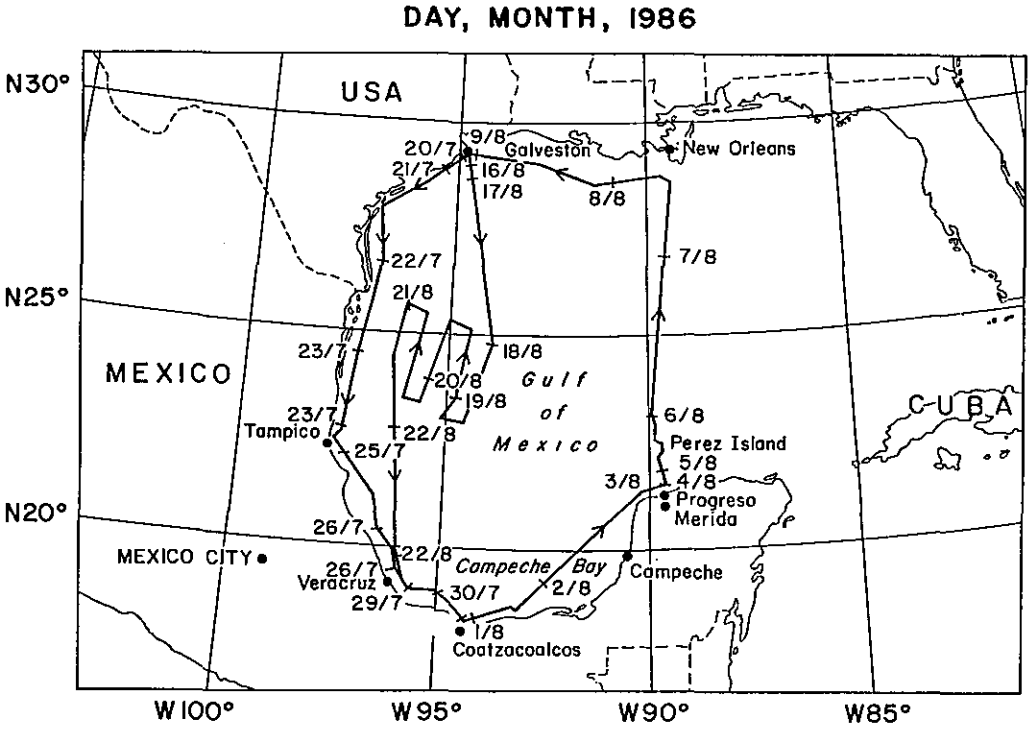

Figure 1. Approximate track for H-02 oceanographic research cruise, 20 July - 22 August 1986.

References

Andreae, M.O., and H. Raemdonck, 1983: Dimethyl sulfide in the surface ocean and marine atmosphere. Science, 221:744-747.

Andreae, M.O., W.R. Barnard, and J.M. Ammons, 1983: The biological production of DMS in the ocean and its role in the global atmospheric sulfur budget. Ecol. Bull. (Stockholm) 35:167-177.

Ayers, G.P., and J.L. Gras, 1980: Ammonia gas concentrations over the Southern Ocean. Nature, 284:539-540.

Blanchard, D.C., and A.H. Woodcock, 1957: Bubble formation and modification in the sea and its meteorological significance. Tellus, 9:145-158.

Conover, J.T., 1958: Seasonal growth of benthic marine plants as related to environmental factors. Publ. Inst. Mar. Sci., 5, 97-147.

Dumka, N., 1966: Investigations on the Central American Seas. Akademiya Nauk UKSSR. Translation Available from the U.S. Department of Commerce National Technical Information Service, Springfield, VA 22151.

El-Sayed, S.Z., W.M. Sackett, and L.M. Teffrey, 1972: Chemistry, primary productivity, and benthic algae of the Gulf of Mexico. Serial Atlas of the Marine Environment, 22:1-29. Amer. Geogra. Soc.

Jones, J.I., R.E. Rinz, M.O. Rinkel, and R.Z. Smith, 1973: A summary of knowledge of the eastern Gulf of Mexico. I-1 to III F-9. The State University of Florida, Institute of Oceanography.

Parr, A.E., 1935: Report on hydrographic observations in the Gulf of Mexico. Kraus Reprint Co., Bingham Oceanographic Foundation, 93 pp.

Parungo, F.P., C.T. Nagamoto, and J.M. Harris, 1986: Temporal and spatial variations of marine aerosols over the Atlantic Ocean. Atmos. Res., 20:23-37.

Taylor, W.R., 1972: Marine algae of the Smithsonian-Bredin expedition to Yucatan - 1960. Bull. Mar. Sci., 22, 34-44.

Woodcock, A.H., 1953: Salt nuclei in marine air as a function of altitude and wind force. J. Meteorol. 10:362-371.

PART I. GAS MEASUREMENTS

MEASUREMENTS OF O_3, TOTAL HYDROCARBONS, H_2S, AND SO_2 CONCENTRATIONS

Humberto Bravo A., Rodolfo Sosa E., Francois Perrin G.
Guillermo Torres J., Isabel Saavedra R., Ricardo Torres J.
and Rosaura Cauacho C.

1. INTRODUCTION

On 20 July 1986, the S.M.N. (Mexican Navy Secretariat) Research Vessel H-02 sailed from Galveston, Texas, U.S.A. (29°N, 95°E) around the Gulf of Mexico, 10 miles from the coast of the U.S.A. and U.S.M., touching the ports of Tampico, Veracruz, Coatzacoalcos, and Progreso and crossing the Gulf along 90°E, North bound, arriving back at Galveston on 12 August, and ending at Veracruz on 22 August 1986. The objective was to measure gaseous pollutants (ozone, hydrogen sulfide, total hydrocarbons, and sulfur dioxide) over the coastal and remote marine atmosphere.

2. METHODS OF SAMPLING AND ANALYSIS

The locations of the sampling ports and instruments are shown in Fig. 1. The gas samples were collected on a deck 10 m above the sea surface and upwind of the ship's exhaust.

The following instruments were used during the study.

2.1 Sulfur Dioxide: Monitor Labs. Model 8850

Fluorescent SO_2 analyzer: for a continuous dry gas analysis for SO_2 in the range 0 to 10 ppm. Model 8850 works on the principle of U.V. excitation of the SO_2 molecule in the far-ultraviolet, and the resultant fluorescent output is proportional to concentration. With a flow rate of 500 cc/min the lower detectable limit is 1 ppb; precision is ±5 ppb, and lag time is 20 s. We worked with a range up to 250 ppb.

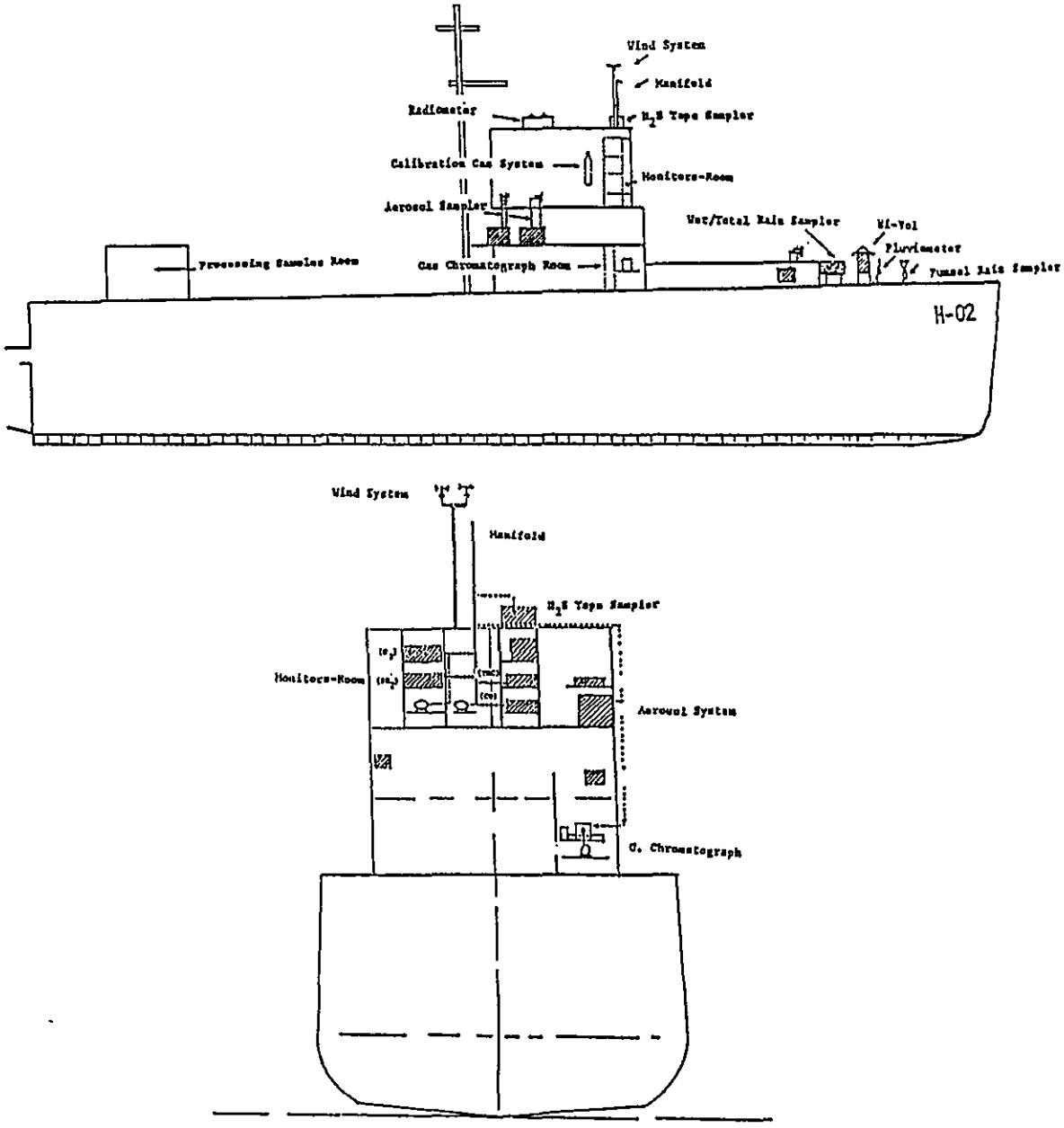

Figure 1. Sampling equipment locations.

Calibration procedure

Zero: with nitrogen gas

Span: with permeation device and dynamic calibration system (Bendix model 8251)

2.2 Ozone: Beckman Instrument Model 950 Ozone Analyzer

The principle of operation is the chemiluminescent gas-phase reaction of ozone with ethylene.

A temperature control of the detector and flow control devices provide a sensibility of 0.5 ppb, a lag time shorter than 1 s, and a precision of ±1% (2 ppb in the range of 0-0.05 ppm).

Calibration procedure

Zero: with nitrogen gas

Span: ozone generator, calibrate with a KI sampling train, in Veracruz

Output: 0.15 ppm and 0.30 ppm O_3.

2.3 Total Hydrocarbons: Beckman Instrument Model 400

Hydrocarbon analyzer: The analyzer uses the flame ionization method of detection. A temperature controller and an internal sample bypass feature provide a full-scale sensiivity of 2% CH_4 and a response speed of 0.5 s. We used it in a range of 0-10 ppm.

Calibration procedure

Zero: with nitrogen gas

Span: cylinder of standard gas CH_4 (Scott Specialty Gases)

Output: 9.2 ppm CH_4

2.4 Hydrogen Sulfide: RAC Model G2 H_2S Sampler

The sampler operates in a range of 0.20-20 ppm; H_2S reacts with the lead acetate of the filter paper tape to produce stains. We used it with a flow sample of 0.15 CFM and a sampling cycle of 3 h. The spots were read with an RAC spot evaluator instrument and compared with the calibration curve that correlates the degree of staining in a spot with the ppm of H_2S.

3. RESULTS

3.1 Meteorology

Wind direction and wind velocity were determined each hour during the cruise. The results are shown in Fig. 2.

3.2 Gaseous Pollutants

The data obtained for the gaseous pollutants were plotted on a logarithmic ordinate, and the cumulative frequency distribution was plotted on the abscissa. Considering that the air quality measurements tend to fit a general mathematical model, the pollutant concentrations are log normally distributed for all covering times (Larsen, 1971, and Aitchinson and Brown, 1966).

For a lognormal distribution the arithmetic mean, geometric mean, standard deviation, and standard geometric deviation are related as follows:

$$sg = \exp\left[\ln^{0.5}\left(\frac{s^2}{m^2} + 1\right)\right]$$

$$mg = \frac{m}{\exp(0.5\ \ln^2 sg)} \qquad (1)$$

where exp = the base of natural logarithms, 2.718, raised to the power that follows in brackets

m = the arithmetic mean

mg = the geometric mean

s = the standard deviation

sg = the standard geometric deviation.

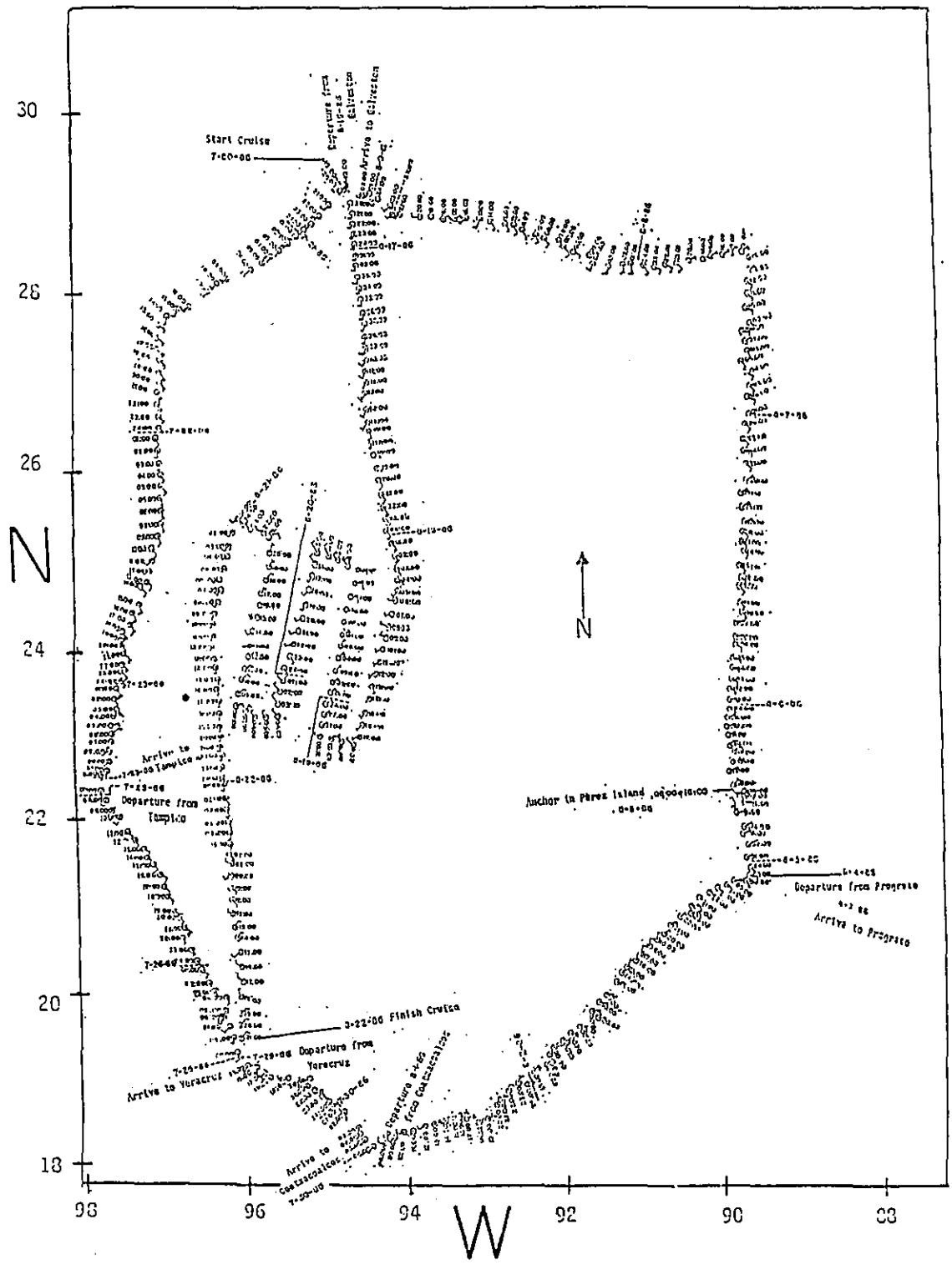

Figure 2. Wind direction and wind velocity during the cruise.

Because the most valuable information is how often air pollutant concentrations equal or exceed certain values, in our representations the abcissa values are used to represent the frequency with which a certain concentration is equal to or exceeds (1).

3.2.1 Ozone analysis

Figure 3 shows the values found for ozone during the sea-coast portion of the cruise. The median values are of the same order of magnitude with the exception of the values found in the Veracruz-Coatzacoalcos portion where mg = 8.50 ppb. In most other times of this portion of the cruise O_3 was in the range from 0.9-4.4 ppb. This could be explained as being due to the high emissions of photochemical oxidant precursors (hydrocarbons and nitrogen oxides). The sea-sea portion of the cruise (Progreso-New Orleans and Galveston-Tampico) shows a well-defined distribution (Fig. 4). Table 1 presents the data.

The ozone average concentrations in the ports represent the highest values found during the cruise, (except the Veracruz-Coatzacoalcos, sea-coast-position where values were even higher) (see Fig. 4). The classical ozone bell-shaped curve observed daily in Mexico City was not present at all during the cruise. Note in Fig. 5 that no increase in ozone concentration took place during the noon hours. When the sampling was performed 10 miles from the coast of Texas, Tampico, Veracruz, and Coatzacoalcos, an increase in the ozone concentration was observed. This effect could be the result of industrial activities in those areas, which produce emissions of hydrocarbons and nitrogen oxides (well-known ozone precursors).

3.2.2 Hydrocarbon analysis

Figures 6 and 7 and Table 1 record the concentrations of total hydrocarbons (THC) found during the cruise (the values include methane). The medians reported in this cruise are in the same order of magnitude. The highest values are believed to correspond to pollution generated in the harbors where stops were made. Typical behavior of the THC during the day is shown in Fig. 8.

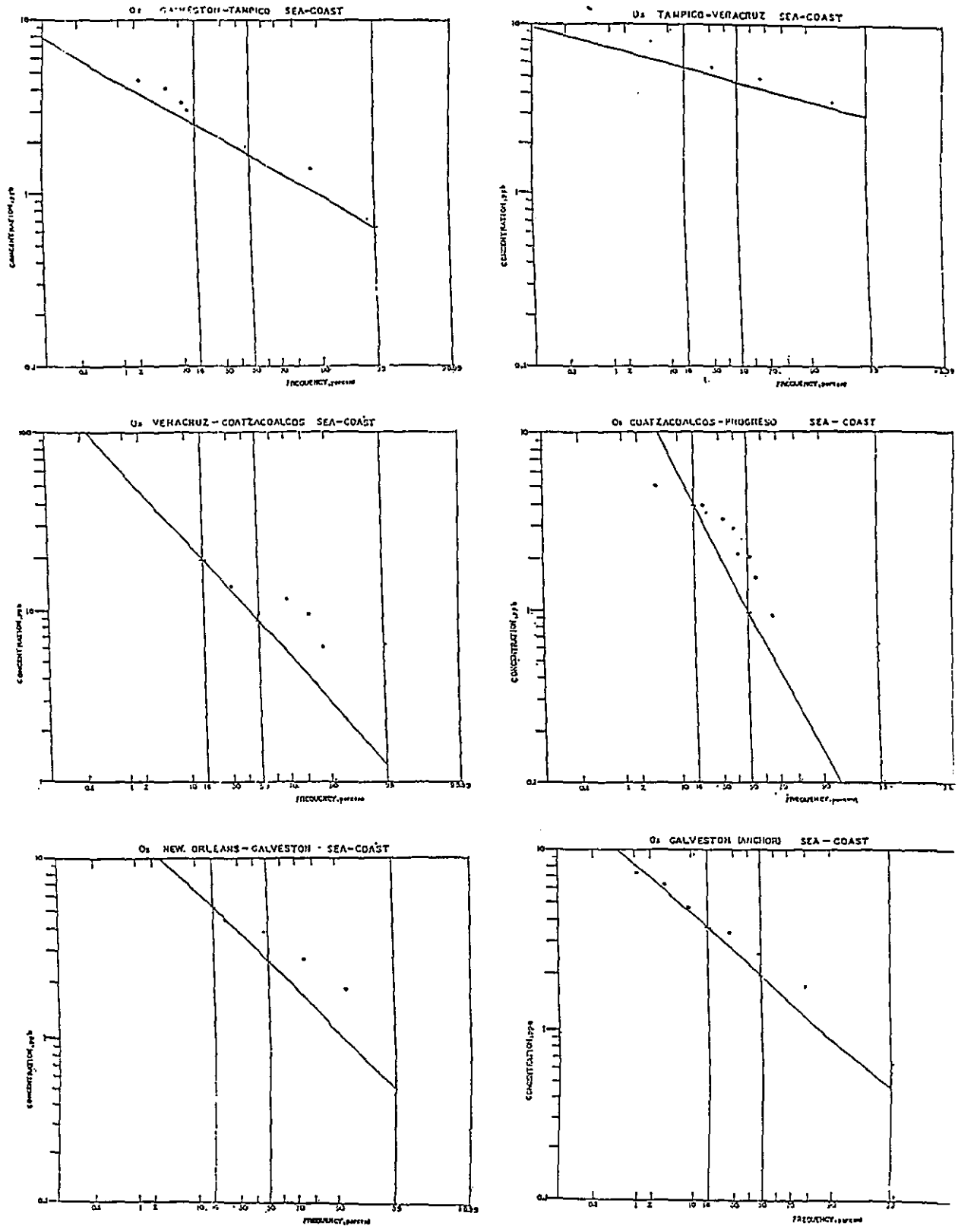

Figure 3. Ozone concentrations during the cruise (sea-coast).

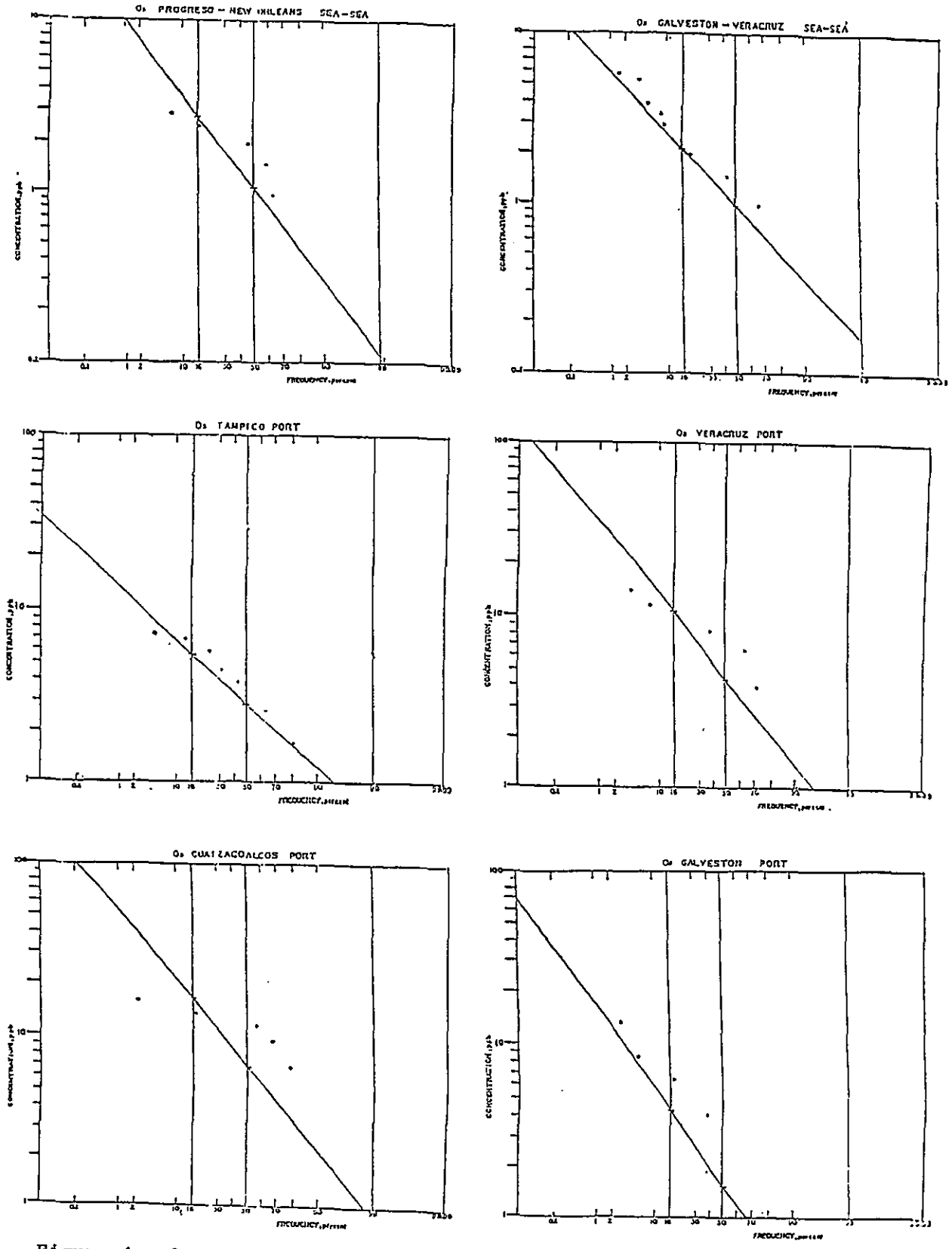

Figure 4. Ozone concentrations during the cruise (sea-sea and ports).

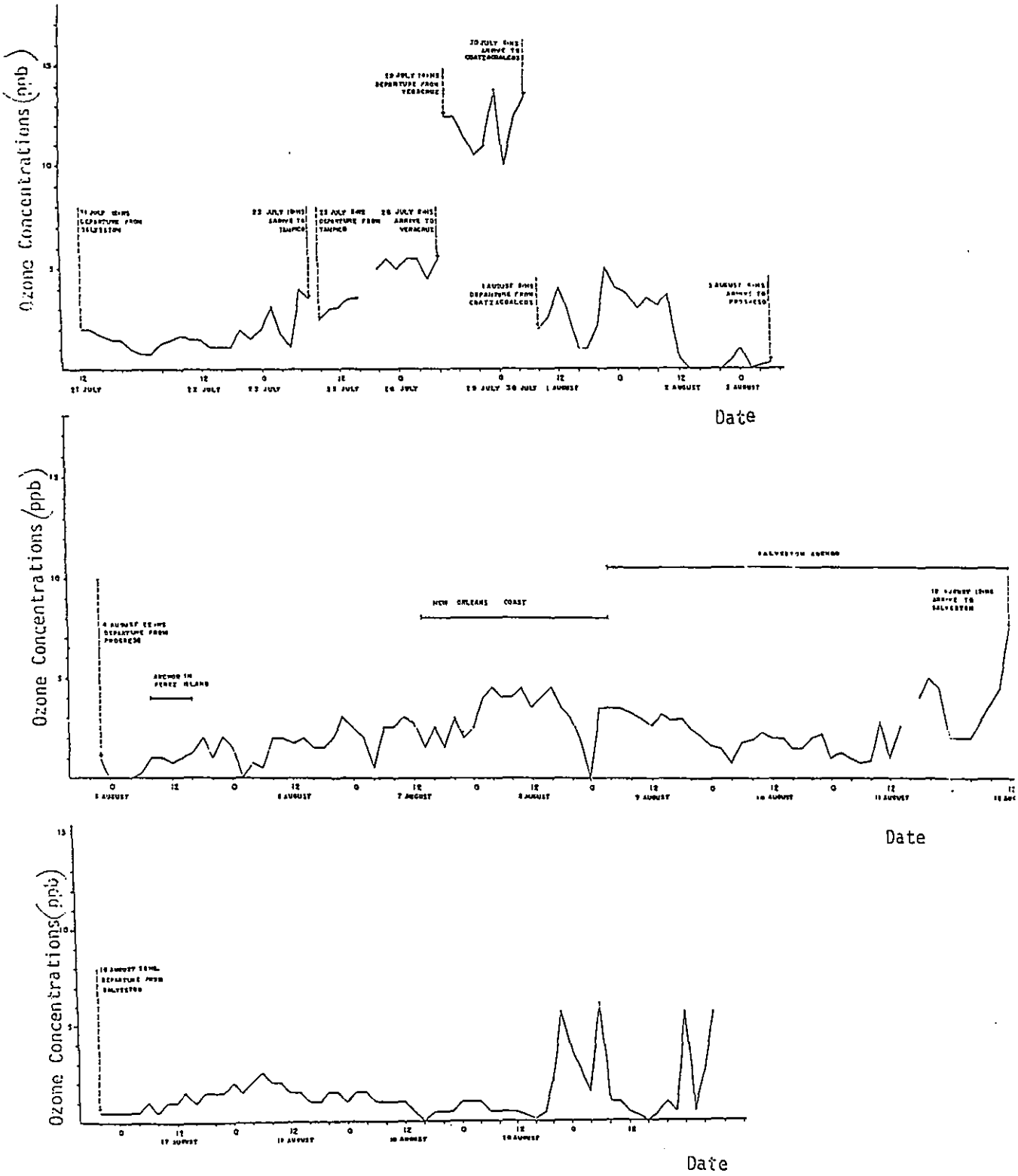

Figure 5. Ozone behavior during the cruise.

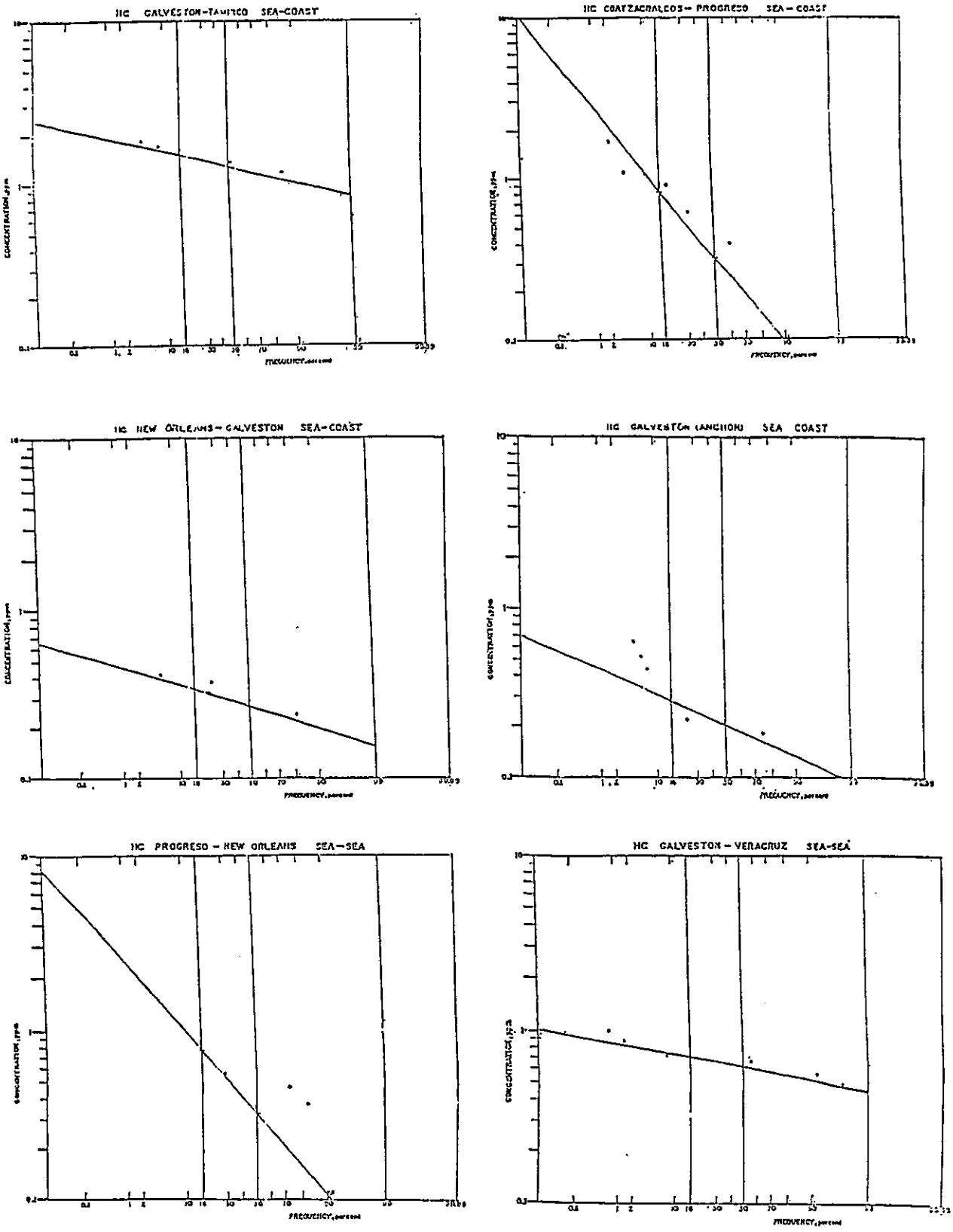

Figure 6. Total hydrocarbon concentrations during the cruise (sea-coast and sea-sea).

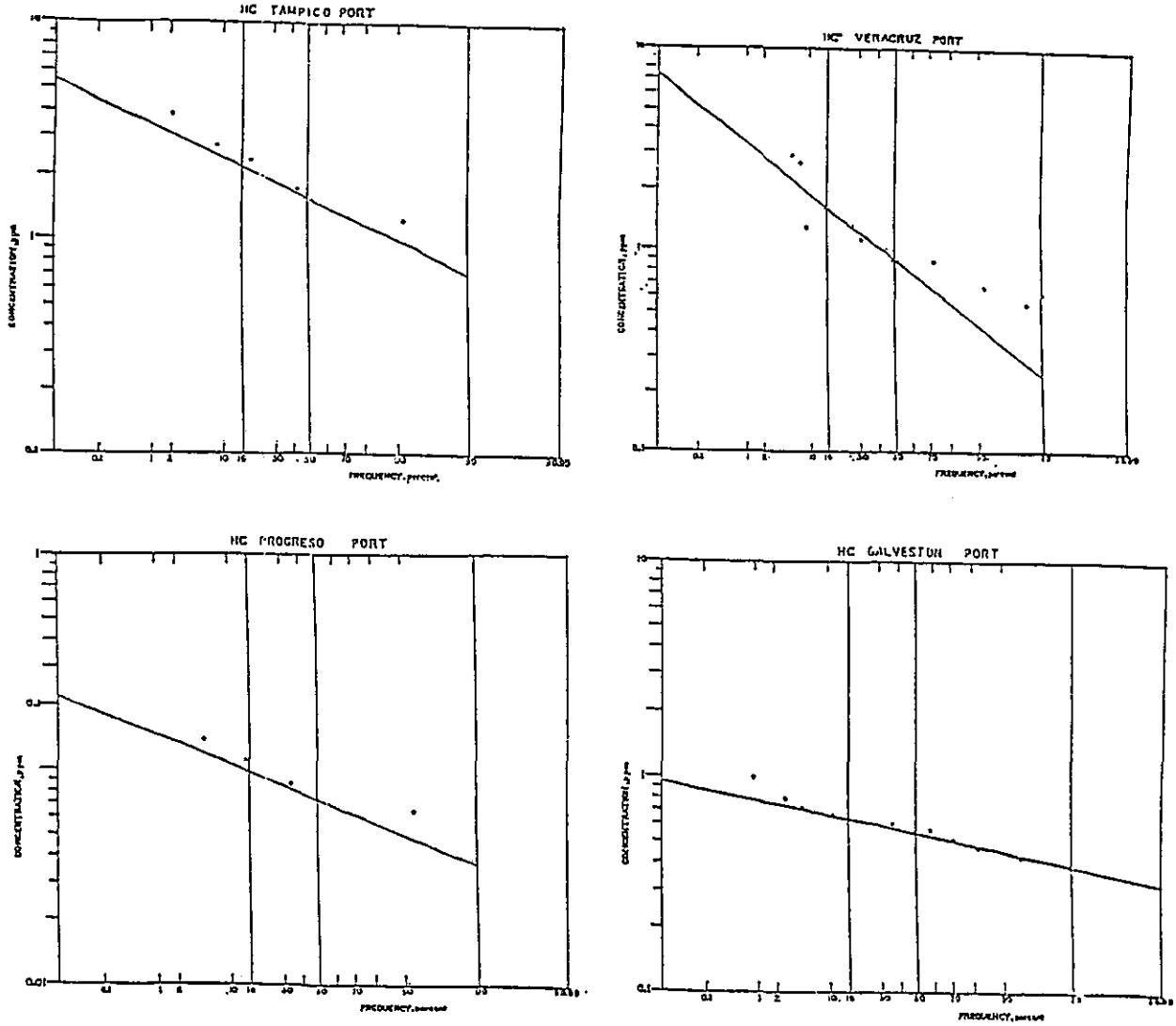

Figure 7. Total hydrocarbon concentrations during the cruise (ports).

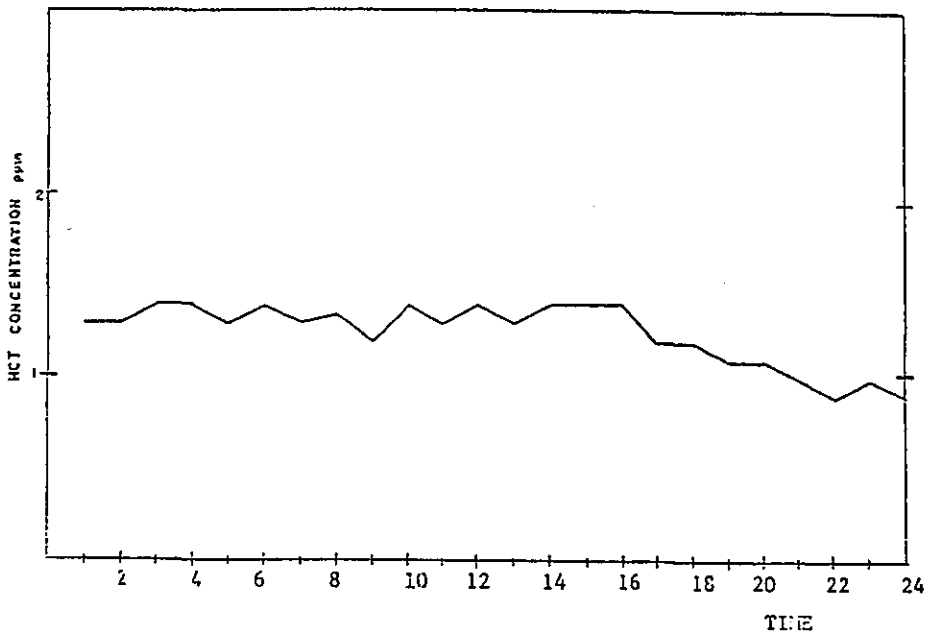

Figure 8. Typical behavior of total hydrocarbons during the day.

Table 1. Concentrations of Ozone and Total Hydrocarbons During the Cruise

Monitoring zone	O_3 (ppb)		THC (ppm)	
	$\bar{X}$	σ	$\bar{X}$	σ
Galveston-Tampico	1.63	1.48	1.26	1.18
Tampico Port	2.73	2.10	1.51	1.40
Tampico-Veracruz	4.43	1.24	0.72	1.18
Veracruz Port	4.32	2.44	0.89	1.76
Veracruz-Coatzacoalcos	8.58	2.25	NM	NM
Coatzacoalcos Port	6.77	2.45	NM	NM
Coatzacoalcos-Progreso	0.95	4.09	0.32	2.53
Progreso Port	0.079	4.53	0.07	1.34
Progreso-Nueva Orleans	1.05	2.60	0.32	2.42
Nueva Orleans-Galveston	2.57	2.01	0.26	1.28
Galveston Anchor	1.93	1.86	0.21	1.34
Galveston Port	1.54	2.73	0.55	1.20
Galveston-Veracruz	0.99	2.18	0.61	1.15

3.2.3 Hydrogen sulfide

Figure 9 shows the concentration distribution of hydrogen sulfide after a discrimination of values was done (deleting the data concentrations obtained from contaminated samples). Note that the median concentration is lower than 1 $\mu g/m^3$ and the geometric standard deviation is 3 $\mu g/m^3$. These data are semi-quantitative because the sampling and analysis were carried out with the lead acetate tape sampler equipment.

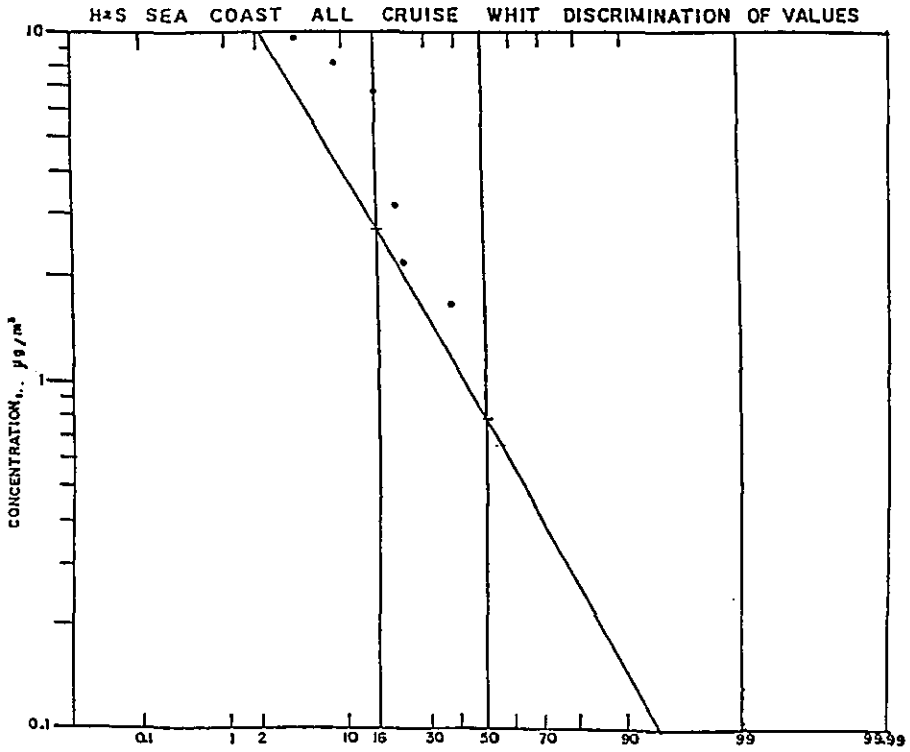

Figure 9. Hydrogen sulfide concentrations during the cruise.

4. SUMMARY

(a) Figure 2 shows the hourly meteorological information, with regard to true wind velocity and direction.

(b) The daily ozone cycle observed in the urban atmospheres (a bell-shaped curve) was not present during the cruise.

(c) The highest values of THC and O_3, found along the coast of Tampico-Veracruz-Coatzacoalcos, may be caused by the oil refining and petrochemical activity.

(d) The concentrations of O_3 were generally very low.

(e) The values found on the different legs suggest the role of the ocean as a sink of ozone.

(f) The sea-coast measurements indicate a pollution transport from the continent to the Gulf.

(g) The hydrogen sulfide concentrations show a geometric mean of 1 $\mu g/m^3$. (Contamination from the ship was detected in many of our samples; such samples were deleted.)

(h) The sulphur dioxide measurement presented uncertainty owing to malfunction of instrumentation.

REFERENCES

Aitchinson, J., and J.A.C. Brown, 1966: The Lognormal Distribution. Cambridge University Press, New York.

Larsen, R.I., 1971: A mathematical model for relating air quality measurements to air quality standards. E.P.A. Office of Air Programs.

MEASUREMENT OF DIMETHYL SULFIDE IN AIR AND SEAWATER

Steven D. Hoyt and Lisa H. Hoyt

1. INTRODUCTION

Acid precipitation and the transport of acid rain precursors has become a major environmental concern to all countries. The objectives of the joint United States and Mexico acid rain cruise in the Gulf of Mexico are to identify sources and transport of acid rain precursors in the Gulf region.

Recent evidence suggests that some of the acidity in precipitation could be caused by the conversion to sulfur dioxide and natural acids formed from reduced sulfur compounds produced by the ocean (Charlson and Rodhe, 1982; Nguyen et al., 1983; Graedel, 1979). Measurements of ocean surface concentrations of sulfur gases have shown that the ocean is an important source of OCS, DMS, and other sulfur gases (Hoyt, 1982; Rasmussen et al., 1982, Nguyen et al., 1978; Cline and Bates, 1983; Andreae and Barnard, 1983; Andreae and Raemdonck, 1983). The results of these measurements indicates that DMS is the most important natural sulfur species produced in the Ocean, and would be expected to contribute significantly to the sulfate burden in the region.

Measurements of the seawater concentrations of DMS have been made in several regions of the ocean (Andreae and Raemdonck, 1983b; Cline and Bates, 1983; Bernard et al., 1982). Measurements in the Gulf of Mexico gave average values for the seawater concentration of DMS as 52 ng S/L. This value was lower than the average value in other ecologically productive regions of the oceans. Upwelling areas along the equatorial region of the Pacific Ocean have average seawater concentrations of 155 ng S/L. Atmospheric concentrations of DMS in the Gulf of Mexico gave average concentrations of 9.7 ng S/m^3 (n=4); this is much lower than the average value 167 ng S/m^3 in the upwelling region of the Pacific Ocean (Andreae and Raemdonck, 1983).

2. ANALYTICAL METHODS

The DMS measurements were made on an instrument developed for oceanographic work. It uses a 30-m DB-1 fused silica capillary column with a 5.0-μm film thickness and an FPD detector. The detector was modified with a wideband filter for increased sensitivity. A similar system had been previously used in the South Pacific for air and water measurements of reduced sulfur gases. The system was constructed from Teflon and silanized glass to minimize adsorption losses. The seawater samples were collected in 50 mL glass syringes and filtered with disposable 25-mm, 0.45-μm filters. The DMS in seawater was concentrated by stripping a 20-mL seawater sample with an inert gas and passing the gas through a potassium carbonate dryer to remove the water vapor. The DMS was cryogenically trapped on silanized glass beads by using liquid oxygen. The sample was (1) desorbed from the glass beads by using hot water and (2) cryofocused on a section of the capillary column. This procedure is similar to the method of Farwell et al. (1979) and Farwell and Gluck (1980). The analysis was run at room temperature, and the DMS concentration was measured by the high-sensitivity FPD detector.

The air samples were collected from an air sampling tower located above the bridge of the ship. The air was continuously pumped down to the gas chromotograph (GC) through Teflon tubing. The DMS measurements in air were made by passing a 1000 mL air sample through a Nafion dryer to a glass bead trap where it was concentrated and then desorbed to the cryofocus loop.

The DMS concentration was determined by integrating the peak areas using a HP 3393A computing integrator. The area was standardized against a DMS gas standard prepared by transferring a 10-ppm DMS standard to a passivated aluminum cylinder and standardizing it before and after the trip against a Scott Environmental Standard.

3. RESULTS

The results for the seawater measurements are shown in Fig. 1 and Table 1. The sample locations are given by date and latitude/longitude.

The equation used to calculate the flux is based on the two film model (Hoyt, 1982; Liss and Slater, 1974):

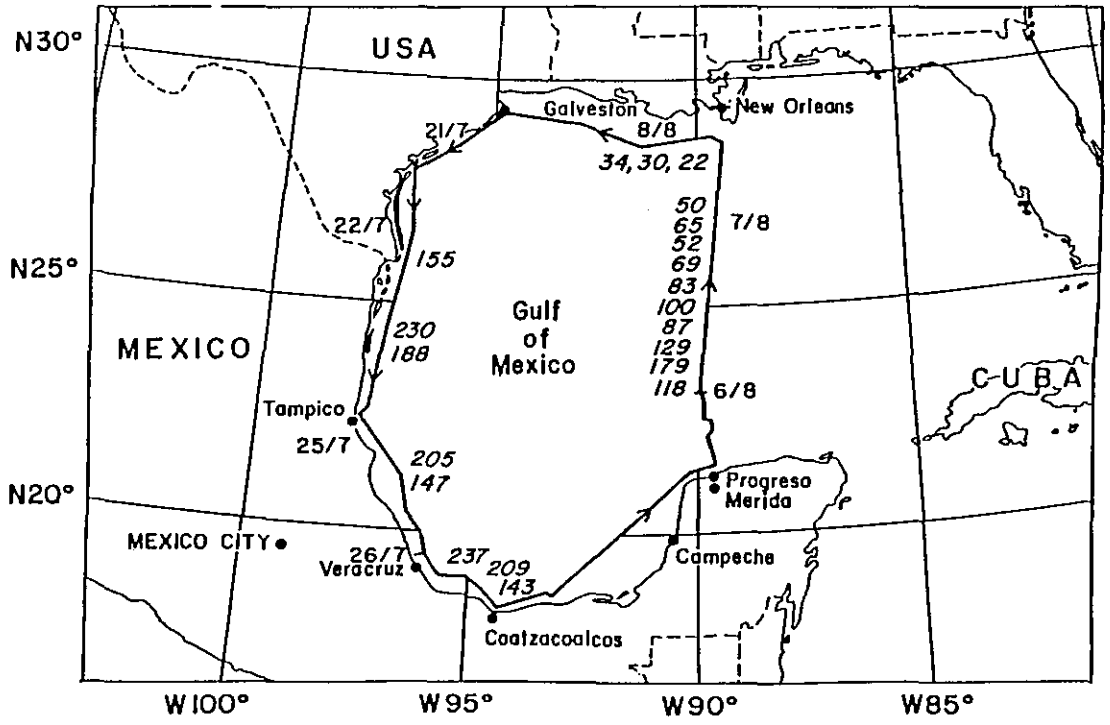

Figure 1. Concentrations of DMS (ng/L) in surface seawater measured along the cruise track.

$$F = K(Cl - Cg/H) \ .$$

The value for the transfer coefficient, K, is estimated from the average value for Radon exchange in the Pacific and Atlantic Oceans (Broecker and Peng, 1974) and is adjusted for the diffusivity of DMS (Hoyt, 1982). For DMS, the value of K is 2.3 m/day. Since the concentration of DMS in air, Cg, is very small compared with the seawater concentration, Cl, the flux is calculated directly as the product of Cl and K. This equation illustrates that the flux of DMS in a region cannot be estimated from atmospheric concentration measurements.

$$F = K\ Cl \ .$$

The concentration of DMS in air was measured at least once each day of the cruise (except 7/22). On all days except 7/23 the results were below the detection limit of 20 ng DMS/m^3. On 7/23 a value of 20 ng DMS/m^3 (10.3 ng S/m^3) (at the detection limit) was determined at a time when the seawater concentration was high. These values are much lower than the concentrations

Table 1. NOAA Gulf of Mexico DMS measurements 20 July - 13 August 1986

Date	Lat.	Long.	T (°C)	DMS (ng/L)	Flux*
July					
22	24°05'	97°17'	29	155	357
	24°28'	97°18'	29	205	472
23	23°03'	97°38'	28	230	529
	22°33'	97°39'	28	188	432
25	21°07'	96°57'	28	205	472
	20°59'	96°50'	28	147	339
29	19°02'	95°33'	29	237	544
	18°58'	95°25'	29	209	481
August					
	18°55'	95°21'	29	143	329
1	18°22'	94°05'	29	182	418
	18°33'	93°08'	29	244	561
	18°53'	92°45'	29	100	229
2	19°45'	91°48'	29	110	254
	19°50'	91°40'	29	70	162
	20°20'	91°14'	29	135	311
	20°40'	90°52'	29	134	308
	20°45'	90°46'	29	160	367
5	24°12'	89°45'	29	202	465
	24°21'	89°45'	29	81	186
6	24°21'	89°45'	30	118	271
	24°37'	89°43'	30	179	413
	25°09'	89°42'	30	129	297
	25°40'	89°39'	30	87	199
	25°54'	89°41'	30	100	230
7	27°47'	89°33'	31	83	191
	28°04'	89°31'	31	69	158
	28°21'	89°29'	31	52	120
	28°32'	89°35'	31	65	149
	28°28'	90°00'	31	50	116
8	28°38'	91°58'	31	22	52
	28°54'	92°54'	31	30	70
	28°54'	92°54'	31	34	78
			Average	130	299

* μg of DMS per meter^2 per day
Flux = K(Cl-Cg/H) Cg <<< Cl
2.3 m/day is the adjusted transfer velocity (K) for DMS

measured in the South Pacific (167 ng S/m^3) and agree with the findings of Andreae and Raemdonck (1983). Because of the low concentrations no diurnal variations were observed.

The average of the DMS concentration in seawater for the Gulf of Mexico was 130 ng/L DMS (67 ng S/L), compared with an average of about 300 ng/L DMS for the equatorial upwelling region of the Pacific Ocean (Andreae and Raemdonck 1983; Cline and Bates, 1983). This would correspond to a smaller average flux value for the Gulf region (300 µg of DMS per $meter^2$ per day). The DMS concentrations in the seawater samples collected along the coast region averaged about 170 ng/L DMS whereas the concentrations across the Gulf averaged about 100 ng/L DMS. The reason for the extremely low values obtained at the end of the trip is not completely understood, unless there was some influence of the Mississippi river outlet.

4. DISCUSSION

In the surface seawater, the biota (e.g., algae, fungi, bacteria and plants) carries out assimilatory sulfate reduction and synthesizes organo-sulfur compounds. Volatile products (e.g., DMS) are transferred across the air/sea interface by a combination of molecular and turbulent diffusion processes (Maroulis and Bandy, 1977). The global marine flux of DMS is estimated at 60 Tg/yr. Thus, DMS is an important precursor for atmospheric sulfate including H_2SO_4. The global average concentration of DMS in seawater is ~3 nM (Andreae, 1986). According to the Henry's Law constant for DMS, measured to be 0.074 (Bingemer, 1984), the atmospheric concentration of DMS in equilibrium with seawater should be 220 nM/m^3. Since the DMS average concentration in Gulf water was only 2.1 nM (130 ng/L), the DMS concentration in Gulf air should be 155 nM/m^3 (~9 µg/m^3). However, the actually measured atmospheric concentration was <0.32 nM/m^3 (≤20 ng/m^3) which is 485-fold below the calculated value. The results suggest that as DMS evicted from sea to air, it was oxidized rapidly and transformed to other sulfur gases (e.g., CH_3SOCH_3, CH_3SO_2, $CH_3SO_3CH_3$, CH_3SSCH_3, SO_2, and SO_3) or sulfate particles (e.g., CH_3SO_3H, H_2SO_4, $(NH_4)_2SO_4$, NH_4HSO_4, Na_2SO_4, and $CaSO_4$). The pathways and rates of oxidation have been widely studied. However, current information is mostly hypothetical. The important products are CH_3SO_3H (a strong acid) and

SO_2 (which will be converted to a strong acid H_2SO_4). As a result, the end products of DMS will acidify or neutralize atmospheric aerosols; thus DMS has an important role in acid cloud and acid rain formation.

Earlier, Pueschel (1984) used aircraft to measure DMS concentrations at various altitudes over the Gulf of Mexico. On the basis of measurements showing very low DMS concentrations in the air, he claimed that natural sources (DMS) had been eliminated as a significant contributor to acid rain. Two years later, the same research group (Luria et al., 1986) used the same measurements and concluded that DMS has significance for the global surface cycle and can cause significant acidification of cloud water. In either case it is inaccurate to foretell the significance by their method, because the atmospheric concentration of DMS does not relate to its flux from the ocean. Our measurements of DMS in Gulf water and in the air provide a more accurate assessment of DMS flux from sea to air, which is ~300 $\mu g/m^2$/day. The Gulf area is 1.5×10^{13} m^2. This means that the Gulf water releases 4.5×10^9 g of DMS into the atmosphere every day. Although DMS concentrations in the air were very low (<20 ng/m^3), the contribution of DMS to acid rain should not be "eliminated" or even underestimated. The rate of oxidation of DMS in air is a central factor for its concentration. The rate depends on solar radiation and other gases and aerosols in the environment. The residence time (τ) of DMS can be calculated by the equation $\tau = C/F$, where C = concentration of DMS in boundary-layer air (assuming the mixing depth is 1 km), $C \leq 20$ $ng/m^3 \times 1000$ m = 20 $\mu g/m^2$, and F = flux of DMS = 299 $\mu g/m^2/D$. Thus, $\tau \leq 0.07$ D = 1.6 h. Therefore, the resident time of DMS in the air is ≤1.6 h, which is shorter than in the marine environment elsewhere (0.2-0.8 day). This may be explained by the fact that in the Gulf the high concentration of pollution, both gases and aerosols, probably catalytically accelerates oxidation and causes low DMS concentration in the air.

5. CONCLUSIONS

The DMS concentrations in seawater measured around the Gulf of Mexico provided information about the flux of natural sulfur to this region. From this data set of 30 measurements an average flux of 300 μg of DMS per $meter^2$ per day was calculated. This would correspond to a flux of 2.3×10^9 g of sulfur

released into the atmosphere of the Gulf each day (0.84 Tg S per year). The atmospheric concentration was <20 ng/m^3 and below the detection limit most of the cruise. By using this value, a lifetime for CMS of ≤1.6 h can be calculated. For future measurements in the Gulf region a preconcentration system capable of concentrating more than 1000 mL of air would be recommended to obtain values for the atmospheric concentration of DMS at these low levels.

REFERENCES

Andreae, M.O., 1986: The ocean as a source of atmospheric sulfur compounds The Role of Air-Sea Exchange in Geochemical Cycling, (Buat-Menard, Ed.) D. Reidel Publishing Co., 331-362.

Andreae, M.O., W.R. Barnard, 1983: Determination of trace quantities of dimethyl sulfide in aqueous solutions. Anal. Chem., 55:608-623.

Andreae M.O., and H. Raemdonck, 1983: Dimethyl sulfide in the surface ocean and the marine atmosphere: A global view. Science, 221:744.

Bernard, W.R., M.O. Andreae, W.E. Watkins, H. Bingemer, and H.-W Georgii, 1982: The flux of dimethyl sulfide from the oceans to the atmosphere. J. Geophys. Res., 87:8787-8794.

Bingemer, H., 1984: DMS in ozen und mariner atmosphare. Ph.D. Dissertation. J.W. Goethe University, Germany.

Broecker, W.S., and T.H. Peng, 1974: Gas exchange rates beween air and sea. Tellus, 26:21-35.

Charlson, R.J., and H. Rodhe, 1982: Factors controlling the acidity of natural rainwater. Nature, 295:683-685.

Cline, J.D. and T.S. Bates, 1983: Dimethyl sulfide in the equatorial Pacific Ocean: A natural source of sulfur to the atmosphere. Geophys. Res. Lett., 10:949.

Farwell, S.O., and S.J. Gluck, 1980: Glass surface deactivants for sulfur containing gases. Anal. Chem., 52:1968-1971.

Farwell, S.O., S.J. Gluck, W.L. Bamesberger, T.M. Schutte, and D.F. Adams, 1979: Determination of sulfur-containing gases by a deactivated cryogenic enrichment and capillary gas chromatographic system. Anal. Chem., 51:606-615.

Graedel, T.E., 1979: Reduced sulfur emission from the open oceans. Geophys. Res. Lett., 6:329-331.

Hoyt, S.D., 1982: Ocean-air exchange of carbonyl sulfide and halocarbons. Ph.D. Thesis, Oregon Graduate Center, Beaverton, OR.

Liss, P.S., and P.G. Slater, 1974: Flux of gases across the air-sea interface. Nature, 247:181-184.

Luria, M., C. Van Valin, D. Wellman, and R. Pueschel, 1986: Contribution of Gulf area natural sulfur to the North American sulfur budget. Environ. Sci. Tech., 91-95.

Maroulis, P.J., and A.R. Bandy, 1977: Estimate of the contribution of biologically produced dimethyl sulfide to the global sulfur cycle. Science, 196:647.

Nguyen, B.D., A. Gaudry, B. Bonsand, and G. Lambert, 1978: Reevaluation of the role of dimethyl sulfide in the sulfur budget. Nature, 275:637-639.

Nguyen, B.D., B. Bonsand, and A. Gaudry, 1983: The role of the ocean in the atmospheric sulfur cycle. J. Am. Chem. Soc., 88:10903.

Pueschel, R., 1984: Gulf coast insignificant as source of acid rain. Dept. of Commerce News NIL 84-236.

Rasmussen, R.A., M.A.K. Khalil, and S.D. Hoyt, 1982: Oceanic source of carbonyl sulfide. Atmos. Environ., 16:1591-1594.

MEASUREMENTS OF ATMOSPHERIC CARBON DIOXIDE AND METHANE

Thomas J. Conway and L. Paul Steele

1. INTRODUCTION

The National Oceanic and Atmospheric Administration's Geophysical Monitoring for Climatic Change program (NOAA/GMCC) measures the concentration of atmospheric CO_2 and CH_4 through a cooperative global flask sampling network (Komhyr et al., 1985; Conway et al., 1988; Steele et al., 1987). The purpose of the measurements is to determine the rates of increase and global distribution of these species. Knowing the increase is important, because of the potential for these infrared-absorbing gases to alter climate. Knowing the global distribution will aid in determining the globally significant regional-scale sources and sinks of CO_2 and CH_4.

The network sites are generally located in remote marine locations to maximize the probability of measuring well-mixed, regionally representative air while minimizing the influence of local sources or sinks. For these purposes the Gulf of Mexico would be a less than ideal sampling site owing to the proximity of coastal and marine anthropogenic sources of CO_2 and CH_4 as well as presumably large and variable biospheric fluxes. However, in July and August 1986, 26 samples were collected on a joint U.S.A./U.S.M. cruise aboard the U.S.M. Research Vessel H-02 in the Gulf of Mexico. As expected, the CO_2 and CH_4 concentrations measured in these samples tend to be higher and more variable than at GMCC network sites at similar latitudes, although the lowest measured concentrations are similar to those at the network sites.

2. THE EXPERIMENT

The details of sample collection and analysis have been given elsewhere (Komhyr et al., 1983, 1985; Conway et al., 1988; Steele et al., 1987), so only a brief description is given here.

The samples are collected in cylindrical, 0.5-L glass flasks with greased (Apiezon-N), ground-glass stopcocks at each end. Two flasks are connected in series and flushed for 5 min, using a battery-powered, noncontaminating pump.

The flasks are pressurized to 1.2-1.5 atm and stored for later analysis in Boulder.

One flask from each sample pair is analyzed for CH_4, using a Hach Carle Series-400 gas chromatograph (G.C.) equipped with a flame ionization detector (FID). The 2-cc sample loop of the G.C. is flushed with cryogenically dried sample gas using the overpressure in the flask. Each sample injection is bracketed by injections of calibration gas, and the CH_4 concentration in the sample is determined by the ratio of sample peak height to calibration gas peak height (Steele et al., 1987). Concentrations are reported in parts per billion by volume in dry air (ppb). The measurement precision is estimated to be ±3 ppb.

Both flasks are then analyzed for CO_2 concentration, using a UNOR 4N non-dispersive infrared (NDIR) analyzer. The NDIR analyzer cell is flushed with cryogenically dried sample gas by means of a noncontaminating gas transfer apparatus. The CO_2 concentration is determined by linearly interpolating from the analyzer response to two bracketing calibration gases (Komhyr et al., 1983). The concentration values assigned to the calibration gases are directly traceable to the World Meteorological Organization (WMO) CO_2 standards maintained at Scripps Institution of Oceanography. The CO_2 concentrations (ppm) are reported in the WMO X85 mole fraction scale. The estimated measurement precision is ±0.2 ppm.

3. RESULTS

Thirteen pairs of flask samples were collected at the locations shown in Fig. 1. The sampling time and position, and the CO_2 and CH_4 concentrations are given in Table 1. The measured concentrations are plotted vs. time in Fig. 2 (CO_2) and Fig. 3 (CH_4). These figures include data from the GMCC sampling sites at Key Biscayne, Florida, and St. Croix, American Virgin Islands, for comparison with the shipboard data (GMCC, unpublished data).

Table 1. Flask samples of CO_2 and CH_4, collected during the cruise.

Sample number	Date	Time (GMT)	Lat. (Deg. min N)	Long. (Deg. min W)	Flask I.D.	CO_2 (ppm)	Δ	CH_4
1	21 Jul 86	2125	27 40	96 58	1-83	348.94		
					G2-83	348.70	0.24	1658
2	23 Jul 86	0330	23 59	97 27	753-83	348.30		
					G754-83	348.13	0.17	1733
3	25 Jul 86	1845	21 42	97 18	859-83	347.47		
					G860-83	349.09	1.62	1683
4	26 Jul 86	0930	20 02	96 26	709-85	351.25		
					G710-85	353.95	2.70	1689
5	30 Jul 86	0615	18 45	95 01	365-85	351.27		
					G366-85	350.35	0.92	1658
6	6 Aug 86	0615	23 29	89 51	699-83	345.35		
					G700-83	346.02	0.67	1658
7	6 Aug 86	1830	24 54	89 43	1307-82	348.85		
					G1308-82	348.74	0.11	1667
8	7 Aug 86	1330	27 40	89 33	385-85	346.22		
					G386-85	344.23	1.99	1654
9	7 Aug 86	1830	28 28	90 00	815-83	345.12		
					G816-83	345.02	0.10	1652
10	7 Aug 86	1840	28 28	90 00	627-83	348.82		
					G628-83	346.16	2.66	1669
11	8 Aug 86	1430	28 38	91 58	745-82	346.73		
					G746-82	346.96	0.23	1681
12	8 Aug 86	2000	28 52	92 45	341-85	345.97		
					G342-85	344.59	1.38	1666
13	8 Aug 86	2215	28 59	93 57	371-85	355.08		
					G372-85	354.26	0.82	---

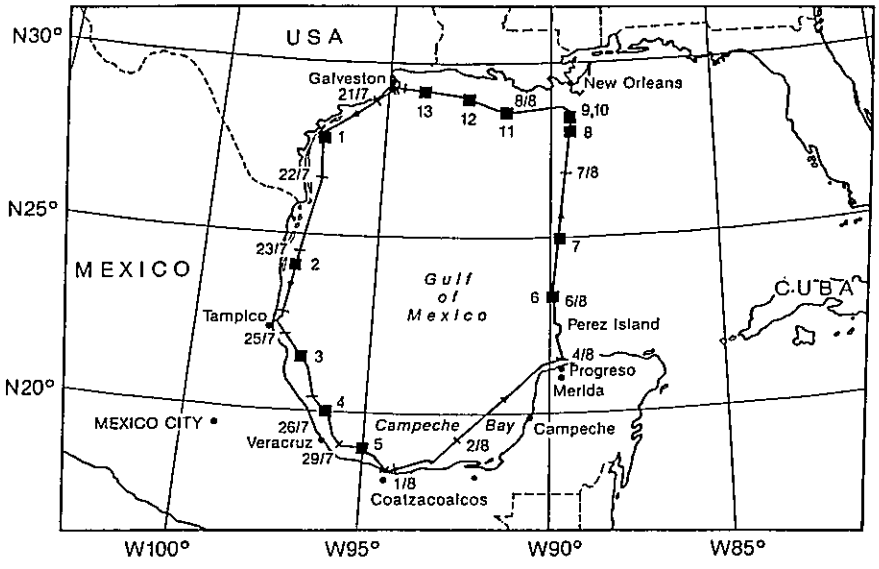

Figure 1. Locations where flask samples were collected during July-August 1986.

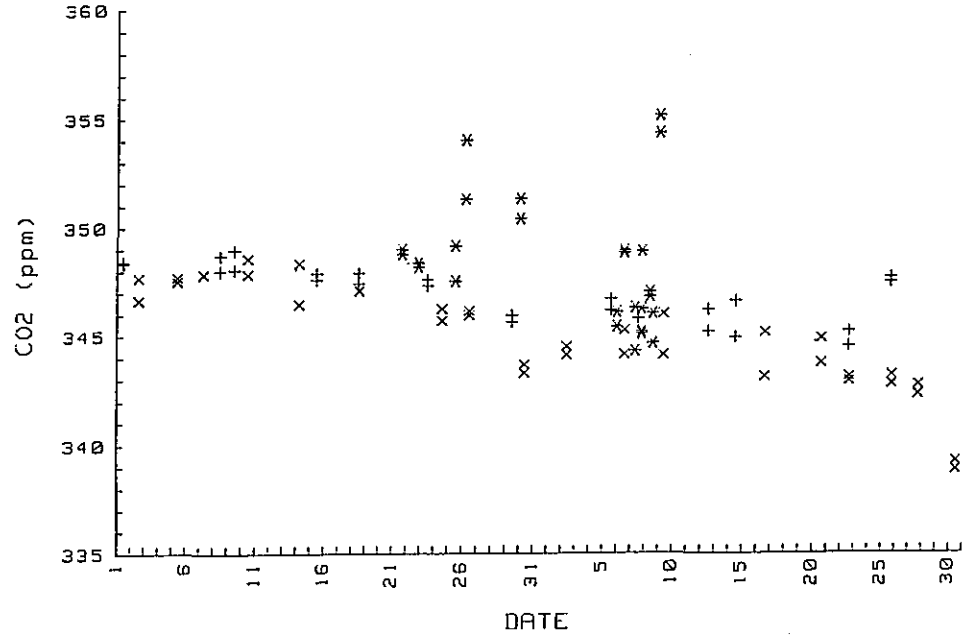

Figure 2. CO_2 concentrations measured in shipboard flask samples (*). Flask sample data from Key Biscayne, Florida (+), and St. Croix, American Virgin Islands (x), are shown for comparison.

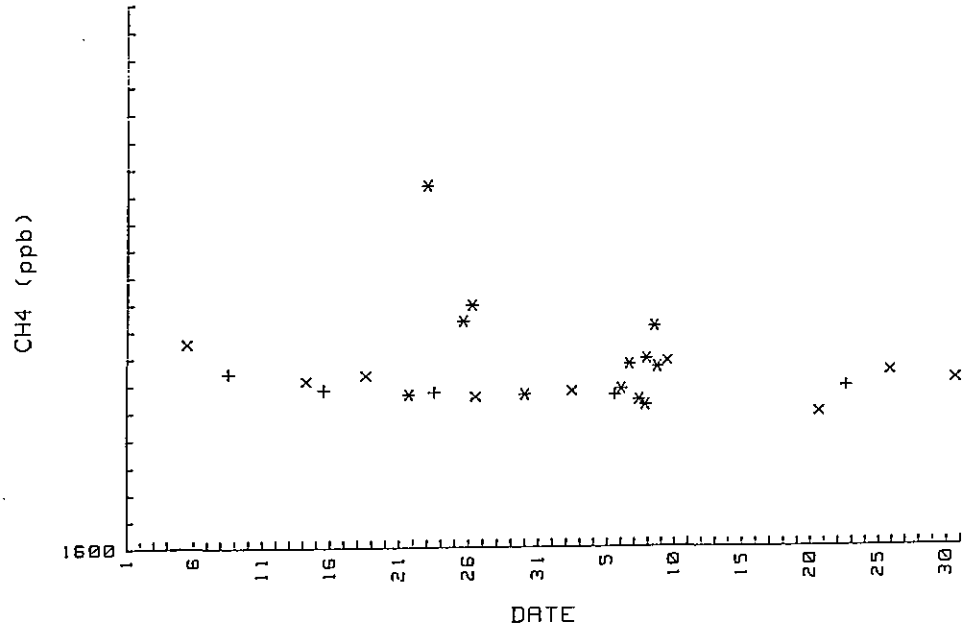

Figure 3. As in Fig. 2, but for CH_4.

4. DISCUSSION

Flask samples for CO_2 analysis are collected in pairs to aid in evaluating the sample collection and analysis techniques. In general, ~80% of sample pairs meet a pair difference criterion of $D \leq 0.5$ ppm (Conway et al., 1988). When this value is exceeded it is probable that an error occurred during sampling, a stopcock leaked subsequent to sampling, or the air mass being sampled was so inhomogeneous with respect to CO_2 that different concentrations were sampled even though the flasks were collected in series, simultaneously. At the GMCC flask network sites this last possibility is not very likely and sample pairs not meeting the 0.5-ppm criterion are rejected or flagged as being probably contaminated. In the present small data set, rather than reject bad pairs (8 of 13 pairs), we consider each flask sample individually, but note the possibility that some flasks may have been contaminated.

In Fig. 2 the cruise CO_2 data are compared with the July and August CO_2 data from Key Biscayne (KEY) (25°40' N, 80°12' W) and St. Croix, American Virgin Islands (AVI) (17°45' N, 64°45' W). The CO_2 concentrations at both KEY and AVI are decreasing during this period and the mean value at KEY is higher than at AVI. These features are due to the seasonality in CO_2 concentration resulting from biospheric uptake of CO_2 during summer, and the meridional gradient in CO_2 concentration resulting from fossil fuel CO_2 emissions in middle altitudes of the Northern Hemisphere (see, for example Pearman and Hyson, 1986).

The lowest CO_2 concentrations measured in the cruise samples tend to agree with the baseline measurements at KEY and AVI. The remainder of the cruise samples are higher and show more variability than the baseline data.

The results for CH_4 are similar to those for CO_2 (Fig. 3). The CH_4 concentrations are essentially at the seasonal minimum, so only a slight variation with time is observed at both KEY and AVI (Steele et al., 1987). Again the lowest cruise values fit in well with the baseline measurements; higher values are more variable.

The pattern observed in these data suggests that the air over the Gulf of Mexico consists of a zonally well-mixed air mass into which point or regional sources have injected air containing higher concentrations of CO_2 and CH_4.

Combustion sources of CO_2 and CH_4 include power plants, industrial activity, automobiles, ships, drilling platforms, and gas flaring. Natural gas drilling is also a source of CH_4 to the atmosphere. Possible biospheric sources are heterotrophic respiration for CO_2 and methanogenesis in anoxic sediments. All these sources are prevalent in and around the Gulf of Mexico. The variability observed in the CO_2 and CH_4 data is the result of proximity to the sources and limited mixing of plumes with background air. Because of the limited number of samples and the possibility that some samples are contaminated, we are not able to draw conclusions concerning individual samples or specific sources. However, it may be possible to extend this analysis by combining these data with measurements of other species (e.g., condensation nuclei and SO_2) made simultaneously during the cruise.

REFERENCES

Conway, T.J., P. Tans, L.S. Waterman, K.W. Thoning, K.A. Masarie, and R.H. Gammon, 1988: Atmospheric carbon dioxide measurements in the remote global troposphere, 1981-1984. Tellus (in press).

Komhyr, W.D., L.S. Waterman, and W.R. Taylor, 1983: Semiautomatic nondispersive infrared analyzer apparatus for CO_2 air sample analysis. J. Geophys. Res., 88:1315-1322.

Komhyr, W.D., R.H. Gammon, T.B. Harris, L.S. Waterman, T.J. Conway, W.R. Taylor, and K.W. Thoning, 1985: Global atmospheric CO_2 distribution and variations from 1968-1982 NOAA/GMCC CO_2 flask sample data. J. Geophys. Res., 90:5567-5596.

Pearman, G.I., and P. Hyson, 1986: Global transport and inter-reservoir exchange of carbon dioxide with particular reference to stable isotopic distributions. J. Atmos. Chem., 4:81-124.

Steele, L.P., P.J. Fraser, R.A. Rasmussen, M.A.K. Khalil, T.J. Conway, A.J. Crawford, R.H. Gammon, K.A. Masarie, and K.W. Thoning, 1987: The global distribution of methane in the troposphere. J. Atmos. Chem., 5:125-171.

PART II. AEROSOL MEASUREMENTS

ION CONCENTRATIONS OF ATMOSPHERIC AEROSOLS

Robin E. Madel and Farn P. Parungo

1. INTRODUCTION

To study temporal and spatial variations of aerosol characteristics in the Gulf of Mexico we first need to know the aerosol mass concentrations, specifically the ion concentrations. This report concerns the chemical analysis of aerosol bulk samples with an ion chromatograph.

2. SAMPLING AND ANALYSIS

The samples were collected on Zefluor (Teflon) filters (90-mm diameter, 1-μm pore size) with a regulated flow rate (~175 L min^{-1}). The samples were collected on the forward upper deck of the ship. The sampling time was 6 or 7 hours except when rain or other incidents cut it short. The volumes of air samples were calculated (Table 1). The filters were stored in sealed polyetheylene bags and were analyzed after the cruise in our laboratory. The sample filters were extracted with a calculated amount of deionized and degased water (1 mL of water per 1 m^3 air) by performing two 10-minute washings under ultrasonic action. The extract solutions were standardized per unit of air volume for comparison (Lazrus et al., 1983; Parungo et al., 1986). The solutions were analyzed with an anion column for Cl^-, NO_3^-, and $SO_4^=$ (other anions were too dilute to be detected), with a monovalent cation column for Na^+, NH_4^+ and K^+, and with a bivalent cation column for Mg^{++} and Ca^{++} (Table 2). The concentrations of these ions in water soluble aerosols are in ppm (μg per g of water) which should be equivalent to μg of ions in aerosol form, per m^3 of air.

3. RESULTS AND DISCUSSION

A most commonly used tracer of marine-origin aerosols is Na^+, which has a definite ratio with other ions in seawater. The variation of Na^+ concentrations in aerosol samples is shown in Fig. 1. The lowest Na^+ concentrations (<1 μg m^{-3}) were found SW of Galveston and SW of Merida where

Table 1. Hi-volume aerosol sample data

Sample	Date	Local time	Flow rate (L min^{-1})	Minutes	Volume (m^3)	pH*
HV1	7/21/86	0900-1505	165	365	60	4.7
HV2	7/21/86	2100-0300	185	360	67	4.8
HV3	7/22/86	0900-1455	170	355	60	5.6
HV4	7/22/86	2125-0315	167	350	59	5.5
HV5	7/25/86	0900-1500	167	360	60	6.3
HV6	7/25/86	2055-0300	172	365	63	6.4
HV7	7/29/86	2100-0300	175	350	63	5.6
HV8	8/01/86	0900-1500	172	360	62	6.4
HV9	8/01/86	2110-0410	177	420	74	5.7
HV10	8/02/86	0900-1500	177	360	64	5.5
HV11	8/02/86	2105-0405	175	420	74	6.2
HV12	8/03/86	No sample taken--		---	--	---
HV13	8/05/86	2100-0300	172	360	62	6.0
HV14	8/06/86	0900-1500	177	360	64	5.7
HV15	8/06/86	2100-0300	175	360	63	5.9
HV16	8/07/86	0900-1500	172	300	54	5.3
HV17	8/07/86	2100-2400	177	180	32	5.3
HV18	8/08/86	0900-1500	172	300	54	5.6
HV19	8/08/86	2100-2400	172	180	31	5.0

* Extract standardized to 1 m^3 air per 1 mL H_2O.

Table 2. Ion concentrations in aerosol samples ($\mu g\ m^{-3}$)

Sample	Na	NH_4	K	Mg	Ca	Cl	NO_3	SO_4
HV1	0.90	0.28	0.16	0.09	0.00	1.39	1.08	1.55
HV2	1.45	0.21	0.13	0.16	0.01	2.35	0.66	1.44
HV3	0.67	0.42	0.04	0.02	0.10	1.06	0.43	1.35
HV4	1.00	0.34	0.06	0.13	0.13	1.59	0.28	1.37
HV5	1.46	0.36	0.15	0.20	0.65	2.36	0.48	1.79
HV6	3.04	0.30	0.14	0.46	1.36	6.33	1.90	2.61
HV7	1.41	0.18	0.11	0.22	0.25	2.76	0.61	1.06
HV8	1.52	0.42	0.11	0.20	0.51	2.50	0.52	1.29
HV9	1.40	0.31	0.13	0.24	0.25	2.70	0.41	1.52
HV10	0.54	0.44	0.01	0.05	0.13	0.77	0.00	1.42
HV11	0.77	1.06	0.03	0.10	0.58	0.76	13.52	2.56
HV12	----	----	----	----	----	----	----	----
HV13	2.37	0.39	0.11	0.29	0.20	5.12	0.89	1.53
HV14	1.31	0.25	0.03	0.14	0.11	2.86	0.63	0.89
HV15	2.90	0.23	0.10	0.30	0.30	5.57	0.92	1.40
HV16	2.26	0.22	0.09	0.25	0.19	4.44	0.71	1.37
HV17	11.85	0.56	0.51	1.24	0.93	14.51	2.93	4.80
HV18	2.67	0.29	0.18	0.27	0.26	3.76	0.76	1.63
HV19	7.60	0.85	0.39	0.84	1.21	11.17	1.93	5.89

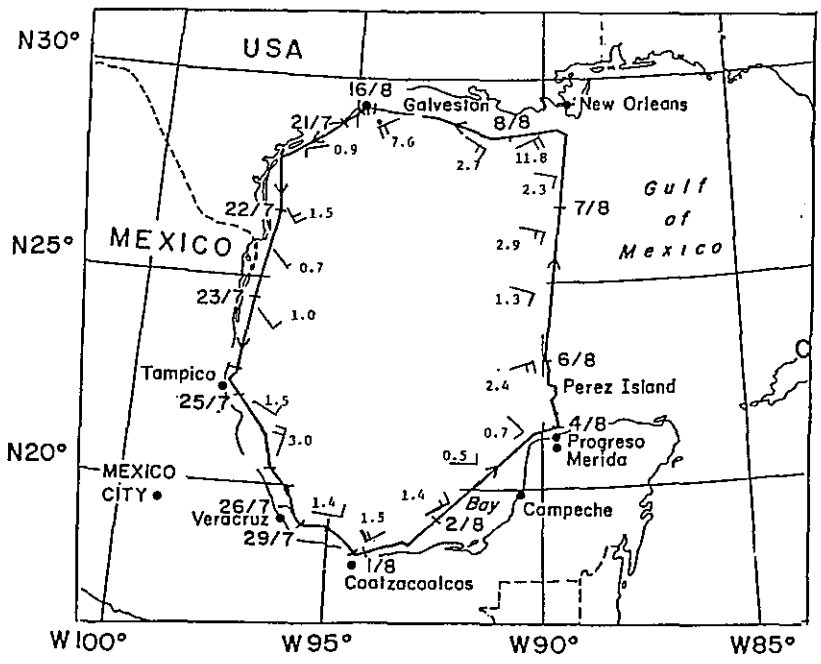

Figure 1. Na^+ ion concentrations ($\mu g\ m^{-3}$) in aerosol samples and surface winds.

surface winds were from land, and wind speeds were <10 kn during the sampling periods. As reported by Woodcock (1953) and Blanchard and Woodcock (1980) that seasalt concentration is a function of surface wind speed, we observed that Na^+ concentrations, which are ~1/3 of seasalt concentration, fluctuated with surface wind speed. The degree of fluctuation (Fig. 2) is also in general agreement with previous reports.

The ratios of Cl^-/Na^+ in seawater samples collected in various locations of the Gulf were measured to have an average $X = 1.94$ ($\sigma = 0.15$; $n = 11$). The ratio over the open sea is known to be 1.80. However, the ratios of Cl^-/Na^+ in aerosol samples collected over the Gulf varied widely with location (Fig. 3). Along the coast of the U.S.A., the ratios (1.22 to 1.60) were distinguishably lower than seawater's value. This is probably due to urban air pollution gases, e.g., SO_2 and NO_x, replacing Cl^- in seasalt and releasing HCl gas in the air. Very low ratios (0.99 and 1.42) were also found SW of Merida City where oil refineries may also affect the aerosol chemistry. The aerosol samples collected across the middle of the Gulf showed that the ratio of Cl^-/Na^+ was as high as that of seawater. This indicates that aerosols in the area are less affected by anthropogenic pollution.

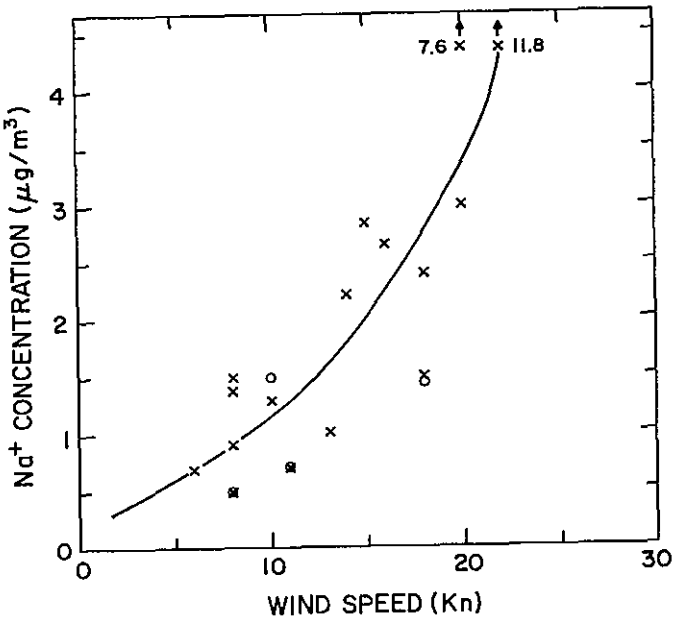

Figure 2. Variation of Na^+ ion concentrations with wind speed.

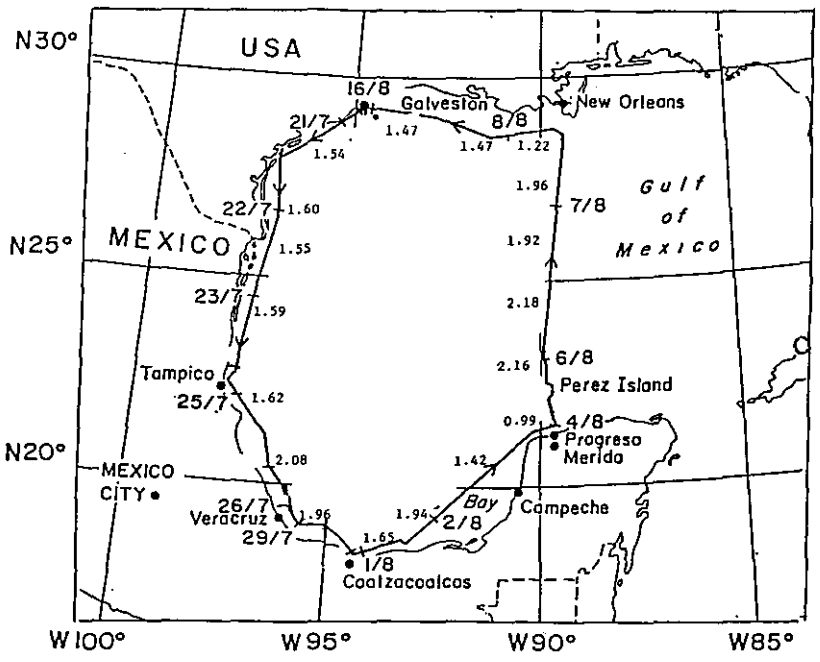

Figure 3. Ion concentration ratios, Cl^-/Na^+, in aerosols.

Sulfate aerosols can be classified into two groups on the basis of the sources: (a) the seasalt particles whose concentration can be calculated as $0.25 \times [Na^+]$ because in seawater, the concentration ratio between $SO_4^=$ and N_a^+ is 0.25; (b) the non-seasalt particles whose concentration can be calculated as total sulfate concentration minus seasalt sulfate concentration. Figure 4 shows the spatial variation of seasalt sulfate concentration, which, like Na^+, fluctuated with wind speed and direction. Figure 5 shows the spatial variations of non-seasalt sulfate concentrations, which reflect the effects of anthropogenic air pollution. Near big cities--Galveston, New Orleans, Veracruz, and Merida--the non-seasalt sulfate concentrations were high, with a maximum 3.99 $\mu g\ m^{-3}$. In the middle of the Gulf the concentrations were low, with a minumum of 0.56 $\mu g\ m^{-3}$.

Figure 6 shows the spatial variations of aerosol nitrate concentrations. As non-seasalt sulfate, the high nitrate concentrations were found near the cities, with maxima of 3.52 and 2.93 $\mu g\ m^{-3}$ SW of Merida and New Orleans respectively. Urban pollution and nearby oil refinery plumes may have contributed to the high content of nitrate in aerosols.

The aerosol sample extractions were also used to determine the acidity of the aerosols. The pH of a solution that was extracted from a filter with 1 mL of water for every m^3 of air samples simulates the pH of cloud water formed by rising air parcels containing these aerosols to yield liquid water content (LWC) of 1 $g\ m^{-3}$, provided that all the particles are scrubbed into cloud drops. The pH of aerosol samples (Fig. 7) ranged from 4.7 to 6.4 with a mean = 5.6 (σ = 0.5). If the simulated cloud has a higher or lower LWC, the pH of the cloud may also be slightly lower or higher.

The seawater samples from the Gulf had a pH of 7.8 to 8.1. The mass ratio H^+/Na^+ in seawater is $\sim 10^{-9}$. The mean ratio of H^+/Na^+ in the aerosol samples was 5.4×10^{-3} ($\sigma = 9.3 \times 10^{-3}$). The fact that the enrichment factor of H^+ in aerosols (compared with seawater) is 5.4×10^6 suggests that many acidic particles had been formed or transported into the Gulf region and mixed with seasalt particles.

The most acidic aerosols were found near Galveston (pH = 4.7, 4.8, 5.0) and south of New Orleans (pH = 5.3). This suggests that the alkaline seasalt

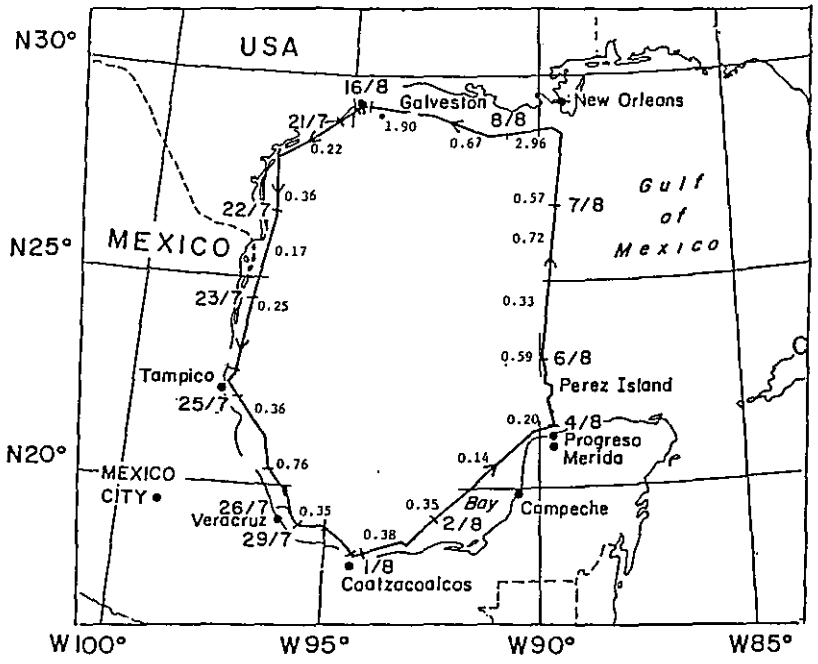

Figure 4. Seasalt sulfate concentrations ($\mu g\ m^{-3}$).

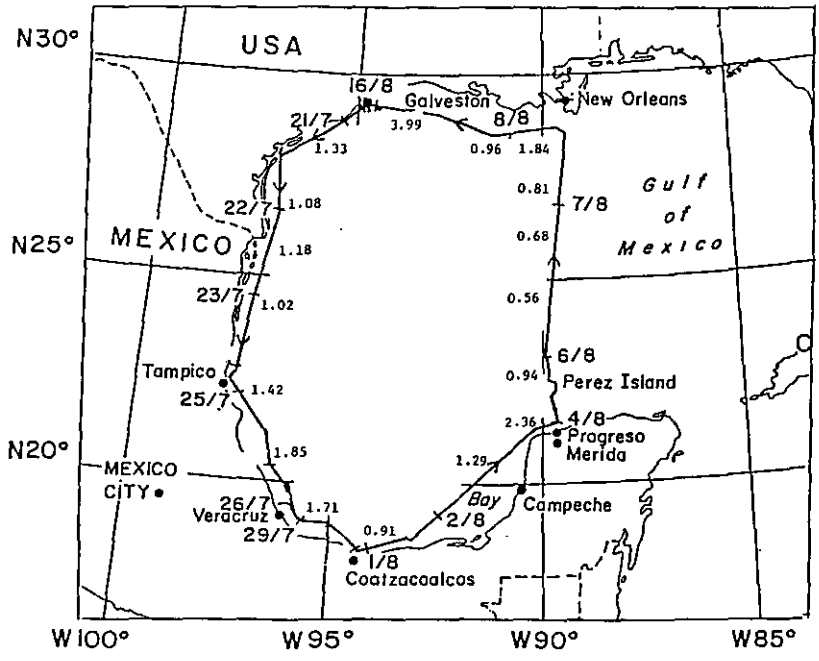

Figure 5. Non-seasalt sulfate concentrations ($\mu g\ m^{-3}$).

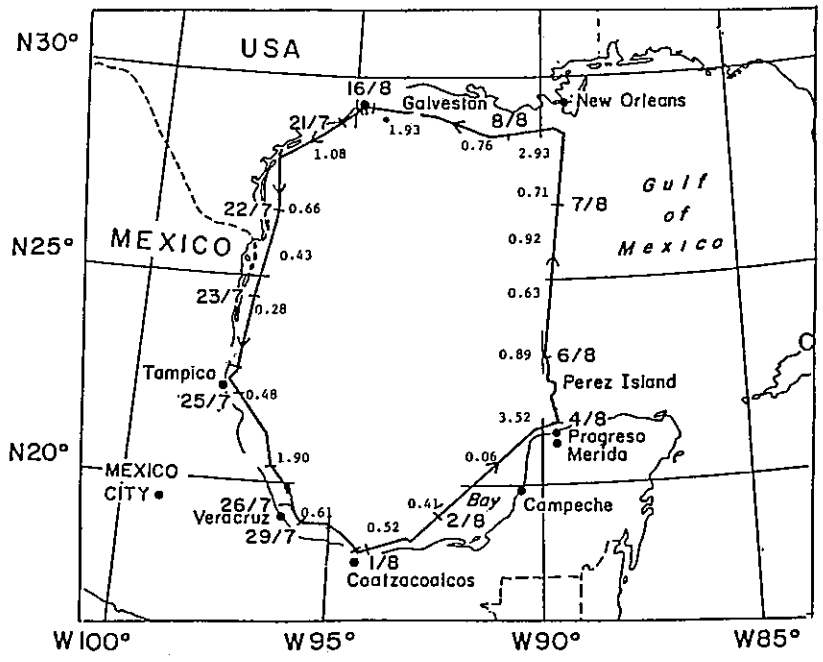

Figure 6. Aerosol nitrate concentrations ($\mu g\ m^{-3}$).

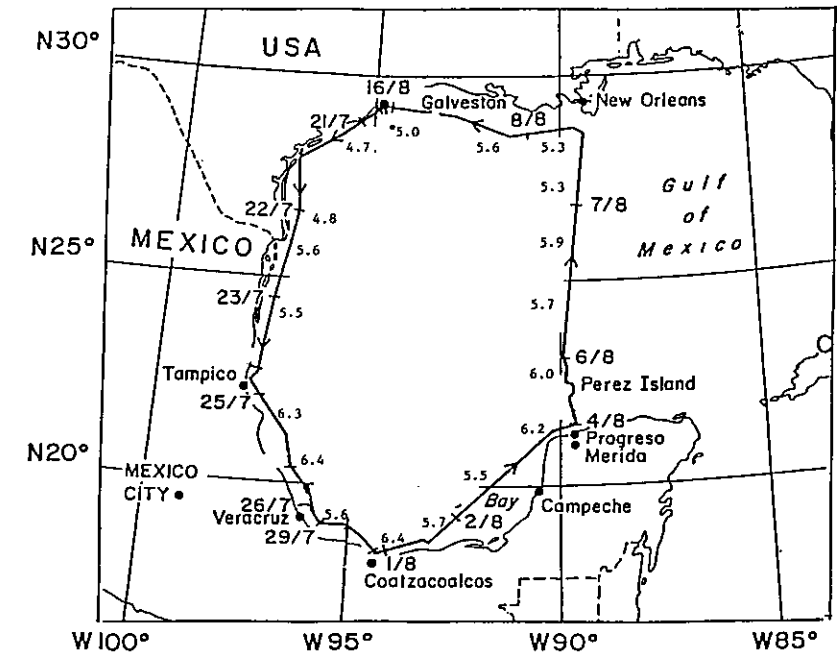

Figure 7. pH of the aerosol samples, of 1 m^3 or air per mL water.

particles could have been neutralized or even acidified by anthropogenic pollution. These acidic particles in addition to seasalt particles, could serve as cloud condensation nuclei to form clouds. Therefore, in the polluted marine environment the acid rain formation may be initiated by condensation nucleation at cloud base.

REFERENCES

Blanchard, D.C., and A.H. Woodcock, 1980: The production, concentration and vertical distribution of seasalt aerosol. Ann. N.Y. Acad. Sci., 338:330-347.

Lazrus, A.L., P.L. Haagenson, G.L. Kok, B.J. Huebert, and J.W. Winchester, 1983: Acidity in air and water in a case of warm frontal precipitation. Atmos. Environ., 17:581-591.

Parungo, F.P., C.T. Nagamoto, J. Rosinski, and P.L. Haagenson, 1986: A study of marine aerosols over the Pacific Ocean. J. Atmos. Chem., 4:199-226.

Woodcock, A.H., 1953: Salt nuclei in marine air as a function of altitude and wind force. J. Meteorol., 10:362-371.

NUMBER CONCENTRATIONS OF ATMOSPHERIC AEROSOLS

Clarence T. Nagamoto and Farn P. Parungo

1. INTRODUCTION

Knowledge of aerosol number concentration and size distribution is as important as knowledge of mass concentration because it reveals the mechanisms of aerosol formation, the information of aerosol sources, the ability of aerosol transport, the duration of aerosols in the air, the velocity of dry deposition, and the effect of aerosols on cloud microphysics and wet deposition.

2. SAMPLING AND ANALYTICAL PROCEDURES

The concentrations and size distributions of the aerosol particles were obtained using two different methods. (1) A condensation nucleus (CN) counter was set up on the highest deck of the ship, and a continuous concentration of particles ($d > 0.003$ μm) was obtained. The instrument used was a modified G.E. CN counter, which basically detects condensation particles at very high supersaturations by a light-scattering system. The sampling rate of the air was 6 Lpm. [Detailed procedures have been reported by Bodhaine and Murphy (1980) and Parungo et al. (1987)]. (2) Aerosol particles were also collected on 47-mm-diameter, 0.2-μm-pore Nuclepore filters on the upper deck, two decks above the main deck, forward on the ship. The sampling flow was 10 Lpm for 2 hours, which gave a volume of 1.2 m^3 of air passing the filter. A small portion of the filter was examined under the scanning electron microscope (SEM), and the concentrations and size distributions of particles larger than 0.05 μm were determined.

3. RESULTS

Concentrations of aerosol particles measured by the CN counter in-situ during the cruise are shown in Fig. 1. Along the rural coast, the concentrations averaged ~10^3 cm^{-3}; near or at the port cities the concentrations were high and variable, ranging from 2×10^3 to 2×10^5 cm^{-3}; in the middle of the Gulf the concentration decreased to ~2×10^2 cm^{-3}.

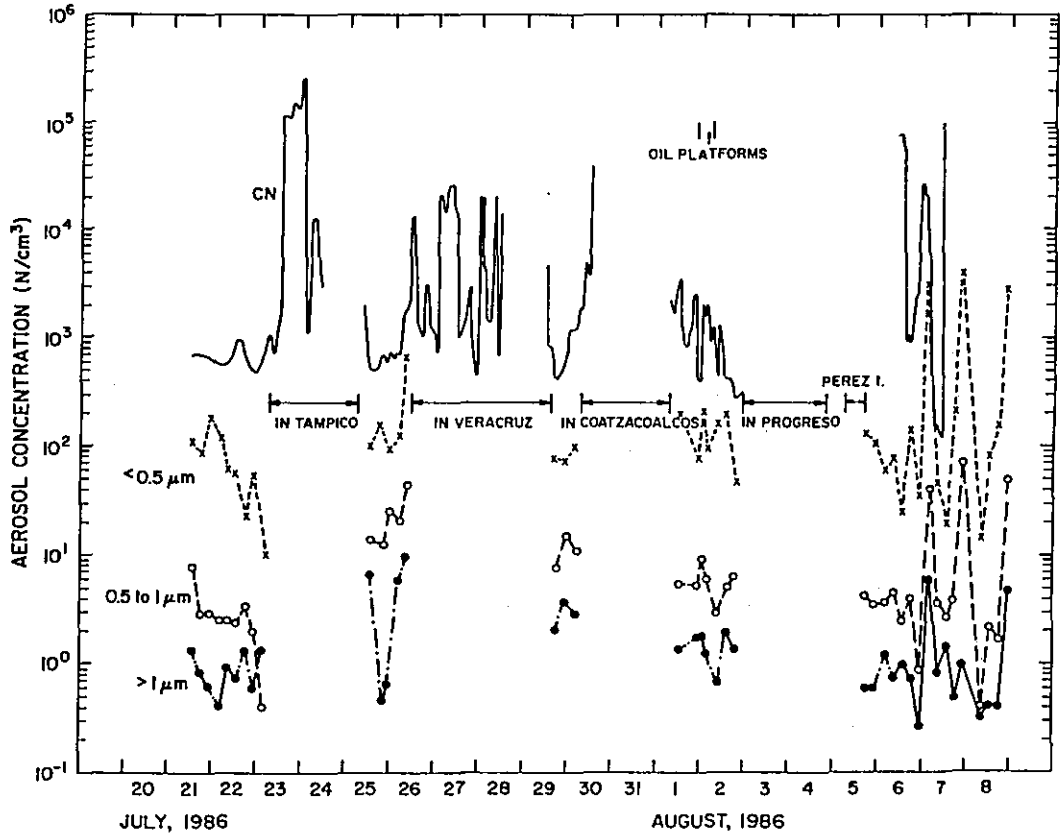

Figure 1. Temporal and spatial variations of aerosol number concentrations.

Aerosol samples on Nuclepore filters were analyzed with an SEM; examples of electronmicrographs are shown in Fig. 2. Particles were segregated into three size ranges: d > 1 μm, d = 0.5 to 1 μm, and d = <0.5 μm, particle concentrations in each range are also shown in Fig. 1. Unlike the condensation nuclei, which showed a great variability, the larger particles showed less spatial or temporal variations of concentration. No samples were taken when the ship was in port because the shifting winds might blow the ship's exhaust and contaminate samples. In fact, even when the ship cruised slowly along the the Louisiana coast on 7-8 August, strong tailwinds occasionally blew the ship exhaust plume to the sampling site. The high variation of particle concentrations on those days might be the result of contamination.

Figure 3 shows the size distributions of samples taken on 22, 25, 26 July and 6-7 August. The highest concentrations of particles occurred near the port cities, e.g., near Veracruz (26 July) and south of New Orleans (7 August). On 22 July when the ship cruised along the west coast of the Gulf

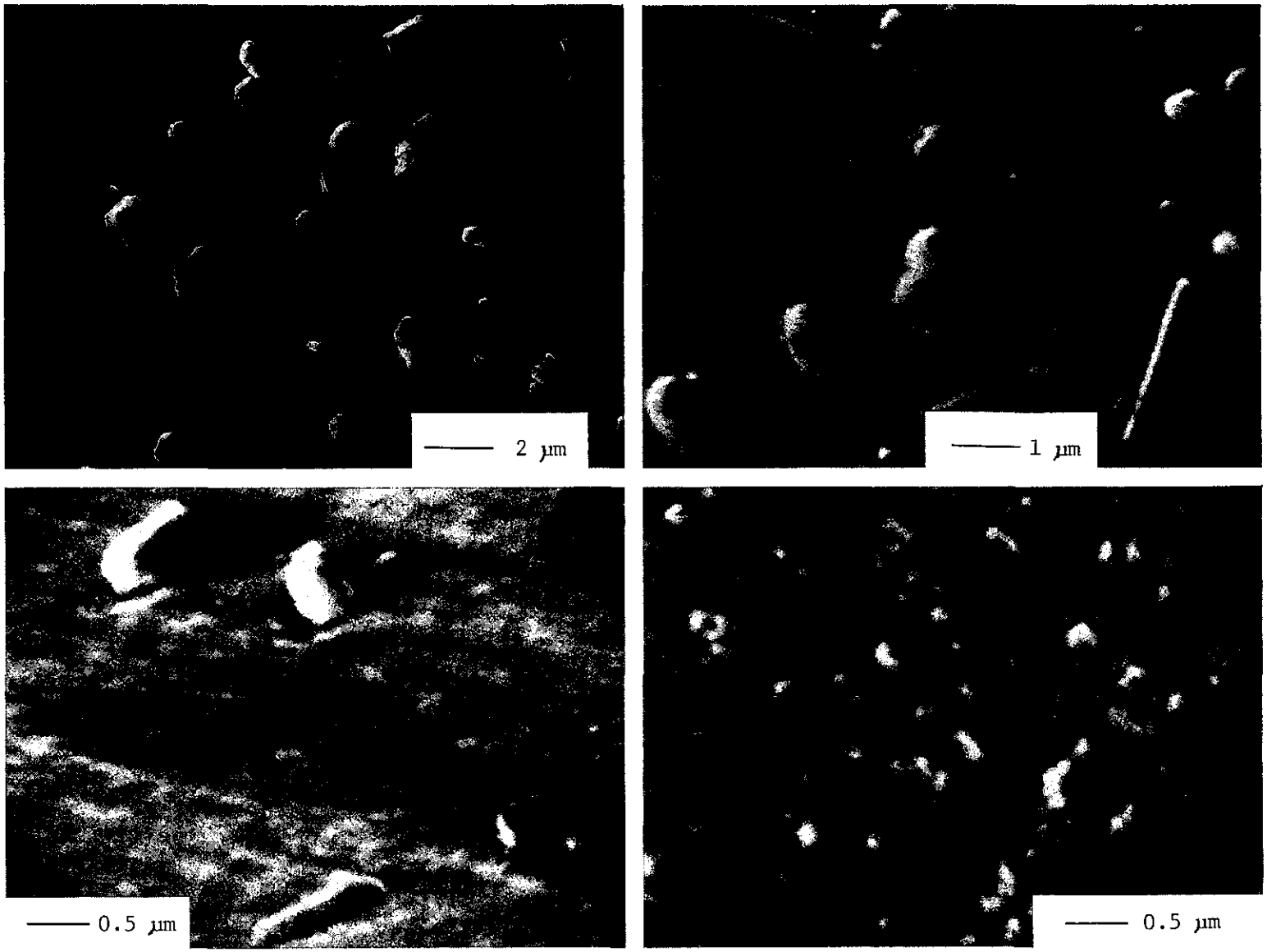

Figure 2. Scanning electron micrographs of aerosol particles on nuclepore filter.

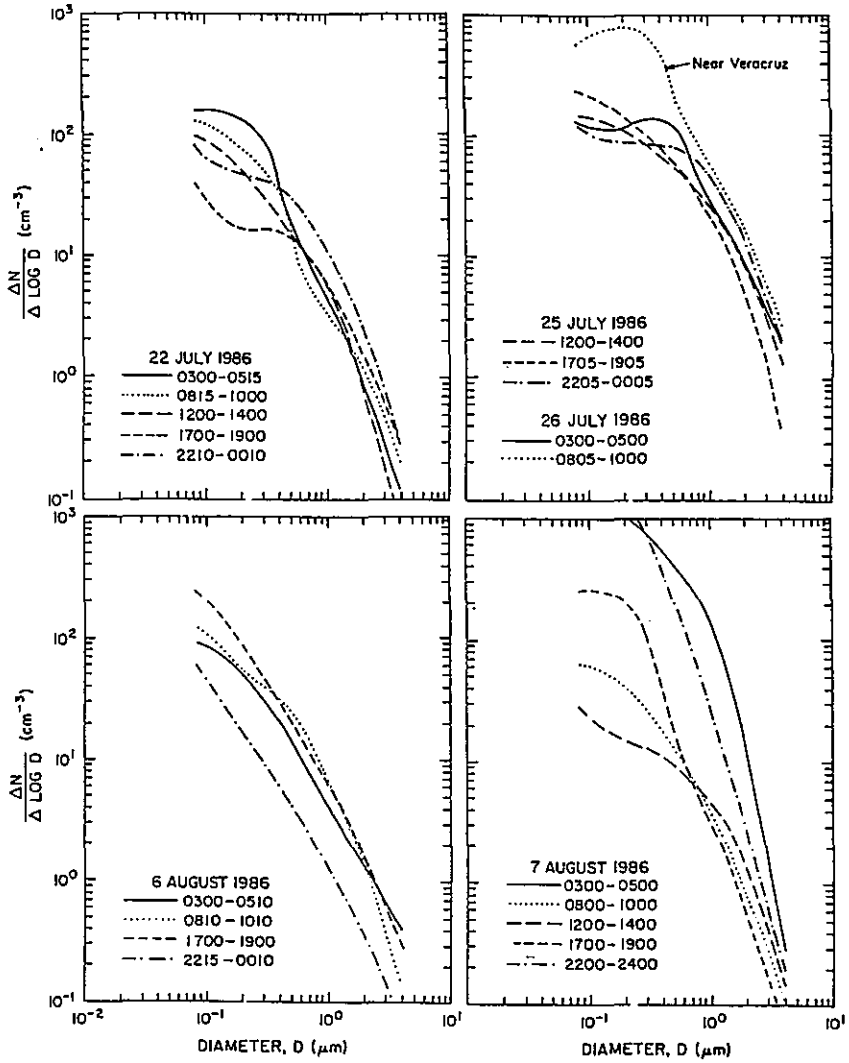

Figure 3. Aerosol particle size distributions at various dates and times.

the highest concentrations of small particles ($d < 1$ μm) were observed from midnight to dawn. This is probably because of land breezes that carried air pollution into the Gulf. In the daytime, especially in late afternoon (1700-1900), the sea breeze brought a cleaner air mass to the sampling site, and thus lower particle concentrations were observed. On 6 August when the ship sailed in the open Gulf where the air probably was not affected by land breeze and sea breeze oscillation, aerosol samples collected before dawn showed lower concentrations than daytime samples. This was probably because photo-oxidation in the daytime enhanced gas-to-particle conversion. Such diurnal variation had frequently been observed in the Pacific Ocean (Parungo et al., 1986).

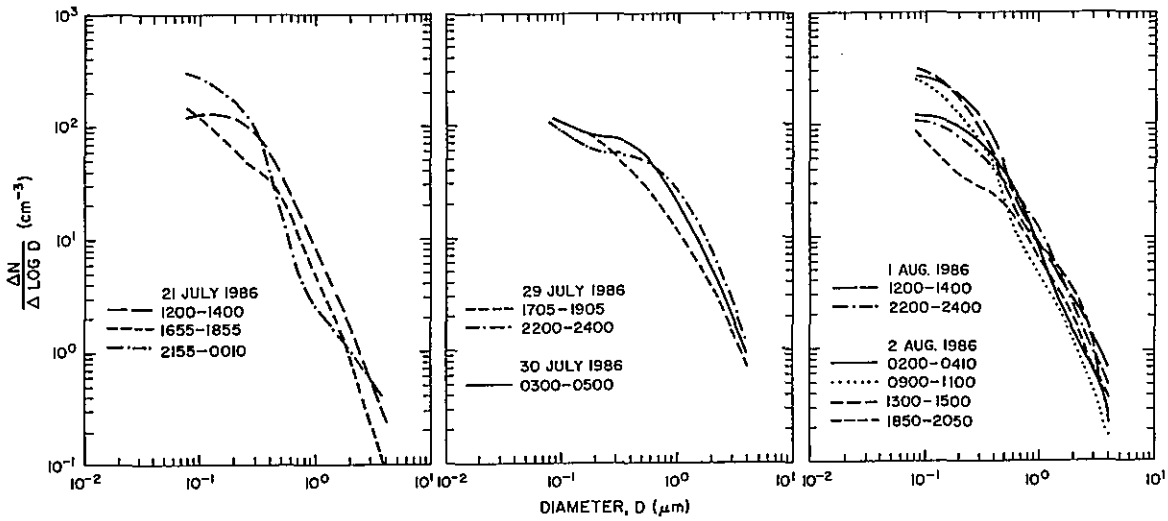

Figure 4. Aerosol particle size distributions on three different days.

On some days the diurnal variations of particle concentrations were not evident (Fig. 4). The air mass was probably influenced by several complex and opposite factors.

The elemental compositions of individual particles collected on Nuclepore filters were analyzed with an x-ray energy spectrometer (XES), interfaced with a scanning electron microscope (SEM). Figure 5 shows examples of particle x-ray spectra. The peaks indicate all the constituent elements (except light elements with atomic number less than 10). The peak heights reflect the relative concentrations of each element in that particle. The analytical results of samples collected on four different days are shown in Fig. 6. Particles were divided into two groups according to size. For group A diameter $d \geq 1$ μm; for group B, $d < 1$ μm. Approximately 150 particles were randomly selected in each group. Among the larger particles, >85% contained Si, >60% contained Fe, and >50% contained Al. These particles generally represented continental origin. The maritime-origin elements such as Na and Cl were found in <50% of the particles and often coexisted with Si, Al, Fe, Mg, P, K, Ca, or S. The crustal elements (e.g., Si, Al, Fe) were less frequently present in smaller particles. Nonetheless, they are still the major components. Since these elements are usually in compounds that are insoluable or slightly soluble in water, their concentrations in aerosols cannot be measured with an ion chroma-

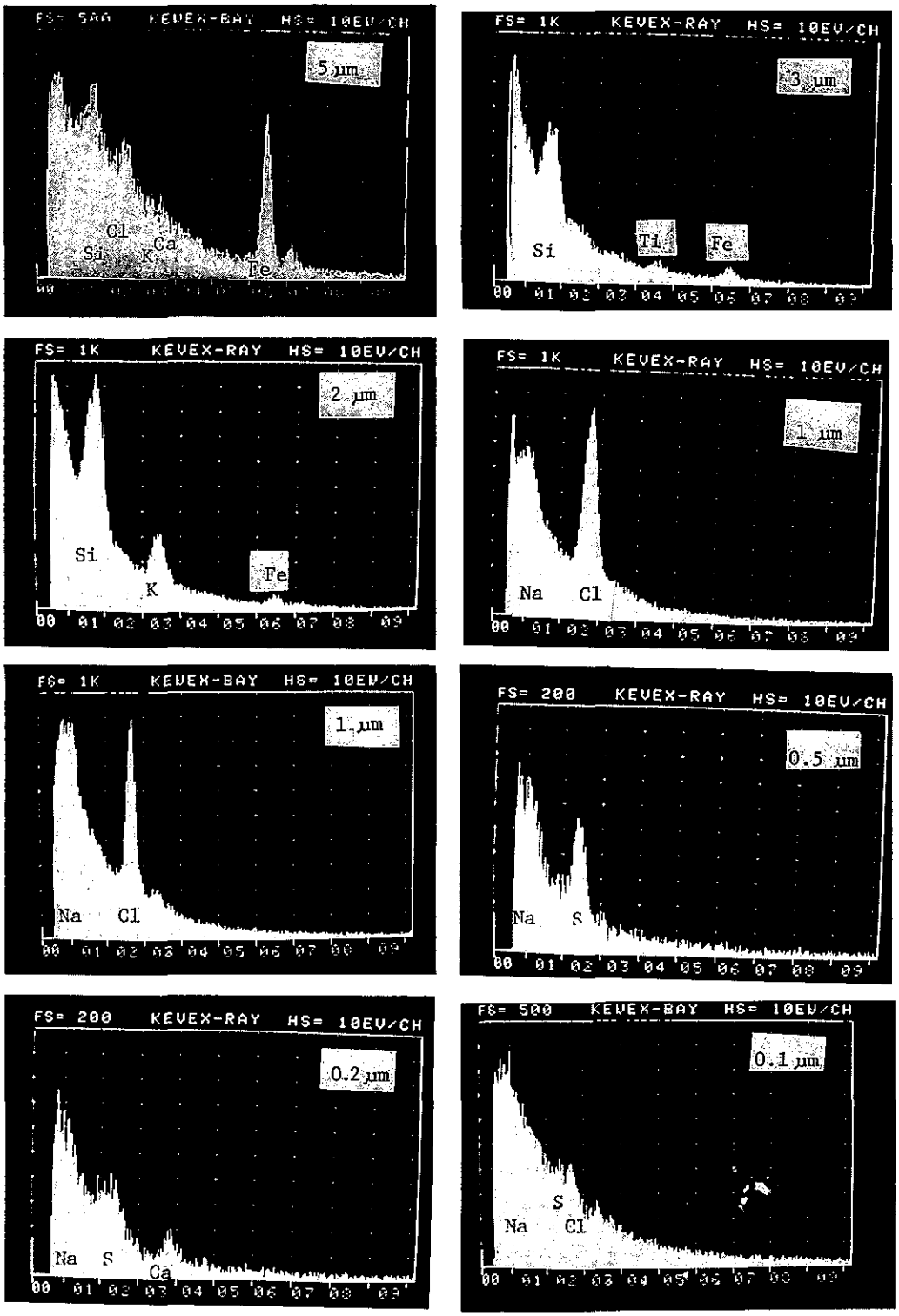

Figure 5. Examples of x-ray energy spectra (XES) of individual aerosol particles of various sizes.

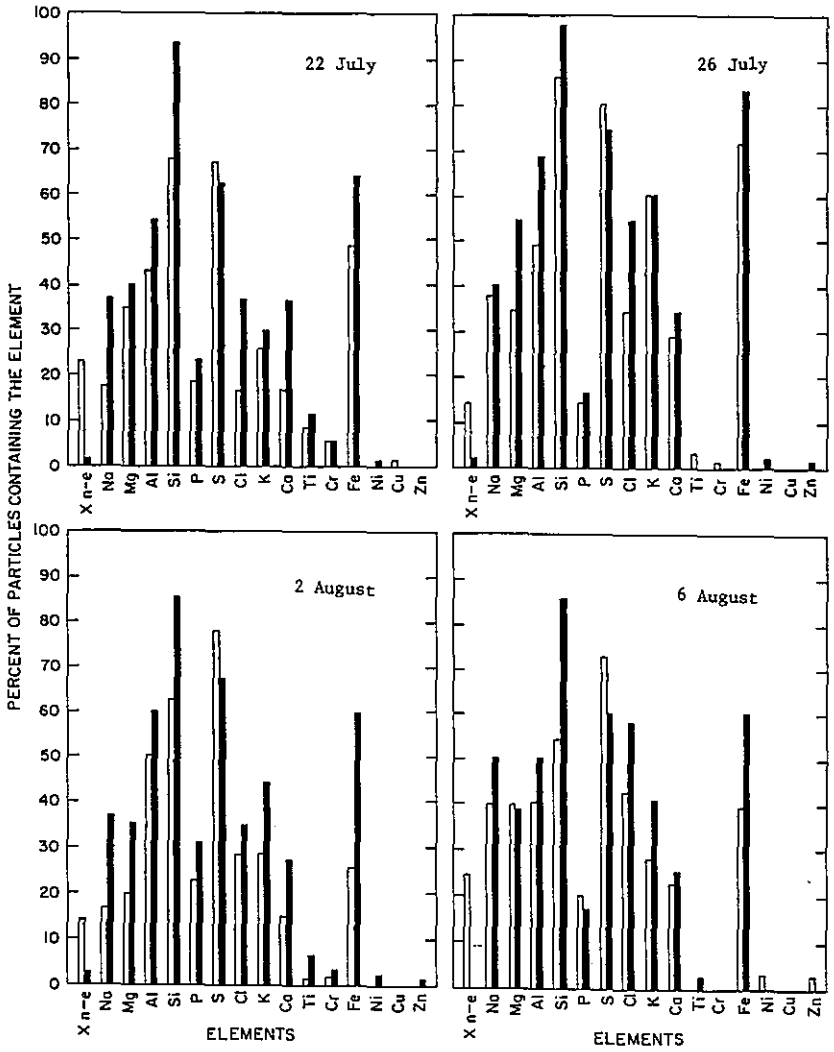

Figure 6. Frequencies of elements appearing in 150 individual particles of the samples collected on various days. Open bar: d < 1 μm; solid bar: d ⩾ 1 μm.

tograph and thus their existence in aerosols may easily be ignored by researchers. Now with the SEM-XES system, we found that they are the predominant components in the aerosols over the Gulf. It may appear incredible that seasalt aerosols are second in abundance over seawater. However, if we compare the size distributions of aerosol samples taken over the Gulf and over the Pacific Ocean, we notice that the average particle concentration in all sizes over the Gulf is at least twice as much as over the Pacific. The excess particles over the Gulf must come from the surrounding land, either as soil particles consisting of Si, Al, Fe, etc., or as anthropogenic fly ash, which is mainly aluminum silicates. Therefore it is reasonable that the majority of the particles consisted of crustal elements.

Approximately 60-70% of the particles contained S. More small particles than large ones consisted of S. Since S-compounds are present in seawater, soil , and air pollution, it is difficult to trace their origins. Generally the very fine S-particles ($d < 0.2\ \mu m$) are believed to be the product of gas-to-particle conversion. However, in SEM-XES analysis the fine particles, e.g., $(NH_4)_2SO_4$ and NH_4HSO_4, may evaporate in the high vacuum and under the intense beam. Thus, many small sulfate particles failed to be detected. A supplemental method (spot test) is used to remedy this deficiency (see the next chapter, by Quintana and Parungo).

In the small particles, 10-20% did not emit any detectable x-ray. These particles are probably organic consisting of H, C, N, and/or O and could be either anthropogenic or natural.

REFERENCES

Bodhaine, B.A., and M.E. Murphy, 1980: Calibration of a condensation nucleus counter at South Pole. J. Aerosol. Sci., 11:305.

Parungo, F.P., C.T. Nagamoto, R. Madel, J. Rosinski, and P.L. Haagenson, 1987: Marine aerosols in Pacific upwelling regions. J. Aerosol Sci., 18, 277-290.

Parungo, F.P., C.T. Nagamoto, J. Rosinski, and P.L. Haagenson, 1986: A study of marine aerosols over the Pacific Ocean. J. Atmos. Chem., 4:199-226.

SULFATE, NITRATE, AND BIOLOGICAL PARTICLES IN AEROSOLS

Barbara A. Quintana, Farn P. Parungo, and Humberto Bravo, A.

1. PROCEDURE

Aerosol samples were collected on electron microscope specimen grids mounted on a Casella Cascade Impactor and analyzed with a transmission electron microscope (TEM) in order to determine sulfate, nitrate, and biomass particle concentrations.

To collect the samples, we mounted the Impactor at the bow of the ship and attached a pump to the end of the Impactor in order to draw air through the Impactor. The rate of air intake was maintained at 17.5 L/min as constant as possible for comparisons to be valid.

The Cascade Impactor has four stages. Each stage contains progressively smaller slits through which air is drawn, producing a system of four air-jets. These air-jets impinge in series on 1-inch-diameter glass discs. Each stage produces a jet that is progressively finer than the previous stage. The progressively finer jets result in an increase in speed and efficiency of impaction of the particles on the discs.

The system of four air-jets produces a size-grading of particles that impinge on the discs. Stage 1 particles are ≥ 5 μm; stage 2 particles range from ≥ 2 μm to <5 μm; stage 3 particles range from ≥ 0.7 μm to <2 μm; stage 4 particles range from ≥ 0.2 μm to <0.7 μm.

Three electron-microscopic-sampling grids were mounted on each glass disc under the jets. First, all Formvar film on the screens was coated with carbon. In addition one screen was coated with barium chloride, and one was coated with Nitron. The screen with only Formvar and carbon coating was denoted the "control" sample, and the particles showed no reactions.

The screen coated with barium chloride is used to determine which particles contain sulfate. The procedure used is a modified spot test (Bigg et al., 1974). If a particle containing sulfate is brought into contact with the barium chloride, and if the relative humidity is adequate, as in a marine

environment, a reaction occurs. The reaction produces a distinctive halo (Fig. 1). When observed through the TEM the layer of humidified barium chloride appears as a series of fine crystals. The thinner the layer, the finer the crystals. The size of these grains depends on the relative humidity and the thickness of the film. It is important to maintain a small enough grain size so that the atmospheric particles can be distinguished easily.

The Nitron-coated screen is used to detect particles that contain nitrate. The method used is also a spot test modified by Mamane and Pueschel (1980). A reaction occurs when a particle containing nitrate comes into contact with the Nitron, if the relative humidity is adequate. The reaction spot that occurs is made up of nitron nitrate. The thickness of the Nitron coating is important, because too thin a coating will result in an incomplete reaction, and too thick a coating will mask some of the smaller particles. The reaction spot can be identified by distinctive needle-shaped crystals of the Nitron nitrate (Fig. 2).

The screen coated with Formvar and carbon is used both as a control sample and to identify biomass particles. Figure 3 shows typical particles found on the blank screen, and Figs. 4 and 5 show examples of biomass particles. During the cruise, five samples were taken at various times of every day (no sample was taken when the ship stopped because the air was contaminated with ship exhaust). Stages one and two were sampled for the full 2 hours; stage three was sampled for 30 minutes, and stage four for 15 minutes.

2. RESULTS

Figures 6-9 show the particle concentration variations of each stage during the entire cruise. Particles were separated into four classes: the giant particles ($d > 5$ μm) collected on stage 1, the large particles ($2 \leq d \leq 5$ μm) collected on stage 2, the medium particles ($0.7 < d < 2$ μm) collected on stage 3, and small particles ($0.2 \leq d \leq 0.7$) collected on stage 4. The giant particle concentrations were 0.01 to 0.2 cm^{-3} with an average ~0.02 cm^{-3}. The large particles were 0.2 to 2 cm^{-3}; with an average ~1 cm^{-3}; the medium particles were 10 to 300 cm^{-3} with an average ~100 cm^{-3}; and the small particles were 200 to 3000 cm^{-3} with an average ~1000 cm^{-3}. No distinguishable diurnal

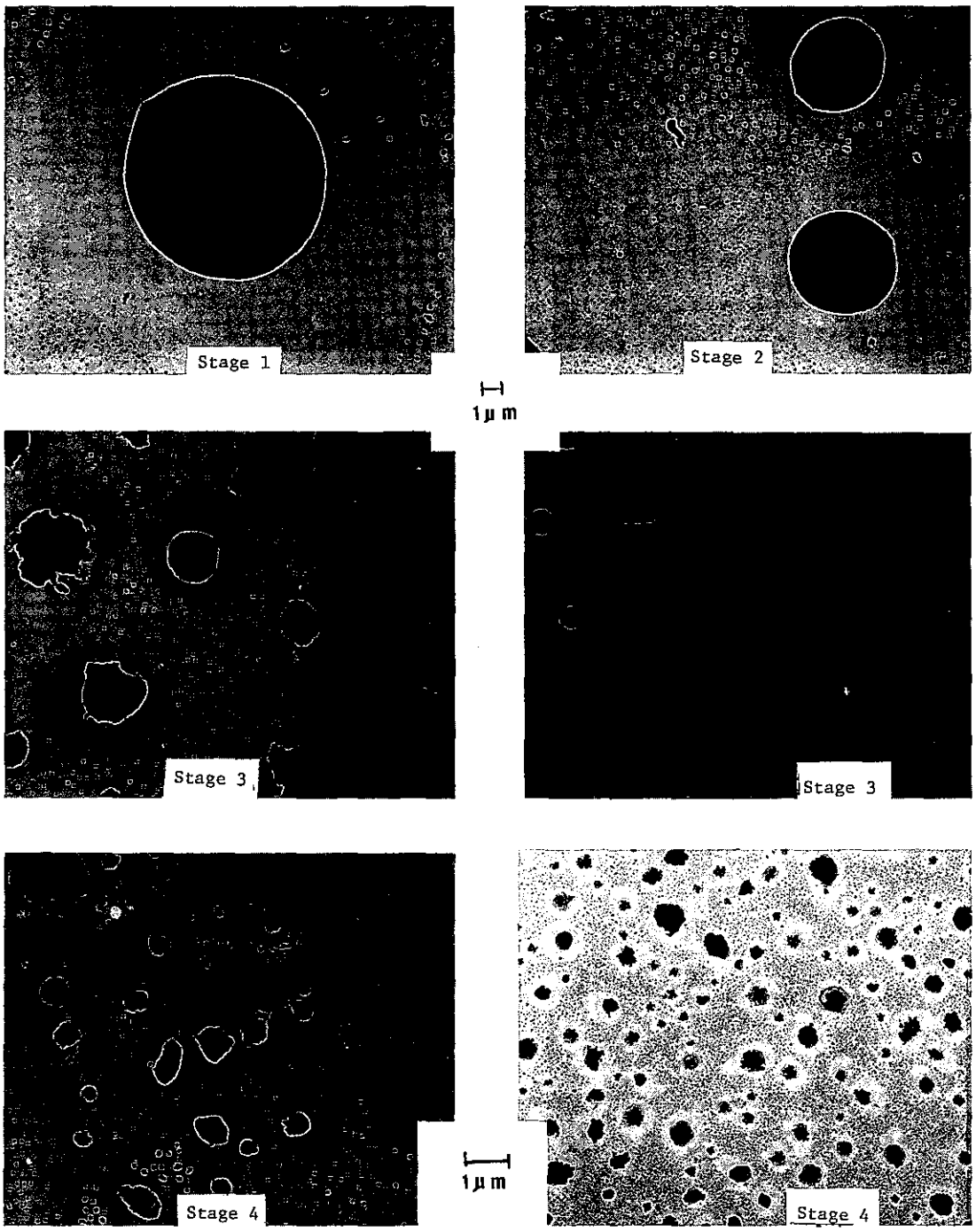

Figure 1. Transmission-electron-micrographs of aerosol particles that reacted with $BaCl_2$ coating to yield a halo ring indicating sulfate-containing particles.

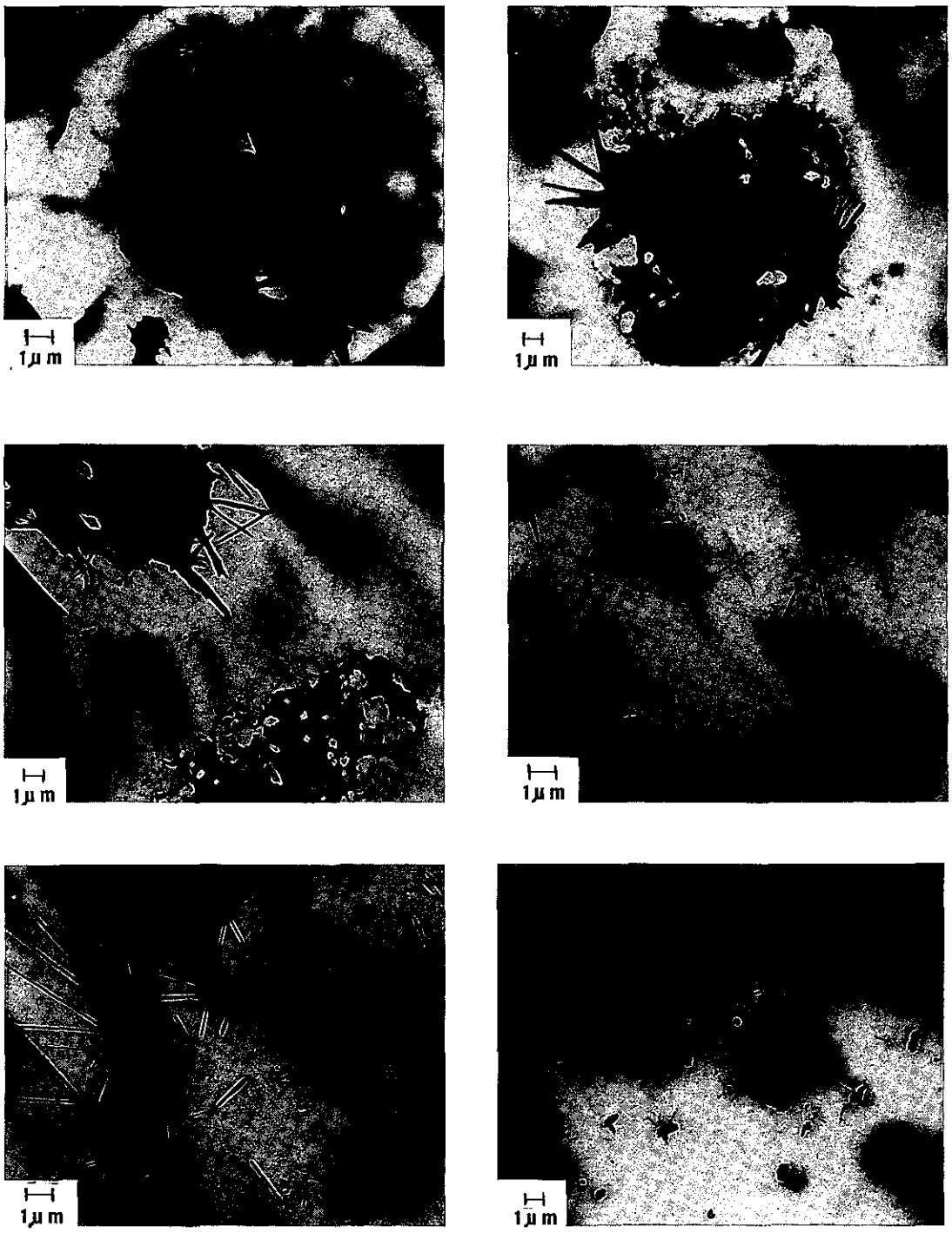

Figure 2. Aerosol particles that reacted with Nitron coating; the presence of needle-shaped crystals indicated particles containing NO_3^-.

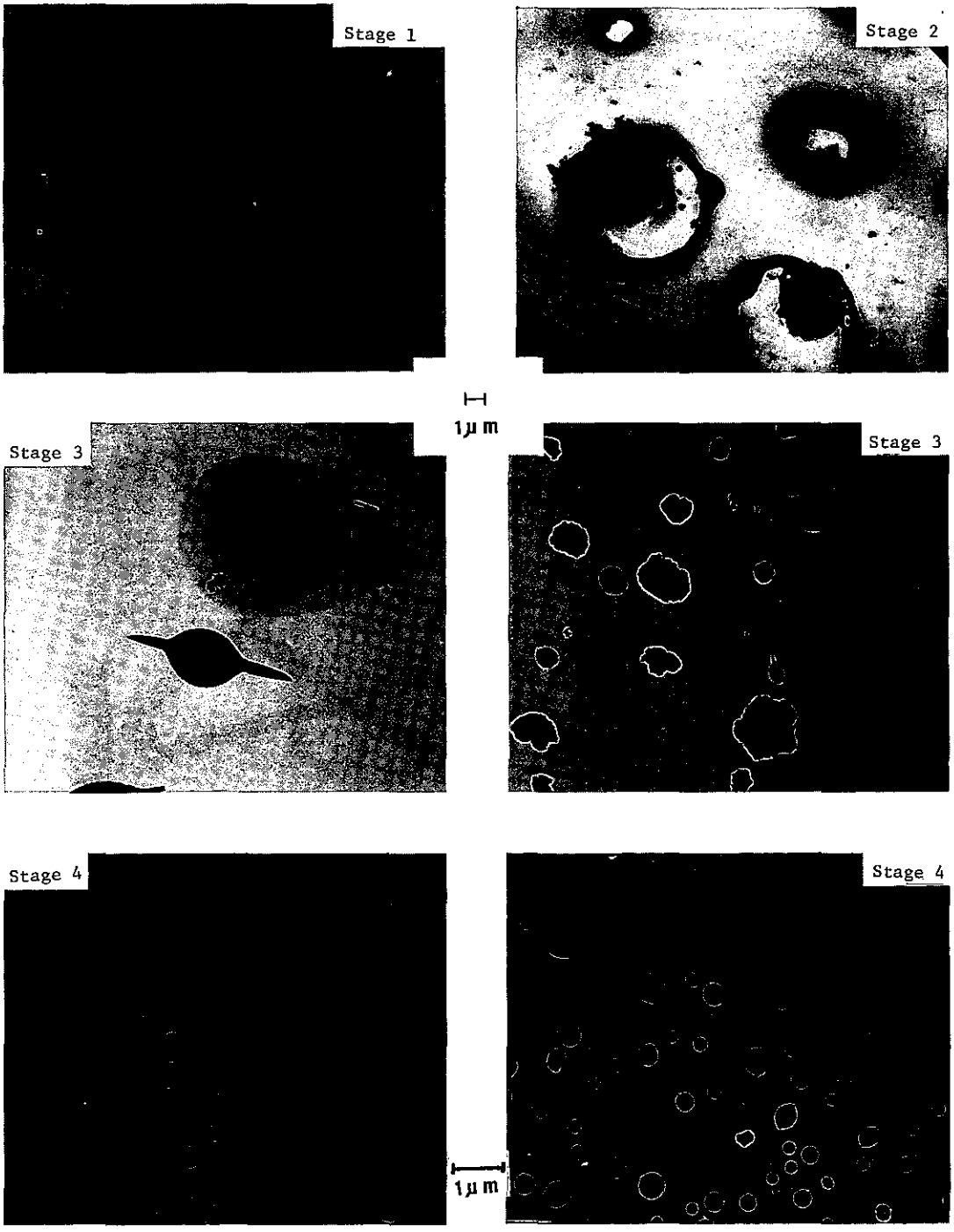

Figure 3. Typical particles collected on the Formvar-carbon-coated EM screens, which were mounted on four stages of an impactor to classify particles according to their sizes.

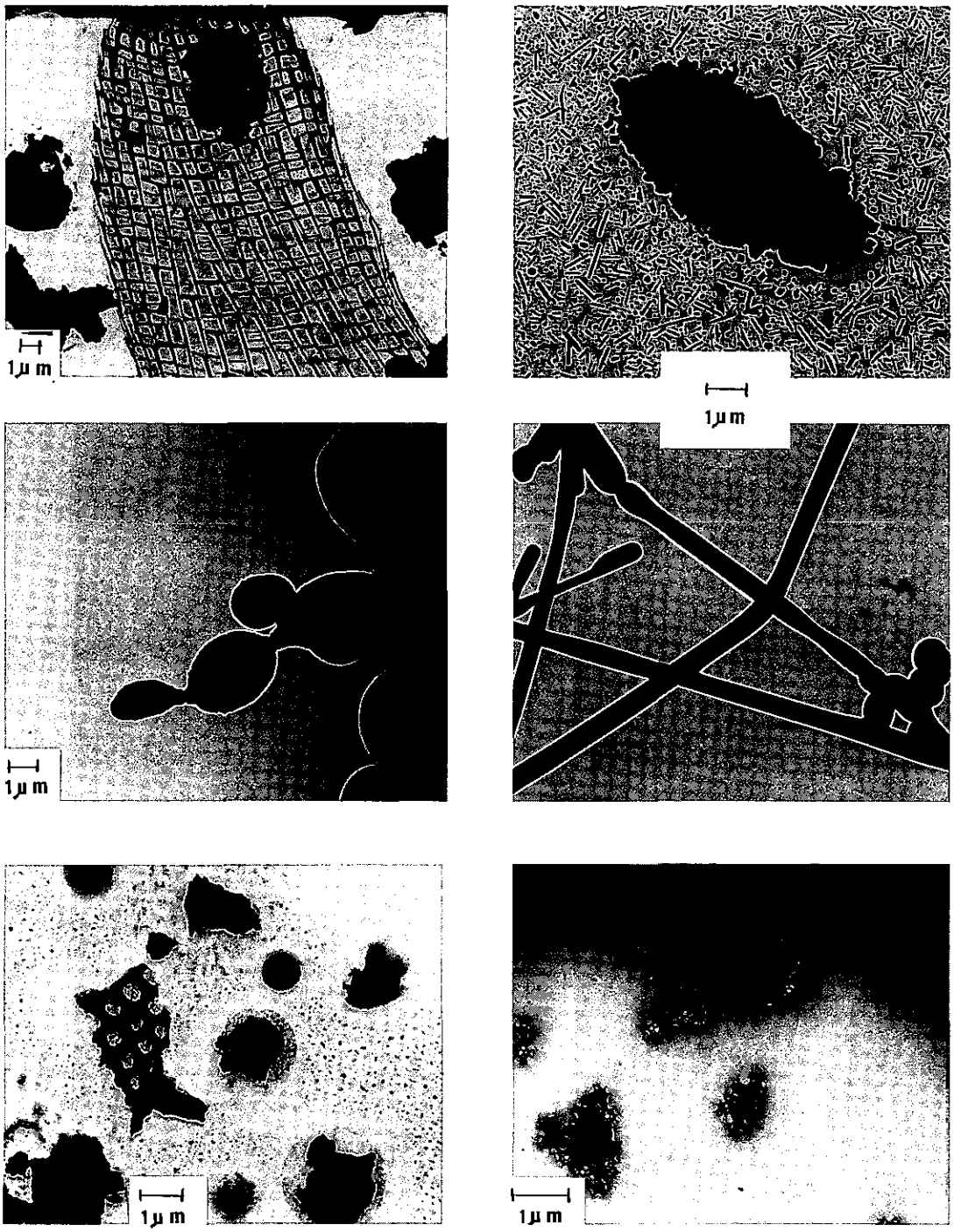

Figure 4. Particles with special morphology identified as biota.

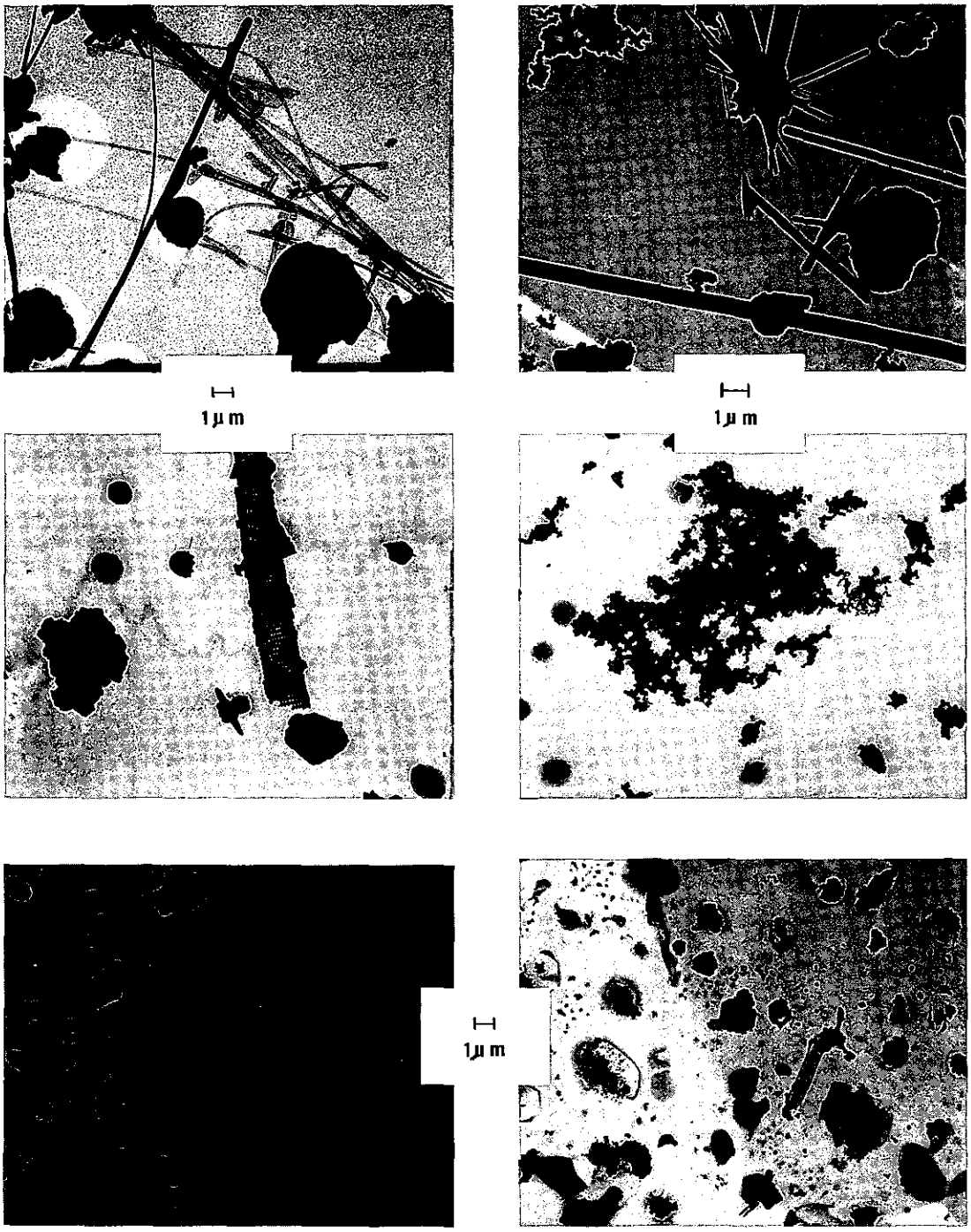

Figure 5. Some biological particles mixed with inorganic aerosols.

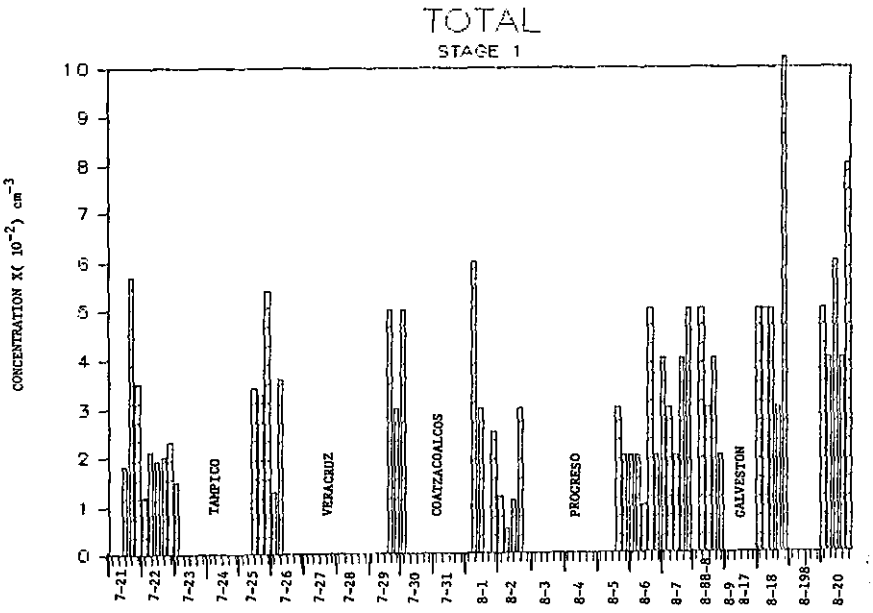

Figure 6. Temporal variation concentrations of particles collected on stage 1 ($d > 5$ μm).

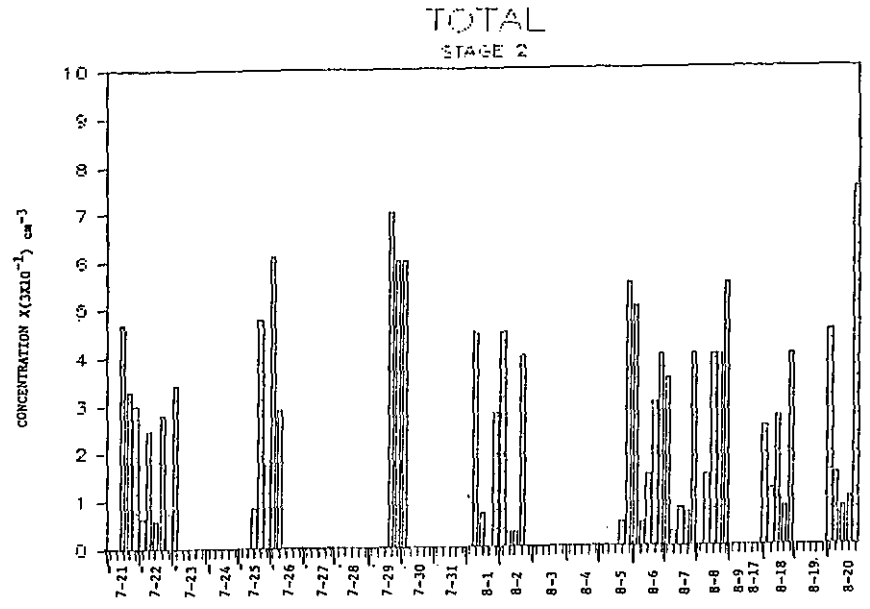

Figure 7. Temporal variation concentrations of particles collected on stage 2 ($2 < d < 5$ μm).

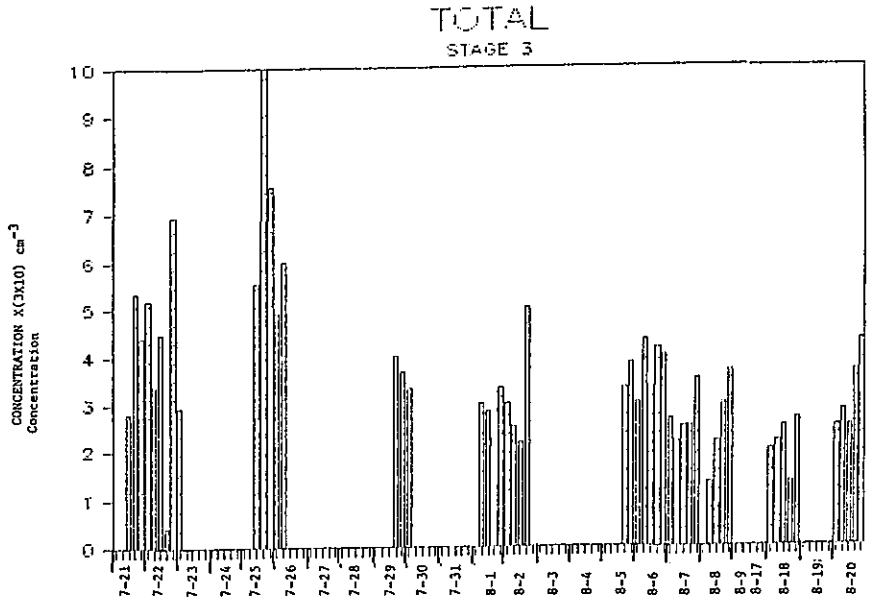

Figure 8. Temporal variation concentrations of particles collected on stage 3 ($0.7 < d < 2$ μm).

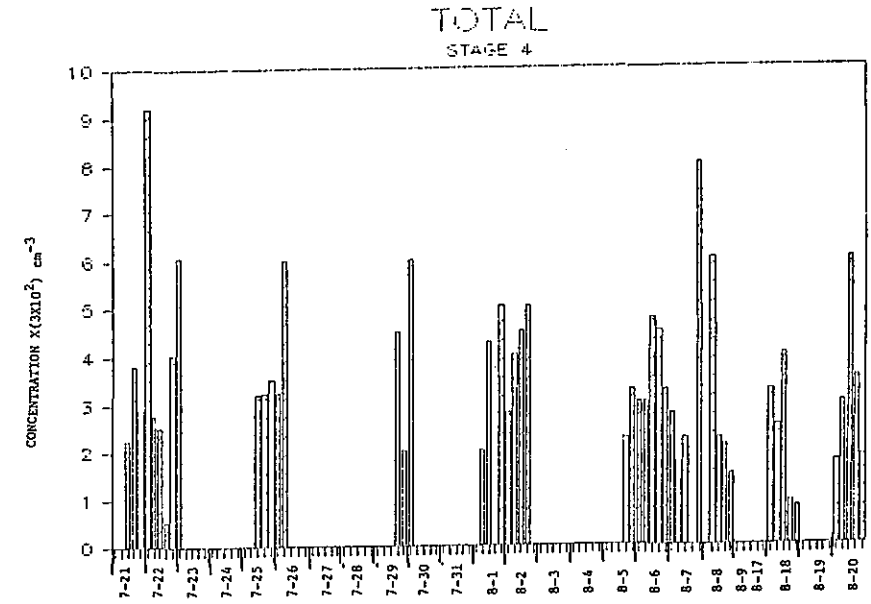

Figure 9. Temporal variation concentrations of particles collected on stage 4 ($0.2 < d < 0.7$ μm).

variations were observed in giant, large, and medium particles. However, in small particles, higher concentrations were observed before dawn when the ship was near shore. This was probably because the land breeze carried industrial air pollution to the sea. The lowest concentrations in all sizes were found 5-7 August when the ship was crossing the center Gulf where such pollution was least expected.

Figures 10-13 show the sulfate particle concentrations and Fig. 14 shows the percentages of particles containing sulfate. The sulfate particle concentration for stage 1 ranged from 0 to 9×10^{-2} cm^{-3}, and the average percentage of particles containing sulfate was ~75%. Stage 2 ranged from 0 to 1.2 cm^{-3}, and the average percentage of particles containing sulfate was >80%. Stage 3 ranged from 10 to 200 cm^{-3}, with an average of ~120 cm^{-3}; >85% of the particles contained sulface. Stage 4 ranged from 100 to 3000 cm^{-3}; >90% of the particles contained sulfate.

By comparing the plots of the relative sulfate particle density, some tentative conclusions could be drawn. Samples taken near the coast exhibit a trend of two peaks per day. The first and smaller peak occurs in the late afternoon. The second, larger, peak occurs in the very late evening to early morning. Samples taken in areas farther from the coast exhibit only one peak per sampling day. One-peak days occurred in the open sea during the trip from Progreso up to the New Orleans coast and on the return from Galveston to Veracruz. The peaks occurred generally in the late afternoon.

The trends observed for the samples tested for sulfate concentrations appeared to agree with the expected behavior. While near the coast, one expects to observe two peak periods, one in the late afternoon due to photochemical reaction to convert SO_2 to sulfate particles and a second at night when the land cools and land breeze forces air pollution out to sea. Farther from the coast, the early morning peak due to cooling of the land diminishes. Only the peak in the afternoon due to photochemical production remains. Stage 4 particularly shows this trend.

The actual percentage of sulfate particles does not vary much. The plots show that in the majority of samples 75%-95% of the particles contained sulfate on all stages. A slight decrease in percentage occurred in the

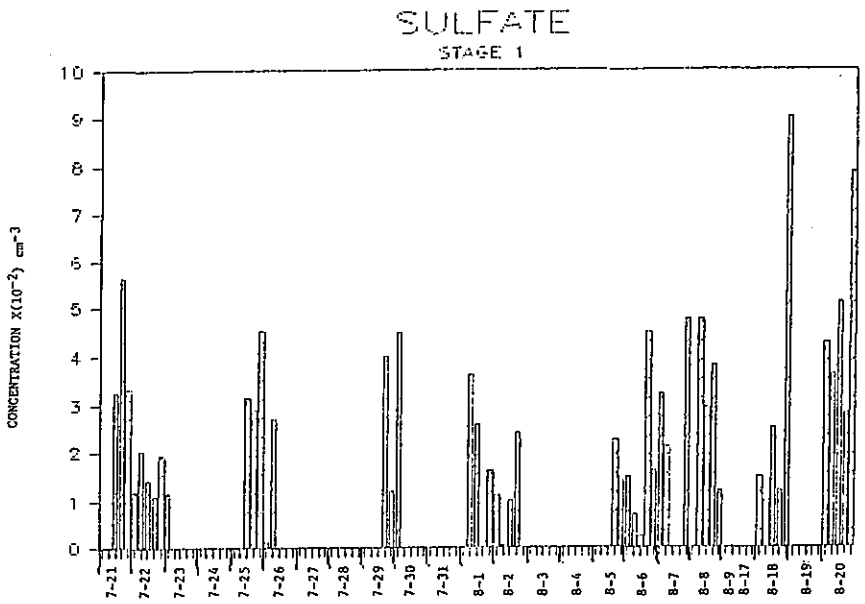

Figure 10. Temporal variation of sulfate-containing particles on stage 1.

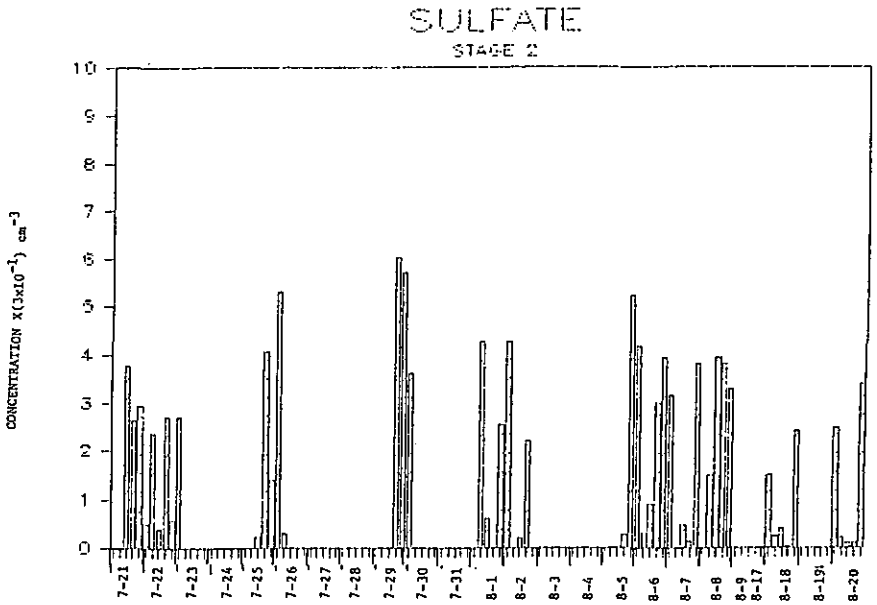

Figure 11. Temporal variation of sulfate-containing particles on stage 2.

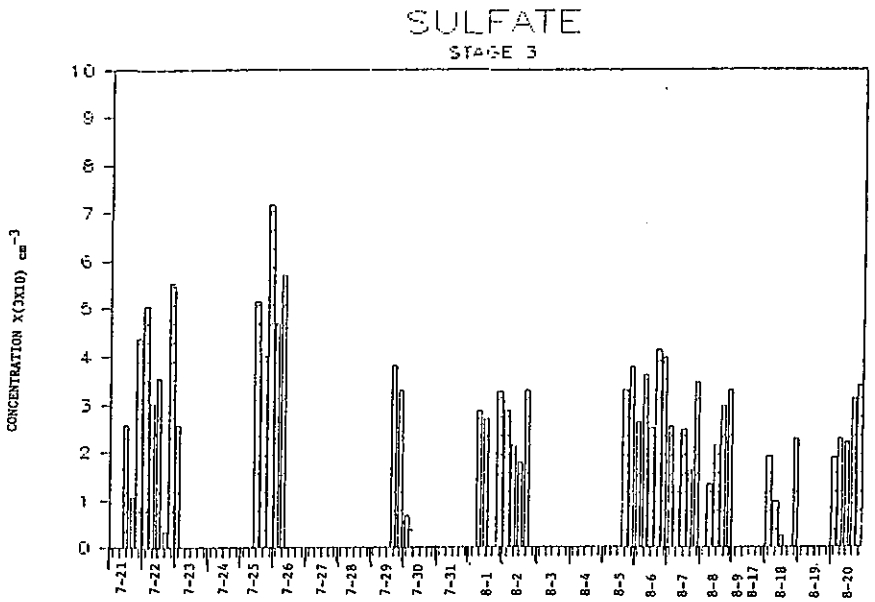

Figure 12. Temporal variation of sulfate-containing particles on stage 3.

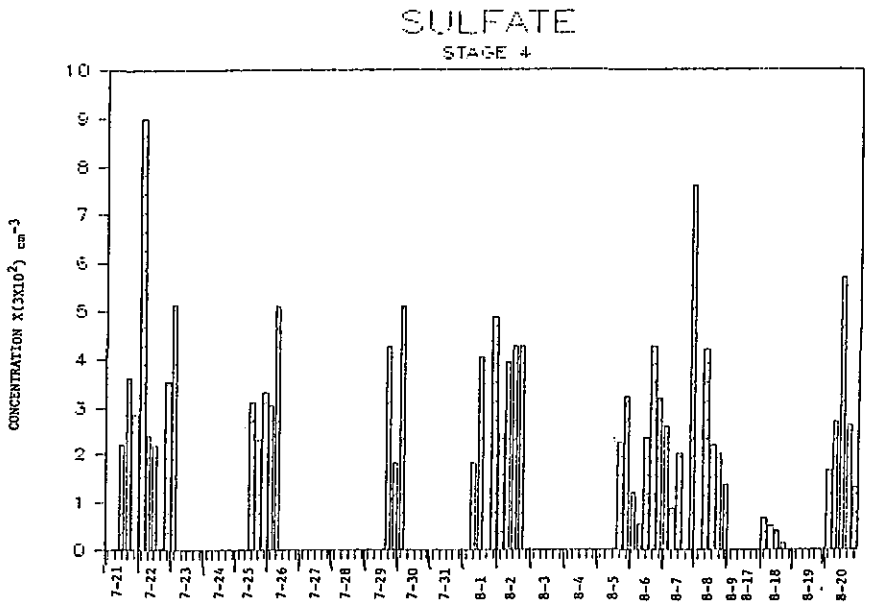

Figure 13. Temporal variation of sulfate-containing particles on stage 4.

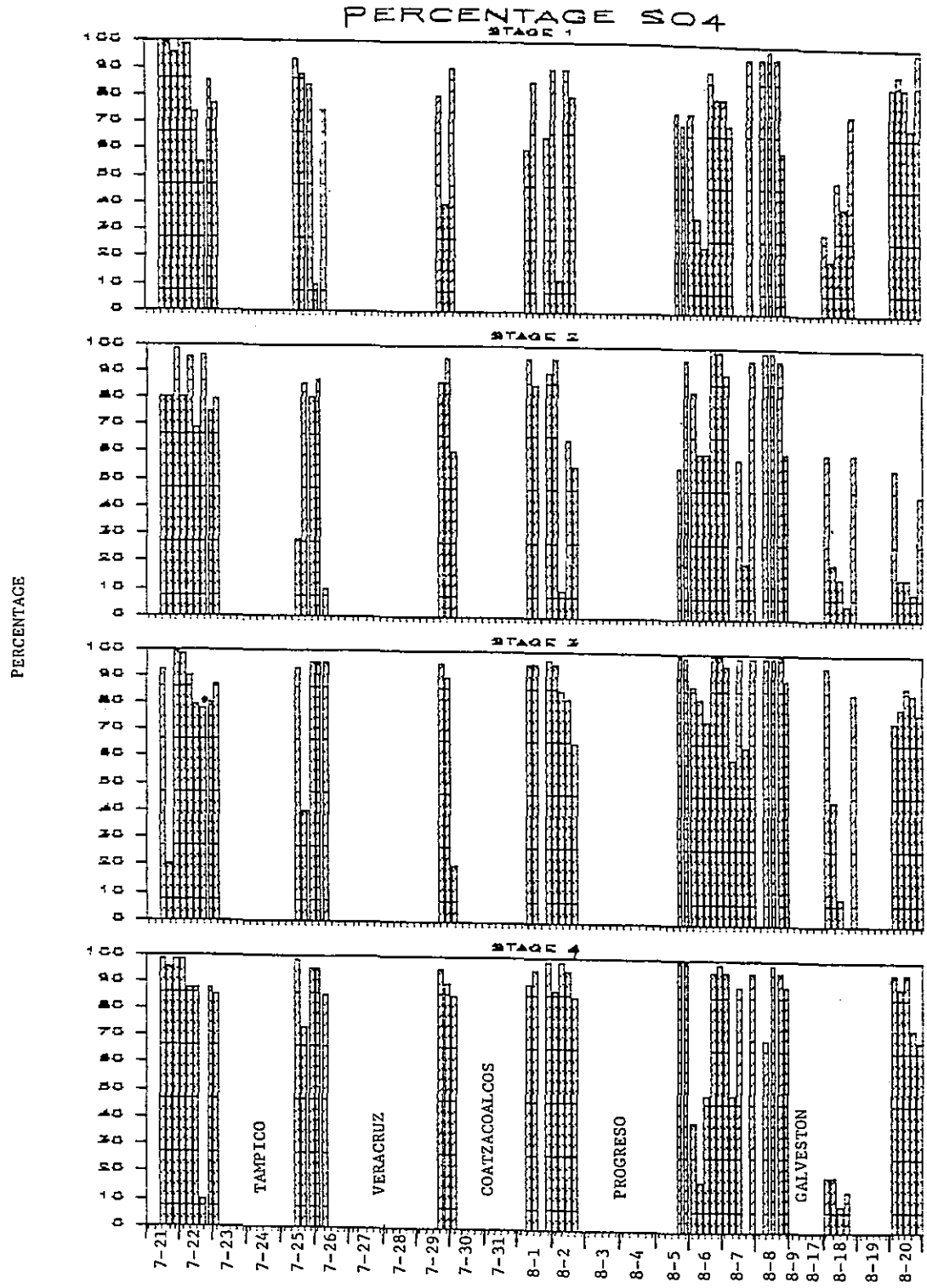

Figure 14. Percentage of particles containing $SO_4^=$ on the four stages along the cruise.

samples collected in areas farther from the coast--between Progreso and the New Orleans coast, and also between Galveston and Veracruz on the return of the ship. The 18 August samples show the most dramatic and consistent decrease in sulfate concentration for all four stages, in both the percentage plots and the relative density plots. These results support previous conclusions, as these samples were obtained in an area far from the coast.

Figures 15-16 show the results of the analysis for nitrate concentrations. The relative nitrate particle concentration for stage 1 ranged from 0 to 8 × 10^{-2} cm^{-3}; an average of ~75% of total particles reacted with Nitron. Stage 2 ranged from 0 to 0.7 cm^{-3}; an average of <75% reacted with Nitron. Stage 3 ranged from 0 to 200 cm^{-3}; an average of 70% reacted with Nitrate. Stage 4 ranged from 0 to 1500 cm^{-3}; an average of 50% reacted with Nitrate.

A distinct diurnal variation was much harder to obtain from the total nitrate particle analysis. The relative particle density on stages 2 and 3 (d = 0.7 to 5 μm) shows the pattern most similar to that of the sulfate reactions, where in the coastal regions there is an afternoon peak and a late night peak, the late night peak being the larger. The areas farther from the coast show only the late afternoon peak. Also, the same pattern occurs on 18 August, when the samples were taken in the center of the Gulf where the nitrate particle concentrations were the lowest.

Figure 17 shows the biomass concentrations that were determined by morphology. Biological particles as shown in Fig. 4 andof samples contained either zero or very few. Figure 17 shows the biological particle concentrations. Stages 1 and 2 show that the concentrations ranged from 0 to 0.02 cm^{-3}, with an average ~2 × 10^{-3} cm^{-3}. Stages 3 and 4 show a range from 0 to 25 cm^{-3} with an average ~2 cm^{-3}. The percentage of biomass concentrations for Stages 1 and 2 had a mean of ~5%; stages 3 and 4 had a mean of ~1%. Approximately half of the samples contained no biomass particles at all. The highest concentrations occurred around the Campeche Bay area. Other peak concentrations occurred right out of Veracruz and in the area between Progreso and the New Orleans coast.

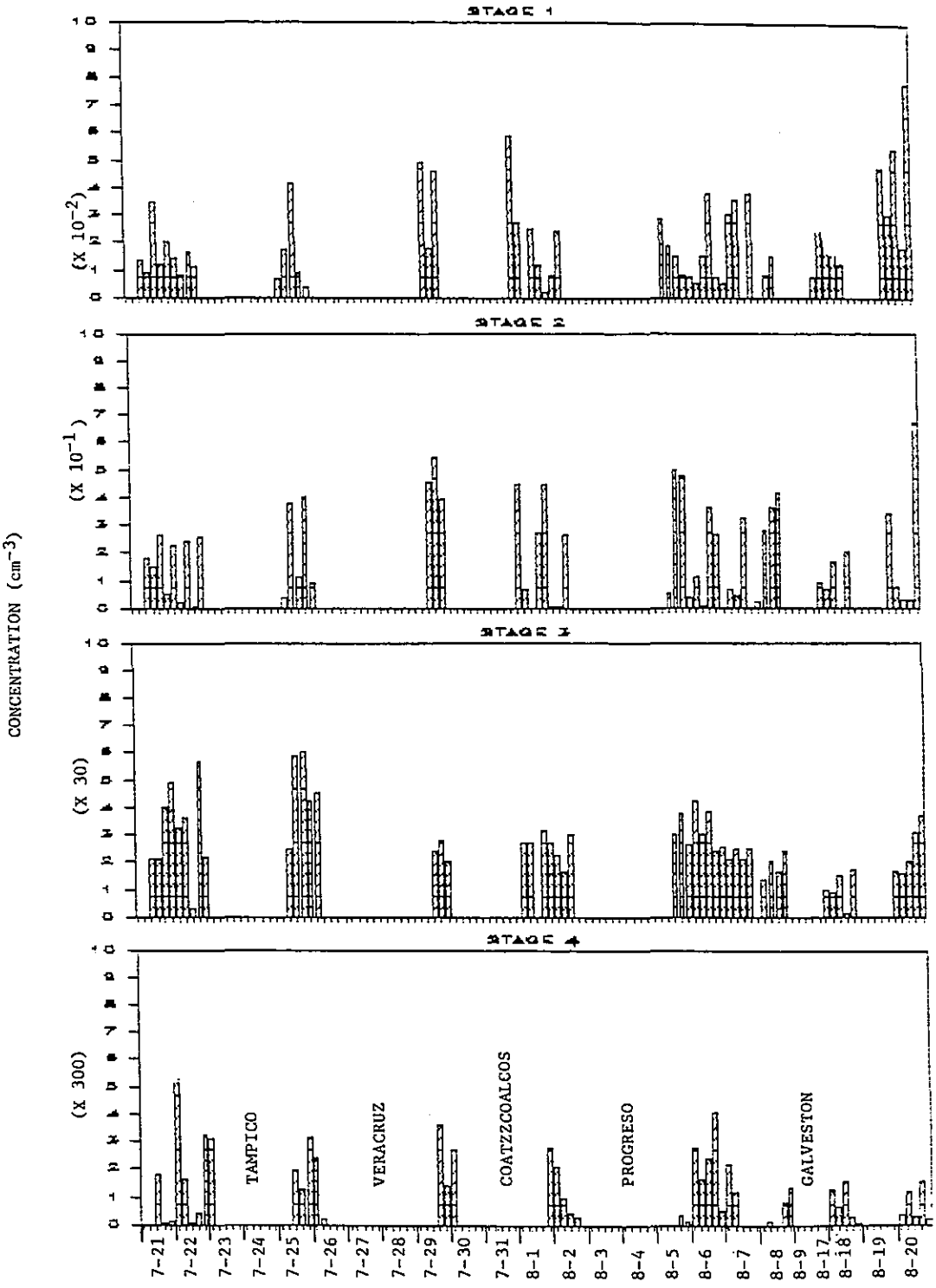

Figure 15. Temporal variation of concentrations of nitrate-containing particles on stages 1-4.

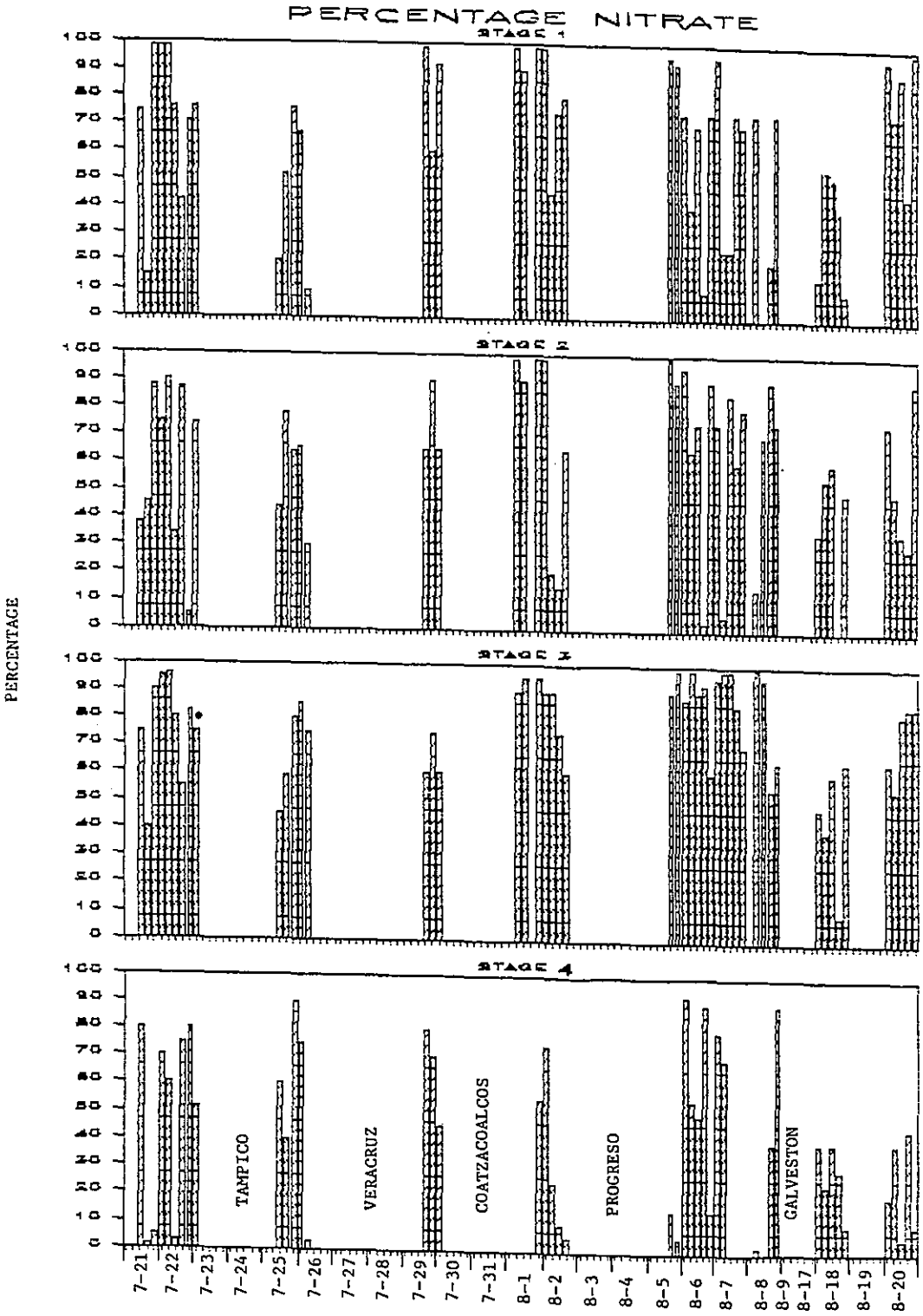

Figure 16. Percentage of particles containing NO_3^- on the four stages along the cruise.

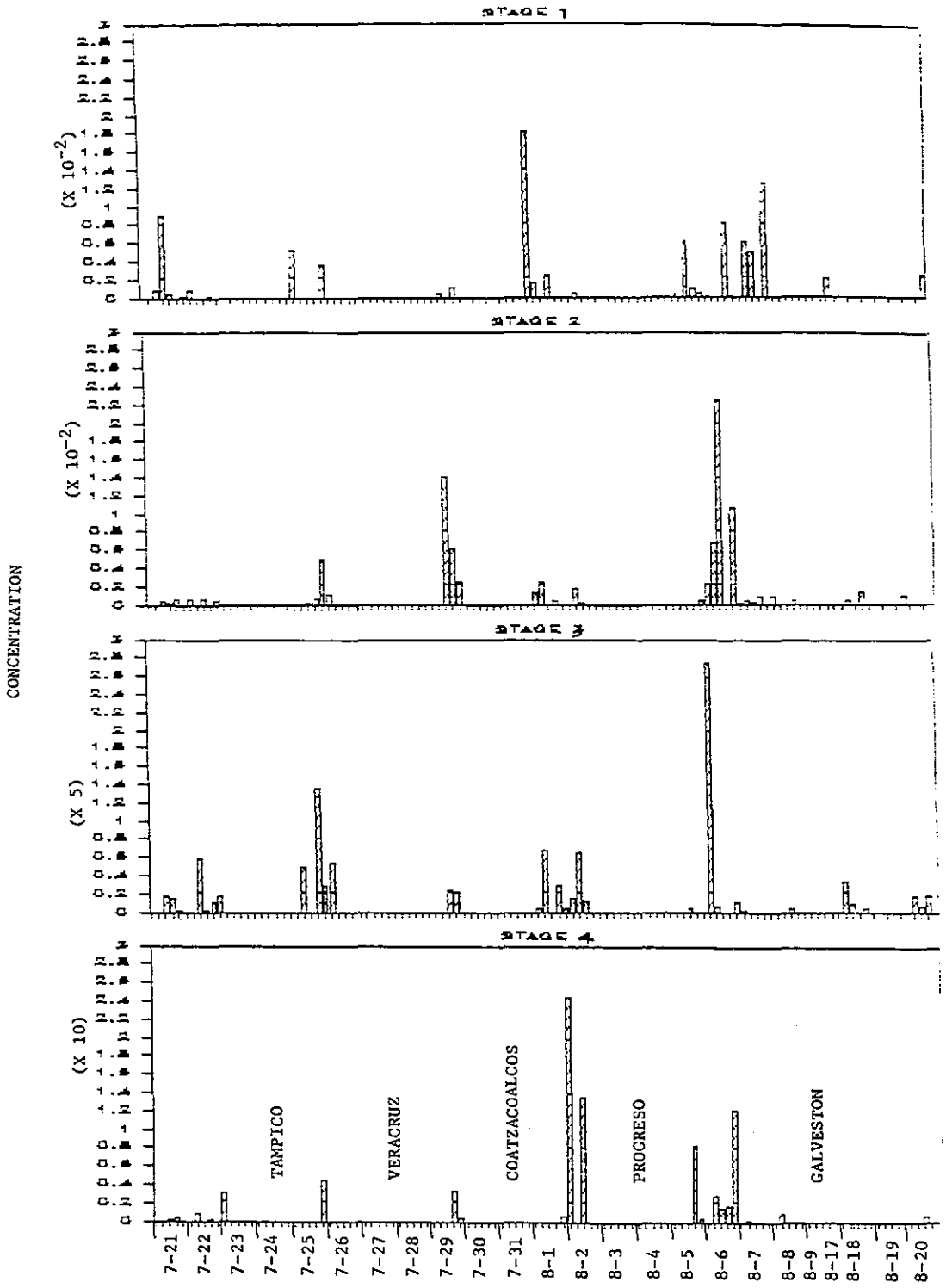

Figure 17. Temporal variation of concentrations of biomass particles on stages 1-4.

3. CONCLUSION

(1) The highest concentrations of total particles, sulfate particles, and nitrate particles were found near cities, e.g., Galveston, Tampico, Veracruz, and New Orleans. The lowest concentrations were measured on the way across the open Gulf. As expected, anthropogenic air pollution indeed has an important role in the aerosol chemistry over the Gulf.

(2) A high percentage (>80%) of particles contained sulfate; in most samples, a higher percentage (>90%) of smaller particles ($d < 1$ μm) than of larger particles containing sulfate. The observations agree with our previous investigations on marine aerosols (Parungo et al., 1986a, 1986b).

(3) Nitrate-containing particles were less numerous than sulfate-containing particles. However, in the majority of the samples >70% of larger particles and >40% of smaller particles contained nitrate. The nitrate concentrations, which were very much higher than marine aerosols measured in the Atlantic Ocean (Parungo et al., 1986a) and in the Pacific Ocean (Parungo et al., 1986b; 1987), indicated that the Gulf air was severely polluted with nitrate compounds.

(4) Near the coast, sulfate particle concentrations showed a definite two-peak-per-day pattern, one at late afternoon and another before dawn. The first peak was probably caused by photochemical reactions that generated particles from gases; the second peak was probably due to land breeze which brought air mass from land toward the sampling site. In the open Gulf far away from the shore the second peak was no longer observed. Similar diurnal variation of nitrate particle concentration was observed on some days but it was not evident on other days.

(5) The highest biological particle concentrations were observed around the Campeche Bay area where fishery has been known to be most prosperous. The high concentration observed on 5-7 August when the ship was crossing the open Gulf has not been explored.

REFERENCES

Bigg, E.K., A. Ono, and J.A. Williams, 1974: Chemical test for individual submicron aerosol particles. Atmos. Environ., 8, 1-13.

Mamane, Y., and R.F. Pueschel, 1980: A method for the detection of individual nitrate particles. Atmos. Environ., 14, 629-639.

Parungo, F., C.N. Nagamoto, and J. Harris, 1986a: Temporal and spatial variations of marine aerosols over the Atlantic Ocean. Atmos. Res., 20, 23-37.

Parungo, F., C.N. Nagamoto, J. Rosinski, and P. L. Haagenson, 1986b: A study of marine aerosols over the Pacific Ocean. J. Atmos. Chem., 4, 199-226.

Parungo, F., C.N. Nagamoto, R. Madel, J. Rosinski, and P.L. Haagenson, 1987: Marine aerosols in Pacific upwelling regions. J. Aerosol Sci., 18, 277-290.

AEROSOL MASS CONCENTRATIONS

Humberto Bravo A., Francois Perrin G., Guillermo Torres J.,
Rodolfo Sosa E., Ma Isabel Saavedra, R. Ricardo Torres J.,
and Rosaura Camacho C.

1. INTRODUCTION

The mass of total suspended particles (TSP) at the sampling sites was measured Madel and Parungo report (in Sec. II) on the ion concentrations of aerosols; the sum of all ion concentrations represented only the soluble portion of the total mass of the aerosol samples.) Nagamoto and Parungo (in Sec. II) report on the number concentrations of particles, but unless we know the density of particles in each size range, it is difficult to calculate the accurate mass of total aerosols in the air.

2. PROCEDURE

A direct way to measure TSP mass is to collect aerosols on a preweighed filter and weigh the filter again after sampling. Because the amount of aerosol suspended in the air is minute, a vast air volume must be sampled for even the most sensitive scale to weigh the aerosol collected. We used a high-volume air sampler (General Metal Works), which works on aerodynamic principles to collect particles in the range 0.3 to 100 μm. The sampler consists of a blower motor unit and a supporting screen for the filter. A pressure transducer recorder and a 7-day regular timer are included. Our glass fiber filters had a sampling time of 12 h or 24 h and a flow rate of 100 m^3/h. Calibration was done using the calibration orifice method (GMW-25) and a water manometer. The mass was determined in the laboratory after the cruise.

We also determined the mass concentrations of sulfate and nitrate ions as follows:

Determination of sulfate in atmospheric total suspended particles using the Turbidimetric Barium Sulfate Method:

Suspended particulate matter is collected over a 24-h (or 12-h) period on an 8 x 10-inch glass fiber filter by using a high-volume sampler. A water extract of the sample is treated with barium chloride to form barium sulfate.

The turbidity caused by the barium sulfate is a measure of the sulfate content. Fractioning is adjusted so that samples containing 1 to 20 μg per cubic meter, the expected range of atmospheric samples, can be measured. The sensitivity of the turbidimetric analytical procedure is 50 μg of sulfate (Keily and Rodgers, 1955).

Determination of nitrate in atmospheric total suspended particulates using the 2,4 Xylenol Method:

Suspended particulate matter is collected over a 24-h (or 12-h) period on an 8 × 10-inch glass fiber filter by using a high-volume sampler. A water extract is obtained and nitrated with 2,4 xylenol; the nitrated sample is separated from other water-soluble colored substances by means of extraction with toluene and sodium hydroxide. The color of the purified caustic extract is compared with the standards to estimate the nitrate content. Aliquot values are adjusted so that samples containing 0.1 to 10 $\mu g/m^3$ (the expected range of atmospheric samples) can be measured. Sensitivity is 5 μg of nitrate in up to 5 mL of water (Barues, 1950).

3. RESULTS AND DISCUSSION

The results of the measurements are shown in Tables 1 and 2 and Fig. 1. It is evident that air in port cities (e.g., Tampico and Veracruz) was very polluted with particulate matter including nitrate and sulfate particles. The TSP could be ~10 times higher than over the open sea. It is also noticeable that the concentrations of TSP and sulfate found during the night and early morning sampling (1900-0700 h) are most of the time higher than the concentrations found during the day hours (0700-1900 h), probably owing to the reduction of planetary boundary layers and land breeze carrying pollution to near-by sea. Sulfate values ranged from 2 to 19 $\mu g/m^3$ (Table 1), although the $SO_4^=$ concentrations were generally higher than the results measured by Madel and Parungo (this report); both data sets agree that the high values were measured near the strong emission sources from continental activities. Nitrate concentrations ranged from 0.77 to 1.7 $\mu g/m^3$. The results show a general agreement with Madel and Parungo's data. It was observed that the concentrations of nitrates during nights were sometimes higher and sometimes lower than the values during days.

Table 1. Results of total suspended particle analysis

Sampling zone	Number samples	Sampling period	TSP ($\mu g/m^3$)	$SO_4^=$ ($\mu g/m^3$)	NO_3^- ($\mu g/m^3$)	$\frac{SO_4^=}{PST}$	$\frac{NO_3^-}{PST}$	$\frac{SO_4^=}{NO_3^-}$
Galveston-Tampico	3	12 h	9.405	2.575	0.777	0.27	0.082	3.31
Tampico-Puerto	1	24 h	98.185	18.859	1.746	0.19	0.017	10.80
Tampico-Veracruz	2	12 h	58.540	6.240	0.901	0.11	0.015	6.92
Veracruz-Puerto	3	24 h	90.168	18.437	2.110	0.20	0.023	8.73
	4	12 h						
Veracruz-Coatzacoalcos	0	---	---	---	---	---	---	---
Coatzacoalcos Puerto	2	24 h	54.83	14.08	1.776	0.26	0.032	7.93
Coatzacoalcos Progreso	3	12 h	14.35	6.369	1.376	0.44	0.096	4.63
Progreso-Puerto	0	---	---	---	---	---	---	---
Progreso-New Orleans	3	12 h	13.28	4.66	0.917	0.35	0.069	5.07
New Orleans-Galveston	2	12 h	19.37	12.54	1.60	0.65	0.083	7.83
Galveston Fondeo	0	---	---	---	---	---	---	---
Galveston Puerto	0	---	---	---	---	---	---	---
Galveston-Veracruz	3	24 h	32.698	6.341	0.834	0.19	0.025	7.59
	7	12 h						

Table 2. Variation of total suspended particles between day and night periods

Sample number	Period*	$\mu g/m^3$			$\frac{SO_4^=}{PST} \times 100$	$\frac{NO_3^-}{PST} \times 100$
		TSP	$SO_4^=$	NO_3^-		
1	D	10	2.4	0.58	24	5.8
2	D	7	3.4	0.54	48.6	7.7
3	N	12	1.8	1.18	15	9.8
4	D	38	3.6	0.04	9.5	0.1
5	N	78	7.8	1.76	10	2.3
6	D	28	8.2	1.86	29.3	6.6
7	D	5	2.0	1.00	40	20.0
8	N	10	8.8	1.25	88	12.5
9	N	24	6.8	1.12	28.3	4.7
10	D	9	2.4	0.78	26.7	8.7
11	D	8	5.0	0.84	62.5	10.5
12	N	26	16.8	1.42	64.6	5.5
13	D	12	8.2	1.76	68.3	14.7
14	N	48	5.4	1.08	11.3	2.3
15	D	47	3.4	1.30	7.2	2.8
16	N	27	4.4	0.98	16.3	3.6
17	D	20	8.8	0.94	44	4.7
		$\bar{X}N=32.1$	$\bar{X}N=7.40$	$\bar{X}N=1.26$	$\bar{X}N=35.6$	$\bar{X}N=5.8$
		$\bar{X}D=18.4$	$\bar{X}D=4.74$	$\bar{X}D=0.96$	$\bar{X}D=33.4$	$\bar{X}D=8.2$

* D = Day
N = Night

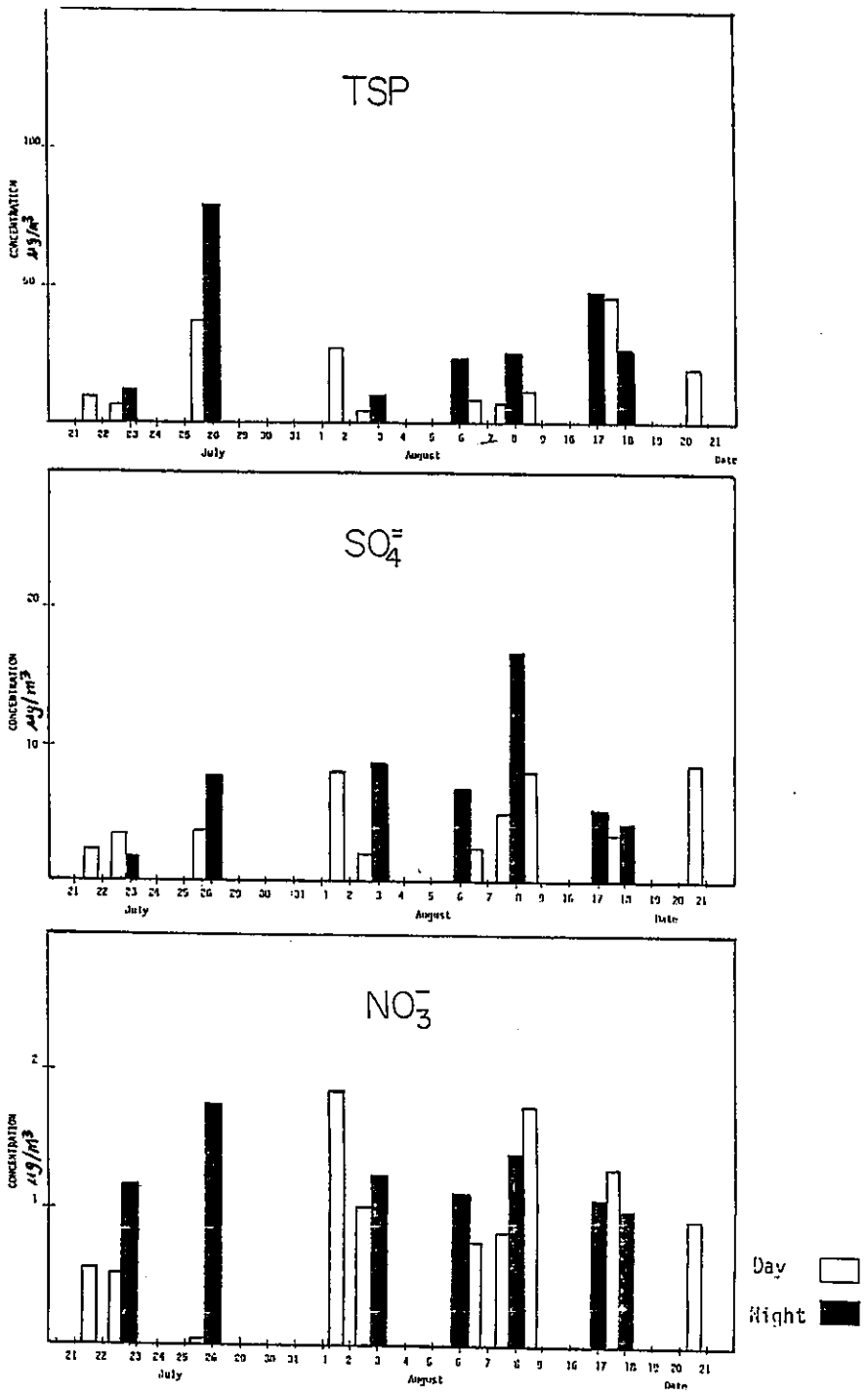

Figuare 1. Total suspended particles, and sulfate and nitrate aerosol concentrations measured at day and night on the cruise.

The average concentrations for all samples were 25.25 μg m^{-3} for TSP, 6.07 μg m^{-3} for $SO_4^=$, and 1.11 μg m^{-3} for NO_3^-.

REFERENCES

Barues, S.H., 1950: A modified 2:4-xylenol method for nitrate estimations. Analyst, 75, 388.

Keily, H.J., and L.B. Rodgers, 1955: Instrumental variability of a Model 7 Coleman photonephelometer. Analyt. Chem., 31, 2052.

ICE-FORMING NUCLEI IN AIR MASSES OVER THE GULF OF MEXICO

Jan Rosinski, Barbara A. Quintana and Philip L. Haagenson

1. INTRODUCTION

Two previous studies (Rosinski et al., 1986, 1987) have shown the presence of aerosol particles active as ice-forming nuclei (IFN) over the Pacific Ocean from 7°N to 10°S latitude and 110° to 170°W longitude. Concentrations of IFN active by condensation-followed-by freezing varied from 0 to 4.5×10^4 m^{-3} active at the initial (the highest) ice nucleation temperature of -4°C, and they were found to be independent of temperature below this initial ice nucleation temperature down to -17°C. The highest ice nucleation temperature found was -3.3°C; the corresponding concentration was 10^2 m^{-3}. These IFN concentrations were patchy over the ocean where upwelling was taking place. The most important and completely unexpected finding was that the sulfate ion was found to be an integral part of the ice nucleating particle. IFN were sulfate-bearing hydrophobic water-insoluble aerosol particles in the 0.1-0.3 μm diameter size range.

Dimethyl sulfide (DMS) originating in the ocean water is a precursor for the SO_4^{-2} ion in the atmosphere. The flux of DMS from the surface of the ocean water into the atmosphere is proportional to the concentration of DMS in water. Preliminary experiments were performed to explore a possible relation between the concentrations of IFN and of DMS. Measurements were made during the joint U.S.A.-U.S.M. cruise aboard the Mexican Research Vessel HO-2 from 20 July to 30 August 1986. The air chemistry over the Gulf of Mexico waters was under investigation.

2. THE EXPERIMENT

2.1 Measurements of IFN Population

The sampling technique used to collect different sized aerosol particles was similar to one described in the previous studies. It had two main features: (1) The two upper stages (1 and 2) were removed, and stages 3, 4, 5, and 6 were used only in the Andersen sampler; (2) three backup filters were used. The

backup filters and filters used in the Andersen sampler were 47-mm-diameter membrane filters with a 0.22-μm nominal pore diameter (Millipore Corp., Bedford, MA 01730). The number of jets impinging on an area of 17.3 cm^2 of a filter at each stage was 149. The area outside a filter mounted on each Andersen plate was coated with silicon grease to minimize travel, to the next stage, of any particles that might be dislodged after impinging on the metal plate. The sampling area of each backup filter was 9.6 cm^2. Filters were mounted by means of a flat Teflon ring; the area under the ring (7.7 cm^2) was not exposed to the sampled air and served as a background.

A dynamic developing chamber (Langer and Rodgers, 1975) was used to detect and to determine concentrations of IFN active by sorption and by condensation-followed-by-freezing. In experiments to detect ice nucleation by sorption, filters were exposed at a constant temperature for 15 minutes to water vapor just below saturation over liquid water (S_w < 0%). Concentrations of IFN active by condensation-followed-by-freezing were determined at a water vapor supersaturation of 2% ± 0.1. The temperature of a filter was changed continuously from -4° to -24°C. A cooling rate of 0.3°C min^{-1} was used.

2.2 Measurements of DMS in Seawater

The DMS measurements were made by Steven Hoyt (see Sec. I) onboard during the cruise.

Isentropic trajectory analysis (constant potential temperature, θ) was used to determine the transport history of the sampled air. The isentropic transport model used is described by Haagenson and Shapiro (1979). It has been used successfully in boundary-layer transport application (Clark et al., 1983; Ferek et al., 1983; Lazrus et al., 1983). Application of the model involving transport in the Southern Hemisphere and in equatorial regions is discussed by Crutzen et al. (1985).

3. RESULTS AND DISCUSSION

Concentrations of IFN active through condensation-followed-by-freezing as a function of aerosol particle diameter and temperature were determined at a simulated updraft speed of 0.5 m s^{-1} during four sampling periods: 21-22 August, 25-26 August, 6-7 September, and 8 September 1986.

During the first sampling period the highest temperature of ice nucleation by aerosol particles in the 0.1-0.4 μm diameter size range changed with time of day; it was -11°C at 1200-1400, -17°C at 1655-1855, -17°C at 2155-0010, -14°C at 0815-1000, and -10°C at 0300-0515 h (Fig. 1). Previous studies over the upwelling regions of the Pacific Ocean have shown that the sulfate ion-bearing aerosol particles in the 0.1-0.3 μm diameter size range nucleated ice at a temperature of -3.3°C; at -4°C the concentrations were up to 4.5×10^4 m^{-3}. Concentrations over that part of the waters of the Gulf of Mexico were less than 10 m^{-3}. Clearly the concentrations of IFN do not resemble previous findings. The simple explanation is that the upwelling regions of the Pacific Ocean are rich in biogenic activity and the ecological region under investigation is oligotrophic (Andreae and Raemdonck, 1983). But the IFN populations from both regions have one property in common, that is, their concentrations are independent of temperature for some temperature range. Over the Pacific Ocean this was present over the temperature range of 13°C (from -4° to -17°C; this dependency was not measured below the temperature of -17°C) and over the Gulf of Mexico it was present over different temperature ranges at different temperatures and for different aerosol particle diameter size ranges. For example, (from Fig. 1) for aerosol particles in the 0.1 - 0.4 μm diameter size range the temperature range was 6°C, for 1.0 - 3.6 μm it was 7°C, and for 0.4 - 1.2 μm it was 6°C and 5°C at two different IFN concentrations. Hydrosol particles present in seawater started to nucleate ice at a temperature of -6°C (1830, 21 July) and at -11°C (1100, 22 July). Hydrosol particles when dispersed into the air could supply aerosol particles for nucleating ice in that temperature range but IFN active at temperatures higher than -10°C were not detected in air. Concentrations of different sized aerosol particles and their size distributions are reported by Nagamoto and Parungo (see Sec. II). The fraction of aerosol particles f(d μm; T °C) in the 0.1-0.4 μm diameter size range active as IFN at -15°C (arbitrarily selected temperature) was found to be between 0 and 10^{-8}; for aerosol particles larger than 0.4 μm it was ~10^{-7}.

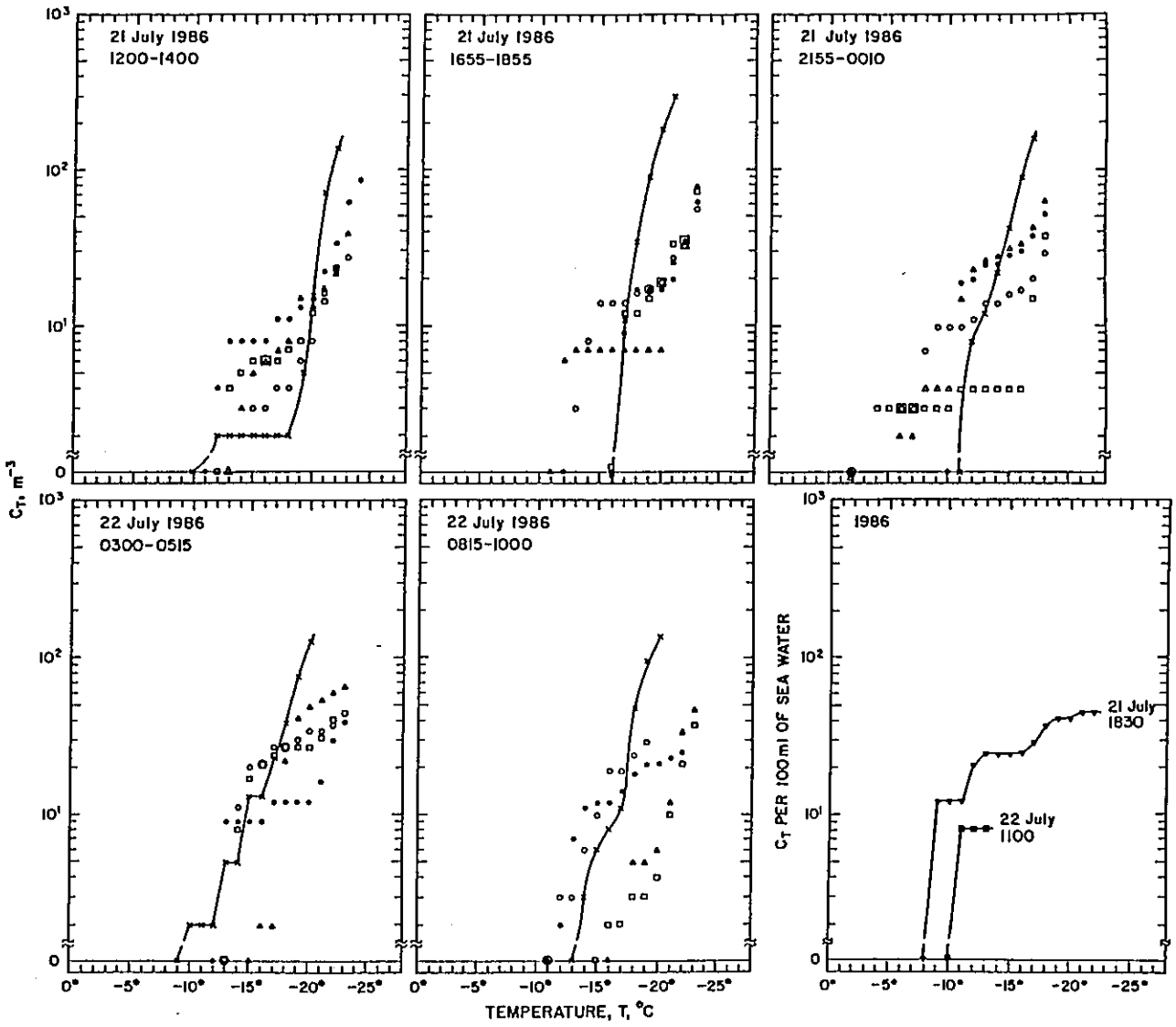

Figure 1. Concentrations of IFN active through condensation-followed-by-freezing during the 21-22 July 1986 sampling period (diameter of aerosol particles, d_a: x and solid line, 0.1-0.4 μm; □, 0.4-1.2 μm; Δ, 1.0-3.6 μm, •, 3.1-5.0 μm; o, <4.5 μm). C_T (last frame) is for particles separated from seawater by filtration.

The results from the second sampling period are presented in Fig. 2. Aerosol particles in the 0.1-0.4 μm diameter size range present between 1200-1400 h nucleated ice at the initial (the highest) temperature, -4°C; their concentration was very low (3 m^{-3}). Larger aerosol particles started to nucleate ice at -10°C. Five hours later this was reversed; larger particles nucleated ice at -5°C, and particles in the 0.1-0.4 μm diameter size range

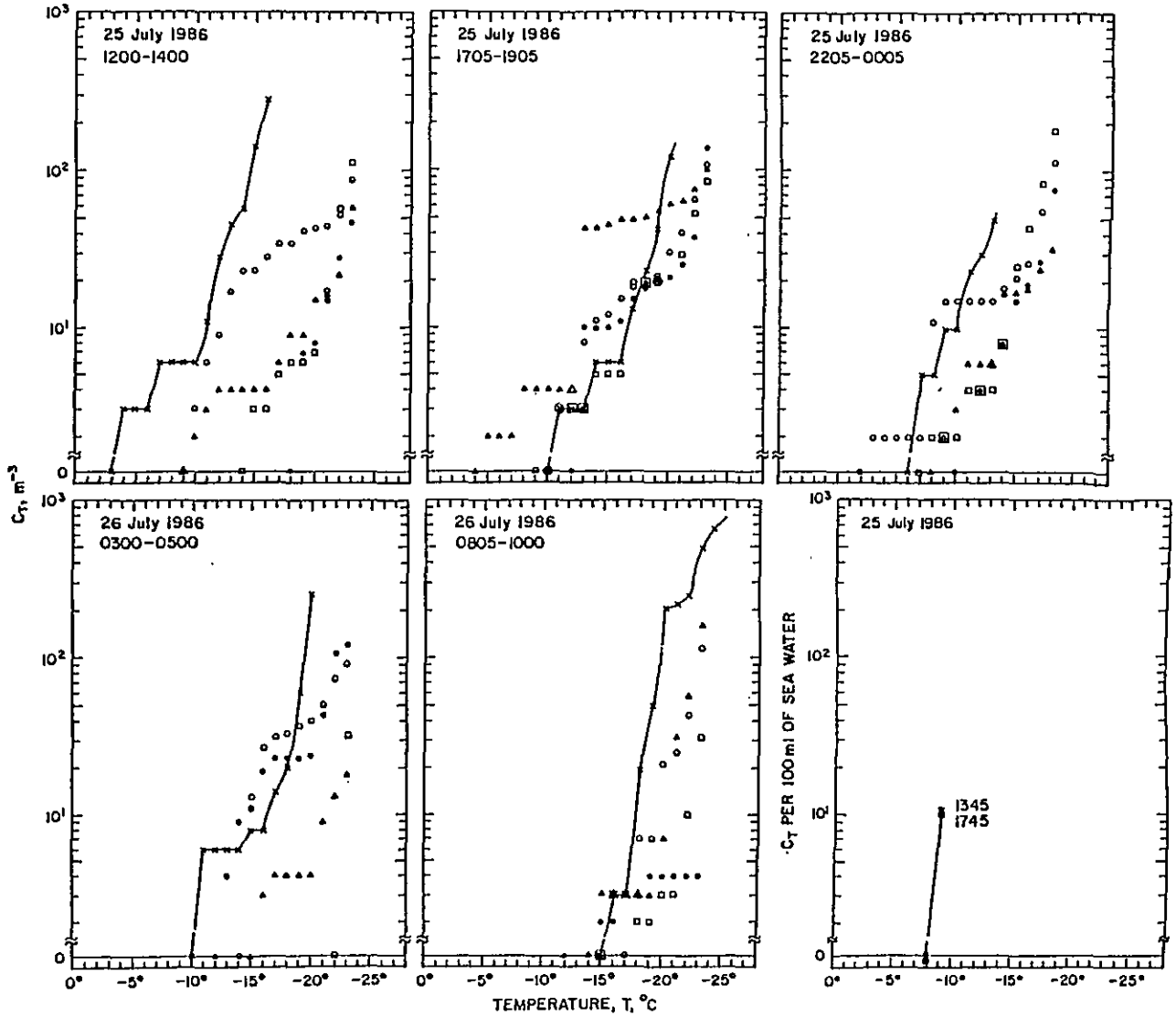

Figure 2. Concentrations of IFN active through condensation-followed-by-freezing during the 25-26 July 1986 sampling period (diameter of aerosol particles, d_a: x and solid line, 0.1-0.4 μm; □, 0.4-1.2 μm; Δ, 1.0-3.6 μm, •, 3.1-5.0 μm; o, <4.5 μm). C_T (last frame) is for particles separated from seawater by filtration.

nucleated ice at -11°C. During the night the highest temperature of ice nucleation dropped, reaching -16°C in the morning hours. The IFN in the 0.1-0.4 μm diameter size range were similar to those found over the Pacific Ocean in respect to the highest temperature of ice nucleation but they were found to be independent of temperature over different short ranges of temperatures at different IFN concentrations. The highest temperature of ice nucleation by par-

ticulate matter present in seawater was -9°C. The larger aerosol particles nucleating ice at higher temperatures (-5° to -8°C) later in the day (1705-1905 h) were therefore aggregates formed through coagulation of the 0.1-0.4 μm diameter particles with the larger ones. Fractions F(0.1 - 0.4 μm; -4°C) and F(0.1 - 0.4 μm; -15°C) were about 10^{-8} and 2×10^{-6} respectively.

The third and fourth sampling periods were over seawaters containing hydrosol particles nucleating ice at the initial temperature of -5°C (Figs. 3 and 4). Aerosol particles nucleated at initial temperatures as follows: -9°C at 1205-1405, 8 August; -12°C on four occasions; between -13°C and 16°C the rest of the time. Aerosol particles nucleating ice at higher temperatures (beween -5°C and -8°C) were not released from seawater unless the hydrosol particles lost their ability to nucleate ice when transferred from seawater into the air. Fractions F(0.1 - 0.4 μm; -11°C) and F(0.1 - 0.4 μm; -9°C) were about 10^{-7} and 5×10^{-8} respectively; at -15°C they were about 2×10^{-7} and 3×10^{-7}.

Dimethyl sulfide (DMS) concentrations in seawater and in the air were measured by Hoyt onboard in this cruise (see Sec. I). It has been shown that SO_4^{-2} ions are an integral part of IFN of marine origin in the 0.1-0.5 μm diameter size range over the equatorial upwelling regions of the Pacific Ocean. DMS is the precursor of the SO_4^{-2} ion and consequently it was thought that it might correlate with the initial temperature of ice nucleation of aerosol particles in that size range. Concentrations of DMS (in ng m^{-3} of air) from Andreae and Raemdonck (1983) were plotted together with the highest temperatures of ice nucleation. Concentrations of DMS in air over the Gulf of Mexico were below the detectable level. But concentrations in air are proportional to the concentrations in seawater and thus can be plotted (Fig. 5). The data show a distinct peak in the temperature curves between 1200 and 1400 hours. The peak concentration of DMS in air occurred between 0600 and 1000 hours. The time difference between the midpoints of sampling times is ~5 h; this is the time sufficient to oxidize S(-II) in $(CH_3)_2S$ to S(+VI) in SO_4^{-2} ion and to coagulate with aerosol particles, thus producing SO_4^{-2}-bearing mixed aerosol particles active as IFN through condensation-followed-by-freezing. Another finding supporting the relation between the initial temperature of ice nucleation and the concentration of DMS is given in Fig. 6. The highest temperature of ice nucleation by aerosol particles in the 0.1 - 0.4 μm diameter size range is associated with the largest

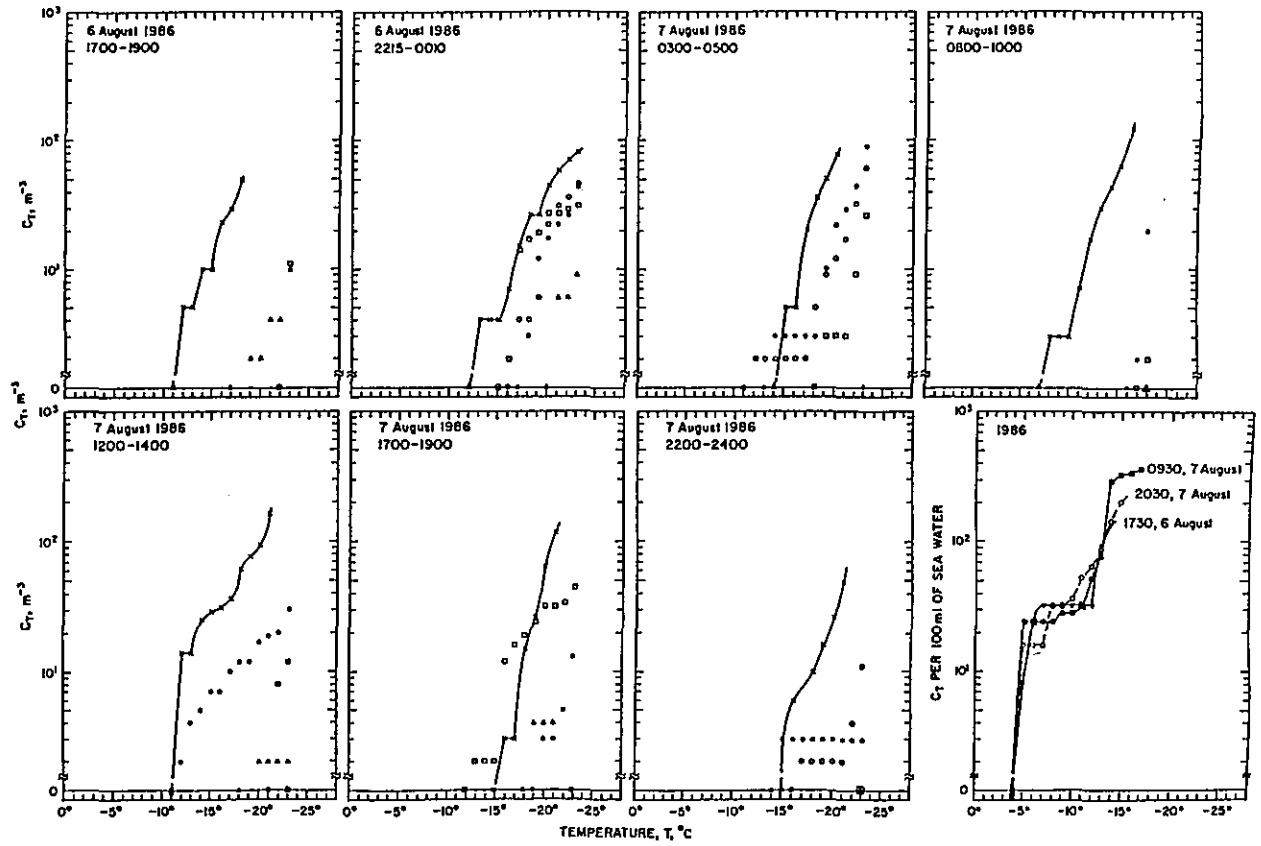

Figure 3. Concentrations of IFN active through condensation-followed-by-freezing during the 6-7 August 1986 sampling period (diameter of aerosol particles, d_a: x and solid line, 0.1-0.4 μm; □, 0.4-1.2 μm; Δ, 1.0-3.6 μm, •, 3.1-5.0 μm; o, <4.5 μm). C_T (last frame) is for particles separated from seawater by filtration.

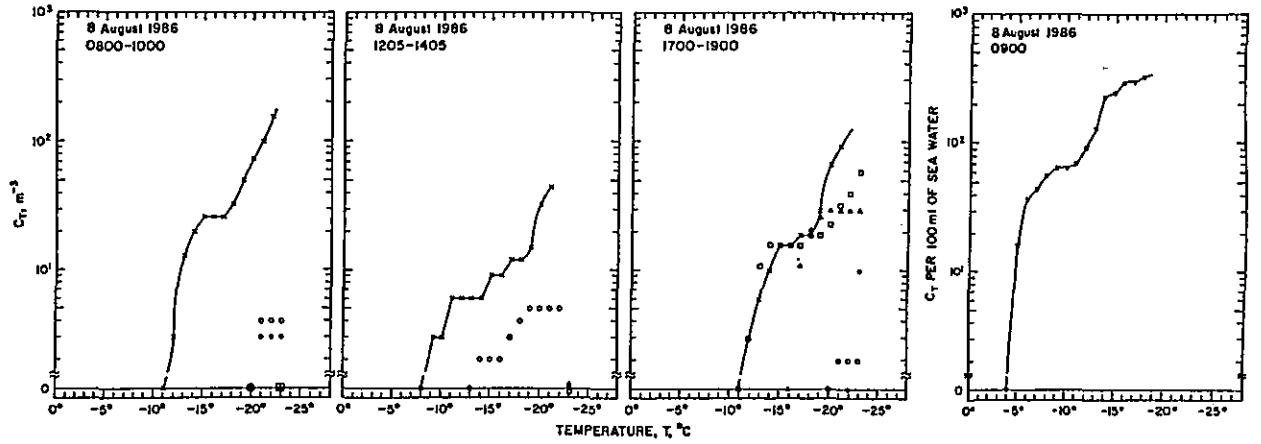

Figure 4. Concentrations of IFN active through condensation-followed-by-freezing during the 8 August 1986 sampling period (diameter of aerosol particles, d_a: x and solid line, 0.1-0.4 μm; □, 0.4-1.2 μm; Δ, 1.0-3.6 μm, •, 3.1-5.0 μm; o, <4.5 μm). C_T (last frame) is for particles separated from seawater by filtration.

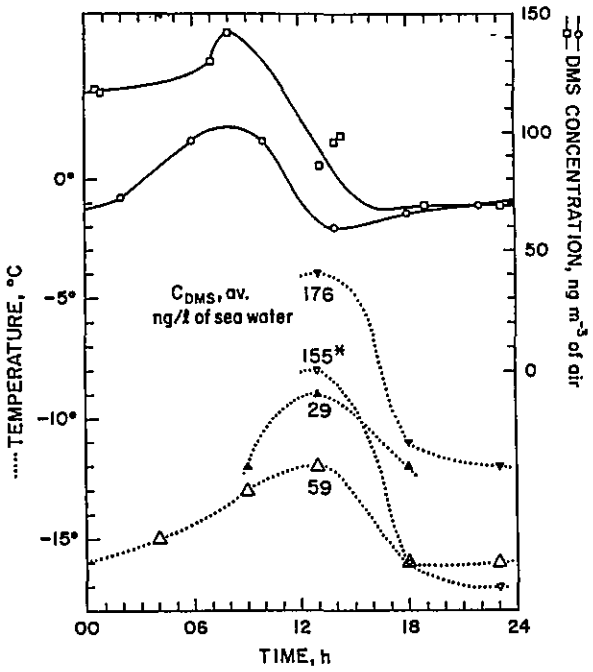

Figure 5. Concentrations of DMS (ng per m^3) in air over the equatorial Pacific. Solid lines and o, Andreae and Raemdonck, (1983); □, Hoyt and Rasmussen (unpublished data collected in Pacific Equatorial Region on 25 May 1984 on the NOAA ship Researcher); dotted lines, temperatures of ice nucleation; (▼, 25 July; ∇, 21 July; ▲, 8 Aug.; Δ, 7 Aug. 1986) vs. time of day; *, the datum closest to the sampling time for aerosol particles.

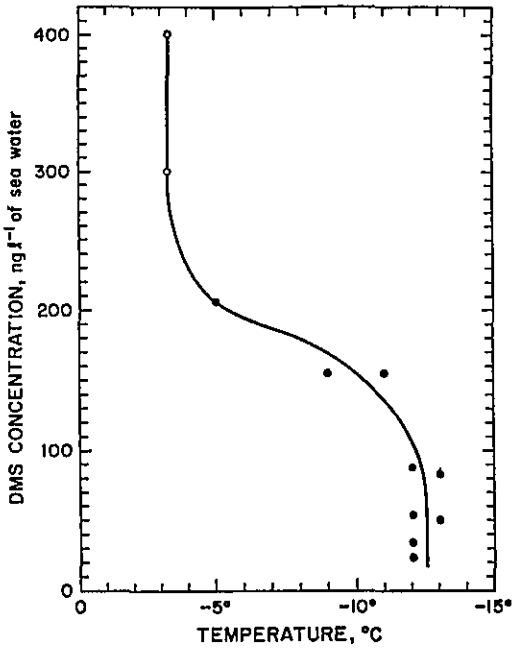

Figure 6. The highest temperatures of ice nucleation vs. concentration of DMS in seawater and in air. o, from Andreae and Raemdonck (1983) and Rosinski et al. (1986); o, present data.

concentration of DMS in seawater and consequently in air. It is possible that high biogenic activity is producing specific chemical compounds that nucleate ice at high temperatures (-3.3° to 7°C). But it is also possible that a specific ratio of mass of an organic particle to a concentration of SO_4^{-2} ions in the surface of a particle is necessary to be produced during the exchange of matter at the air-sea interphase; formation of high-temperature IFN may be restricted to the high biogenic activity.

IFN of marine origin were found to be independent of temperature. Data from the upwelling regions of the equatorial Pacific Ocean are shown together with data from the Gulf of Mexico (Fig. 7). The presence of large number con-

centrations of IFN nucleating ice at high temperatures was associated with large concentrations of DMS. The grey area in Fig. 7 represents typical temperature spectra of aerosol particles of continental origin; the entire area is typical of IFN present in marine-continental mixed air masses. The presence of SO_4^{-2} ions that are produced from their precursor molecules (DMS) is an essential but insufficient condition for formation of IFN of marine origin. Presence of derivatives of, e.g., the C-16 hydrocarbon (it is used here as an example because its derivatives constitute the most abundant group in the ocean waters) is necessary for production of IFN. The two components, SO_4^{-2} ions and aerosol particles made of the derivatives of the C-16 hydrocarbon, must be present at the same time in the atmosphere. Concentration of DMS is proportional to biogenic activity and, if it is low, SO_4^{-2} ions may be relatively abundant but organic particles will be scarce; the result may be the presence of aerosol particles nucleating ice at a high temperature but at a very low concentration. And this is what was found over the waters of the Gulf of Mexico.

An example of the elemental chemical composition of aerosol particles collected over the sea is shown in Fig. 8. Nearly all aerosol particles consist of mixed particles containing salts from the sea water attached to an organic (X n-e particles) or an inorganic matrix. There is also a bias toward detection of chemical elements in larger particles. Organic particles probably contain traces of most of the elements. The presence of different concentrations of organic particles and of trace elements (Cr, Mn, Ni, and Cu) at different times of sampling indicate a different biogenic activity and a different chemical composition of the seawater along the ship's path. This explains the observed non-uniform character in the population of IFN over the sea.

To establish the origin of aerosol particles nucleating ice along the path of the ship, we constructed backward 72-h isentropic trajections of air parcels arriving at the sampling sites (Fig. 9). A sampling of aerosol particles was taking place in the air mass that just arrived along a trajectory. Sampled aerosol particles consist, therefore, of those that originated at some distance and of those that were produced locally at the place of sampling. Concentrations of DMS molecules in seawater were measured at the sampling sites and they were not affected by the air motions. It was determined that all prevailing air masses under investigation were staying below the marine boundary layer and there were no intrusions of air from the upper layers of the atmosphere.

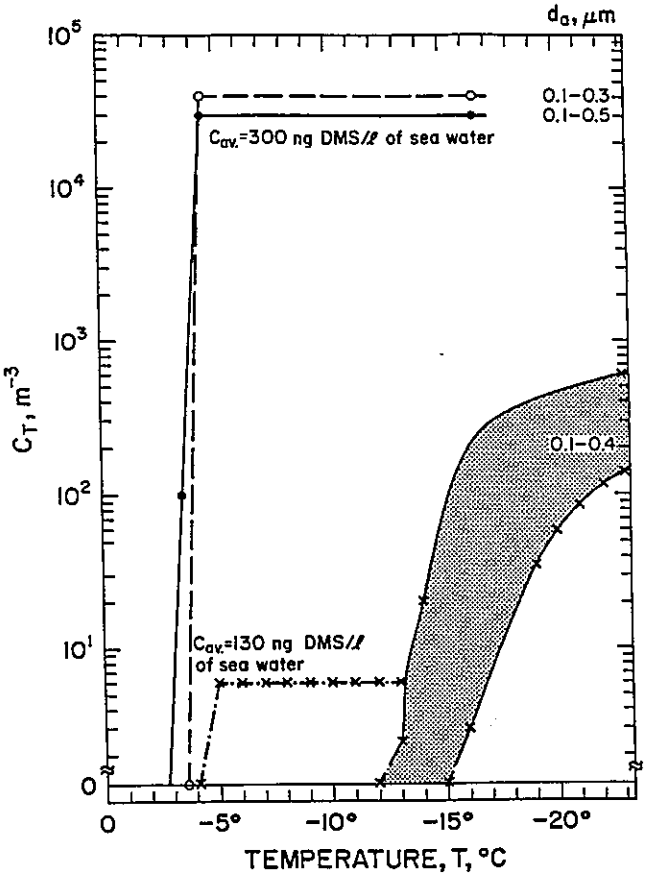

Figure 7. Temperature spectra of IFN of marine origin. The gray area represents IFN spectra of continental origin.

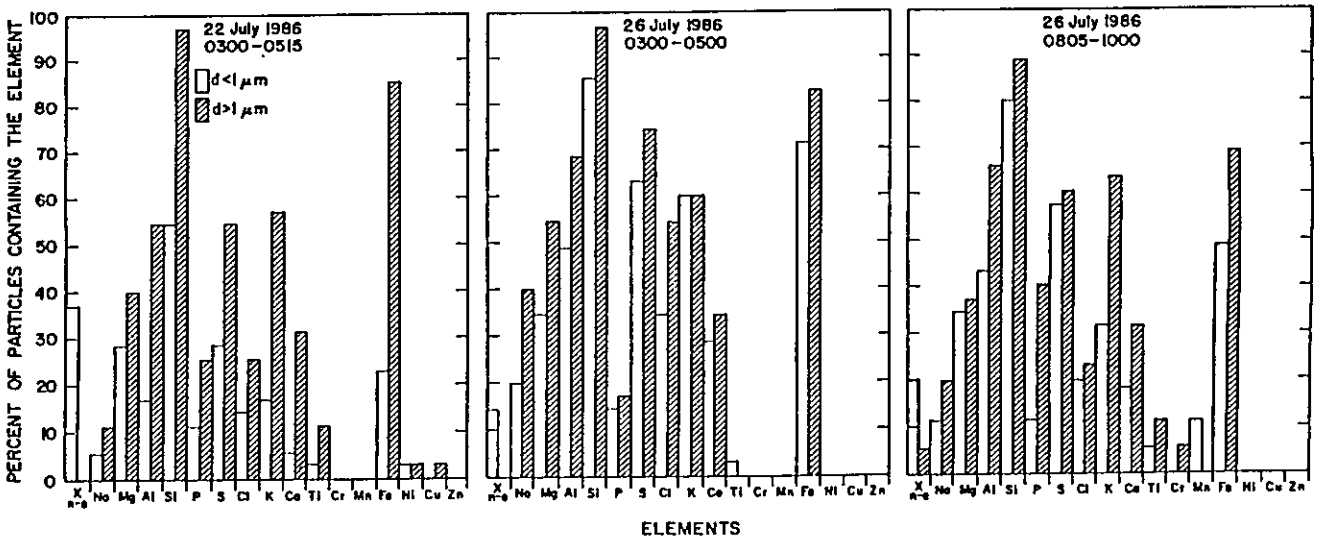

Figure 8. Frequency of chemical elements in aerosol particles. X n-e indicates x-ray non-emitting particles.

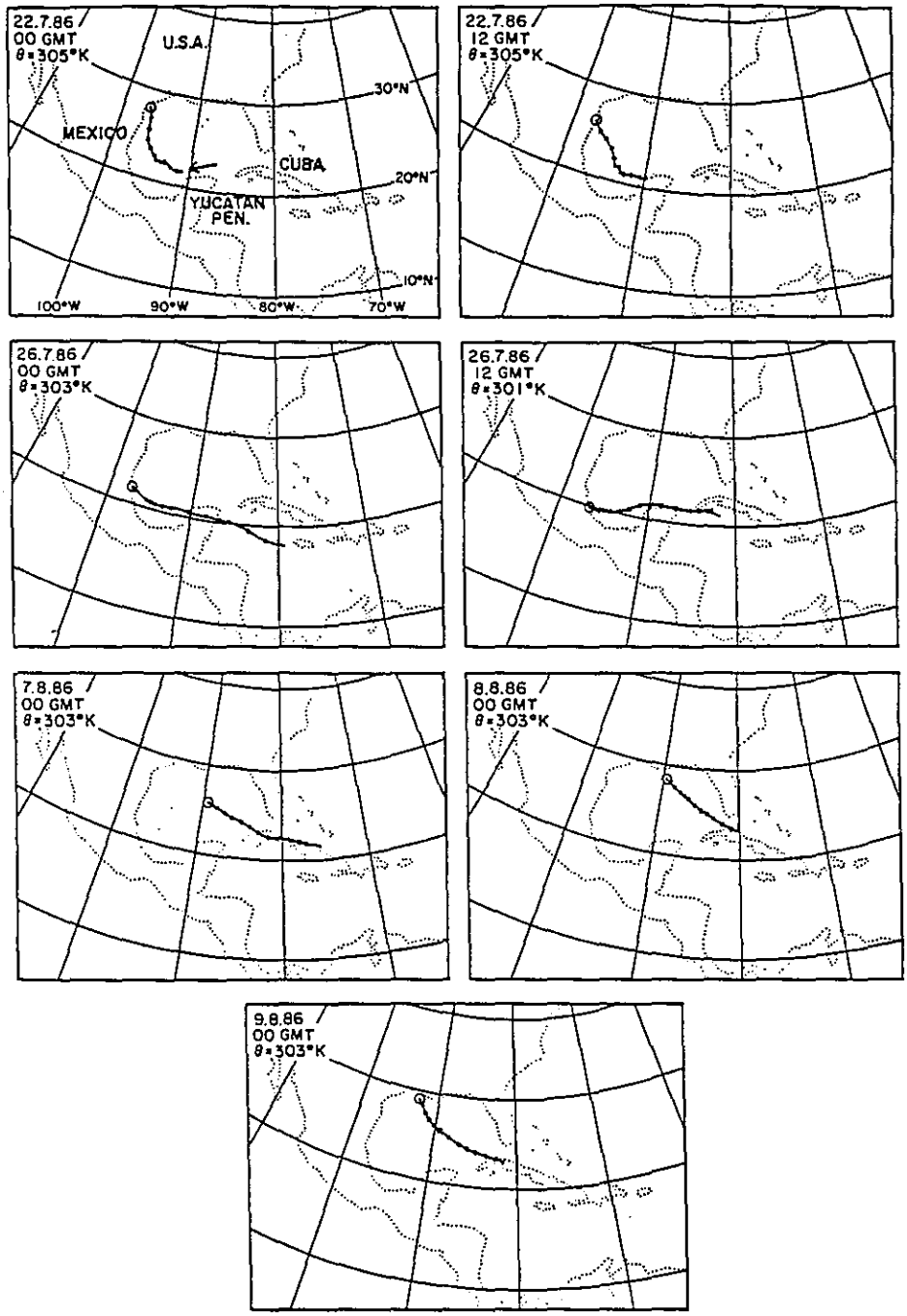

Figure 9. Backward 72-h isentropic trajectories of air parcels having different θ values. Segments between block dots are of 6-h duration; o is position of the ship.

Fractions of the aerosol particle population of continental origin were from the Yucatan Peninsula and from Cuba. Their contribution was shown in characteristic dependency of IFN on temperature of ice nucleation.

4. CONCLUSIONS AND OBSERVATIONS

(1) IFN of marine origin active at the highest temperature of -4°C were present at extremely low concentrations (2 to 10 m^{-3}). Fractions of aerosol particles in the 0.1-0.4 μm diameter size range nucleating ice at the initial (the highest) temperatures were between 10^{-8} and 10^{-7}.

(2) Aerosol particles in the 0.1-0.4 μm diameter size range nucleated ice at the highest temperatures during daytime hours (1200-1400 local time).

(3) Aerosol particles larger than 0.4 μm in diameter nucleated ice at higher temperatures than the smaller ones in the afternoon hours (1700-1900 local time).

(4) Peaks in the concentration of dimethyl sulfide preceded peaks in ice nucleating temperatures by ~5 h; this gives sufficient time for DMS molecules to be oxidized to sulfates and to produce mixed aerosol particles through coagulation of different sized aerosol particles and absorption of sulfur-bearing gas molecules.

(5) The temperature of ice nucleation by aerosol particles in the 0.1-0.4 μm diameter size range was found to be proportional to the DMS concentration in seawater and consequently in air.

(6) All IFN displayed characteristic features of mixed IFN, that is, of marine origin (part of IFN concentration independent of temperature) and of continental origin (part of IFN concentration dependent on temperature).

(7) Hydrosol particles present in seawater were nucleating ice on some occasions at temperatures higher than those of the aerosol particles, indicating that these hydrosol particles were not transferred from seawater into the air unless the aerosolized particles lost their ability to nucleate ice at high temperatures.

REFERENCES

Andreae, M.O., and H. Raemdonck, 1983: Dimethyl sulfide in the surface ocean and the marine atmosphere: A global view. Science, 221, 744-747.

Clark, J.F., T.L. Clark, J.S. Ching, P.L. Haagenson, R.B. Husar, and D.E. Patterson, 1983: Assessment of model simulations of long-distance transport. Atmos. Environ., 17, 2449-2462.

Crutzen, P.J., A.C. Delany, J. Greenberg, P.L. Haagenson, L. Heidt, R. Lueb, W. Pollock, W. Seiter, A. Wartburg, and P. Zimmerman, 1985: Tropospheric chemical composition measurements in Brazil during the dry season. J. Atmos. Chem., 2, 233-256.

Ferek, R.J., A.L. Lazrus, P.L. Haagenson, and J.W. Winchester, 1983: Strong and weak acidity of aerosols collected over the northeastern United States. Environ. Sci. Technol., 17, 315-324.

Haagenson, P.L., and M.A. Shapiro, 1979: Isentropic trajectories for derivation of objectively analyzed meteorological parameters. NCAR Tech. Note, NCAR TN-149.

Langer, G., and J. Rodgers, 1975: An experimental study of the detection of ice nuclei on membrane filters and other substrata. J. Appl. Meteorol, 14, 560-570.

Lazrus, A. L., P.L. Haagenson, B.J. Heubert, G.L. Kok, C.W. Kreitzberg, G.E. Likens, V.A. Mohnen, W.E. Wilson, and J.W. Winchester, 1983: Acidity in air and water in a case of warm frontal precipitation. Atmos. Environ., 17, 581-591.

Rosinski, J., P.L. Haagenson, C.T. Nagamoto, and F. Parungo, 1986: Ice-forming nuclei of maritime origin. J. Aerosol Sci., 17, 23-46.

Rosinski, J., P.L. Haagenson, C.T. Nagamoto, and F. Parungo, 1987: Nature of ice forming nuclei in marine air masses. J. Aerosol Sci., 18, 291-309.

PART III. RAINWATER CHEMICAL ANALYSES

ION CONCENTRATIONS AND pH OF RAINWATER

Farn P. Parungo, Humberto Bravo A., William C. Keene and James N. Galloway

1. SAMPLE COLLECTION AND ANALYSES

Rain samples were collected independently by the American team and the Mexican team during the cruise. The American team collected simultaneously two types of samples, (a) the event samples (from beginning to end of every rain event) and (b) the sequential samples (with intervals of 5 or 10 minutes depending on rainfall rate--more or less than 2 cm h^{-1}). Both types of samples were collected with a polyethylene funnel (20-cm diameter) with a neck that could be screwed onto a receiving bottle (a 1-L bottle for event sample and 30-mL bottles for sequential samples).

The collectors were cleaned with deionized water and stored inside the cabin in a clean plastic bag. The bottles contained deionized water, which was used to rinse the funnels prior to use. The collectors were brought out to the open deck and mounted at the front rail of the ship just before rain. After rain they were washed, rinsed, and stored for the next event.

The pH of rain was measured with a pH meter immediately after each sample collection. There were seven rain events during the cruise; only three events produced sufficient sequential rain samples. The pH values of sequential rain samples collected at different locations are shown in Fig. 1. The rain samples had a pH range from 4.0 to 6.1. In some events the pH varied at different stages of the same event. After the rain, samples were sealed in clean bottles that had been pre-conditioned by the University of Virginia scientists (Keene, private communication); they were stored in a refrigerator for post-cruise analyses. Each rain-event sample was divided into three bottles--one to be analyzed by NOAA scientists at Boulder and two to go to the University of Virginia (UV) (0.5 mL of chloroform, $CHCl_3$, was added to one of these twin samples to prevent bacterial reactions). The NOAA samples were analyzed with an ion chromatograph, within a month after the collection. Concentrations of anions Cl^-, NO_3^-, and $SO_4^=$ and cations Na^+, NH_4^+, K^+, Mg^{++}, and Ca^{++} were determined. The UV samples were analyzed 6 months after collection. In addition to common anions and cations, organic ions were also measured by UV scientists (if the sample was

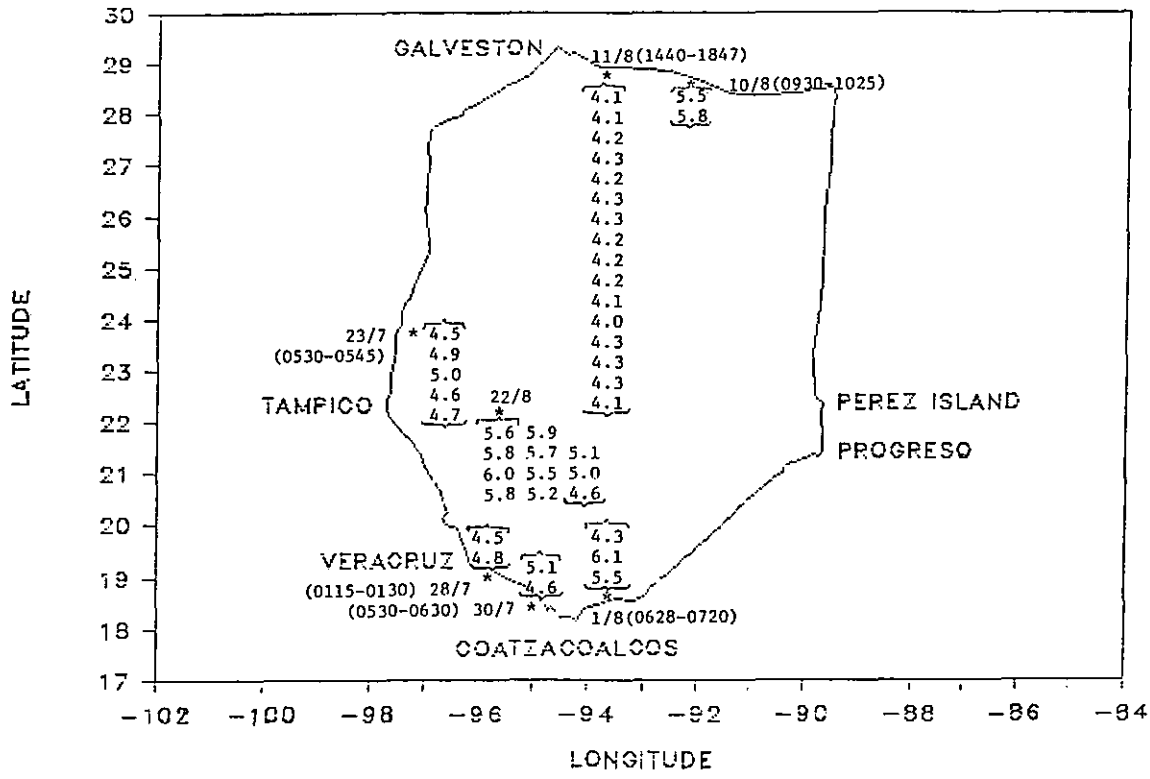

Figure 1. The pH values of sequential rain samples collected during the cruise (* marks locations where samples were collected).

sufficient). The pH of the samples was measured again in the laboratory. Generally the acidity (hydrogen ion concentration) of rain samples was found to decrease during storage (Fig. 2). The chemical analytical results of rain-event samples are listed in Table 1. NOAA's and UV's analyses showed fair agreement. Comparison between samples with and without $CHCl_3$ showed no systematic trends among all ions. In fact, of the last twin samples collected on 11 August, the sample with $CHCl_3$ showed almost half as much concentration as the one without. No logical explanation can be offered except possible handling error. Rain samples for 23 July and 1 August contained significant amounts of formate and acetate ions. However, these organic ions were absent in the 11 August rain samples. Sequential samples collected on 23 July and 11 August were analyzed by NOAA Scientists, The results are shown in Figs. 3 and 4.

Rain samples were collected by the Mexican team, which encountered three additional rain events on the way home from Galveston to Veracruz. They used an automatic rain collector (Aerochemmetric model 301). The pH and conductivity

Table 1. Ion concentrations of rain samples (mg L^{-1}) measured by the U.S.A. team

Date	Time (local)	Sample	$CHCl_3$	Na^+	NH_4^+	K^+	Mg^{++}	Ca^{++}	Cl^-	NO_3^-	$SO_4^=$	HCO_2^-	$CH_3CO_2^-$	H^+ field lab
23 Jul	0530-0555	NOAA1	-	0.76	0.10	0.06	0.08	0.20	0.74	0.47	0.48	---	---	$3\times10^{-2}/1\times10^{-2}$
		UV1	-	0.76	0.01	0.19	0.09	0.27	0.86	0.32	0.66	---	---	$/2\times10^{-3}$
		UV1	+	0.71	0.10	0.19	0.09	0.66	0.91	0.47	0.82	0.56	0.66	$/2\times10^{-3}$
		UV11	+	0.69	---	0.19	0.09	0.65	---	---	---	---	---	---
01 Aug	0628-0720	NOAA4	-	4.82	0.97	0.68	0.57	1.02	7.34	0.62	4.05	---	---	$8\times10^{-4}/6\times10^{-4}$
		UV4	+	---	1.29	---	---	---	---	---	---	2.83	1.29	$/1\times10^{-2}$
11 Aug	1440-1700	NOAA6	-	9.99	0.08	0.57	1.12	0.68	15.16	2.60	3.02	---	---	$5\times10^{-2}/3.2\times10^{-2}$
		UV6	-	11.50	0.04	0.53	1.35	0.68	20.07	1.58	3.89	---	---	$/2.5\times10^{-2}$
		UV6	+	9.82	0.06	0.50	1.16	1.14	17.14	1.48	4.99	0.00	0.00	$/2.5\times10^{-2}$
		UV6	-	9.22	0.03	0.42	1.10	0.83	9.99	2.19	3.18	---	---	$/3.2\times10^{-2}$
		UV6	+	4.35	0.03	0.26	0.51	0.42	7.83	0.94	2.21	0.00	0.00	$/2.5\times10^{-2}$

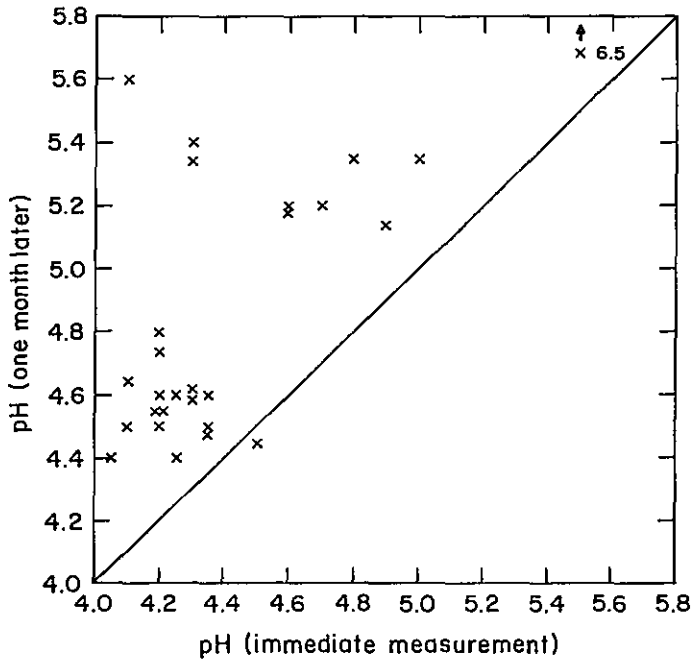

Figure 2. Comparison of pH values of rain samples measured immediately and 1 month later.

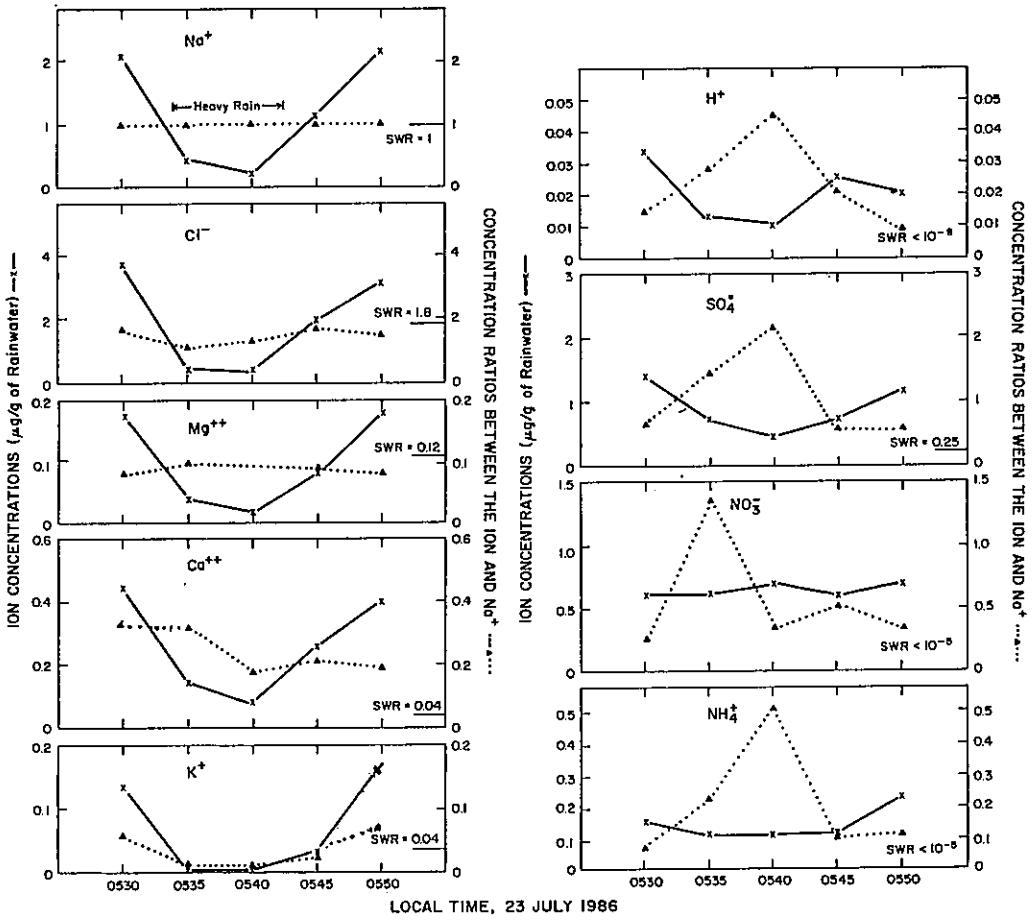

Figure 3. Ion concentrations and concentration ratios with Na^+ of rain samples collected on 23 July 1986.

were measured onboard. Concentrations of $SO_4^=$ and NO_3^- were measured in the University of Mexico (UM) laboratory. Table 2 shows the results. There is good agreement between NOAA and UM data for 23 July; however, on 1 August the UM data for $SO_4^=$ and NO_3^- are ~40% and ~18% higher, respectively, than NOAA's. On 11 August, the UM data for $SO_4^=$ and NO_3^- are ~20% and 40% lower, respectively, than NOAA's. As the data indicate, different collection, treatment, and analysis methods yield different results. To obtain accurate marine precipitation chemical data, rainwater samples must be analyzed immediately after collection. Since we did not have an ion chromatograph onboard the H-02 vessel, the post-cruise analyses may be somewhat uncertain because of sample deterioration and contamination. Nevertheless, all three sets of analyses showed some common findings that rainwater acidities in the Gulf were variable with location and time

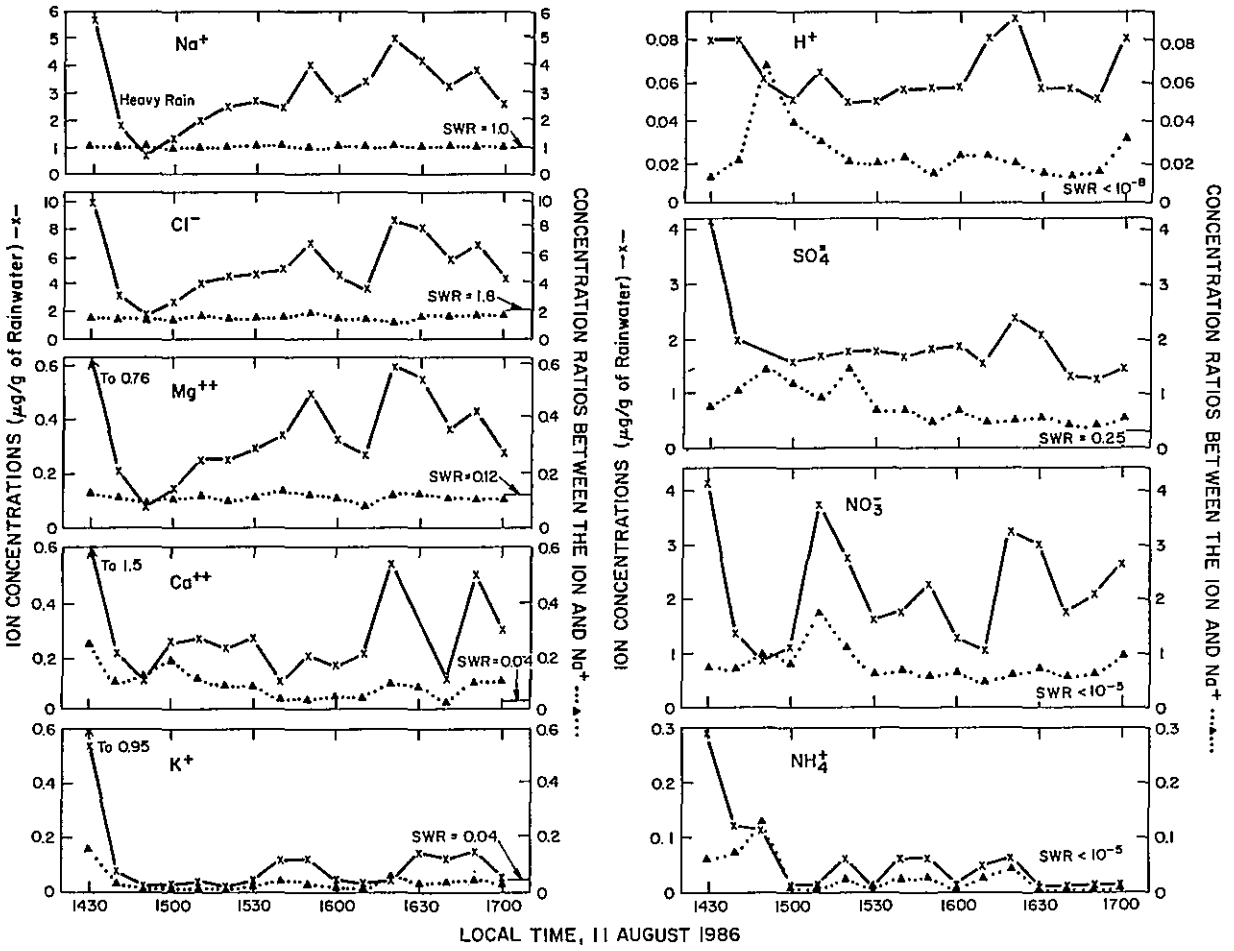

Figure 4. Ion concentrations and concentration ratios with Na^+ of rain samples collected on 11 August 1986.

Table 2. Characteristics of precipitation events measured by the Mexican team

Date	Time (local)	pH	Conductivity (μV)	$SO_4^=$ (mg/L)	NO_3^- (mg/L)
July					
23	0540	5.0	16.35	0.49	0.50
30	0530-0630	4.1	---		0.50
August					
1	0630	5.8	110.4	5.65	1.75
10	0945	5.67	247.0		1.50
11	1437		62.9	2.4	1.45
	1830	4.4			
12	0445-0500	5.88	51.7	4.2	1.50
14	0440-0843	7.22	434.0		5.0
22	0345-0930	5.63	626		1.75
Sequential		5.81	105	5.5	1.00
		6.04	16.84		
		5.80	10.11		
		5.90	15.45		
		5.71	12.83		
		5.53	19.95		
		5.20	17.48	0.6	0.25
		5.21	13.31		
		5.16	17.19		
		5.08	14.07		
		4.96	15.34	0.6	0.30
		4.64	28.7		

as shown in Fig. 1. The most acidic rain (pH ~4.2) was observed south of Galveston and least acidic rain was in the middle of the Gulf (pH ~6.0). The major cation was N_a^+; the concentrations of anions were $Cl^- > SO_4^= > NO_3^-$ regardless of the location. The data suggest that seasalt particles were the dominant components in marine rainwater in spite of the fact that some clouds had a continental origin (see Griffith's paper in this report). The concentration ratios $SO_4^=/Na^+$ and NO_3^-/Na^+ in all rain samples showed much higher values than corresponding seawater ratios (Riley and Chester, 1971), indicating that anthropogenic sulfate and nitrate aerosols had also had significant roles in the precipitation system. The details are discussed in the case studies.

2. CASE STUDIES

On 23 July the ship was north of Tampico. In a 20-min shower that started at 0530, five sequential samples were collected. The ion concentrations in rain samples and ratios between the ions and Na^+ are shown in Fig. 3; seawater ratios (SWR) between the ions are also shown. For ions Na^+, Cl^-, Mg^{++}, Ca^{++}, K^+, H^+, and $SO_4^=$ the concentrations showed a trend: Higher concentrations occurred at the beginning and end of the shower when rainfall rates were lower (~0.5 cm h^{-1}). At the middle of heavy rain (~2 cm h^{-1}) the ions were diluted to yield lower concentrations. Ions NO_3^- and NH_4^+ did not follow this trend and the concentrations remained relatively consistent throughout the event. The ratios H^+/Na^+, $SO_4^=/Na^+$, and NH_4^+/Na^+ had similar trends with maxima 10 minutes after the beginning of the rain; NO_3^-/Na^+ and Ca^{++}/Na^+ had maxima 5 min after; K^+/Na^+ had maxima at the beginning and at the end. However, Cl^-/Na^+ and Mg^{++}/Na were consistent throughout the shower.

On 11 August a prolonged rain occurred from 1430 to 1700. Sequential samples were taken every 10 min. The highest concentrations of ions were found at the beginning. As the rainfall rate increased, the ion concentrations decreased (Fig. 4). When the rain was subsiding the concentrations increased again. The results are evidence that ion concentrations in rain are reversely proportional to rainfall rates, which reflect the liquid water content in clouds.

The ratios Cl^-/Na^+ and Mg^{++}/Na^+ were practically constant throughout the event. As in the 23 July event the ratios were close to the corresponding

ratios in sea water. This indicates that Na^+, Mg^{++}, and Cl^- probably have a common source and common procedures for being incorporated into cloud and precipitation systems. The ratios H^+/Na^+, $SO_4^=/Na^+$, NO_3^-/Na^+, and NH_4^+/Na^+ have greater values than the values of corresponding ratios in sea water. This indicates an enrichment of these ions (from other than a seasalt source) in the rain-developing system. The enrichment factor (E) defined as the ratio between (Ci/Na^+) in rain and (Ci/Na^+) in seawater, is $\sim 10^4$ for H^+, ~4 for $SO_4^=$; $\sim 5 \times 10^3$ for NO_3^-, and $\sim 10^3$ for NH_4^+. The differences between these enrichment factors suggest that these four ions may have diverse sources and strengths. Nonetheless their ratios show a general pattern of low values at the beginning of a rain event, maxima shortly after, and a later decrease to consistent low values. The pattern suggests that these four ions may be incorporated into precipitation by similar mechanisms.

The ratio Ca^{++}/Na^+ is ~5 times higher in rain than in sea water. Its highest values occurred at the early stage of an event. The ratio K^+/Na^+ in rain was close to the ratio in sea water.

3. DISCUSSION

To study precipitation chemistry it is necessary to understand cloud microphysics. Cloud droplets form on cloud condensation nuclei (CCN) at the condensation level. Aerosols, especially hygroscopic particles (e.g., NaCl, $MgCl_2$, $(NH_4)_2SO_4$, NH_4HSO_4, $CaSO_4$) are incorporated into cloud water probably through cloud base-condensation nucleation. As the cloud drops grow the concentration of ions decreases because of dilution. Thus, the ion concentrations are inversely proportional to the liquid water content in a cloud. In marine clouds higher liquid water content generally produces greater rainfall. Our observations agree with the theory that the higher the rainfall rate, the lower the ion concentration. However, if nucleation is the only important mechanism for ion contamination in rain we should observe a constant ratio of ion to Na^+ throughout a rain event. This was almost true for Cl^- and Mg^{++}; but quite different for H^+, $SO_4^=$, NO_3^-, and NH_4^+ (Figs. 3 and 4). The observation suggests that Mg^{++}, and Cl^-, like Na^+, indeed served as CCN incorporated in cloud at cloud base. However for the ions of H^+, $SO_4^=$, NO_3^-, and NH_4^+ present in cloud and rain water, other mechanisms could also have important roles such as in-

cloud scavenging of atmospheric gases and cloud-top entrainments of different air mass.

After a cloud is formed, water-soluble acidic gases (e.g., SO_2 and NO_x) will be continuously adsorbed by cloud drops until a solubility equilibrium is reached. Simultaneously chemical reactions (e.g., oxidation and acidification) may also take place in the drops. As a result, a cloud should be more acidic than the air below, and aged clouds should be more acidic than young clouds. Indeed this was observed by Parungo et al. (1987) and Lazrus et al. (1983). Although NH_3, which is the only important basic gas in the air, may be adsorbed by cloud drops and neutralized acids, the concentrations of NH_3 are generally much less than those of acids, and thus NH_3 may not affect a cloud's acidity significantly. Most clouds do not precipitate, and precipitation is generally initiated by ice nucleation. The clouds in our case studies had a top temperature <-40°C (see Griffith's paper in this report). It is likely that the precipitation was initiated by ice nucleation. When the clouds reach a level at which the temperature is cold enough to activate ice nuclei (IN), then the drops freeze and almost all the contaminants remain in the frozen drops (some less soluble gases, e.g., CO_2, may escape from ice). Once ice crystals appear in a cloud the surrounding liquid drops will evaporate and provide water vapor for ice crystals to grow rapidly because of vapor pressure gradients present between water and ice (Bergeron-Findeisen mechanism). The evaporated drops leave the imbedded particles and gases in the space between the ice crystals. Because ice crystals have higher efficiency for scavenging particles than for scavenging gases, the interim particles including NaCl nuclei may be recaptured by growing and falling ice crystals and leave the gases free in the air. Descending to lower and warmer levels, the ice crystals melt to raindrops. As a result, ratios $SO_4^=/Na^+$ and NO_3^-/Na^+ are low at the start of rainfall as shown in Figs. 3 and 4. However, after the triggering mechanism of ice nucleation, precipitation may proceed by acretion, riming, and coalescence, and heavy rain follows. The raindrops formed by these processes are a combination of individual highly contaminated and aged cloud drops. Thus the ratios of $SO_4^=/Na^+$ and NO_3^-/Na^+ are maxima at the second stage of rainfall. After the aged cloud drops fall off, the clouds approach a static state at which updraft air mass and fallout rain reach an equilibrium. The ratios $SO_4^=/Na^+$ and NO_3^-/Na^+ remain constant at a lower value until the end of the event. Since $SO_4^=$ and NO_3^- are strong acidic

anions, it is reasonable that H^+/Na^+ has a trend similar to that of $SO_4^=/Na^+$ and NO_3^-/Na^+. Qin and Chameides (1986) calculated rainfall rates and concentrations of species dissolved in rainwater for various solubilities (Fig. 5). Our observations of $SO_4^=$ and NO_3^- concentration in rainwater generally agreed with their model calculations in the pattern of evolution. However, the timing showed some difference. This is probably because the rain events we observed were results of cumulus development whereas the model was for stratiform clouds.

The reason for the slightly higher ratios of Ca^{++}/Na^+ and K^+/Na^+ at the beginning of the rainfall could be that these ions were present in the ice nuclei that triggered the precipitation.

In continental precipitation, the major mechanism for incorporating $SO_4^=$ and NO_3^- is probably in-cloud scavenging of precursor gases SO_2 and NO_x, respectively, as reported by many researchers (Hegg and Hobbs, 1981; Scott, 1982; Lazrus et al., 1983; and Parungo et al., 1987). It is important to know if this is also the case with maritime precipitation. Figure 6 and Table 3 compare mass ratios of individual ions and Na^+ in sea water (Riley and Chester, 1971), in atmospheric aerosols, and in rain. The values are the average of all the samples collected in the cruise in each category. Compared with seawater, rainwater has higher ratios for $SO_4^=$, NO_3^-, NH_4^+, K^+, and Ca^{++}; lower ratios for Cl^-; the same ratio for Mg^{++}. The enrichment factors were 3.7 for $SO_4^=$, $>10^3$ for NO_3^-, $>10^3$ for NH_4^+, 1.5 for K^+, 5.3 for Ca^{++}, 1 for Mg^{++}, and 0.9 for Cl^-. The enriched ions in rain can be either anthropogenic or natural or both. It is difficult to distinguish the origins with the available data. However, on the basis of comparison of ion ratios between rainwater and aerosols one can estimate that the enrichment comes either from particle entrainment into clouds through cloud condensation nucleation or from gas scavenging by hydrometeors as shown in Fig. 6. The enrichment factor, $E = (C_i/Na^+)$ in rain $\div$ (C_i/Na^+) in aerosols, was 1.15 for $SO_4^=$; i.e., 87% of $SO_4^=$ in rain comes from sulfate aerosols, and only 13% from SO_2 gas dissolving in hydrometeors. For NO_3^-, E = 1.26, i.e., 80% from aerosols and 20% from NO_x gas. Almost all Mg^{++}, Ca^{++}, K^+, and NH_4^+ in rain came from aerosols. As for Cl^-/Na^+, it decreased 10% in aerosols and another 1% in rain. The explanation is probably that atmospheric gases, e.g., SO_2 and NO_x, reacted with NaCl in aerosols or in cloud drops to replace Cl^-. As SO_2 oxidized to $SO_4^=$ and NO_x oxidized to NO_3^- the acidity increased and

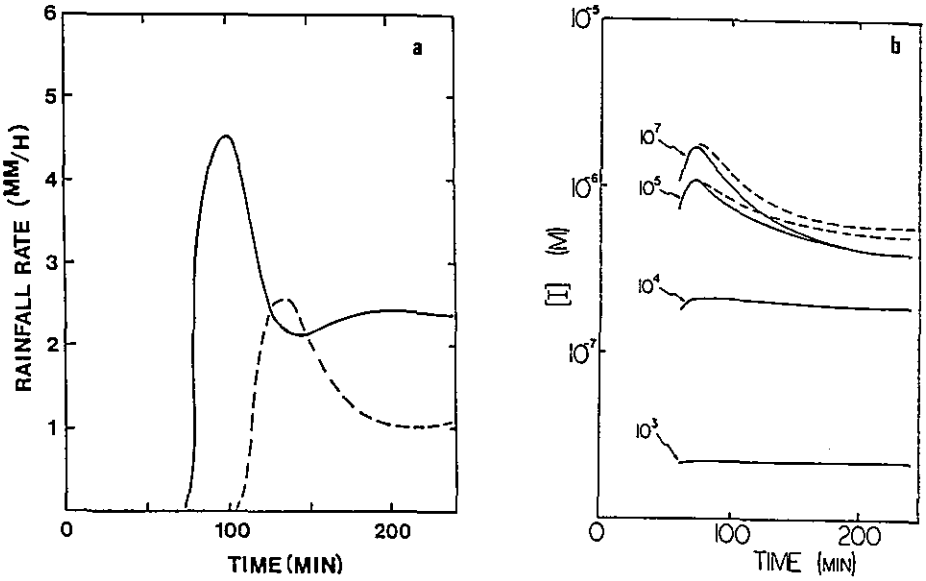

Figure 5. (a) The calculated rainfall as a function of time for updraft velocities 0.1 m/s (solid line) and 0.05 m/s (dashed lines). (b) The calculated concentration (I) in rainwater for various values of solubility constant (Qin and Chameides, 1986).

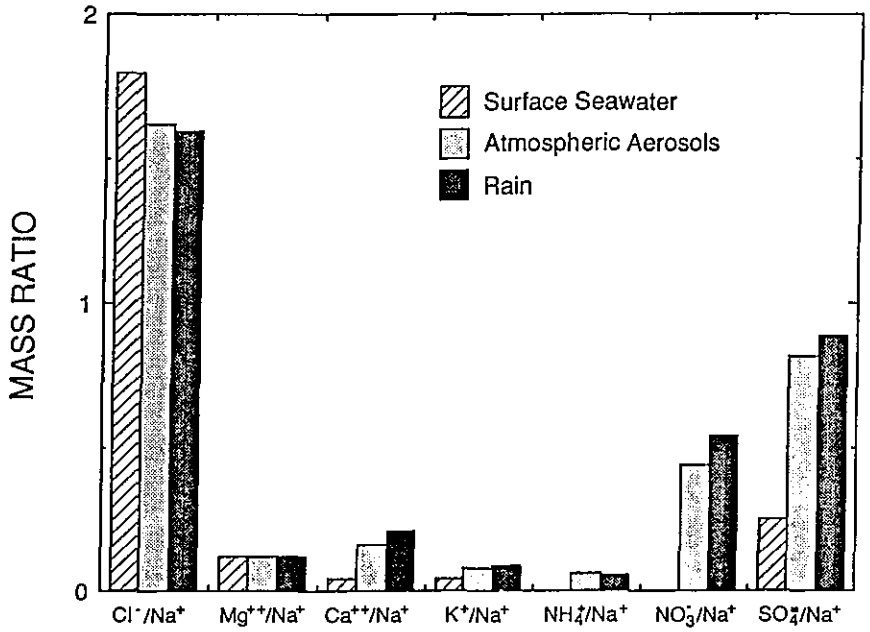

Figure 6. Mass ratios of individual ions to Na^+ in seawater, atmospheric aerosols, and rain.

Table 3. Average ion concentrations (C), ratios (C_i/C_{Na^+}), and enrichment factors (E)

Item	Unit	Na^+	Cl^-	Mg^{++}	K^+	Ca^{++}	HN_4^+	$SO_4^=$	NO_3^-
C_a	$\mu g\ m^3$	2.44	3.94	0.29	0.14	0.48	0.20	1.97	1.94
σ (n=18)	---	2.78	3.64	0.29	0.12	0.39	0.12	1.28	0.91
C_r	ppm	3.18	5.12	0.38	0.20	0.67	0.29	2.97	1.72
σ (n=27)	---	2.61	3.39	0.31	0.14	1.07	0.14	1.39	1.04
C_s	g/kg	10.76	19.53	1.29	0.39	0.41	10^{-4}	2.71	10^{-4}
$[C_i/C_{Na^+}]_a$*	---	1.00	1.62	0.12	0.06	0.14	0.07	0.81	0.43
$[C_i/C_{Na^+}]_r$*	---	1.00	1.61	0.12	0.06	0.21	0.06	0.93	0.54
$[C_i/C_{Na^+}]_s$*	---	1.00	1.80	0.12	0.04	0.04	10^{-5}	0.25	10^{-5}
E(a/s)	---	1.00	0.90	1.00	1.50	3.50	7×10^3	3.24	4×10^4
E(r/a)	---	1.00	0.99	1.00	1.00	1.50	0.86	1.15	1.26
E(r/s)	---	1.00	0.89	1.00	1.50	5.25	10^3	3.72	10^5

* a is aerosol; r is rainfall; s is seawater (C_s from Riley and Chester, 1971).

thus released HCl gas into the atmosphere. These phenomena were discussed by Lodge et al. (1960) and Parungo et al. (1986). Our present data indicate that 90% of the replacement took place in aerosol form and only 10% was in cloud water. The result is quite different from continental precipitation in which we had found that a dominant portion of $SO_4^=$ and NO_3^- in cloud and in rain came from in-cloud scavenging of SO_2 and NO_x (Lazrus et al., 1983; Rosinski et al., 1984; Parungo et al., 1987). The differences are probably caused by different environments. In the maritime atmosphere, there are abundant wet, alkaline sea-salt particles, which can adsorb acidic gases such as SO_2 and NO_x. Followed by oxidation on the particles, the gases are converted to $SO_4^=$ and NO_3^- respectively, forming a layer of solid coating. Furthermore, the high humidity over the sea surface may also accelerate gas-to-particle conversion. Therefore, little of the gases remained to be lifted to the cloud condensation level to be scavenged by cloud drops. On the other hand, in the dry continental air mass,

gases probably have longer life and thus remain in higher concentration at cloud level to be scavenged. In the case of NO_x, even if it is oxidized, neutralized, and converted to particles NH_4NO_3 below clouds, being unstable in dry air it will decompose to HNO_3 and NH_3 gases. Only when the relative humidity is higher than 62% (its deliquescence point) can NO_x exist as wet particles. Therefore, most $SO_4^=$ and most NO_3^- in continental rain water are incorporated through the gas phase, whereas in maritime precipitation most $SO_4^=$ and NO_3^- are incorporated through aerosol phases.

References

Hegg, D.A., and P.V. Hobbs, 1981: Cloud water chemistry and production of sulfate in cloud. Atmos. Environ., 15:1597-1604.

Lazrus, A.L., P.L. Haagenson, G.L. Kok, B.J. Huebert, C.W. Dreitzberg, G.E. Likens, V.V. Mohnen, W.E. Wilson, and J.W. Winchester, 1983: Acidity in air and water in a case of warm frontal precipitation. Atmos. Environ., 17:581-591.

Lodge, J.P., P. MacDonald, and E. Vihman, 1960: A study of the composition of marine atmosphere. Tellus, 12:184-187.

Parungo, F.P., C.T. Nagamoto, J. Rosinski, and P.L. Haagenson, 1986: A study of marine aerosols over the Pacific Ocean. J. Atmos. Chem., 4:199-226.

Parungo et al., 1987: A study of mechanisms of acid rain formation. J. Atmos. Sci. (in press).

Qin, Y., and W.L. Chameides, 1986: The removal of soluble species by warm stratiform clouds. Tellus, 38B:285-299.

Riley, J.P., and R. Chester, 1971: Introduction to Marine Chemistry. Academic Press, London and New York, 465 pp.

Rosinski, J., B. Gandrud, C. Nagamoto, and F. Parungo, 1984: Cumulative chemical composition of atmospheric cloud condensation nuclei. J. Aerosol. Sci., 15:709-718.

Scott, B.C., 1982: Predictions of in-cloud conversion rates of SO_2 to SO_4 based upon a simple chemical and kinematic storm model. Atmos. Environ., 16:1735-1752.

WET AND DRY DEPOSITION OF AEROSOLS

Farn P. Parungo

1. INTRODUCTION

There are two major aerosol sink mechanisms: (a) Wet deposition, which encompasses all processes involving transport of aerosols from air to Earth's surface through precipitation systems; (b) dry deposition, which denotes all fallout processes (except scavenging by rain or snow), such as inertial impact, sedimentation, phoresis, and electric effect. Since we measured many ions' concentrations in aerosol and rain samples collected in the Gulf, we can use these data to estimate wet and dry deposition from air to sea in the region. However, our cruise lasted only 1 month. Sample numbers were limited, and chemical analytical data might not be very representative. Therefore, the estimates should be considered indicative rather than conclusive.

2. DRY DEPOSITION

The rate of dry deposition depends on aerosol concentration and size distribution, the characteristics of the receiving surface, and meteorological effects near the surface. Because of the difficulties of measuring all these parameters, most attempts to determine dry deposition rates directly have resulted only in vast uncertainties (Wesely and Williams, 1981; Sievering et al., 1982). Modeling results of deposition velocity have also presented serious problems, especially among the small particles ($d < 1$ μm) as discussed by Sievering (1984). As a result, dry deposition is not yet completely understood. However, because our measurements of atmospheric aerosols' size distributions (Nagamoto and Parungo, in this report, Sec. II) showed that large particles ($d > 1$) were heavily represented in total aerosol mass, it is probably accurate to use model results, such as those reported by Slinn and Slinn (1980), shown in Fig. 1, to estimate aerosol mass fluxes from air to sea.

During most of the cruise, the sea was calm and the average wind was ~5 m s^{-1} (~10 kn, Fig. 2). The relative humidities measured onboard were

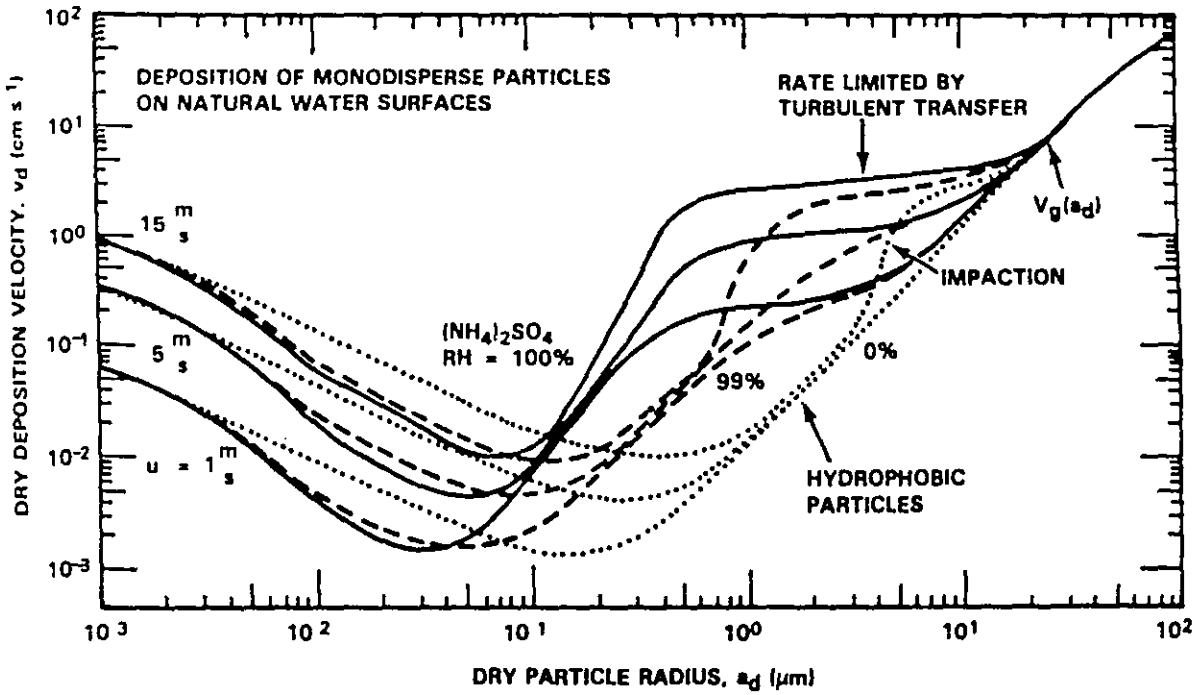

Figure 1. Theoretical predictions of the influence of wind speed and of particle growth by water-vapor condensation, for particle deposition to natural waters. (From Slinn and Slinn, 1980.)

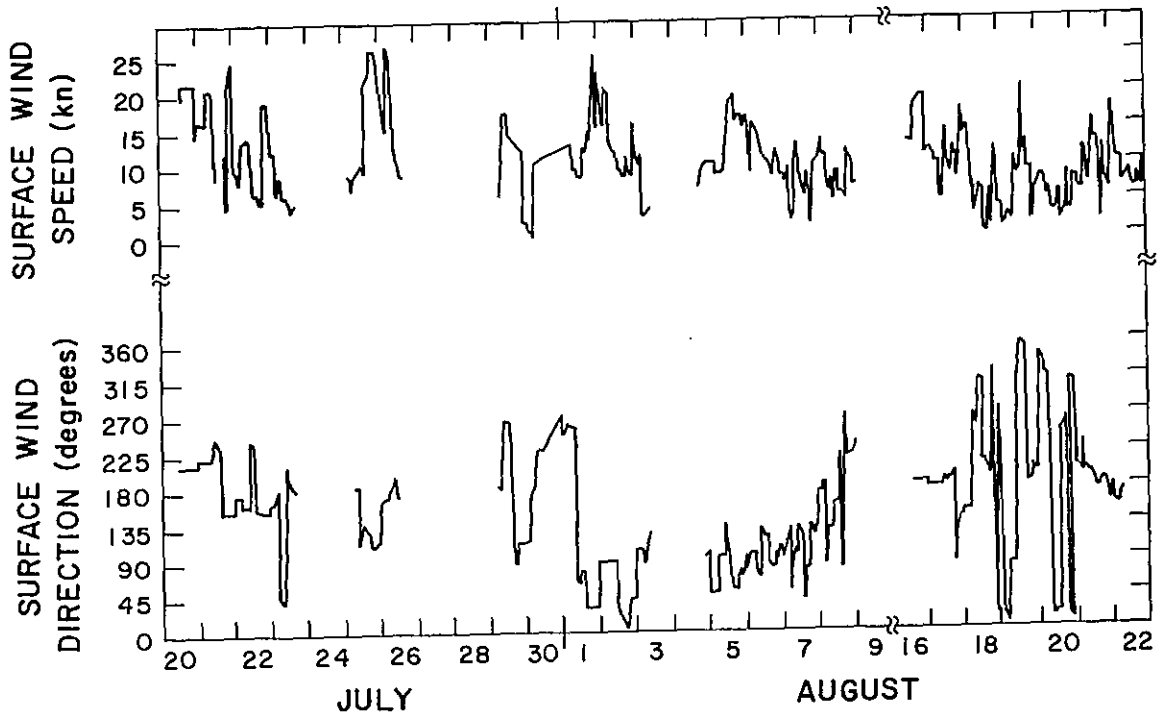

Figure 2. Surface wind direction and wind speed measured during the cruise.

72-90%, and the pressure ranged from 1005 to 1017 mb (Fig. 3). Thus, both sea surface and atmosphere were relatively consistent in these parameters. According to the model calculation, the dry deposition velocity (V_d) should be 1 cm s^{-1} (Fig. 1). The total suspended particle (TSP) mass concentration (C) measured by Bravo et al. (in this report, Sec. II) had an average of 25.25 μg m^{-3}. Since air-to-sea mass flux $F = V_dC$, the total flux was estimated at 0.25 μg m^{-2} s^{-1}, which was equivalent to 90 ng cm^{-2} h^{-1}, or ~8 g m^{-2} y^{-1} (y for year). Since the area of the Gulf of Mexico is 1.5×10^7 km^2, the total dry deposition was estimated to be 120 Tg y^{-1}. McDonald et al. (1982) estimated that when windspeed (W) was 3.4 m s^{-1} the salt aerosol concentration (C_a) was 2.7 μg m^{-3}, air-to-sea flux (F) was 8 ng cm^{-2} h^{-1}, when W = 6.5 m s^{-1}, C_a = 14 μg m^{-3}, and F = 170 ng cm^{-2} h^{-1}; when W = 10 m s^{-1}, C_a = 18 μg m^{-3} and F = 410 ng cm^{-2} h^{-1}. Our estimate of flux fitted in McDonald's general frame. However, Bravo et al's. TSP measurements over the Gulf included not only sea salt but also natural and anthropogenic particles from the surrounding land. Thus the average TSP concentration (25.25 μg m^{-3}) was more than double McDonald et al.'s. measurement of sea salt particles under similar windspeed. Indeed, Nagamoto and Parungo (in this report, Sec. II) observed with SEM-XES that <50% of TSP contained Na and Cl, and most particles consisted of crustal elements, e.g., Si, Al, Fe. Madel and Parungo's data (in this report, Sec. II) showed that the average total ion concentration was 10.50 μg m^{-3}. This means that insoluble particle concentration was 14.75 μg m^{-3}, which is >1.4 times the concentration of sea salt particles. On the basis of these data we can calculate that the flux from air to sea is ~10.42 μg m^{-2} s^{-1} for sea salt particles and ~14.83 μg m^{-2} s^{-1} for insoluble particles.

To estimate the dry deposition flux of individual ions it is necessary to consider each ionic particle size distribution. For Na^+, Cl^-, Mg^{++}, K^+, Ca^{++}, and NO_3^-, we observed mean-mass diameters of ~1 μm; thus we can still use V_d = 1 cm s^{-1} to calculate their fluxes. However, $SO_4^=$ particles had two modes in particle mass distribution, one at d = 0.1 μm and the other at d = 1 μm. Both appear almost equal in weight. We should calculate 50% at $V_d = 10^{-2}$ cm s^{-1} and 50% at V_d = 1 cm s^{-1}. Thus only the large sulfate particles are important for dry deposition. As for NH_4^+, almost all particles were associated with small sulfate particles (Gavenhorst et al., 1979); thus

72-90%, and the pressure ranged from 1005 to 1017 mb (Fig. 3). Thus, both sea surface and atmosphere were relatively consistent in these parameters. According to the model calculation, the dry deposition velocity (V_d) should be 1 cm s^{-1} (Fig. 1). The total suspended particle (TSP) mass concentration (C) measured by Bravo et al. (in this report, Sec. II) had an average of 25.25 μg m^{-3}. Since air-to-sea mass flux $F = V_dC$, the total flux was estimated at 0.25 μg m^{-2} s^{-1}, which was equivalent to 90 ng cm^{-2} h^{-1}, or ~8 g m^{-2} y^{-1} (y for year). Since the area of the Gulf of Mexico is 1.5×10^7 km^2, the total dry deposition was estimated to be 120 Tg y^{-1}. McDonald et al. (1982) estimated that when windspeed (W) was 3.4 m s^{-1} the salt aerosol concentration (C_a) was 2.7 μg m^{-3}, air-to-sea flux (F) was 8 ng cm^{-2} h^{-1}, when W = 6.5 m s^{-1}, C_a = 14 μg m^{-3}, and F = 170 ng cm^{-2} h^{-1}; when W = 10 m s^{-1}, C_a = 18 μg m^{-3} and F = 410 ng cm^{-2} h^{-1}. Our estimate of flux fitted in McDonald's general frame. However, Bravo et al's. TSP measurements over the Gulf included not only sea salt but also natural and anthropogenic particles from the surrounding land. Thus the average TSP concentration (25.25 μg m^{-3}) was more than double McDonald et al.'s. measurement of sea salt particles under similar windspeed. Indeed, Nagamoto and Parungo (in this report, Sec. II)

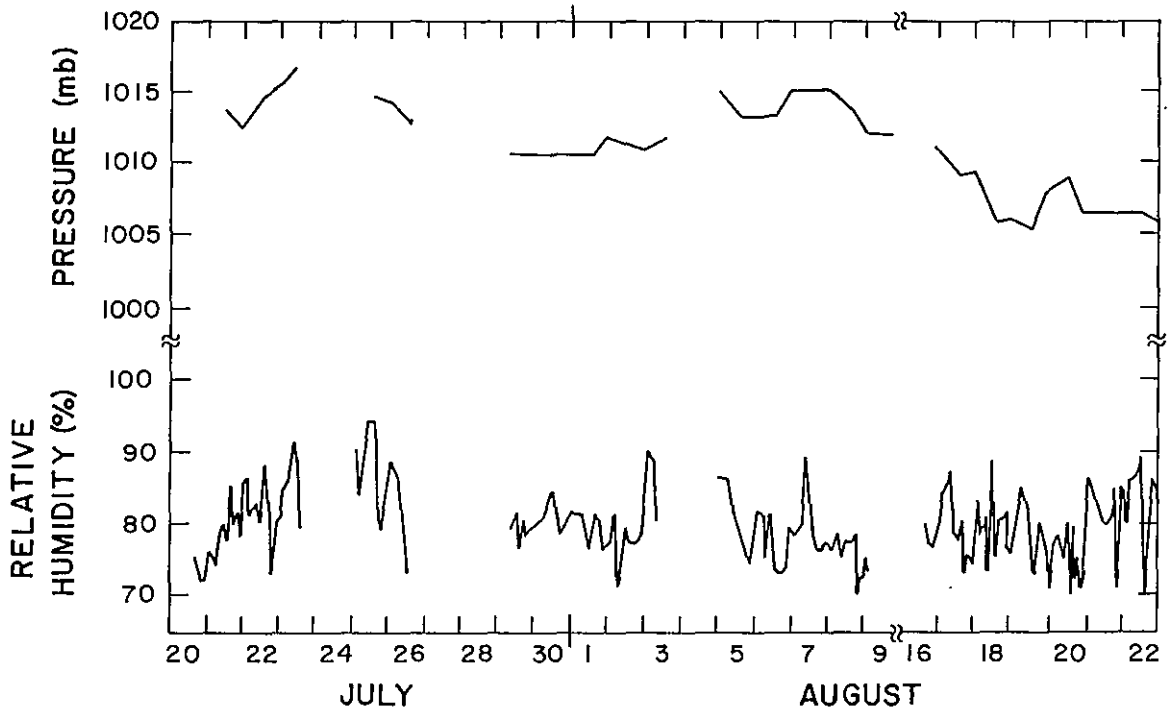

Figure 3. Surface pressure and relative humidity measured during the cruise.

observed with SEM-XES that <50% of TSP contained Na and Cl, and most particles consisted of crustal elements, e.g., Si, Al, Fe. Madel and Parungo's data (in this report, Sec. II) showed that the average total ion concentration was 10.50 $\mu g\ m^{-3}$. This means that insoluble particle concentration was 14.75 $\mu g\ m^{-3}$, which is >1.4 times the concentration of sea salt particles. On the basis of these data we can calculate that the flux from air to sea is ~10.42 $\mu g\ m^{-2}\ s^{-1}$ for sea salt particles and ~14.83 $\mu g\ m^{-2}\ s^{-1}$ for insoluble particles.

To estimate the dry deposition flux of individual ions it is necessary to consider each ionic particle size distribution. For Na^+, Cl^-, Mg^{++}, K^+, Ca^{++}, and NO_3^-, we observed mean-mass diameters of ~1 μm; thus we can still use V_d = 1 cm s^{-1} to calculate their fluxes. However, $SO_4^=$ particles had two modes in particle mass distribution, one at d = 0.1 μm and the other at d = 1 μm. Both appear almost equal in weight. We should calculate 50% at $V_d = 10^{-2}$ cm s^{-1} and 50% at V_d = 1 cm s^{-1}. Thus only the large sulfate particles are important for dry deposition. As for NH_4^+, almost all particles were associated with small sulfate particles (Gavenhorst et al., 1979); thus $V_d \sim 10^{-2}$ cm s^{-1} and dry deposition is relatively unimportant. The calculated results of dry deposition (D_{dry}) of individual ions are listed in Table 1.

3. WET DEPOSITION

The average concentrations (C_R) of individual ions for 27 rain samples collected in the Gulf are also listed in Table 1. Since climatological data show that the rainfall in coast cities, e.g., Galveston and Veracruz, averages ~110 cm y^{-1}, the wet deposition, (D_{wet}) = C_R × 110 g $m^{-2}\ y^{-1}$, was calculated. The results are shown in Table 1. However, one must note the following: (a) The data include not only soluble particles but also gases, e.g., SO_2 and NO_x washed down by rain. (b) Insoluble particles are excluded. (c) C_R is not the annual average; it is merely the average of several rain events that occurred during the cruise. Nonetheless, we can make a crude comparison beween wet and dry deposition. The ratios between wet and dry deposition (Table 1) are 4.5 to 5.0 for Na^+, Cl^-, Mg^{++}, K^+, and Ca^{++}; 5.8 for $NO_3^=$; 10 for $SO_4^=$; and 20 for NH_4^+. These ratios suggest that in this Gulf region wet deposition is 4-20 times more efficient than dry deposition for transporting aerosols from air to

Table 1. Deposition of ions in aerosols

Parameter	Unit	Na^+	Cl^-	Mg^{++}	K^+	Ca^{++}	NH_4^+	$SO_4^=$	NO_3^-
C_a	$\mu g/m^3$	2.44	3.94	0.29	0.14	0.48	0.20	1.97	1.04
σ (n=18)	---	2.78	3.64	0.29	0.12	0.39	0.12	1.28	0.91
D_{dry}	$g/m^2/y$	0.78	1.26	0.09	0.04	0.15	0.01	0.33	0.33
C_R	ppm	3.18	5.12	0.38	0.20	0.67	0.19	2.97	1.72
σ (n=27)		2.61	3.39	0.31	0.14	1.07	0.14	1.39	1.04
D_{wet} (R=1.1 m/y)	$g/m^2/y$	3.5	5.9	0.4	0.2	0.7	0.2	3.3	1.9
D_{wet}/D_{dry}	---	4.5	4.7	4.5	5.0	4.7	20	10	5.8
$W=\rho C_r/C_a$	$\times 10^3$	1.56	1.56	1.57	1.71	1.67	1.20	1.81	1.99
C_c (L=1 g m^3)	ppm	2.44	3.94	0.29	0.14	0.48	0.20	1.97	1.04
C_c (L=2 g m^3)	ppm	1.22	1.97	0.15	0.07	0.20	0.10	0.99	0.52
In-cloud Scav.									
max	%	77	77	76	70	72	100	66	61
min	%	39	39	38	35	35	50	33	31
mean	%	58	58	57	53	54	75	50	46
Bl-cloud Scav.									
max	%	61	61	62	65	65	50	67	69
min	%	23	23	24	30	28	0	34	39
mean	%	42	42	43	47	46	25	50	54

sea. This is especially so with the aerosols that have gaseous precursors, e.g., NH_4^+, $SO_4^=$, and NO_3^-.

To investigate wet depositon of aerosols, a term "washout factor" or "scavenging ratio" is often used by researchers (e.g., Engelmann, 1970; Duce and Woodcock, 1979):

$$W = \rho_a \, C_r/C_a \ .$$

where C_r = concentration of a species in rain ($\mu g/g$ of water),
C_a = concentration of a species in ground-level air ($\mu g/m^3$ of air),
ρ = density of air $\sim 1.2 \times 10^3$ g/m^3 of air at sea level.

W is dimensionless; it does not have any physical meaning by itself. However, it is convenient for assessing the relative washout efficiencies by rain among various species. Duce and Woodcock (1979) reported that W increases with mass-mean radius of aerosol particles. Ng and Patterson (1981) found that the reverse was true. Buat-Menard et al. (1982) observed no particular relationship between W and particle size. It appears that washout efficiency is more complex than a simple particle size effect. Our calculations of W for Na^+, Cl^-, and Mg^{++} were within a narrow range (1.55 to 1.57) $\times 10^3$. Although NH_4^+ and SO_4^+ were present in most small particles ($d < 0.5$ μm), the values of W for NH_4^+ (1.90) and $SO_4^=$ (1.70) are higher than for sea salt particles. NO_3^-, contained mostly in large particles, also has high W (1.99). We believe that the high W for these ions is caused by precursor gases that have been incorporated into cloud drops or raindrops and converted to corresponding salt ions to contribute additional concentrations.

Junge (1963) divided wet deposition into two steps: (a) in-cloud scavenging which includes condensation nucleation, the Facy-effect, and Brownian motion; (b) below-cloud scavenging, which includes capture and evaporation. He named the former "rainout" and the latter "washout." Both terms are misleading; we prefer to use the terms in-cloud and below-cloud scavenging. To investigate in-cloud scavenging of aerosols, one must collect cloud water and analyze its chemical composition as in the experiments conducted by Parungo et al. (1987). Since we did not have the aircraft facility for such collection in this project, we estimated cloud chemical concentrations on the basis of

aerosol data. We simulated surface air being updrafted to condensation level and forming clouds, and assumed that all particles in this air parcel are scavenged into cloud drops. [As indicated by Junge (1963), the scavenging efficiency is 0.9 - 1.0 for marine aerosols.] The concentrations of various ions in cloud water depend on liquid water content in a cloud. Most clouds do not precipitate because of insufficient water or lack of ice nuclei. For raining clouds, the liquid water content appears to be fairly constant and varies between 1 and 2 g m^{-3} (Mason, 1957). Ignoring the slight changes in volume caused by pressure changes at various altitudes we let $C_C = C_a/L$, where C_a = concentration in air ($\mu g\ m^{-3}$), L = liquid water content (g m^{-3}), and C_C = concentration in cloud ($\mu g/g$ of water). We calculated C_C of various ions at L = 1 g m^{-3} (lower limit) and 2 g m^{-3} (upper limit) (Table 1). The results are the likely concentration range in clouds as approximated by aerosol concentrations at the surface. Since we measured the ion concentrations in rain (C_R), the difference between C_R and C_C will be below-cloud scavenging (C_B), $C_B = C_R - C_C$. Lacking measurements of liquid water content in clouds, we could only estimate that in-cloud scavenging for most inorganic ions was between 30% and 70% of total scavenging; the estimate for below-cloud scavenging was similar. (This estimate method may be inaccurate for ions, e.g., $SO_4^=$, NO_3^-, and NH_4^-, because precursor gases, in addition to aerosols, were incorporated in the precipitation system.) If we use the mean L = 1.5 g m^{-3}, in-cloud scavenging is almost equal to below-cloud scavenging. It appears that both in-cloud and below-cloud scavenging are important processes for wet deposition.

4. CONCLUSION

(1) The Gulf of Mexico is a large sink of atmospheric aerosols. The dry deposition is 120 Tg y^{-1}. The fluxes are 8 g m^{-2} y^{-1} for total particles, 3 g m^{-2} y^{-1} for salt (soluble) particles, and 5 g m^{-2} y^{-1} for insoluble particles. The wet deposition flux for total soluble particles is 16 g m^{-2} y^{-1}. The combined aerosol influx from air to sea may affect surface water ecology and ocean sedimentation.

(2) The wet deposition of inorganic ions in aerosols is 4-20 times higher than dry deposition. This is probably due to the large amount of rainfall in the Gulf region.

(3) Washout factors for Na^+, Cl^-, and Mg^{++} are very close to one another (1.56 to 1.57 x 10^3), indicating that these ions were incorporated into precipitation by similar mechanisms (i.e., cloud-base condensation nucleation). Washout factors for K^+ (1.71 x 10^3), Ca^{++} (1.67 x 10^3), SO_4 (1.80 x 10^3), and NO_3^- (1.99 x 10^3) are higher, indicating that cloud-top entrainment or precursor-gas enrichment in clouds provided additional ion concentrations in rain.

(4) Estimates of in-cloud and below-cloud scavenging of various ions suggest that both mechanisms have equal importance in the precipitation chemistry of the region.

REFERENCES

Buat-Menard, P., U. Ezat, and A. Gaudichet, 1982: Size distribution and minerology of alumino-silicate dust in air and rain. 4th Internal. Conf. on Precipitation, Santa Monica, CA.

Duce, R. A., and A. H. Woodcock, 1979: Difference in chemical composition of atmospheric sea salt particles produced in the surf zone and on the open sea in Hawaii. Tellus, 23:427-435.

Engelmann, R. J., 1970: Scavenging prediction using ratios of concentrations in air and in precipitation. Precipitation Scavenging, U.S. Atomic Energy Commission, 475-455.

Gavenhorst, G., K. P. Miller, and H. Franken, 1979: Inorganic nitrogen over the north Atlantic. Gesellschaft für Aerosolforschung, 7:182-187.

Junge, C. E., 1963: Air Chemistry and Radioactivity. Academic Press, New York, 382 pp.

Mason, B. J., 1957: The Physics of Clouds. Oxford Univ. Press, London.

McDonald, R. L., C. K. Unni, and R. A. Duce, 1982: Estimation of atmospheric sea salt dry deposition wind speed and particle size dependence. J. Geophys. Res., 87:1246-1250.

Ng, A., and C. Patterson, 1981: Natural concentration of lead in ancient Arctic and Antarctic ice. Geochim. Cosmochim. Acta, 45:2109-2122.

Parungo, F., C. Nagamoto, and R. Madel, 1987: A study on mechanisms of acid rain formation. J. Atmos. Sci. (in press).

Slinn, S. A., and W. G. N. Slinn, 1980: Predictions for particle deposition on natural waters. Atmos. Environ. 14:1013-1016.

Sievering, H., 1984: Small-particle dry deposition on natural waters: Modeling uncertainty. J. Geophys. Res., 89:9679-9681.

Sievering, H., J. Eastman, and J. A. Schmidt, 1982: Air-sea particle exchange at near-shore oceanic site. J. Geophys. Res., 87:11,027-11,037.

Wesely, M. L., and R. M. Williams, 1981: Eddy correlation measurements of particle fluxes over Lake Michigan. Annual Report Argonne Nat. Lab., Argonne, Ill, 36-38.

PART IV. SEA WATER ANALYSES

ANTICYCLONIC RING DISPLACEMENT IN THE WESTERN GULF OF MEXICO

Luis D. Salastorrea and Diego López Veneroni

1. INTRODUCTION

The circulation in the eastern Gulf of Mexico is dominated by the Loop Current, which forms a continuous system between the current that enters through the Yucatan Channel and the out-going flow at the Straits of Florida. Leipper (1970) suggested that when this current attains its maximum penetration into the gulf, anticyclonic rings (ACRs) may become detached from its northern edge; Cochrane (1972) concluded that the growth of two cyclonic meanders (from Campeche Bank and Florida Shelf) produce an ACR separation.

Ichiye (1962) indicated that there is a lack of continuity in the flow between the eastern and western parts of the Gulf of Mexico; instead, water transport seems to occur by the westward migration of detached ACRs (Ichiye, 1962; Cochrane, 1972; Nowlin and Hubertz, 1972). Using historical temperatures averaged by 1° squares and by month, Behringer et al. (1977) proposed that these rings enter the western gulf during the summer. Elliot (1982) characterized a series of ACRs and concluded that they are important in the heat and salt balance of the western gulf. In the western Gulf of Mexico there is a great ACR of permanent character (Ichiye, 1962; Nowlin and McLellan, 1967; Vázquez, 1975), although its position and dimensions may vary. According to Elliot (1982) the migration of ACRs must be taken into consideration in the study of the forcing mechanism for this great ring; Sturges and Blaha (1976) proposed instead that the circulation in the western gulf is maintained by the curl of the wind stress.

Rings of high and low geopotential have been reported for different years and seasons at the northern part of the western gulf (e.g., Austin, 1955; Vázquez, 1975; Elliot, 1982). Merrell and Morrison (1981) noted a two-ring system to the west of 90°W (whose centers were 220 km apart) that occurred in early spring; they supposed that both the ACR and the cyclonic ring (CR) migrated from the eastern gulf and were directly influenced by the wind-induced circulation, particularly by the extension of the Texas shelf current. Almost immediately after, Merrell and Vázquez (1983) observed that this CR had inten-

sified while the ACR had weakened, and suggested that this was due to a severe norther or, alternatively, to the spindown of the ACR as it reached the gulf's western boundary. Apparently the presence of ACRs and CRs is common in the western Gulf of Mexico.

During July and August 1986, on the interdisciplinary cruise of Research Vessel H-02, two series of expendable bathythermograph (XBT) surveys were done in the western gulf, less than a month apart. The temperature structure and the changes that occurred between the two surveys were used to estimate the position and movement of an anticyclonic ring.

2. RESULTS AND DISCUSSION

Figure 1 shows the locations of the XBT stations for 15-17 July 1986. The 34 stations lie on a NNE-SSW section, between 27°45'N, 94°30'W, and 22°30'N, 95°30'W. XBTs were used every 10 miles; thus the horizontal interpolation approximates real behavior. Stations 1-27 have a depth to the bottom of more than 1000 fathoms; stations 28-34 lie on the continental slope.

Figure 2 and Table 2 shows the route of the four-section survey on 17-22 August 1986. The 100 stations lie between latitudes 27°00'N and 21°30'N, and longitudes 94°00'W and 96°30'W. Most of the stations have a depth to the bottom of more than 1000 fathoms.

The isotherm distributions from the surface to a depth of 800 m for the July section, and for stations 1-25 (section AB) in August, are shown in Figs. 3 and 4. The slopes of the subsurface isotherms (22°-6°C) in the two surveys show the presence of an ACR off the western boundary of the Gulf of Mexico, whose center was displaced in 1 month. The positions of the ring's center and edges, and the depths of selected isotherms for July and August are compared in Table 1. Temperature observations during July were limited to only one section; for the August survey four transects were used, which give a vertical and horizontal appreciation of the data set.

Table 1. Positions of an ACR and depths of selected isotherms in July and August 1986

Isotherm (°C)	Depth-July (m)			Depth-August (m)	
	Center	N. edge	S. edge	Center	N. edge
	24°15'N 95°05'W	26°05'N 94°40'W	22°35'N 94°20'W	23°00'N 94°58'W	26°01'N 94°15'W
20	250	94	94	255	105
14	420	178	233	420	155
8	700	356	417	720	313

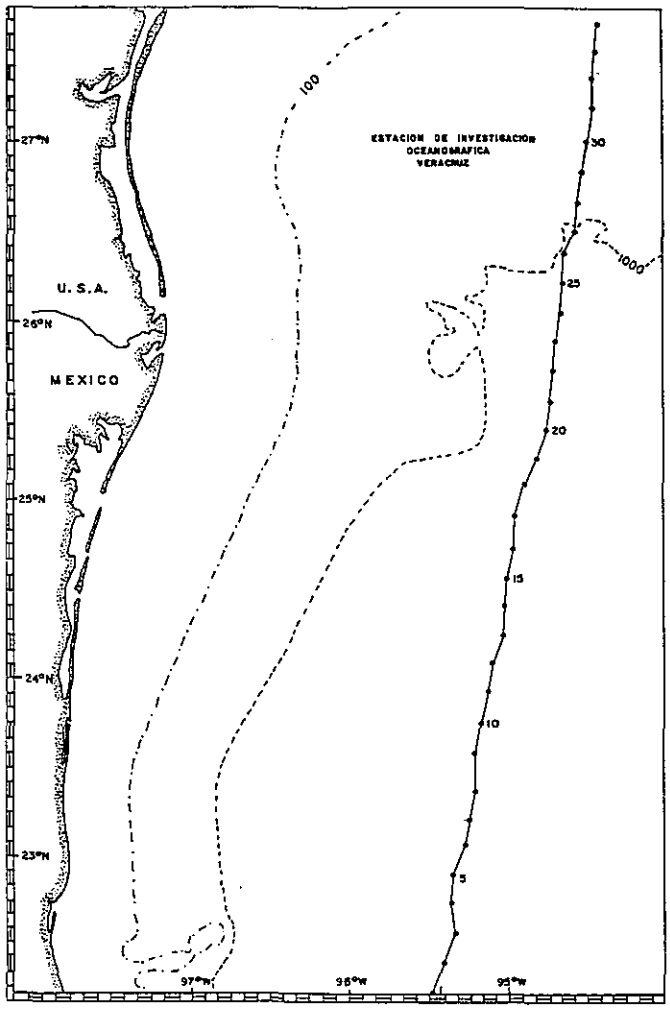

Figure 1. Station locations, 15-17 July 1986.

Table 2. Station locations on 17-22 August

Station No.	Latitude N	Longitude W	Time	Date	Depth (m)
1	26°56.0'	94°24'	18:52	17 Aug 86	209.4
2	26°46.2'	94°23.1'	20:00	"	203.3
3	26°36.3'	94°21.6'	21:10	"	191.5
4	26°26.43'	94°19.6'	22:20	"	174.0
5	26°16.1'	94°17.8'	23:33	"	167.5
6	26°06.0'	94°16.2'	00:46	18 Aug 86	158.3
7	25°56.1'	94°14.3'	01:54	"	158.0
8	25°46.2'	94°11.6'	03:05	"	163.9
9	25°35.9'	94°08.4	04:17	"	167.9
10	25°27.1'	94°06.0'	05:22	"	200.8
11	25°17.9'	94°03.8'	06:34	"	235.3
12	25°07.9'	94°02.3'	07:45	"	231.6
13	24°57.9'	94°01.7'	09:00	"	278.3
14	24°47.2'	94°00.5'	10:20	"	302.8
15	24°38.0'	94°02.7'	11.28	"	31 .2
16	24°28.1'	94°05.2'	12:42	"	327.8
17	24°18.4'	94°08.0'	13:58	"	331.5
18	24°07.3'	94°11.1'	15:18	"	335.9
19	23°58.3'	94°14.7'	16:26	"	332.3
20	23°49.2'	94°17.8'	17:31	"	337.6
21	23°39.2'	94°21.0'	18:43	"	353.9
22	23°29.2'	94°24.5'	19:50	"	366.2
23	23°19.0'	94°27.5'	21:00	"	375.5
24	23°09.2'	94°30.0'	22:05	"	389.1

Table 2. Station locations on 17-22 August (continued)

Station No.	Latitude N	Longitude W	Time	Date	Depth (m)
25	23°00.0'	94°32.8'	23:07	10 Aug 86	399.4
26	22°54.3'	94°37.5'	00:08	19 Aug 86	421.2
27	22°56.7'	94°47.4'	01:19	"	420.4
28	22°59.5'	94°57.9'	02:30	19 Aug 86	418.9
29	23°07.2'	95°01.5'	03:54	"	421.2
30	23°16.0'	94°58.0'	05:05	"	406.1
31	23°26.1'	94°55.8'	06:16	"	388.1
32	23°36.2'	94°52.3'	07:29	"	362.2
33	23°46.1'	94°49.2'	08:40	"	348.4
34	23°56.2'	94°47.5'	09:51	"	342.7
35	24°06.0'	94°45.4'	10:57	"	
35	24°07.0'	94°44.9'	11.10	"	325.4
36	24°17.3	94°42.5'	12:16	"	320.7
37	24°27.6'	94°39.9'	13:28	"	312.0
38	24°37.3'	94°37.4'	14:35	"	312.4
39	24°46.9'	94°33.0'	15:45	"	310.5
40	24°55.7'	94°29.2'	16:51	"	293.0
41	25°01.6'	94°39.0'	18:21	"	293.3
42	25°02.0'	94°40.5'	18:35	"	285.3
43	25°05.0'	94°49.1'	19:32	"	265.5
44	25°08.1'	94°58.5'	20:44	"	281.5
45	24°59.4'	95°02.8'	22:02	"	285
46	24°51.5'	95°04.8'	22:58	"	299
47	24°47.4'	95°06.1'	23:30	"	293

Table 2. Station locations on 17-22 August (continued)

Station No.	Latitude N	Longitude W	Time	Date	Depth (m)
48	24°42.0'	95°08.0'	00:05	20 Aug 86	286
49	24°32.1'	95°11.4'	01:15	"	298.6
50	24°23.7'	95°14.0'	02:15	"	304.6
51	24°14.1'	95°16.9'	03:18	"	331.7
52	24°04.3'	95°19.8'	04:20	"	335.4
53	23°54.9'	95°22.9'	05:22	"	345
54	23°42.4'	95°26.7'	06:42	"	368
55	23°34.8'	95°28.8'	07:35	"	393
56	23°24.9'	95°31.1'	08:43	"	394
57	23°14.9'	95°33.4'	09:51	"	408
58	23°13.6'	95°42.6'	11:11	"	394
59	23°17.1'	95°52.8'	12:20	"	386
60	23°21.0'	96°03.0'	13:34	"	373
61	23°22.9'	96°06.0'	13:52	"	370.384
62	23°26.5'	96°05.2'	14:26	"	380.8
63	23°37.3'	96°01.8'	15:33	"	382.3
64	23°46.0'	95°58.7'	16:35	"	380.4
65	23°56.0'	95°54.8'	17:49	"	370.2
66	24°06.0'	95°51.9	18:56	"	353.1
67	24°07.8'	95°51.0'	19:06	"	345.6
68	24°16.0'	95°50.1'	20:00	"	334.5
69	24°26.0'	95°47.3'	21:09	"	316
70	24°36.0'	95°42.9'	22:23	"	304
71	24°46.1'	95°39.2'	23:31	"	308.1

Table 2. Station locations on 17-22 August (continued)

Station No.	Latitude N	Longitude W	Time	Date	Depth (m)
72	24°57.0'	95°35.9'	00:53	21 Aug 86	295
73	25°09.7'	95°33.3'	02:15	"	276
74	25°16.0'	95°33.0'	03:02	"	266.4
75	25°20.7'	95°40.0'	04:06	"	262.3
76	25°25.8'	95°52.5'	05:27	"	252.3
77	25°26.5'	96°01.3'	06:49	"	245.9
78	25°19.0'	96°04.6'	07:59	"	243.8
79	25°14.5'	96°06.1'	08:35	"	246.2
80	25°06.8'	96°08.6'	09:40	"	234.6
81	24°58.5'	96°11.0'	10:52	"	257.2
82	24°49.0'	96°13.6'	12.11	"	287.7
83	24°30.2'	96°17.7'	14:34	"	326
84	24°26.0'	96°19.4'	15:15	"	322.9
85	24°20.4'	96°20.4'	16:00	"	320.9
86	24°10.2'	96°22.1'	17:25	"	335.7
87	24°00.0'	96°21.9'	18:43	"	355.0
88	23°50.0'	96°20.2'	19:52	"	355.4
89	23°40.1'	96°19.9'	21:07	"	362.4
90	23°30.0'	96°19.6'	22:22	"	365.7
91	23°20.0'	96°19.2'	23:35	"	369.9
92	23°10.3'	96°19.1'	00:46	22 Aug 86	372.9
93	23°00.6'	96°19.2'	02:01	"	363.3
94	22°50.8'	96°19.1'	03:05	"	358.0
95	22°42.2'	96°18.4'	04:15	"	358.8

Table 2. Station locations on 17-22 August (continued)

Station No.	Latitude N	Longitude W	Time	Date	Depth (m)
96	22°30.7'	96°17.9'	05:45	22 Aug 86	349.5
97	22°20.0'	96°16.1'	07:16	"	352.5
98	22°09.0'	96°16.4'	08:40	"	333.1
99	21°59.0'	96°15.7'	09:58	"	314.1
100	21°49.0'	96°14.2'	11:10	"	303.4
101	21°39.0'	96°14.5'	12:40	"	290.1

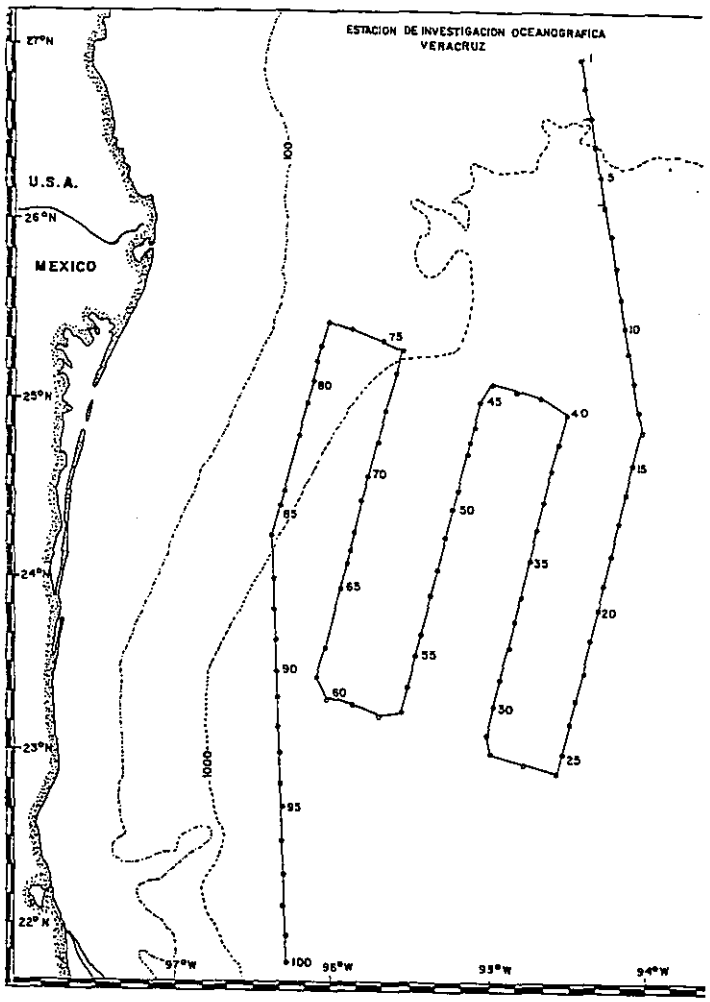

Figure 2. Station locations, 17-22 August 1986.

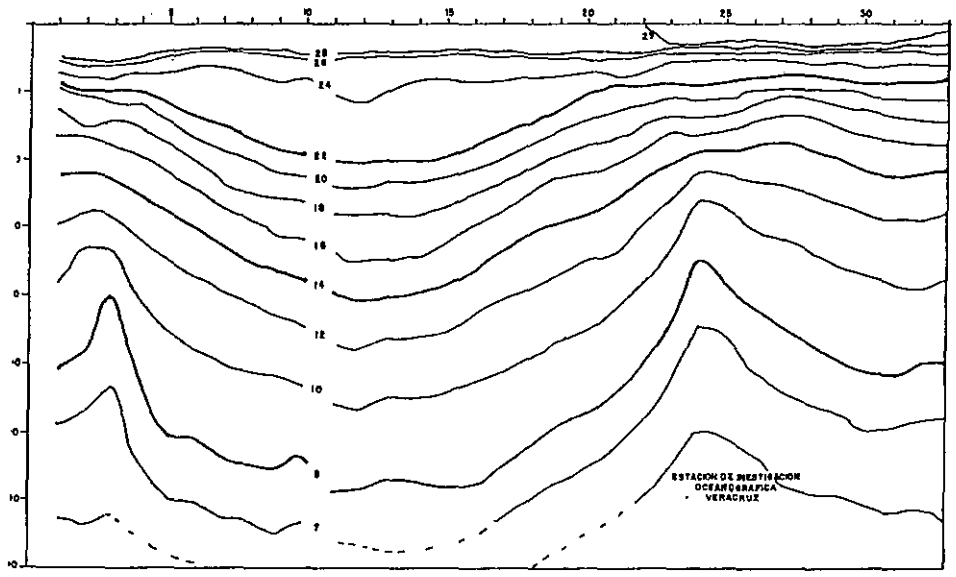

Figure 3. Temperature section, 15-17 July 1986.

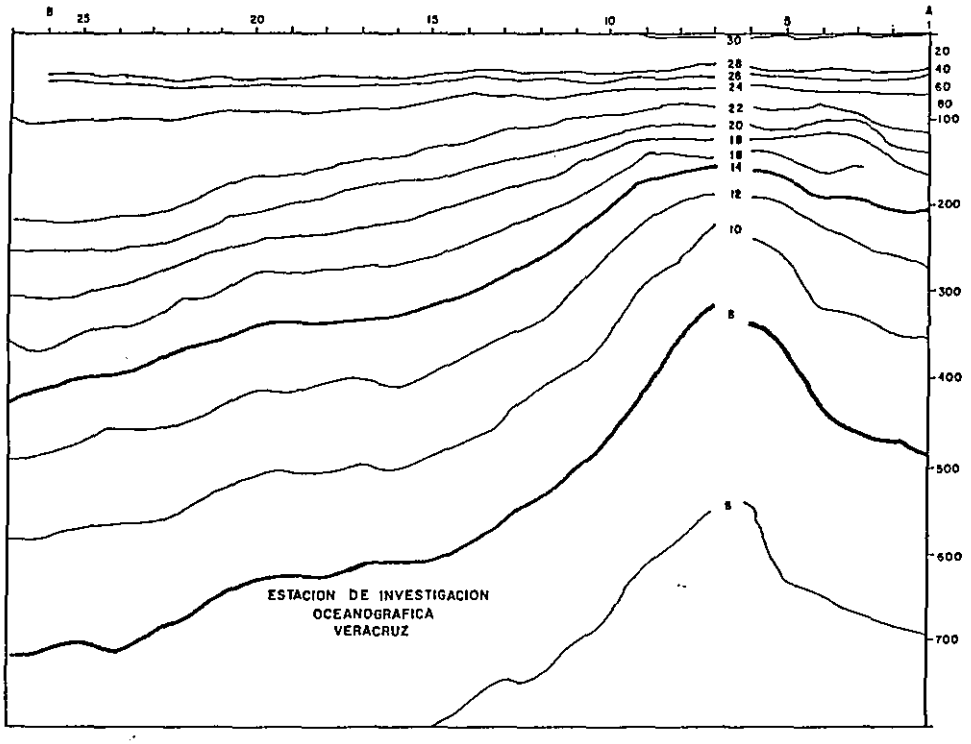

Figure 4. Temperature section for segment AB, 17-19 August 1986.

2.1 Conditions in July

On 15–17 July, the center of the ACR intersected the section at 24°15'N, 95°05'W, according to the maximum depth of selected isotherms (Fig. 3 and Table 1); its northern edge, denoted by the raising of subsurface isotherms, was located at 26°05'N, and its southern edge was detected at 22°35'N. The maximum depth of the 20°C, 14°C, and 8°C isotherms occurred at 225, 420, and 720 m, respectively. Its meridional radius, calculated as the distance between the positions where the 20°C isotherm changes slope (Elliot, 1982), was 200 km.

2.2 August Observations

On 17–22 August, the center of the ring had been displaced 140 km to the south (to 23°00'N, 94°58'W). The ACR's northern limb remained near 26°N but its southern end migrated out of the station grid (Fig. 4). The ring's meridional radius had grown 352 km at 95°W. Considering the displacement of the center of the ring and the increment of the meridional radius, it can be estimated that the ACR's maximum radius was oriented almost parallel to the Mexican continental slope.

The 14°C isotherm surface (Fig. 5) in August shows that the ring's center (at 420 m) had a NW–SE elongation, with an eastward flow between the ring's center and its northern end, and a northwestward flow at its southern end. In comparison, the 8°C isotherm surface (Fig. 6) shows an E–W orientation at 700 m. Both surfaces had a gentle slope between 25°N and 24°N, and a greater gradient near the ring's core (Figs. 5 and 6). The change in direction of the 14°C isotherm at 260 m, and of the 8°C isotherm at 560 m, seems to be the reflection of the small cape off the continental slope, near 25°30'N (Sturges and Blaha, 1976).

2.3 Upper-Layer Conditions

Above the seasonal thermocline (28°–24°C) an intrusion of water warmer than 29°C was observed north of 26°N. This layer was present in both surveys and it can reflect the presence of Texas-shelf water, although its influence on the ACR seems negligible. Merrell and Morrison (1981) suggested that flow from the

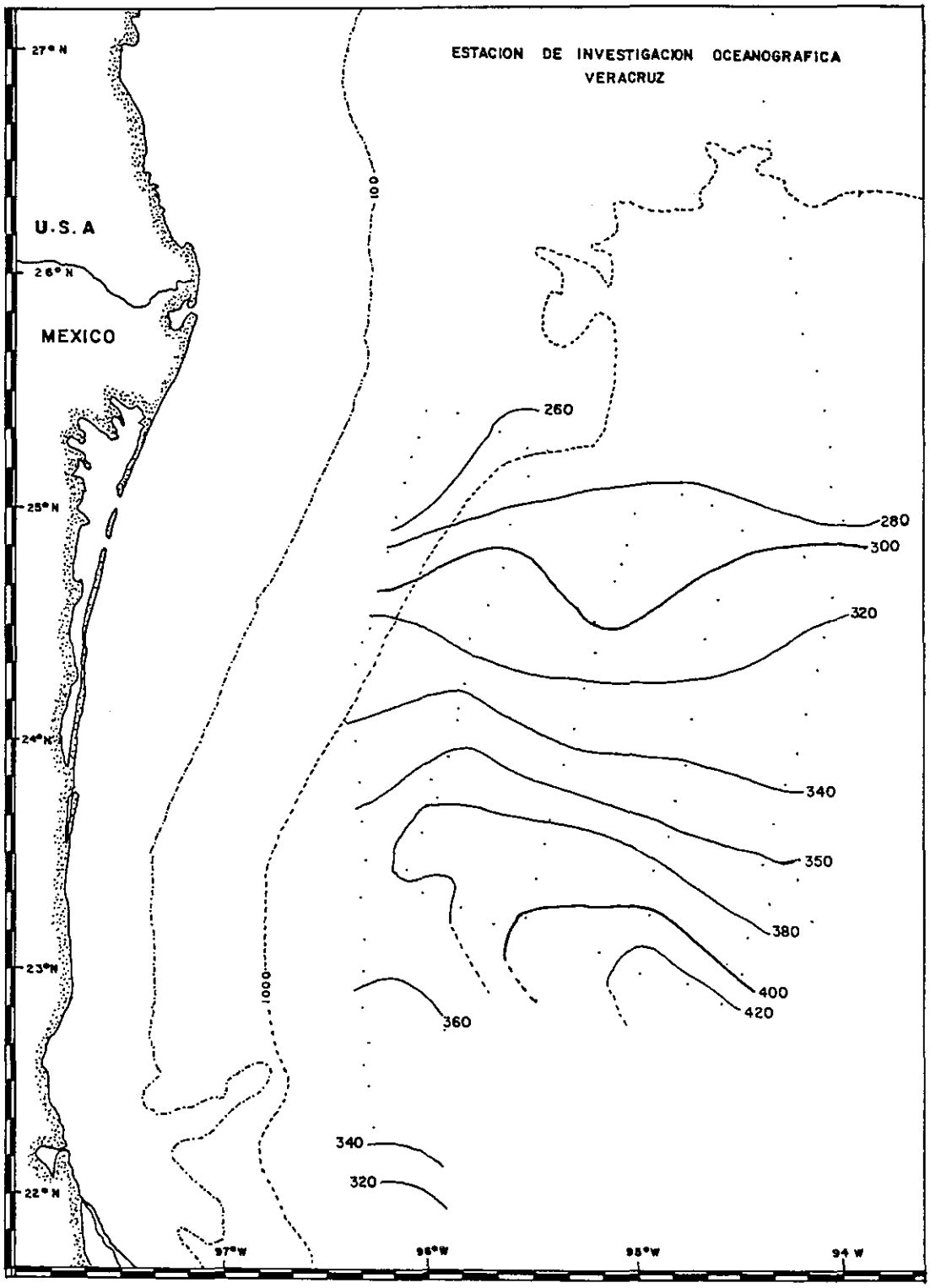

Figure 5. Topography (m) of the 14° isothermal surface, 17-22 August 1986.

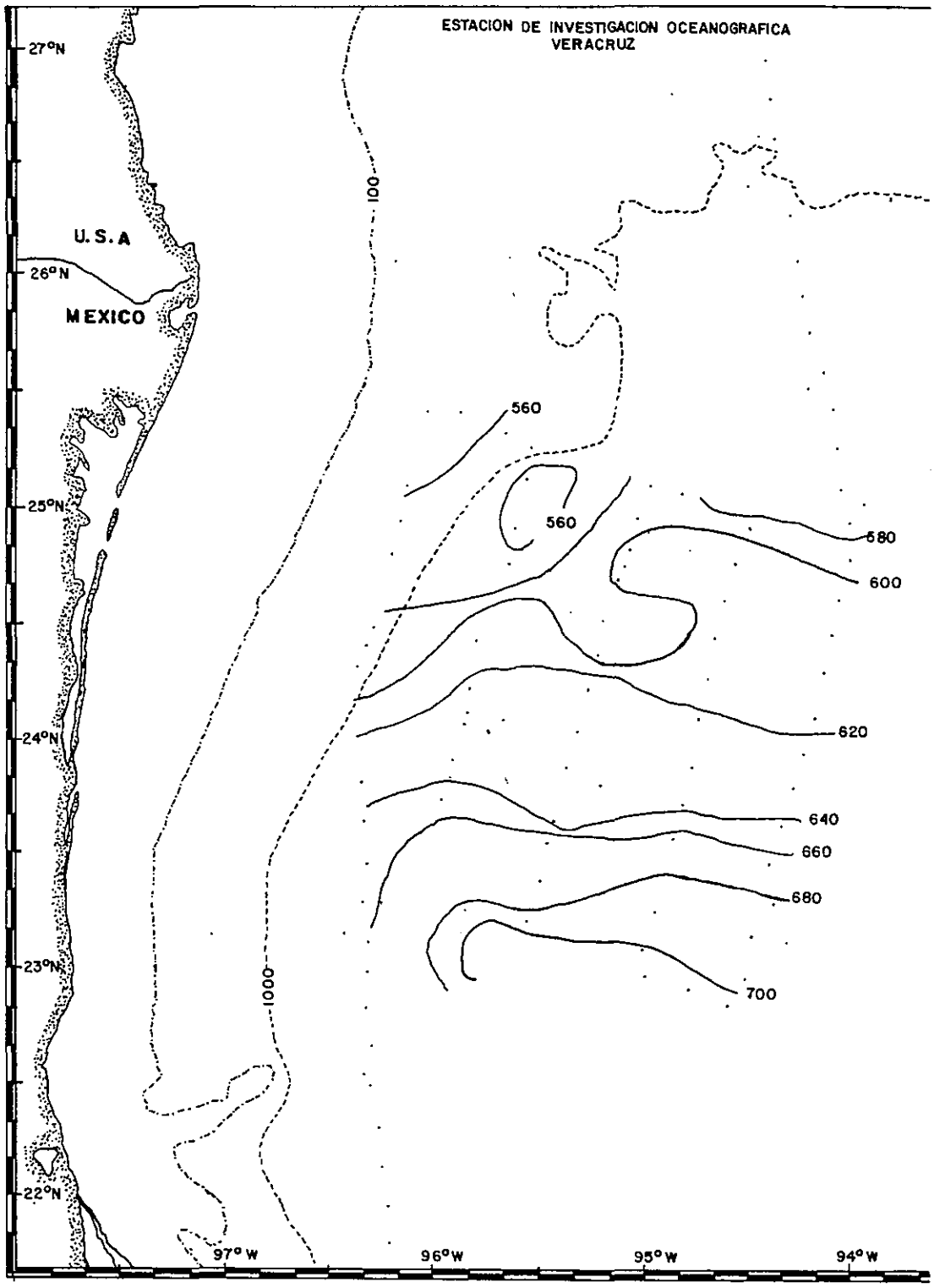

Figure 6. Topography (m) of the 8°C isothermal surface, 17-22 August 1986.

Texas shelf intensified a CR centered at 25°20'N, 95°20'W. In this study, there was no evidence of a well-developed CR, like, for example, a raising of isotherms on the continental slope north of the ACR's northern edge (at 26°N).

Below the thermocline, an almost isothermic (24°-22°C) lens of water with a maximum thickness of 120 m was observed in both surveys. Its greatest depth was 220 m at the ring's core; it was shallower and thinner at its northern limb, and at its southern edge, as well, in July. This isothermic lens can be used to characterize the ACR's upper layer during the summer of 1986. The ACR observed by Vázquez (1975) in May 1971, along a section at 22°30'N, had a 24°-22°C layer between 50 and 100 m depth. Elliot (1982) found an isothermic layer (23°-22°C) between 100 and 150 m depth, below the thermocline, in a ring off the Mexico-Texas slope during September 1967, and explained that it is the deep mixed layer produced by cold fronts (northers) and by the loss of sensible and latent heat during the preceding winter. In this study, the 22°C isotherm was 50-70 m deeper than reported for the western gulf; this suggests a deeper-than-normal mixed layer for the winter of 1985-1986, or an ACR intensification off the northwest continental slope.

2.4 Size of the Ring

The meridional radius at 95°W was incremented from 200 km during July, to 352 km in August. The dimensions of the ACR described by Merrell and Morrison (1981), in terms of the 15°C isotherm at 225 m, are equivalent to a minimum radius of 113 km and a maximum of 225 km, with an E-W elongation. Both rings are greater than the western gulf's ranged 109-141 km, but the ring in 1986 was greater than the eastern gulf's with interval of 102-244 km (Elliot, 1982).

An ACR's intensity can be appreciated with the maximum depth of a given isotherm, and with the depth range of the isotherm between the core and the limits of the ring. The greatest depth of the 20°C isotherm is 250 m in July and August, 50 m deeper than Elliot's (1982) ACR at 26°N, 95°W, in September 1967, and at the same depth as in the Loop Current region (Molinari, 1977). The 15°C isotherm at 390 m had a thickness of 238 m, 73 m deeper and 46 m thicker than for the ACR observed in early April 1978 (Merrell and Morrison, 1981).

2.5 Displacement of the ACR

Apparently, the thermal structure observed in July along 90°W was a cross section of the minimum radius, or of one end of the ACR; in August, the ring's core had been displaced to the 95°W meridian (thus the increase in the meridional radius), and its southern limb had moved out of the grid of stations. The permanence of its northern edge at 26°N suggests that the ACR translated along the Texas continental slope, and/or its maximum axis rotated.

The meridional radius was as large as in the biggest rings in the Gulf of Mexico. Although the limits of the ACR could not be contoured, its radius and location make it likely that this ring could be a part of the great ACR. Behringer et al. (1977) showed that it is found at 24°N and has permanent characteristics. The orientation of the topography of the 14°C and 8°C isotherms shows that during August, the center of the ring had a NW-SE elongation, and that part of the ACR was located on the Mexico-Texas continental slope. There was no evidence of a CR during the summer of 1986. It is known that the rings tend to change form, intensity, and position during a scale of time on the order of weeks (Nowlin and Hubertz, 1972; Elliot, 1982; Merrell and Vázquez, 1983); thus it is possible that the ACR moved during the summer of 1986.

Historical data sets (e.g., Austin, 1955; Vázquez, 1975; Elliot, 1982) show that the presence of a low geopotential anomaly on the continental slope to the west of 95°W and north of 23°N, tends to displace the ACRs offshore. In the absence of this low geopotential, the ACRs are in their northernmost position. Merrell and Morrison (1981) concluded that the wind-induced low in Bay of Campeche during the winter prevents a southward migration of ACRs; according to them, the region to the north of 25°N has a cyclonic character with a high variability, due to the occasional migration of CRs generated in the Loop Current region. If the presence of an ACR off the Mexico-Texas continental slope is part of a cycle of arrival, residence, and departure or dissipation, a low geopotential anomaly between the northern or western sides of the ACR could be the forcing mechanism for its displacement or weakening.

It is likely that the observed ACRs in the gulf's northwestern boundary come from the eastern region. Elliot (1982) observed a detached ring in the Loop

Current region during November 1966, and tracked it to the Mexico-Texas continental slope in September of 1967, with a much reduced salinity at its core. We estimated a mean translational velocity of 2.1 km/day and a direction of 279° for migrating ACRs in the Gulf of Mexico. Merrell and Morrison (1981) found high salinity (36.60 o/oo at 180 m) in their ACR, and concluded that it was the Subtropical Underwater maximum remnant from the Loop Current waters.

An ACR that arrives in the western region during summer or winter can be affected by the curl of the wind stress (Sturges and Blaha, 1976). The depth of the 20°C isotherm and the thickness of the 24°-22°C isothermic lens show that for the summer of 1986 the ACR was similar in intensity to the eastern gulf's ACRs. According to the temperature sections (Figs. 3 and 4), the ring was evident to at least 800 m depth; Vázquez (1975) showed isotherm sloping at 1200 m, and Nowlin and McLellan (1967) detected movement to at least 1500 m depth. The gulf's northwestern continental slope is steep north of 25°N; also its contour changes direction. These geomorphological characteristics must influence isotherm sloping and direction of flow. Sturges and Blaha (1976) indicated that near 26°N there is a wind-induced isotherm rising on the coastal side of the flow field, which contributes to the ACR's intensification during late fall and winter. Nowlin and McLellan (1967) showed velocities of 70-100 cm/s in the ring's coastal edge.

Between July and August, the ACR's northern edge (26°N) isotherms rose 20-40 m (Table 1). If the ACR's intensity is persistent, the rising of isotherms could produce a low geopotential meander on the continental slope and shelf, similar to the cyclonic meander described by Leipper (1970) and Cochrane (1972) for the Yucatán Shelf. Elliot (1982: Fig. 5) shows the presence of a cyclonic region on the Mexico-Texas continental slope in February and March 1967, and an ACR near 26°N, 94°W. The cyclonic meander can become intensified by the extension of the Texas shelf current (Merrell and Morrison, 1981); according to Merrell and Vázquez (1983), CRs can also be intensified by the effects of severe northers.

The average monthly temperature charts by Behringer et al. (1977) suggest that the 15°C isotherm at 200 m can be used to localize the low geopotential region north of 25°N. In February and March, this isotherm forms a diagonal line in relation to the gulf's northern boundary, and reaches 24.5°N at 96°W.

During July and August, the isotherm runs parallel to the northern boundary, at 26°30'N. A CR can be detected in May, September, October, and December. Cyclonic meanders appear during January, June, and November, to the east of 94°W. Although these charts show no data for April to the west of 94°30'W, the presence of a CR during this month has been observed (Merrell and Morrison, 1981; Merrell and Vázquez, 1983). In agreement with these charts, no CR or cyclonic meander was detected in the summer of 1986, and the 15°C isotherm at 200 m was localized near 26°N.

Behringer et al. (1977) showed that the ACR in the western Gulf of Mexico is a permanent feature, with a maximum development in winter and summer, and a minimum during spring and fall. Therefore, the ACR seems to respond inversely to the growth and decline of the low geopotential region north of 25°N, being weakest when CRs are well developed, and strongest in the absence of cyclonic meanders and CRs. In the northwestern Gulf of Mexico, the intensification of a CR can probably cause ACR displacement offshore; historical data by Vázquez (1975) and Merrell and Morrison (1981), for example, illustrate this.

The displaced ACR probably interacts with other ACRs in the western gulf. Merrell and Morrison (1981) concluded that the wind-induced low in the Bay of Campeche (near 22°N) prevents the southward migration of ACRs. On the other hand, the charts by Behringer et al. (1977) show that the ACR responds to the changing size and intensity of the low geopotential region in the gulf's northern boundary (at 25°N). A well-developed CR would constrain the ACR between both lows, and favor ACR coalescence. Figures by Austin (1955), Nowlin and McLellan (1967), Merrell and Vázquez (1983), and Elliot (1982) show ACR interaction.

In summary, ACR displacement off the Mexico-Texas continental slope seems to be a response to a cycle of arrival from the eastern Gulf of Mexico: intensification by local wind and current patterns; offshore displacement produced by the intensification of a cyclonic meander or a CR in the gulf's northern boundary; and coalescence with other ACRs in the western gulf. Possibly, the ACR observed during the summer of 1986 had been intensified.

REFERENCES

Austin, G.B., Jr., 1955: Some recent oceanographic surveys of the Gulf of Mexico. Trans. Amer. Geophys. Union, 36:885-892.

Behringer, D.W., R.L. Molinari, and J.F. Festa, 1977: The variability of anticyclonic current patterns in the Gulf of Mexico. J. Geophys. Res., 82:5469-5476.

Cochrane, J.D., 1972: Separation of an anticyclone and subsequent developments in the Loop Current (1969). Texas A&M University Oceanogr. Stud., Vol. 2, L.R.A. Capurro and J.L. Reid, Eds., Gulf Publ. Co., Houston, 91-106.

Elliot, B.A., 1982: Anticyclonic rings in the Gulf of Mexico. J. Phys. Oceanogr., 12:1292-1309.

Ichiye, T., 1962: Circulation and water mass distribution in the Gulf of Mexico. Geofis, Int., 2:47-76.

Leipper, D.F., 1970: A sequence of current patterns in the Gulf of Mexico. J. Geophys. Res., 75:637-657.

Merrell, W.J., Jr., and J. Morrison, 1981: On the circulation of the western Gulf of Mexico with observations from April 1978. J. Geophys. Res., 86:4181-4185.

Merrell, W.J., Jr., and A.M. Vázquez, 1983: Observations of changing mesoscale circulation patterns in the western Gulf of Mexico. J. Geophys. Res., 88:7721-7723.

Molinari, R.L., 1977: Synoptic and mean monthly 20°C topographics in the eastern Gulf of Mexico. Tech. Memo. ERL-AOML 27, Nat. Oceanic and Atmos. Admin., Boulder, Colo., 33 pp.

Nowlin, W.D., Jr., and J.M. Hubertz, 1972: Contrasting summer circulation patterns for the eastern Gulf-Loop Current versus anticyclonic ring. Texas A&M University Oceanogr. Stud., Vol. 2, L.R.A. Capurro and J.L. Reid, Eds., Gulf Publ. Co., Houston, 119-138.

Nowlin, W.D., Jr., and H.J. McLellan, 1967: A characterization of the Gulf of Mexico waters in winter. J. Mar. Res., 25:29-59.

Sturges, W., and J.P. Blaha, 1976: A western boundary current in the Gulf of Mexico. Science, 192:367-369.

Vázquez, A.M., 1975: Currents and waters of the upper 1200 meters of the southwestern Gulf of Mexico. M.S. Thesis, Dept. Oceanogr., Texas A&M University, 108 pp.

SUSPENDED PARTICLES IN SEA WATER

Clarence T. Nagamoto, Farn P. Parungo, and Evelyn Ackerman

1. INTRODUCTION

Investigations of suspended particles in surface sea water have three purposes: (1) to study the relationship between the characteristics of particles in sea water and in the atmosphere, (2) to correlate particle concentration in sea water with the concentration of dimethyl sulfide (DMS) in sea water, and (3) to compare ice nucleation activities of the particles collected from sea water and from the air above.

During the cruise, surface sea-water samples were taken at the locations shown in Fig. 1. Sea water (100 mL) was filtered through a Nuclepore filter (pore size 0.2 μm) and washed with 100 mL of deionized water. Another 100 mL of sea water was filtered through a millipore filter (0.22 μm) and also washed with 100 mL of deionized water. The filters were stored individually and dried in a decanter that was refrigerated. After the cruise the Nuclepore-filter samples were examined with a scanning electron microscope (SEM). The millipore-filter samples were tested for ice nucleus concentrations by Dr. Jan Rosinski (see Sec. II). A third portion of sample sea water was analyzed onboard for DMS by Dr. Steven Hoyt (see Sec. I). The temperature and pH of sea water were also measured onboard; (Fig. 2). This paper reports only the SEM-XES analysis.

2. RESULTS

Three classes of particles, based on morphology and elemental composition, were observed. (1) Inorganic particles consisting of Si, Al, Fe, S, Ca, K etc. They were generally between 1 to 5 μm with a mean ~2 μm, irregular shaped and without definite texture. The results for samples 4, 7, and 10, which were analyzed with Tracn-Northern "Particle Recognition Characterization" software, are shown in Table 1. The average shape factor is ~2 on a scale of 1 to 6 (1 is "perfect sphere" and 6 is "totally irregular"). The computer printouts of size distribution of all particles and of certain

Table 1. Characteristics of suspended particles in sea water

Sample no.	Particles analyzed	Shape 1-6	Diameter (μm) max.	min.	ave.	Elements (relative x-ray intensities) Si	Al	Mg	Cl	K	Fe	Ca	S
4	104	1.64	2.70	1.44	1.95	56	18	0	1	3	11	6	2
	σ	0.72	1.72	1.04	1.26	27	12	0	1	4	22	16	8
7	122	1.90	2.77	1.17	1.78	55	23	0	0	4	14	0	0
	σ	0.84	2.07	0.89	1.30	25	15	1	1	5	24	3	0
10	113	2.15	3.81	1.27	2.12	24	11	0	41	1	14	--	--
	σ	1.01	4.74	1.63	2.53	30	14	1	39	3	28	--	--

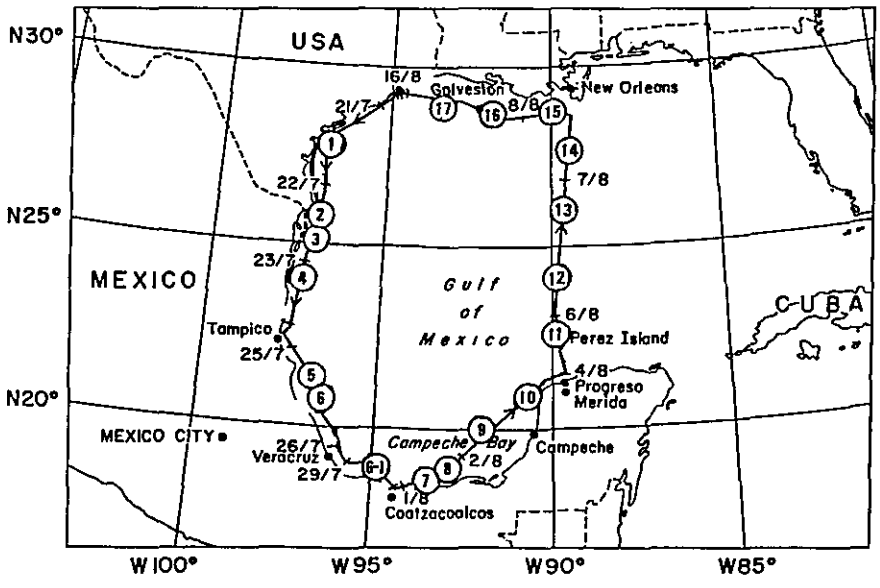

Figure 1. Locations where surface seawater samples were collected. Numbers identify samples.

element-rich particles are shown in the Appendix. (2) Organic particles, which were similar to inorganic particles except that they did not emit detectable x-rays. They contributed <10% of total particles. (3) The biomass, which depicted specific structures with diameters from 1 μm to 1 mm. Their concentrations were highly variable with location. Most of these particles contained Si. Some contained minute amounts of Ca, Na, S, and Cl. Examples of the biological particles and their x-ray spectra are shown in Fig. 3. Figures 4-15 show the diversities of biomass observed in our samples including bacteria, diatoms, dinoflagellate, and algae. These phytoplanktons are primary products for the vast food networks. Their concentrations depend on nutrients in surface sea water, photosynthesis, and the rate of grazing by zooplanktons. Our measurements of particle concentrations in four size ranges (1-10, 10-30, 30-50, and 50-100 μm) are listed in Table 2. We observed great spatial variability in both biomass diversity and concentrations. The highest concentration (~10^6 cm^{-3}) was found south of Campeche Bay (sample 7) and the lowest (<5 x 10^3 cm^{-3}) was in the middle of the Gulf (samples 10 to 15). Our results generally agreed with the survey conducted by Soviet and Cuban expeditions in the Gulf (Ivanov, 1966).

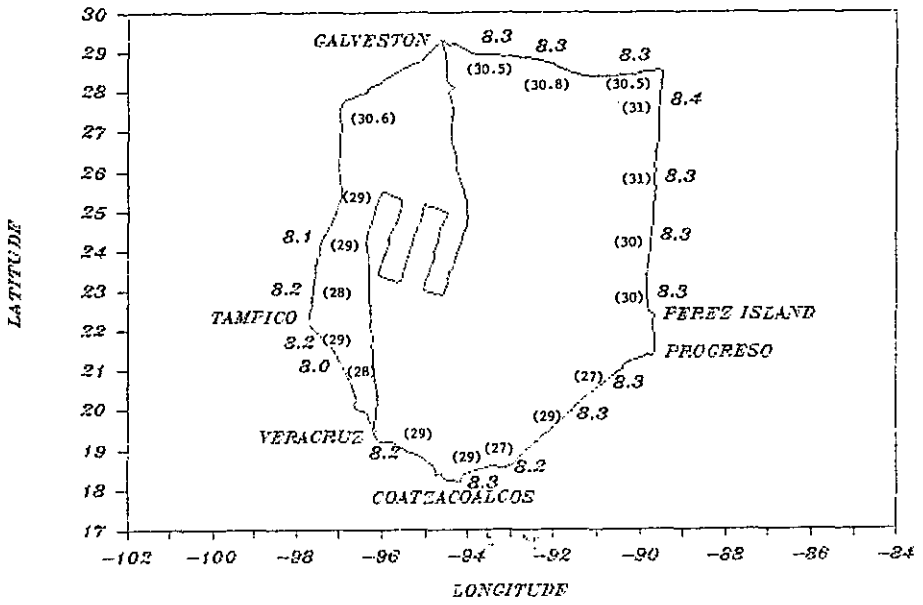

Figure 2. pH and temperature (°C) of surface seawater samples.

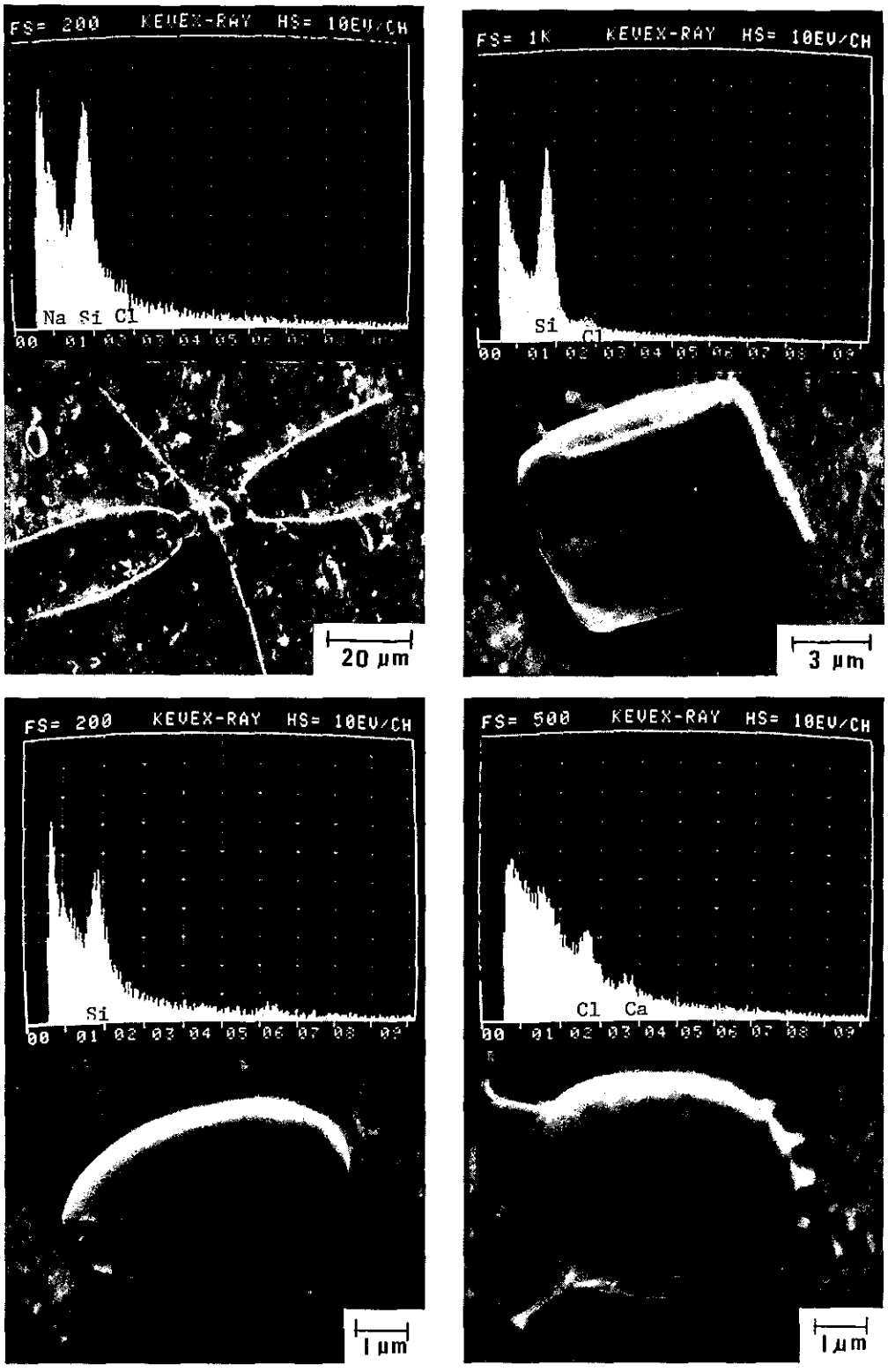

Figure 3. X-ray energy spectra and electron-micrographs of individual biomass.

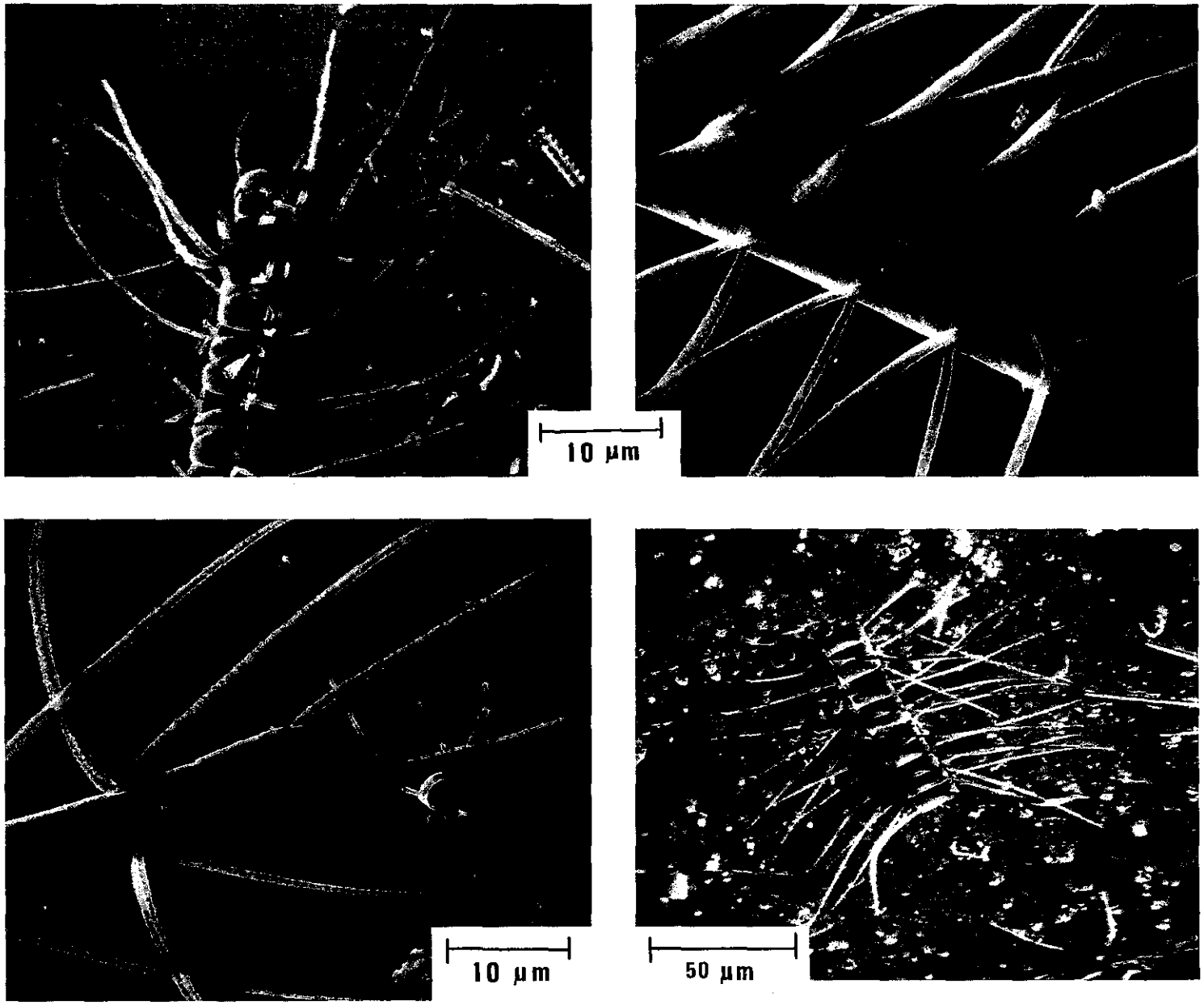

Figure 4. Electron-micrographs of biomass.

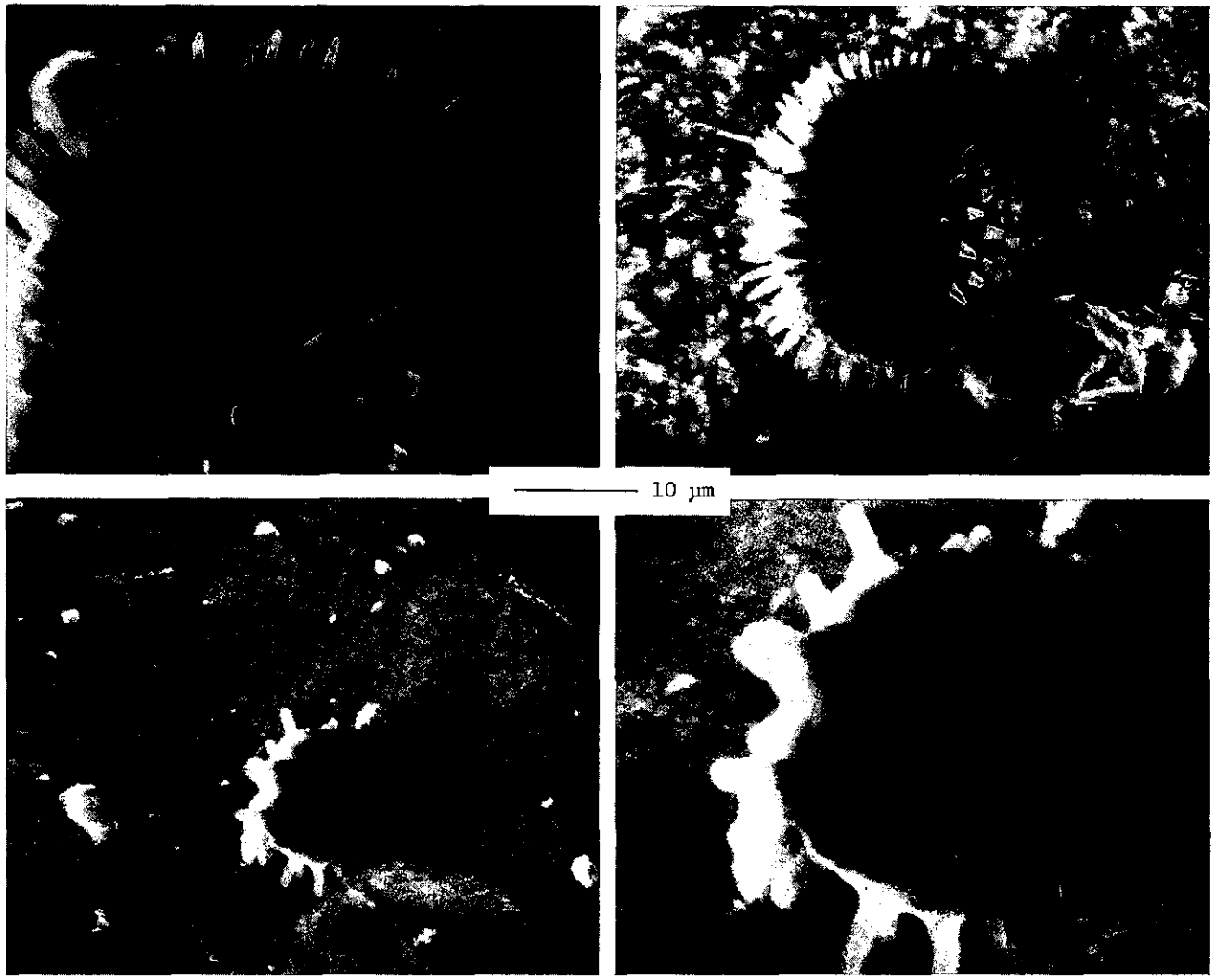

Figure 5. Electron-micrographs of biomass.

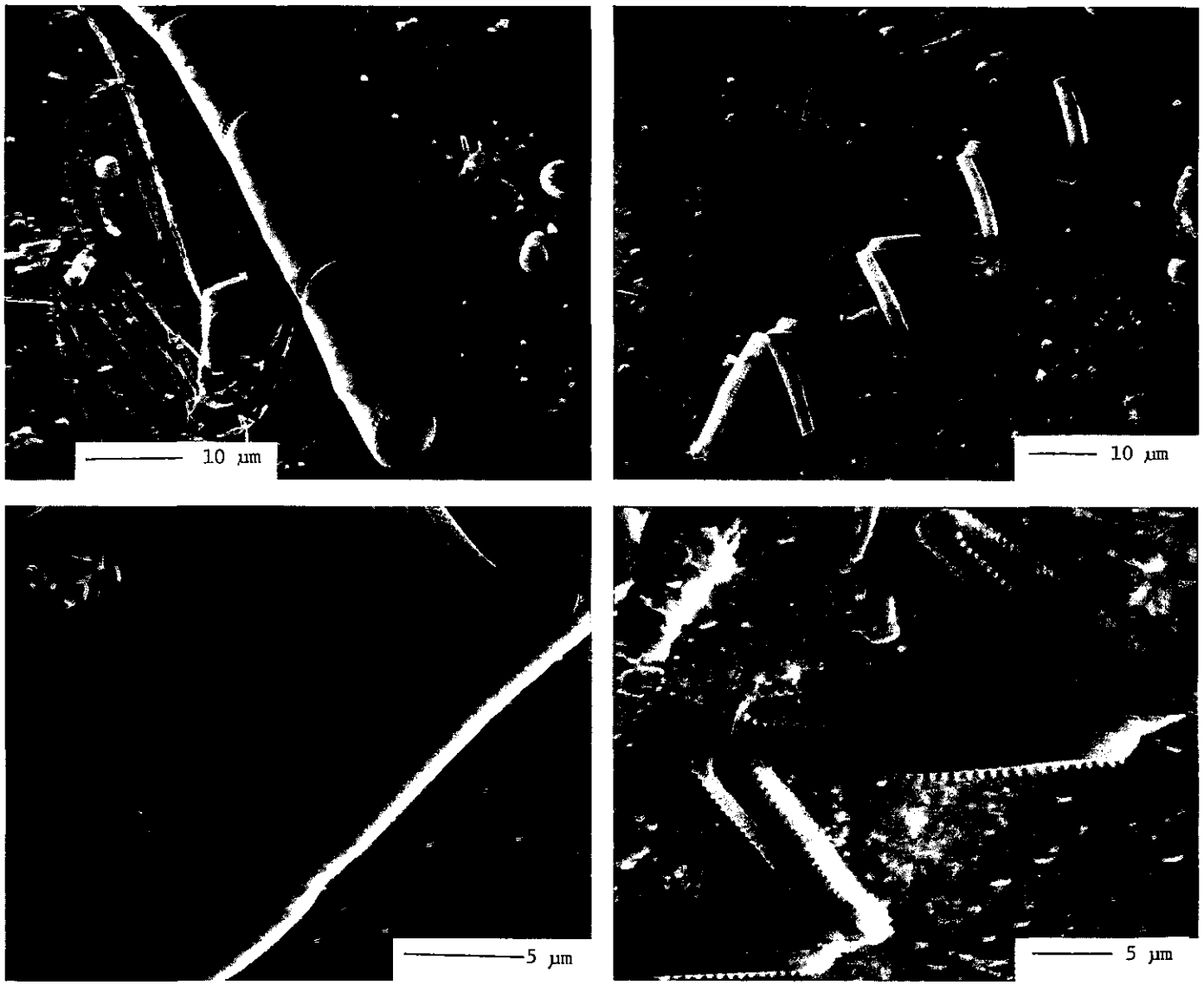

Figure 6. Electron-micrographs of biomass.

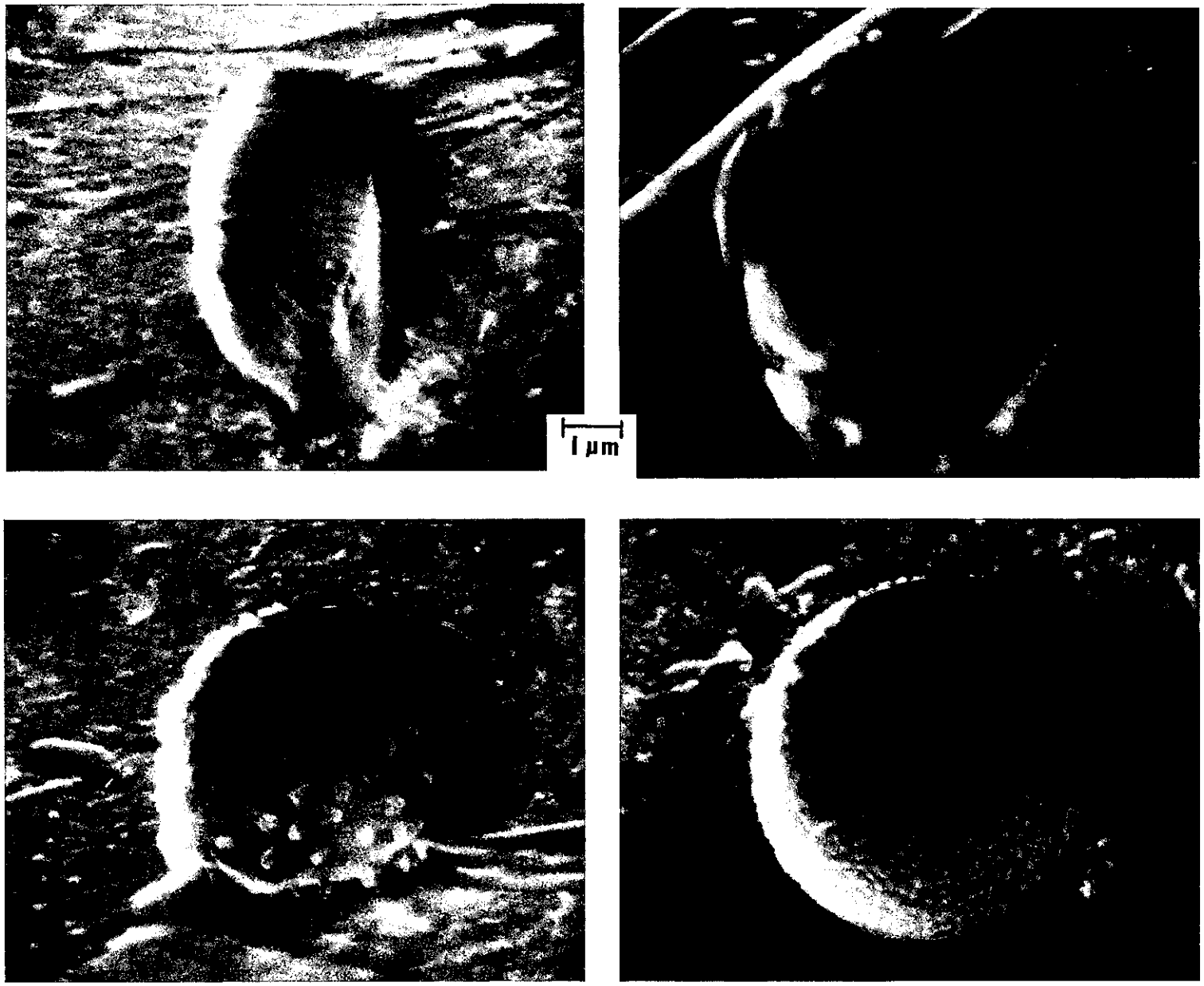

Figure 7. Electron-micrographs of biomass.

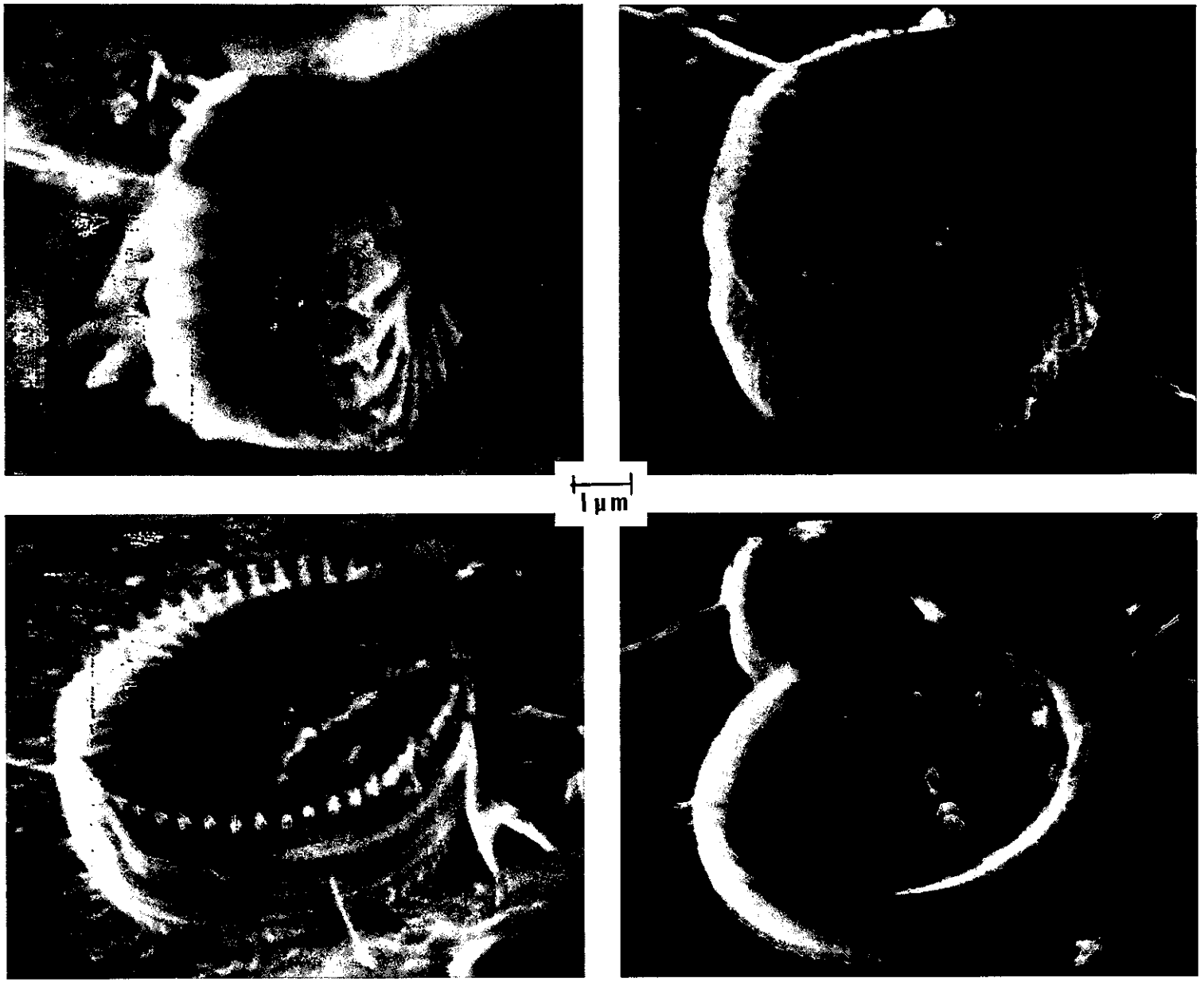

Figure 8. Electron-micrographs of biomass.

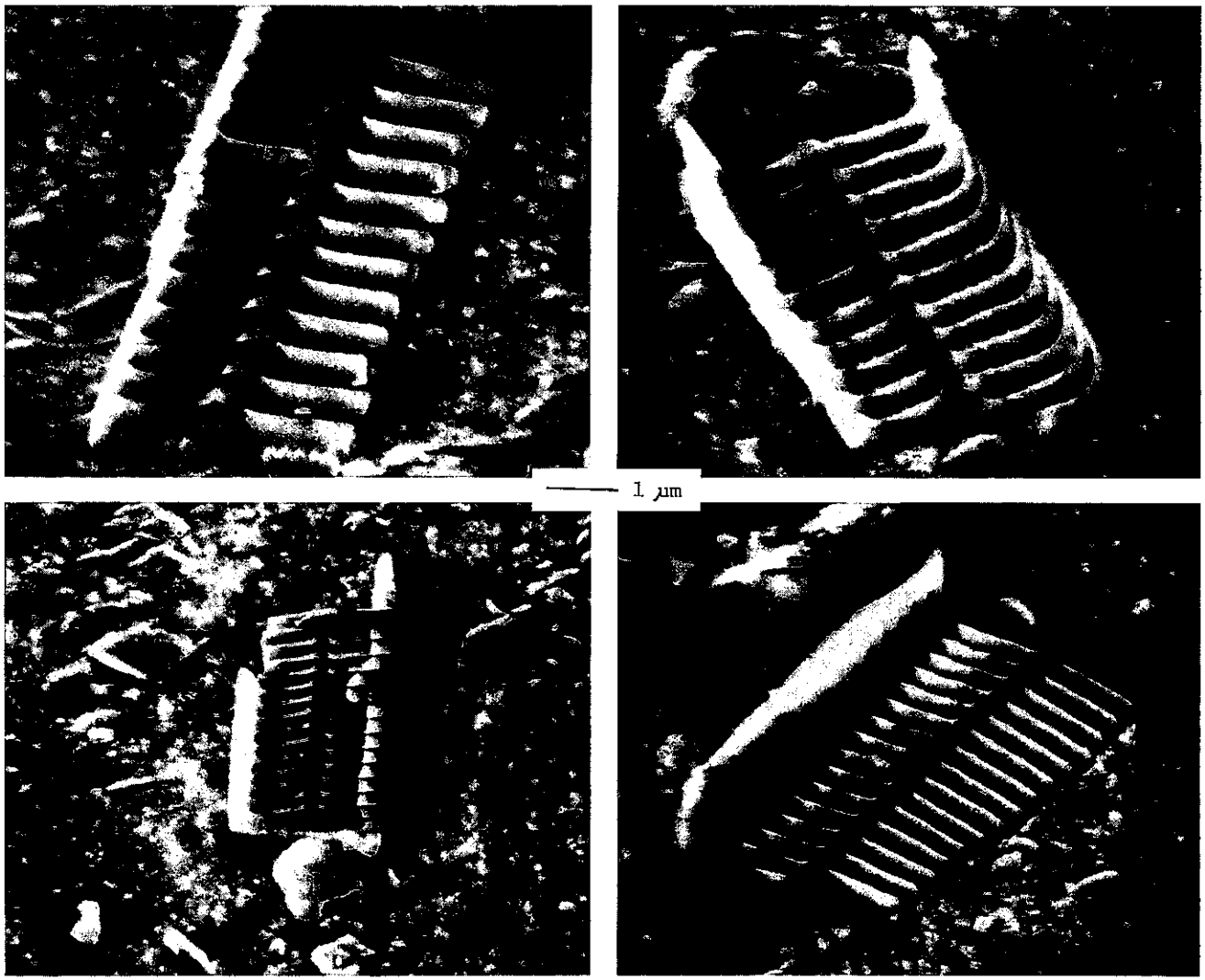

Figure 9. Electron-micrographs of biomass.

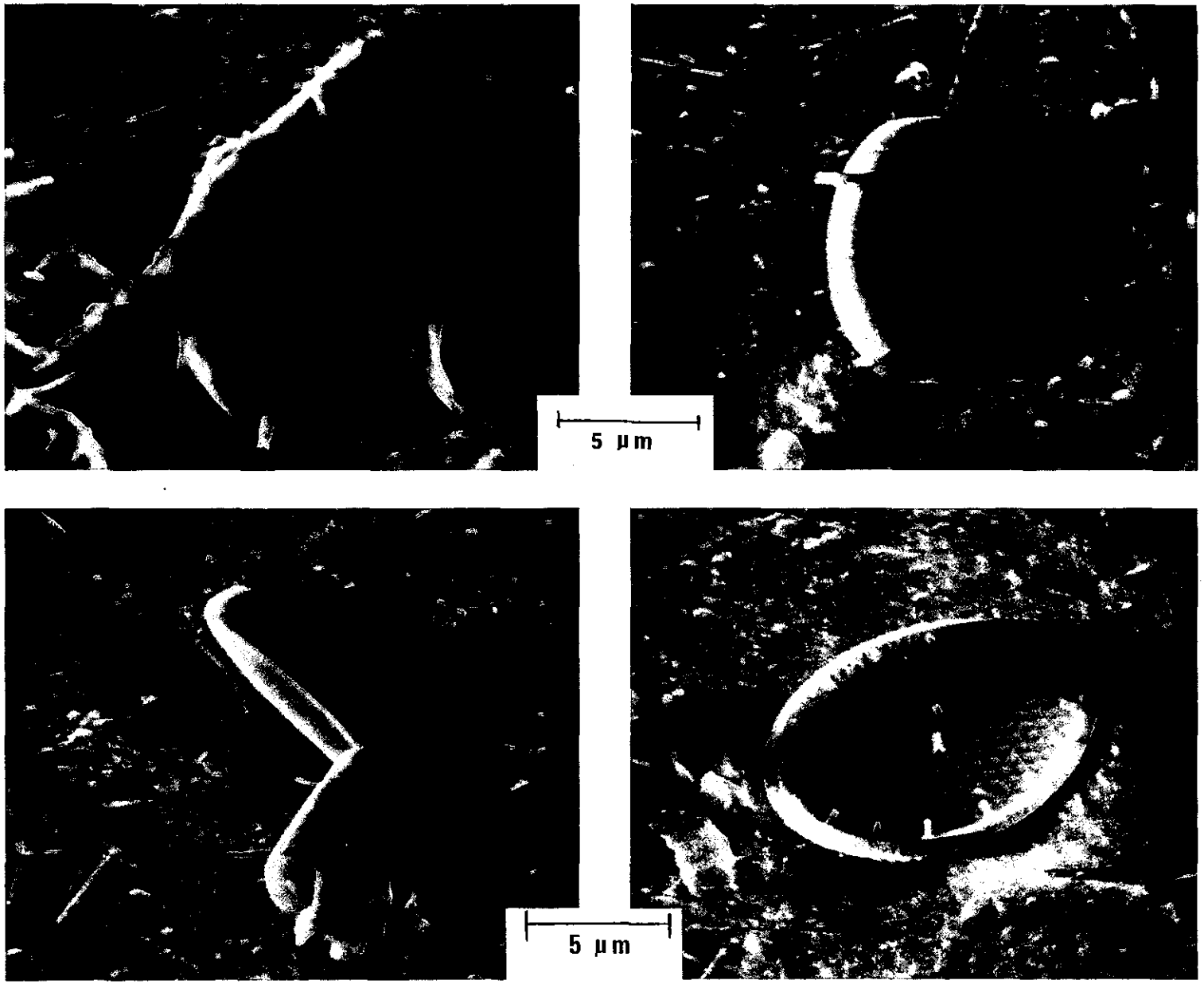

Figure 10. Electron-micrographs of biomass.

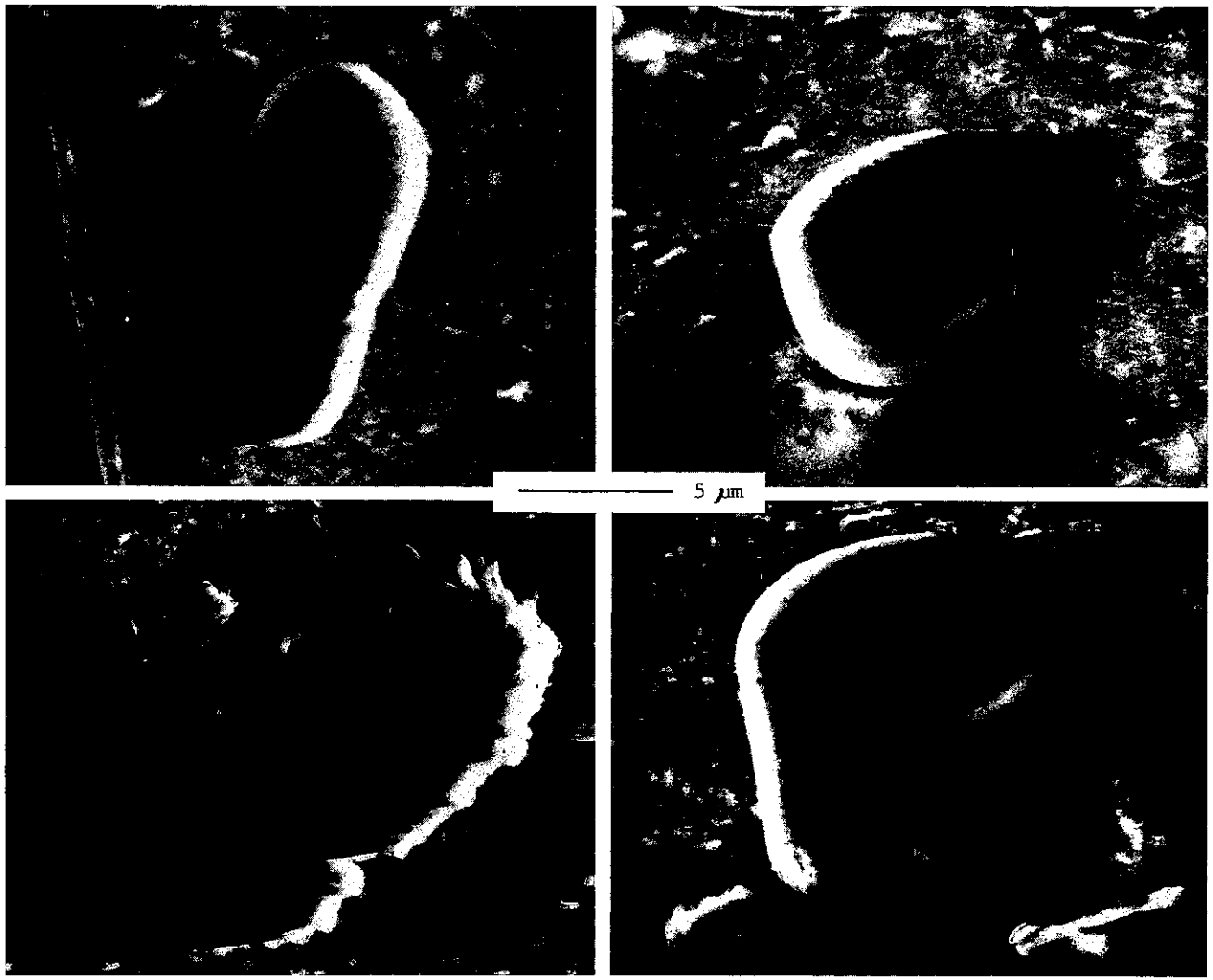

Figure 11. Electron-micrographs of biomass.

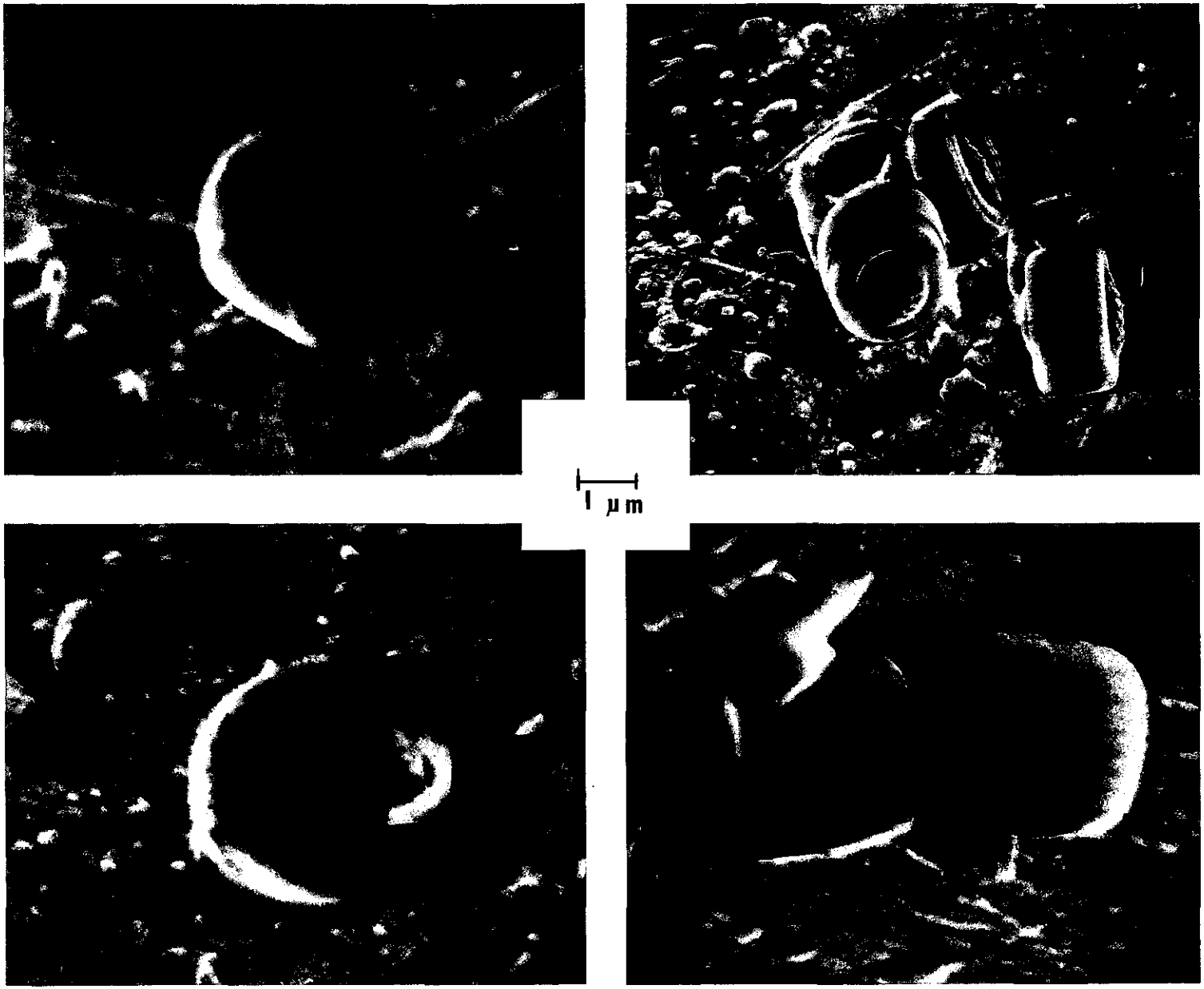

Figure 12. Electron-micrographs of biomass.

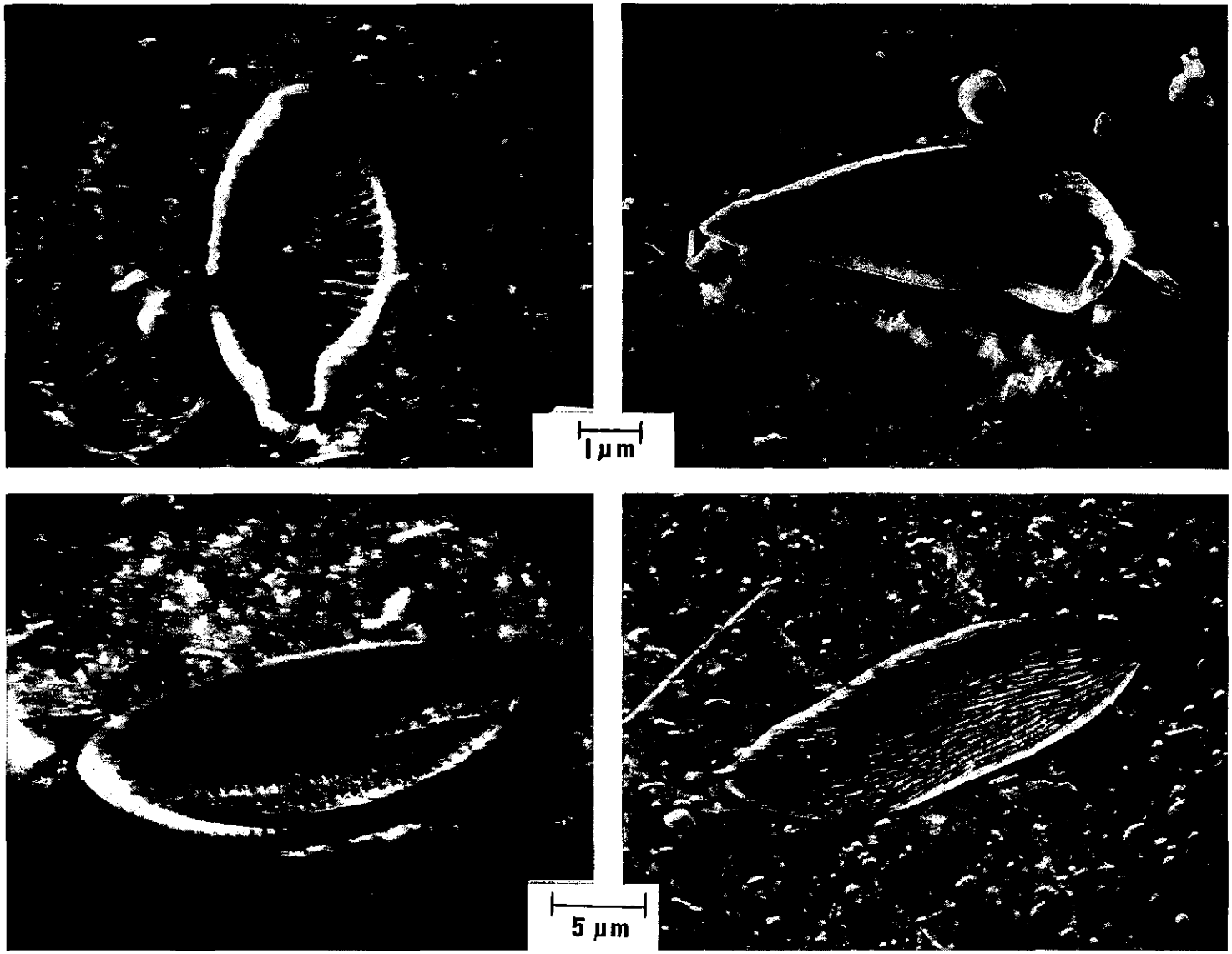

Figure 13. Electron-micrographs of biomass.

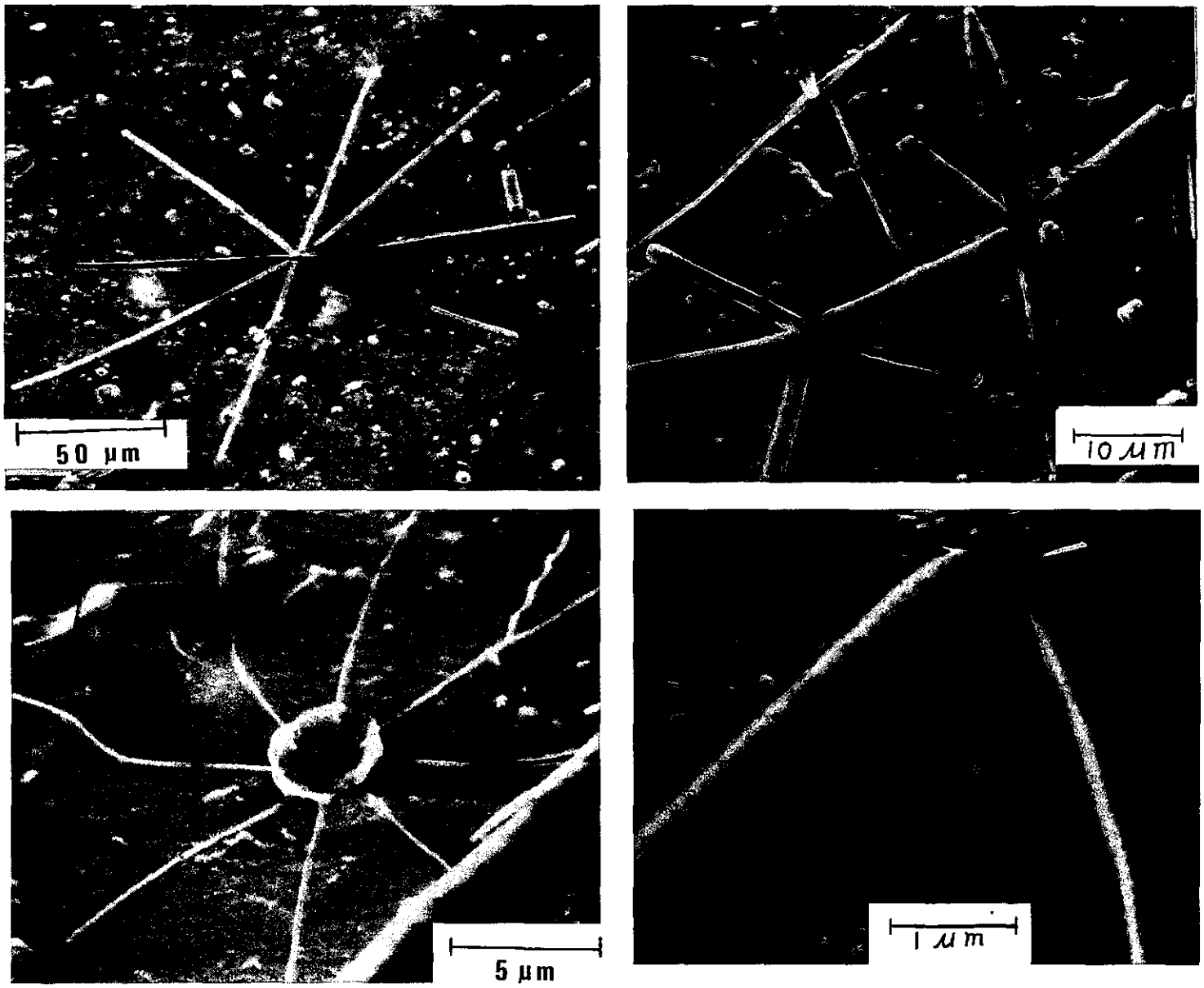

Figure 14. Electron-micrographs of biomass.

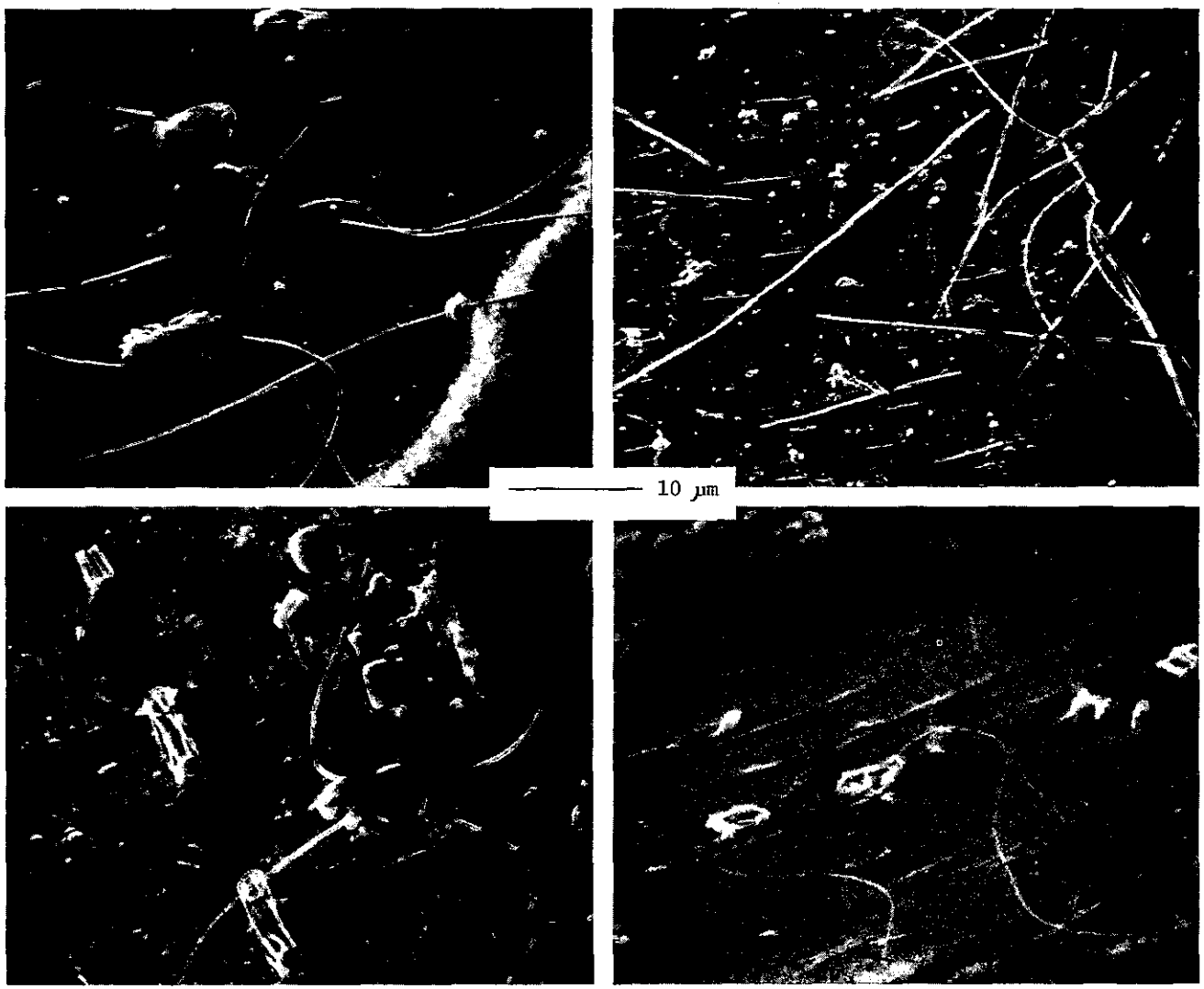

Figure 15. Electron-micrographs of biomass.

Table 2. Approximate concentrations of suspended particles in sea surface water

Sample #	Date 1986	Time (Local)	pH	Size range, μm (number/mL) 1-10	* %	10-30	30-50	50-100	Generalized Observations	conc. DMS ng/L
1	7/21	1830	8.0	10,000	15	930	230	1	Many Types, lots of "Discs", "Barrels", "Balls"	---
2	7/22	1100	8.1	1,800	50	63	25	1	Many Types	155
3	7/22	1645	8.1	2,900	75	310	37	37	Lots of "curly fibers"	205
4	7/23	0600	8.2	28,000	75	2,400	280	88	Lots of "sticks" and large "fuzz patches"	230
5	7/25	1345	8.2	11,000	70	1,100	140	37	Many small "oil drops"	205
6	7/25	1745	8.0	5,300	70	690	90	75	Many different types	147
6-1	7/29	1830	8.2	11,000	80	1,300	150	75	Many "long-leg bugs", several types	143
7	8/1	1000	8.2	89,000	95	6,700	140	25	Many types, lots of "Barrels", "Balls", "Bars"	244
8	8/1	1730	8.2	27,000	80	2,800	200	13	Many types, "Balls", "Bugs", "sticks", "fuzzes"	100
9	8/2	0845	8.2	4,300	75	510	38	13	Lots of "chains" and "fuzz patches"	110
10	8/2	1915	8.2	2 710	15	1,200	38	37	Lots of "long haired bugs"	160
11	8/5	1800	8.2	2,700	10	430	13	25	Some "fuzzy balls"	81
12	8/6	0830	8.2	2,700	10	500	75	25	Mostly "rocks" and "flakes"	118
13	8/6	1900	8.3	4,600	75	490	25	25	Lots of large "fuzz balls"	100
14	8/7	0930	8.4	5,340	10	230	88	1	Mostly "rocks"	83
15	8/7	2030	8.3	5,300	10	640	75	25	Mostly "balls", "rocks"	50
16	8/8	0900	8.3	7,100	50	720	50	25	Many types	22
17	8/8	1730	8.2	1,800	60	390	2	13	Many types	34

*Percent of biologic particles estimated for 1-10μm particles, higher percents for larger particles

Since biomass particles were found in all water samples collected in the Gulf one would expect that proportional amounts could escape to the atmosphere through sea-to-air interactions. Blanchard (1983) and Blanchard and Syzdek (1970, 1974, 1982) conducted a series of laboratory experiments and showed that bacteria content was enriched even in artificial jet and film drops over the bulk water; the enrichment factor was measured as high as 600. Their results suggested a high flux of bacteria from sea to air. In our cruise, aerosol samples were collected with filter and impactor methods. On all the filter samples, few, if any, bioparticles were observed that resembled those found in sea water. The average percentage of bioparticles in total particles was <1%. Among all the impactor samples (which are divided into four size ranges) half of the samples contained no biomass at all (Quintana and Parungo in Sec. II, this volume). The highest concentrations (~20 cm^{-3}) were found south of Campeche Bay where the biomass in the water was the richest. Another patch of high concentrations (~10 cm^{-3}) was found in the open sea where the biomass in the water was the poorest. The average concentration of larger bioparticles ($d > 2$ μm) was ~2×10^{-3} cm^{-3}, which was ~5% of total particles in the same size range. The average concentration of small bioparticles ($d \leq 2$ μm) was ~ 2 cm^{-3}, which was <1% of the total small particles. Since we did not observe a large population of biological particles in marine surface air, we could not determine conclusively any relationship between the biomass concentrations in the air and in the sea water. Our data could not confirm Blanchard's theory that enrichment of bacteria in the film drops could lead to a high flux of bacteria from sea to air.

Schnell and Vali (1976) reported that sea water rich in plankton has high concentrations of ice nuclei. They suggested that bacteria from the sea have an important role in cloud microphysics. We found that biomass concentrations in surface air were very low. The concentration would be even lower at cloud level because of the large size, short life span, and great sedimentation rate of biomass. The importance of bacterial ice nuclei for initiation of snow or rain is highly questionable. Ice nucleation by marine aerosols is discussed further by Rosinski (Sec. II).

Andreae and Raemdonck (1983) and Andreae (1986) reported that phytoplankton were responsible for the production of dimethyl sulfide (DMS) in surface

sea water and that sea-to-air flux of DMS contributed major portions of non-seasalt sulfate particles in the marine atmosphere. Figure 16 and Table 2 compare biomass concentrations in sea water with DMS concentration in sea water (which was measured by Hoyt during the cruise). Our observations generally agree with Andreae's findings that the higher the primary production (biomass) the higher the DMS in water. The correlation coefficient between DMS concentration and biomass number is 0.57 for particles $1 < d < 10$ μm and 0.56 for particles $1 < d < 100$ μm. Thus, there is little if any effect of particle size on DMS concentration. Figure 17 shows that when the biomass number was $<10^4$ cm^{-3}, the DMS concentration was <150 ng L^{-1}. Little correlation was observed. However, when biomass was $>10^4$ cm^{-3}, the DMS concentrations increased with biomass concentration. The correlation coefficient is 0.76. The results suggest that DMS could be produced by the high concentration of a certain biomass that prospers in certain regions of the Gulf.

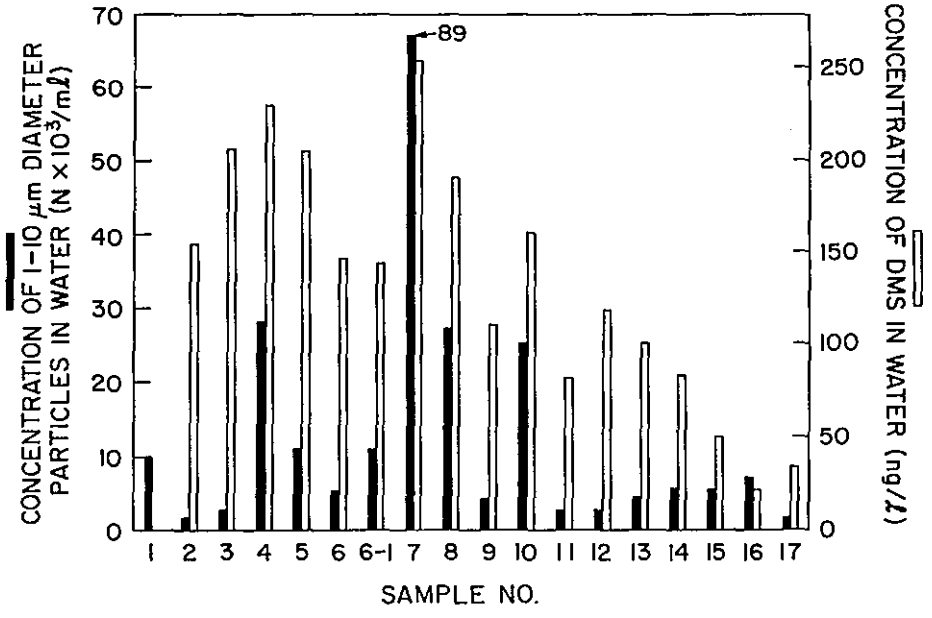

Figure 16. Comparison between DMS concentrations and biomass concentrations in seawater samples.

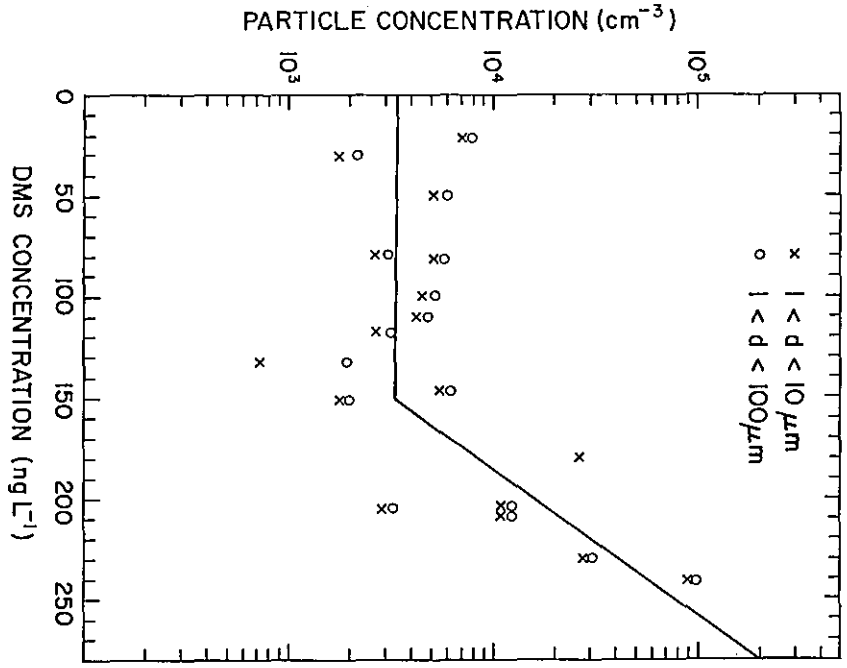

Figure 17. Correlations between DMS concentrations and total suspended particle concentrations in surface seawater samples.

REFERENCES

Andrae, M.O., 1986: The ocean as a source of atmospheric sulfur compounds. In The Role of Air-Sea Exchange in Geochemical Cycling, edited by P. Buat-Menard NATO/ASI Series, C-185, 331-362, D. Reidel Publishing Co.

Andreae, M.O., and H. Raemdonck, 1983: Dimethyl sulfide in the surface ocean and marine atmosphere. Science, 221, 744-747.

Blanchard, D.C., 1983: The production, distribution, and bacterial enrichment of sea-salt aerosols. In Air-Sea Exchange of Gases and Particles, P.S. Liss and W.G.N. Slinn, Eds., Reidel, 407-454.

Blanchard, D.C., and L.D. Syzdek, 1970: Mechanism for the water-to-air transfer and concentration of bacteria. Science, 170, 626-628.

Blanchard, D.C., and L.D. Syzdek, 1974: Importance of bubble scavenging in water-to-air transfer of organic material and bacteria. J. Rech. Atmos., 8, 529-540.

Blanchard, D.C., and L.D. Syzdek, 1982: Water-to-air transfer and enrichment of bacteria in drops. Appl. Environ. Microbiol., 43, 1001-1005.

Ivanov, A.I., 1966: Some data on phytoplankton of the Gulf of Mexico and Florida Strait. Studies on the Central American Seas No. 1, pp. 81-90 (English translation by U.S. Dept. of Commerce, Joint Publ. Res. Serv. 1968).

Schnell and Vali, 1976: Biogenic ice nuclei: Terrestrial and marine sources. J. Atmos. Sci., 33, 1554-1564.

APPENDIX

Size distributions of suspended particles in seawater samples collected at various locations

Sample # 4

AVE DIAMETER VS PARTICLE COUNT HISTOGRAM FOR CHEMICAL TYPE: ALL TYPES
SIZE OR SHAPE RANGE FROM: 0.00 TO 8.00
NO. OF PARTICLES IN HISTOGRAM 104 100.00 % TOTAL NO. PARTICLES
NO. OF PARTICLES OUTSIDE OF SIZE OR SHAPE RANGE 0

BIN MAX	NO.	%	00---10---20---30---40---50---60---70---80---90---100
0.40	0	0.0	[
0.80	19	18.2	[**********
1.20	18	17.3	[*********
1.60	12	11.5	[******
2.00	13	12.5	[*******
2.40	8	7.6	[****
2.80	11	10.5	[******
3.20	7	6.7	[****
3.60	6	5.7	[***
4.00	4	3.8	[**
4.40	1	0.9	[*
4.80	0	0.0	[
5.20	3	2.8	[**
5.60	1	0.9	[*
6.00	0	0.0	[
6.40	0	0.0	[
6.80	0	0.0	[
7.20	1	0.9	[*
7.60	0	0.0	[

ALL TYPES

AVE DIAMETER VS PARTICLE COUNT HISTOGRAM FOR CHEMICAL TYPE: SI RICH
SIZE OR SHAPE RANGE FROM: 0.00 TO 8.00
NO. OF PARTICLES IN HISTOGRAM 45 43.27 % TOTAL NO. PARTICLES
NO. OF PARTICLES OUTSIDE OF SIZE OR SHAPE RANGE 0

BIN MAX	NO.	%	00---10---20---30---40---50---60---70---80---90---100
0.40	0	0.0	[
0.80	7	15.5	[********
1.20	9	20.0	[**********
1.60	5	11.1	[******
2.00	6	13.3	[*******
2.40	1	2.2	[**
2.80	6	13.3	[*******
3.20	4	8.8	[*****
3.60	3	6.6	[****
4.00	2	4.4	[***
4.40	0	0.0	[
4.80	0	0.0	[
5.20	2	4.4	[***
5.60	0	0.0	[

Si-Rich

AVE DIAMETER VS PARTICLE COUNT HISTOGRAM FOR CHEMICAL TYPE: FE RICH
SIZE OR SHAPE RANGE FROM: 0.00 TO 8.00
NO. OF PARTICLES IN HISTOGRAM 10 9.62 % TOTAL NO. PARTICLES
NO. OF PARTICLES OUTSIDE OF SIZE OR SHAPE RANGE 0

```
BIN MAX   NO.  %    00---10---20---30---40---50---60---70---80---90---100
  0.40     0   0.0 [
  0.80     3  30.0 [****************
  1.20     1  10.0 [******                              Fe-Rich
  1.60     3  30.0 [****************
  2.00     1  10.0 [******
  2.40     0   0.0 [
  2.80     0   0.0 [
  3.20     1  10.0 [******
  3.60     0   0.0 [
  4.00     0   0.0 [
  4.40     1  10.0 [******
```

AVE DIAMETER VS PARTICLE COUNT HISTOGRAM FOR CHEMICAL TYPE: CA RICH
SIZE OR SHAPE RANGE FROM: 0.00 TO 8.00
NO. OF PARTICLES IN HISTOGRAM 7 6.73 % TOTAL NO. PARTICLES
NO. OF PARTICLES OUTSIDE OF SIZE OR SHAPE RANGE 0

```
BIN MAX   NO.  %    00---10---20---30---40---50---60---70---80---90---100
  0.40     0   0.0 [
  0.80     0   0.0 [
  1.20     1  14.2 [********                            Ca-Rich
  1.60     1  14.2 [********
  2.00     2  28.5 [****************
  2.40     2  28.5 [****************
  2.80     0   0.0 [
  3.20     0   0.0 [
  3.60     0   0.0 [
  4.00     0   0.0 [
  4.40     0   0.0 [
  4.80     0   0.0 [
  5.20     0   0.0 [
  5.60     0   0.0 [
  6.00     0   0.0 [
  6.40     0   0.0 [
  6.80     0   0.0 [
  7.20     1  14.2 [********
  7.60     0   0.0 [
```

AVE DIAMETER VS PARTICLE COUNT HISTOGRAM FOR CHEMICAL TYPE: SI,AL
SIZE OR SHAPE RANGE FROM: 0.00 TO 8.00
NO. OF PARTICLES IN HISTOGRAM 1 0.96 % TOTAL NO. PARTICLES
NO. OF PARTICLES OUTSIDE OF SIZE OR SHAPE RANGE 0

BIN MAX	NO.	%	00---10---20---30---40---50---60---70---80---90---100
0.40	0	0.0	[
0.80	0	0.0	[
1.20	0	0.0	[
1.60	0	0.0	[
2.00	0	0.0	[
2.40	0	0.0	[
2.80	1	100.0	[**********

Si,Al-Rich

AVE DIAMETER VS PARTICLE COUNT HISTOGRAM FOR CHEMICAL TYPE: UNKNOWN
SIZE OR SHAPE RANGE FROM: 0.00 TO 8.00
NO. OF PARTICLES IN HISTOGRAM 41 39.42 % TOTAL NO. PARTICLES
NO. OF PARTICLES OUTSIDE OF SIZE OR SHAPE RANGE 0

BIN MAX	NO.	%	00---10---20---30---40---50---60---70---80---90---100
0.40	0	0.0	[
0.80	9	21.9	[**********
1.20	7	17.0	[*********
1.60	3	7.3	[****
2.00	4	9.7	[*****
2.40	5	12.1	[*******
2.80	4	9.7	[*****
3.20	2	4.8	[***
3.60	3	7.3	[****
4.00	2	4.8	[***
4.40	0	0.0	[
4.80	0	0.0	[
5.20	1	2.4	[*
5.60	1	2.4	[*
6.00	0	0.0	[

Unknown

AVE DIAMETER VS PARTICLE COUNT HISTOGRAM FOR CHEMICAL TYPE: ALL TYPES
SIZE OR SHAPE RANGE FROM: 0.00 TO 8.00
NO. OF PARTICLES IN HISTOGRAM 122 100.00 % TOTAL NO. PARTICLES
NO. OF PARTICLES OUTSIDE OF SIZE OR SHAPE RANGE 0

BIN MAX	NO.	%	00---10---20---30---40---50---60---70---80---90---100
0.40	0	0.0	[
0.80	24	19.6	[**********
1.20	24	19.6	[**********
1.60	25	20.4	[**********
2.00	13	10.6	[******
2.40	9	7.3	[****
2.80	7	5.7	[***
3.20	4	3.2	[**
3.60	6	4.9	[***
4.00	3	2.4	[**
4.40	0	0.0	[
4.80	2	1.6	[*
5.20	1	0.8	[*
5.60	1	0.8	[*
6.00	0	0.0	[
6.40	0	0.0	[
6.80	2	1.6	[*
7.20	0	0.0	[
7.60	1	0.8	[*
8.00	0	0.0	[

All Types

AVE DIAMETER VS PARTICLE COUNT HISTOGRAM FOR CHEMICAL TYPE: SI RICH
SIZE OR SHAPE RANGE FROM: 0.00 TO 8.00
NO. OF PARTICLES IN HISTOGRAM 74 60.66 % TOTAL NO. PARTICLES
NO. OF PARTICLES OUTSIDE OF SIZE OR SHAPE RANGE 0

BIN MAX	NO.	%	00---10---20---30---40---50---60---70---80---90---100
0.40	0	0.0	[
0.80	15	20.2	[**********
1.20	16	21.6	[**********
1.60	14	18.9	[**********
2.00	6	8.1	[*****
2.40	5	6.7	[****
2.80	3	4.0	[***
3.20	4	5.4	[***
3.60	6	8.1	[*****
4.00	3	4.0	[***
4.40	0	0.0	[
4.80	0	0.0	[
5.20	0	0.0	[
5.60	1	1.3	[*
6.00	0	0.0	[
6.40	0	0.0	[
6.80	0	0.0	[
7.20	0	0.0	[
7.60	1	1.3	[*
8.00	0	0.0	[

Si-Rich

AVE DIAMETER VS PARTICLE COUNT HISTOGRAM FOR CHEMICAL TYPE: AL RICH
SIZE OR SHAPE RANGE FROM: 0.00 TO 8.00
NO. OF PARTICLES IN HISTOGRAM 1 0.82 % TOTAL NO. PARTICLES
NO. OF PARTICLES OUTSIDE OF SIZE OR SHAPE RANGE 0

Al-Rich

BIN MAX	NO.	%	00---10---20---30---40---50---60---70---80---90---100
0.40	0	0.0	[
0.80	1	100.0	[**********

AVE DIAMETER VS PARTICLE COUNT HISTOGRAM FOR CHEMICAL TYPE: FE RICH
SIZE OR SHAPE RANGE FROM: 0.00 TO 8.00
NO. OF PARTICLES IN HISTOGRAM 18 14.75 % TOTAL NO. PARTICLES
NO. OF PARTICLES OUTSIDE OF SIZE OR SHAPE RANGE 0

Fe-Rich

BIN MAX	NO.	%	00---10---20---30---40---50---60---70---80---90---100
0.40	0	0.0	[
0.80	2	11.1	[******
1.20	6	33.3	[**********
1.60	7	38.8	[**********
2.00	1	5.5	[***
2.40	0	0.0	[
2.80	0	0.0	[
3.20	0	0.0	[
3.60	0	0.0	[
4.00	0	0.0	[
4.40	0	0.0	[
4.80	1	5.5	[***
5.20	0	0.0	[
5.60	0	0.0	[
6.00	0	0.0	[
6.40	0	0.0	[
6.80	1	5.5	[***
7.20	0	0.0	[

AVE DIAMETER VS PARTICLE COUNT HISTOGRAM FOR CHEMICAL TYPE: SAKF (Si, Al, K, Fe)
SIZE OR SHAPE RANGE FROM: 0.00 TO 8.00
NO. OF PARTICLES IN HISTOGRAM 7 5.74 % TOTAL NO. PARTICLES
NO. OF PARTICLES OUTSIDE OF SIZE OR SHAPE RANGE Ø

BIN MAX	NO.	%	00---10---20---30---40---50---60---70---80---90---100
0.40	0	0.0	[
0.80	1	14.2	[********
1.20	0	0.0	[
1.60	1	14.2	[********
2.00	3	42.8	[************************
2.40	1	14.2	[********
2.80	0	0.0	[
3.20	0	0.0	[
3.60	0	0.0	[
4.00	0	0.0	[
4.40	0	0.0	[
4.80	0	0.0	[
5.20	0	0.0	[
5.60	0	0.0	[
6.00	0	0.0	[
6.40	0	0.0	[
6.80	1	14.2	[********
7.20	0	0.0	[

Si,Al,K,Fe-Rich

AVE DIAMETER VS PARTICLE COUNT HISTOGRAM FOR CHEMICAL TYPE: UNKNOWN
SIZE OR SHAPE RANGE FROM: 0.00 TO 8.00
NO. OF PARTICLES IN HISTOGRAM 22 18.03 % TOTAL NO. PARTICLES
NO. OF PARTICLES OUTSIDE OF SIZE OR SHAPE RANGE Ø

BIN MAX	NO.	%	00---10---20---30---40---50---60---70---80---90---100
0.40	0	0.0	[
0.80	5	22.7	[************
1.20	2	9.0	[*****
1.60	3	13.6	[*******
2.00	3	13.6	[*******
2.40	3	13.6	[*******
2.80	4	18.1	[**********
3.20	0	0.0	[
3.60	0	0.0	[
4.00	0	0.0	[
4.40	0	0.0	[
4.80	1	4.5	[***
5.20	1	4.5	[***
5.60	0	0.0	[

Unknown

Sample # 10

AVE DIAMETER VS PARTICLE COUNT HISTOGRAM FOR CHEMICAL TYPE: ALL TYPES
SIZE OR SHAPE RANGE FROM: 0.00 TO 17.00
NO. OF PARTICLES IN HISTOGRAM 113 100.00 % TOTAL NO. PARTICLES
NO. OF PARTICLES OUTSIDE OF SIZE OR SHAPE RANGE 0

BIN MAX	NO.	%	00---10---20---30---40---50---60---70---80---90---100
0.57	13	11.5	[***
1.13	43	38.0	[**********
1.70	14	12.3	[*******
2.27	12	10.6	[******
2.83	11	9.7	[*****
3.40	1	0.8	[*
3.97	2	1.7	[*
4.53	3	2.6	[**
5.10	3	2.6	[**
5.67	4	3.5	[**
6.23	1	0.8	[*
6.80	0	0.0	[
7.37	0	0.0	[
7.93	1	0.8	[*
8.50	0	0.0	[
9.07	2	1.7	[*
9.63	1	0.8	[*
10.20	0	0.0	[
10.77	0	0.0	[
11.33	0	0.0	[
11.90	0	0.0	[
12.47	0	0.0	[
13.03	0	0.0	[
13.60	1	0.8	[*
14.17	0	0.0	[
14.73	0	0.0	[
15.30	0	0.0	[
15.87	0	0.0	[
16.43	1	0.8	[*
17.00	0	0.0	[

ALL TYPES

AVE DIAMETER VS PARTICLE COUNT HISTOGRAM FOR CHEMICAL TYPE: SI RICH
SIZE OR SHAPE RANGE FROM: 0.00 TO 17.00
NO. OF PARTICLES IN HISTOGRAM 8 7.00 % TOTAL NO. PARTICLES
NO. OF PARTICLES OUTSIDE OF SIZE OR SHAPE RANGE 0

BIN MAX	NO.	%	00---10---20---30---40---50---60---70---80---90---100
0.57	1	12.5	[*******
1.13	2	25.0	[**********
1.70	0	0.0	[
2.27	0	0.0	[
2.83	0	0.0	[
3.40	0	0.0	[
3.97	0	0.0	[
4.53	0	0.0	[
5.10	0	0.0	[
5.67	2	25.0	[**********
6.23	1	12.5	[*******
6.80	0	0.0	[
7.37	0	0.0	[
7.93	0	0.0	[
8.50	0	0.0	[
9.07	1	12.5	[*******
9.63	0	0.0	[
10.20	0	0.0	[
10.77	0	0.0	[
11.33	0	0.0	[
11.90	0	0.0	[
12.47	0	0.0	[
13.03	0	0.0	[
13.60	0	0.0	[
14.17	0	0.0	[
14.73	0	0.0	[
15.30	0	0.0	[
15.87	0	0.0	[
16.43	1	12.5	[*******
17.00	0	0.0	[

Si-Rich

AVE DIAMETER VS PARTICLE COUNT HISTOGRAM FOR CHEMICAL TYPE: FE RICH
SIZE OR SHAPE RANGE FROM: 0.00 TO 17.00
NO. OF PARTICLES IN HISTOGRAM 17 15.04 % TOTAL NO. PARTICLES
NO. OF PARTICLES OUTSIDE OF SIZE OR SHAPE RANGE 0

BIN MAX	NO.	%	00---10---20---30---40---50---60---70---80---90---100
0.57	2	11.7	[******
1.13	5	29.4	[***************
1.70	3	17.6	[*********
2.27	4	23.5	[************
2.83	2	11.7	[******
3.40	0	0.0	[
3.97	1	5.8	[***
4.53	0	0.0	[

Fe-Rich

AVE DIAMETER VS PARTICLE COUNT HISTOGRAM FOR CHEMICAL TYPE: SI,AL,K,F
SIZE OR SHAPE RANGE FROM: 0.00 TO 17.00
NO. OF PARTICLES IN HISTOGRAM 5 4.42 % TOTAL NO. PARTICLES
NO. OF PARTICLES OUTSIDE OF SIZE OR SHAPE RANGE 0

BIN MAX	NO.	%	00---10---20---30---40---50---60---70---80---90---100
0.57	0	0.0	[
1.13	1	20.0	[**********
1.70	0	0.0	[
2.27	2	40.0	[********************
2.83	1	20.0	[**********
3.40	0	0.0	[
3.97	0	0.0	[
4.53	0	0.0	[
5.10	0	0.0	[
5.67	0	0.0	[
6.23	0	0.0	[
6.80	0	0.0	[
7.37	0	0.0	[
7.93	1	20.0	[**********

Si,Al,K,Fe-Rich

AVE DIAMETER VS PARTICLE COUNT HISTOGRAM FOR CHEMICAL TYPE: AL RICH
SIZE OR SHAPE RANGE FROM: 0.00 TO 17.00
NO. OF PARTICLES IN HISTOGRAM 1 0.88 % TOTAL NO. PARTICLES
NO. OF PARTICLES OUTSIDE OF SIZE OR SHAPE RANGE 0

Al-Rich

BIN MAX	NO.	%	00---10---20---30---40---50---60---70---80---90---100
0.57	1	100.0	[**********

AVE DIAMETER VS PARTICLE COUNT HISTOGRAM FOR CHEMICAL TYPE: CL RICH
SIZE OR SHAPE RANGE FROM: 0.00 TO 17.00
NO. OF PARTICLES IN HISTOGRAM 48 42.48 % TOTAL NO. PARTICLES
NO. OF PARTICLES OUTSIDE OF SIZE OR SHAPE RANGE 0

Cl-Rich

BIN MAX	NO.	%	00---10---20---30---40---50---60---70---80---90---100
0.57	7	14.5	[********
1.13	22	45.8	[**********
1.70	8	16.6	[*********
2.27	2	4.1	[***
2.83	4	8.3	[*****
3.40	0	0.0	[
3.97	1	2.0	[**
4.53	0	0.0	[
5.10	1	2.0	[**
5.67	0	0.0	[
6.23	0	0.0	[
6.80	0	0.0	[
7.37	0	0.0	[
7.93	0	0.0	[
8.50	0	0.0	[
9.07	1	2.0	[**
9.63	1	2.0	[**
10.20	0	0.0	[
10.77	0	0.0	[
11.33	0	0.0	[
11.90	0	0.0	[
12.47	0	0.0	[
13.03	0	0.0	[
13.60	1	2.0	[**
14.17	0	0.0	[

AVE DIAMETER VS PARTICLE COUNT HISTOGRAM FOR CHEMICAL TYPE: NON-INT
SIZE OR SHAPE RANGE FROM: 0.00 TO 17.00
NO. OF PARTICLES IN HISTOGRAM 7 6.19 % TOTAL NO. PARTICLES
NO. OF PARTICLES OUTSIDE OF SIZE OR SHAPE RANGE 0

Organic?

BIN MAX	NO.	%	00---10---20---30---40---50---60---70---80---90---100
0.57	1	14.2	[********
1.13	5	71.4	[**
1.70	0	0.0	[
2.27	1	14.2	[********
2.83	0	0.0	[

AVE DIAMETER VS PARTICLE COUNT HISTOGRAM FOR CHEMICAL TYPE: UNKNOWN
SIZE OR SHAPE RANGE FROM: 0.00 TO 17.00
NO. OF PARTICLES IN HISTOGRAM 27 23.89 % TOTAL NO. PARTICLES
NO. OF PARTICLES OUTSIDE OF SIZE OR SHAPE RANGE 0

Unknown

BIN MAX	NO.	%	00---10---20---30---40---50---60---70---80---90---100
0.57	1	3.7	[**
1.13	8	29.6	[***************
1.70	3	11.1	[******
2.27	3	11.1	[******
2.83	4	14.8	[********
3.40	1	3.7	[**
3.97	0	0.0	[
4.53	3	11.1	[******
5.10	2	7.4	[****
5.67	2	7.4	[****
6.23	0	0.0	[

PART V. METEOROLOGICAL ANALYSES

ATMOSPHERIC TRAJECTORIES

Joyce M. Harris

1. THE TRAJECTORY MODEL

The GMCC atmospheric trajectory program (Harris, 1982) was used to calculate back trajectories for selected locations along the cruise track during the Air Chemistry Experiment over the Gulf of Mexico, July and August 1986.

The trajectory program calculates an interpolated path of the wind back for as many as 10 days in a manner similar to that used by Heffter and Taylor (1975). A 10-day trajectory consists of 80 individually computed 3-h trajectory segments placed end-to-end. To compute a 3-h trajectory segment, the model performs an interpolation in time between two consecutive data fields. The resulting grids are weighted for the midpoint of the 3-h period in question. The latitude and longitude coordinates of the endpoint of the previous trajectory segment are converted to NMC grid units (X,Y). By using bilinear interpolation, the winds at (X,Y) are calculated from the winds at the four grid points surrounding (X,Y). A first-guess trajectory segment is then computed, assuming that this wind is constant for the 3-h duration (Fig. 1). At the midpoint of the first-guess segment (X_m,Y_m) the winds are again calculated by bilinear interpolation. These latter winds are then used to compute the final trajectory segment beginning at (X,Y) because they are assumed to be more representative of winds for the 3-h segment. This iterative approximation technique is called the modified Euler method (Stark, 1970).

2. DATA USED IN THE MODEL

The wind data used to compute the trajectories are analyzed fields of U and V coordinates produced by the U.S. National Meteorological Center's (NMC) global atmospheric model twice daily at 0000 GMT and 1200 GMT. The grid mesh of the data is 2.5 degrees of latitude and longitude, and the data are provided for the entire globe. NMC's model is constrained by availability of data collected from around the globe. The data, consisting of raobs, aircraft

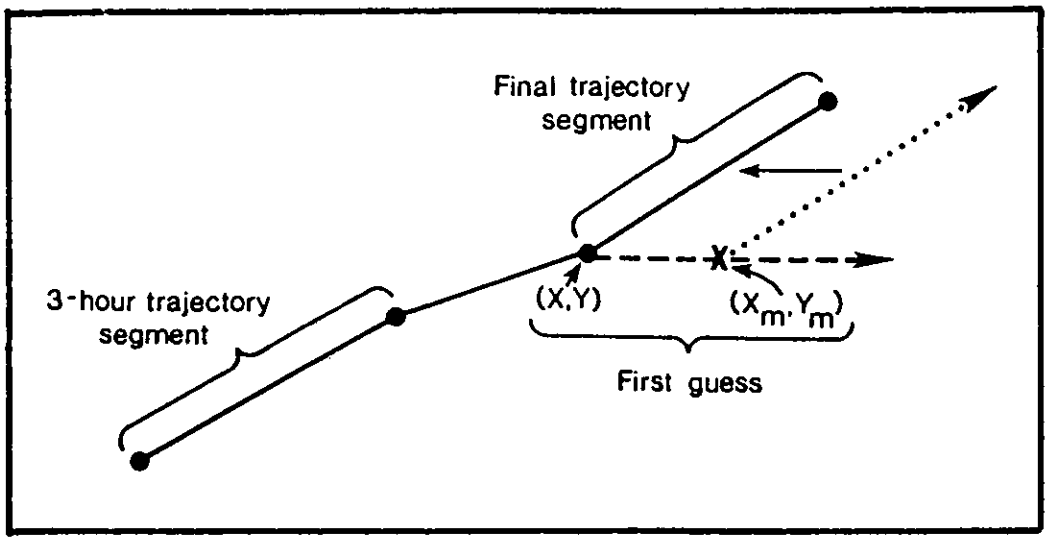

Figure 1. Modified Euler's method for computing a 3-h trajectory segment. The first-guess segment is computed using the interpolated winds at the midpoint (X_m,Y_m) of the first-guess segment.

and ship reports, and satellite data, are most plentiful over the continental U.S.A.; however, there is good coverage over the Gulf of Mexico, provided in part by satellite temperature soundings that are converted hydrostatically to thickness, then to heights, and finally to winds geostrophically. Because of the large scale of the NMC model, local land-sea breezes are not reflected in the trajectories, though they at times may have had considerable influence upon measurements taken during the cruise.

3. DISCUSSION

These plots of the wind path give a sense of the large-scale air flow. The trajectories show that the Gulf of Mexico was dominated by the easterly tradewind regime during the cruise.

Possible sources of error in the trajectories are interpolation, sparse data coverage, observational or NMC model errors, and the approximations made to simulate the real atmosphere. The 1000-mb trajectories must be used with caution because surface friction is not accounted for by the trajectory model, and sometimes 1000-mb winds are extrapolated below the surface. Because any of these errors could be compounded as trajectory segments are added farther

back from the destination, the apparent origin of each trajectory should be considered an approximation, and whenever possible, potential source regions should be corroborated by other atmospheric measurements.

Despite their limitations, atmospheric trajectories have been frequently employed in studies of long-range transport of gases and aerosols. Halter and Harris (1983) investigated causes for CO_2 variability at Barrow, Alaska, using trajectories and other analysis methods. A study of trajectories by Harris (1984) during the Arctic Gas and Aerosol Sampling Program (AGASP) linked a major aerosol event measured on an aircraft near Barrow to transport of industrial pollution from the Ural region of the U.S.S.R. A 7-year back-trajectory climatology by Miller and Harris (1984) characterized air flow to the island of Bermuda and found a strong positive correlation between highly acidic rainfall and trajectories from the North American continent.

4. SAMPLE TRAJECTORIES

The isobaric version of the trajectory program used here follows the winds along surfaces of constant pressure: 1000 mb, 850 mb, and 700 mb. Examples of back trajectories computed along the cruise track are shown in Figs. 2-5 (the complete set of trajectories appears in the Appendix). The numerals along the tracks give the travel time in days from the destination. Figure 2 shows trajectories arriving early in the cruise on 22 July 1986. The northeast tradewind regime that dominated the cruise is evident in both Fig. 2 and 3. Figure 3 shows trajectories arriving about 2 weeks later on 8 August 1986. Both figures indicate little shear among the three layers shown. Agreement among the layers lends confidence to the indicated path of the wind. Figure 4, in contrast, shows one of the few examples during the cruise in which there was a strong shear between 700 mb and the lower-level winds. Relative to potential sources, this situation is more complex. Finally Fig. 5 shows extremely light winds at 1000 mb on 3 August. During stagnant conditions such as these it would be difficult to learn much about the long-range transport affecting sampling.

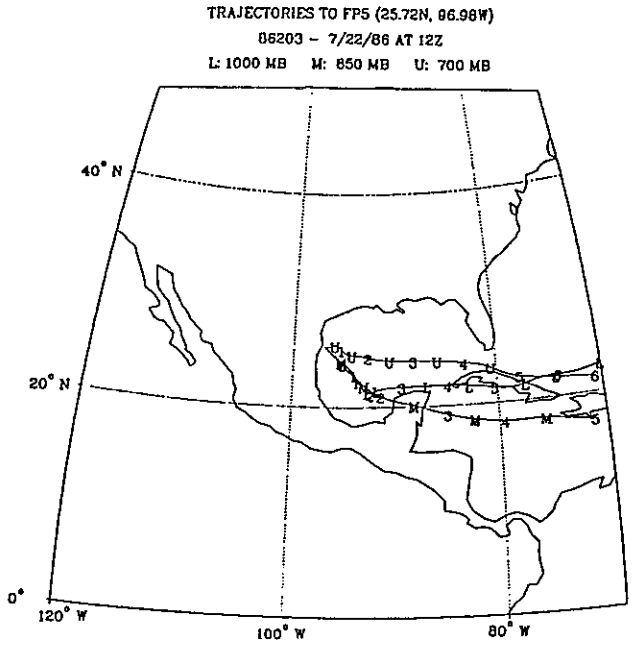

Figure 2. Back trajectories arriving at (25.72°N, 96.98°W) on 22 July 1986 at 1200 GMT on the (L) 1000-, (M) 850-, and (U) 700-mb surfaces.

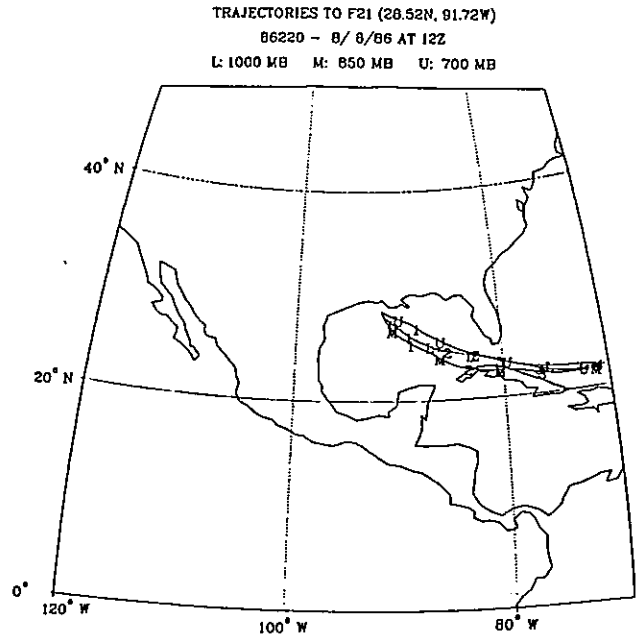

Figure 3. Back trajectories arriving at (28.52°N, 91.72°W) on 8 August 1986 at 1200 GMT on the (L) 1000-, (M) 850-, and (U) 700-mb surfaces.

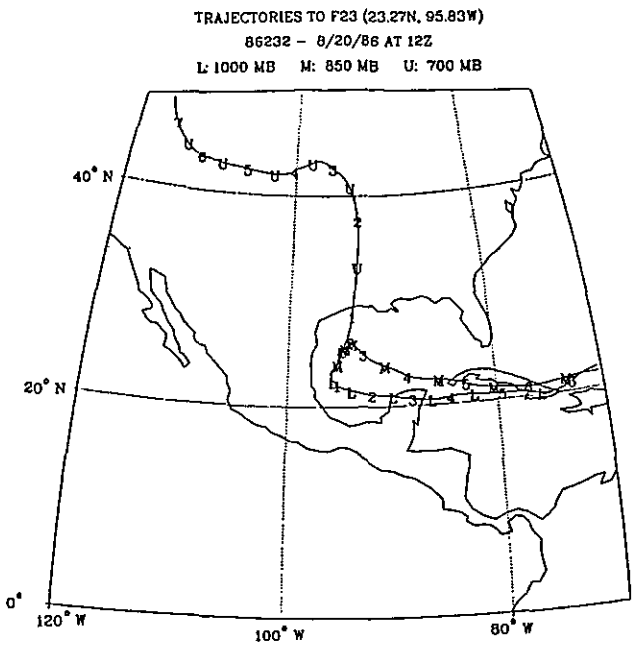

Figure 4. Back trajectories arriving at (23.27°N, 95.83°W) on 20 August 1986 at 1200 GMT on the (L) 1000-, (M) 850-, and (U) 700-mb surfaces.

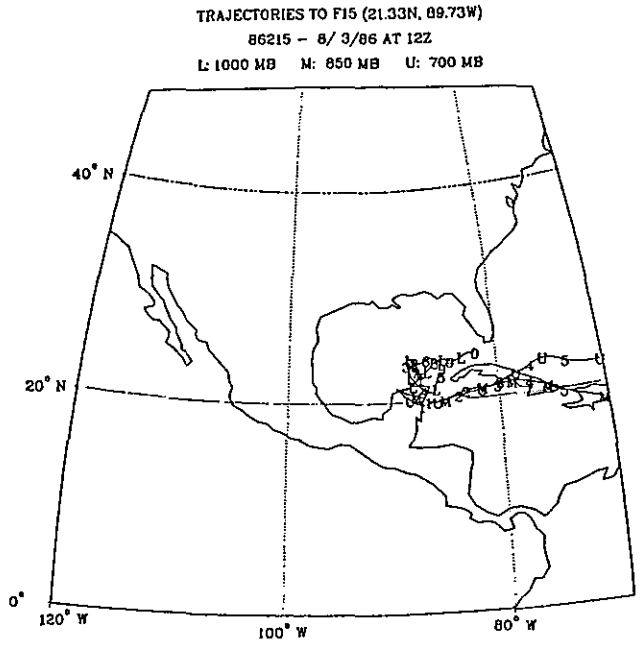

Figure 5. Back trajectories arriving at (21.33°N, 89.73°W) on 3 August 1986 at 1200 GMT on the (L) 1000-, (M) 850-, and (U) 700-mb surfaces.

REFERENCES

Halter, B.C., and J.M. Harris, 1983: On the variability of atmospheric carbon dioxide concentration at Barrow, Alaska, during winter. J. Geophys. Res., 88:6858-6862.

Harris, J.M., 1982: The GMCC atmospheric trajectory program. NOAA Tech. Memo. ERL-ARL-116, NOAA Environmental Research Laboratories, Boulder, Colo., p. 30.

Harris, J.M., 1984: Trajectories during AGASP. Geophys. Res. Lett. 11:453-456.

Heffter, J.L., and A.D. Taylor, 1975: Trajectory model: Part I, A regional-continental scale transport, diffusion, and deposition model. NOAA Tech. Memo. ERL-ARL-50, NOAA Environmental Research Laboratories, Boulder, Colo., 28 pp.

Miller, J.M., and J.M. Harris, 1984: The flow climatology of Bermuda and its implications on long-range transport. Atmos. Environ., 19:409-414.

Stark, P.A., 1970: Introduction to Numerical Methods. Macmillan, New York 254-257.

APPENDIX

Additional air trajectories

TRAJECTORIES TO FP2 (28.33N, 95.87W)
86202 - 7/21/86 AT 0Z
L: 1000 MB M: 850 MB U: 700 MB

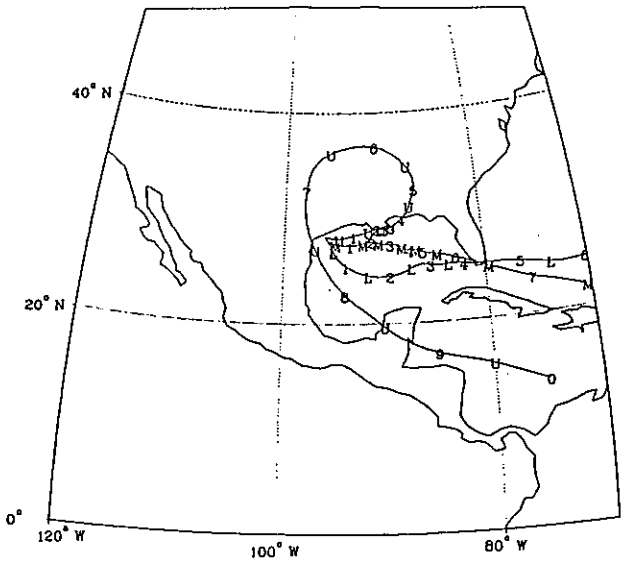

TRAJECTORIES TO FP2 (29.28N, 94.67W)
86202 - 7/21/86 AT 12Z
L: 1000 MB M: 850 MB U: 700 MB

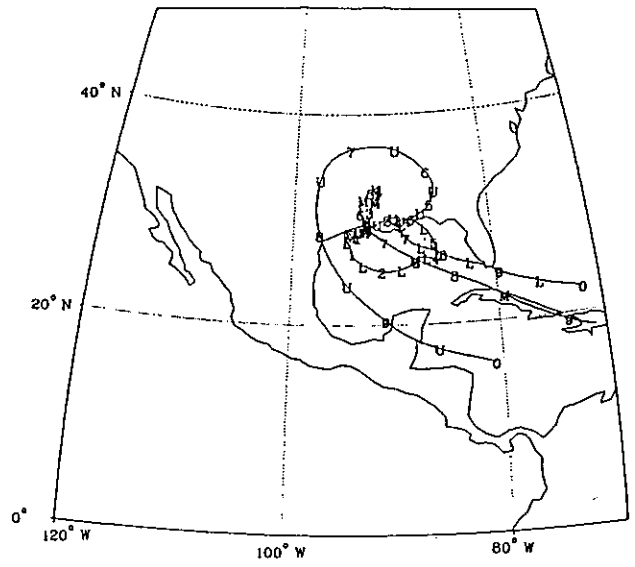

TRAJECTORIES TO FP3 (27.28N, 96.98W)
86203 - 7/22/86 AT 0Z
L: 1000 MB M: 850 MB U: 700 MB

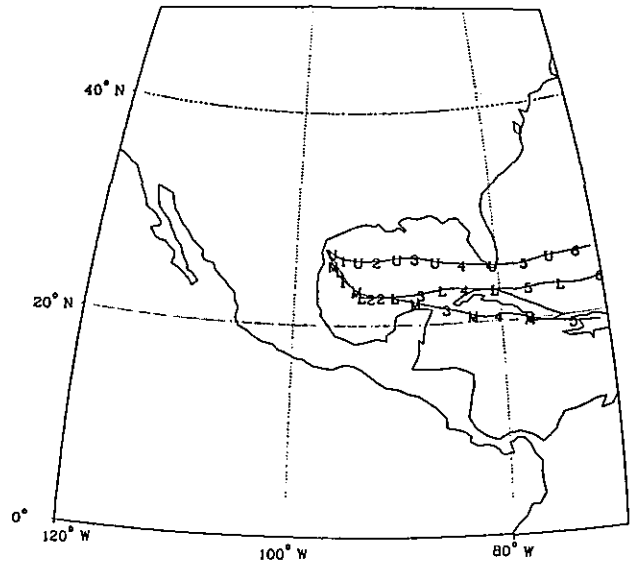

TRAJECTORIES TO FP5 (25.72N, 96.98W)
86203 - 7/22/86 AT 12Z
L: 1000 MB M: 850 MB U: 700 MB

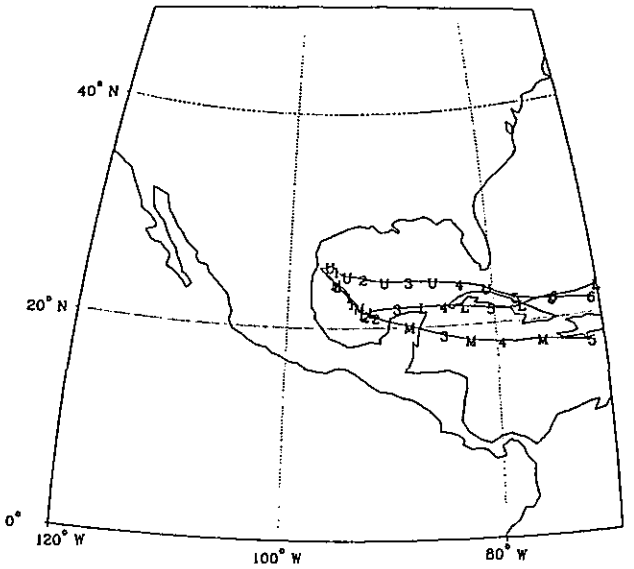

TRAJECTORIES TO FP5 (24.23N, 97.42W)
86204 - 7/23/86 AT 0Z
L: 1000 MB M: 850 MB U: 700 MB

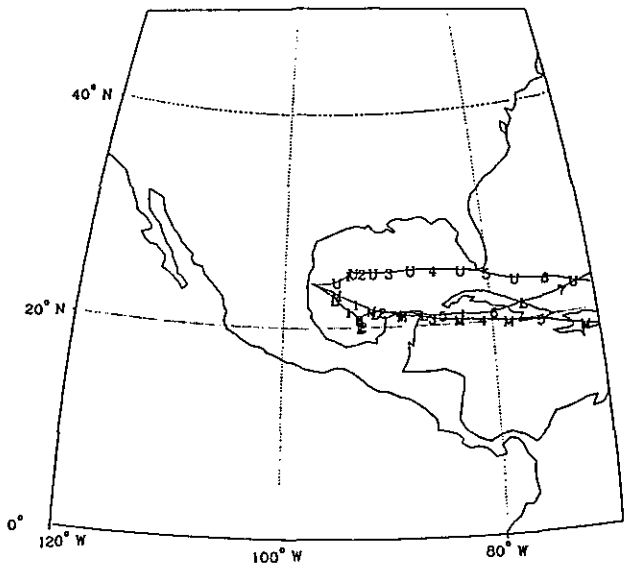

TRAJECTORIES TO FP7 (23.05N, 97.63W)
86204 - 7/23/86 AT 12Z
L: 1000 MB M: 850 MB U: 700 MB

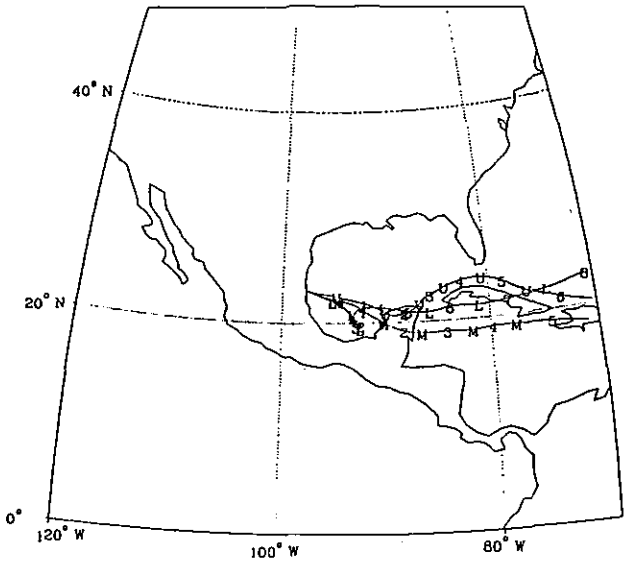

TRAJECTORIES TO FP7 (21.12N, 96.95W)
86207 – 7/26/86 AT 0Z
L: 1000 MB M: 850 MB U: 700 MB

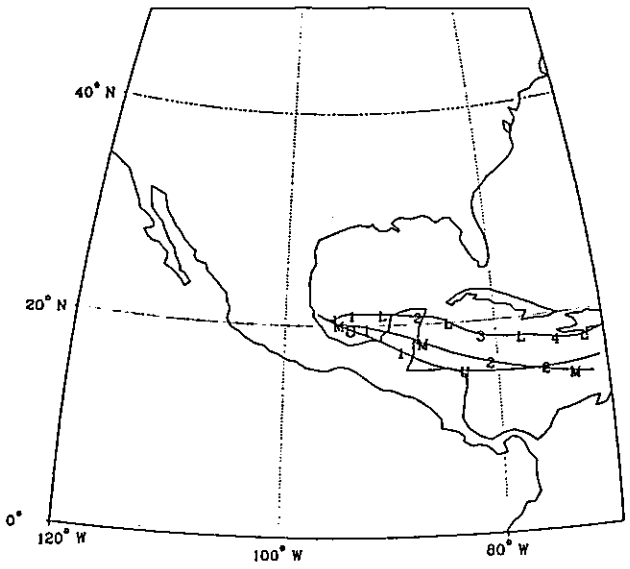

TRAJECTORIES TO FP9 (19.75N, 96.32W)
86207 – 7/26/86 AT 12Z
L: 1000 MB M: 850 MB U: 700 MB

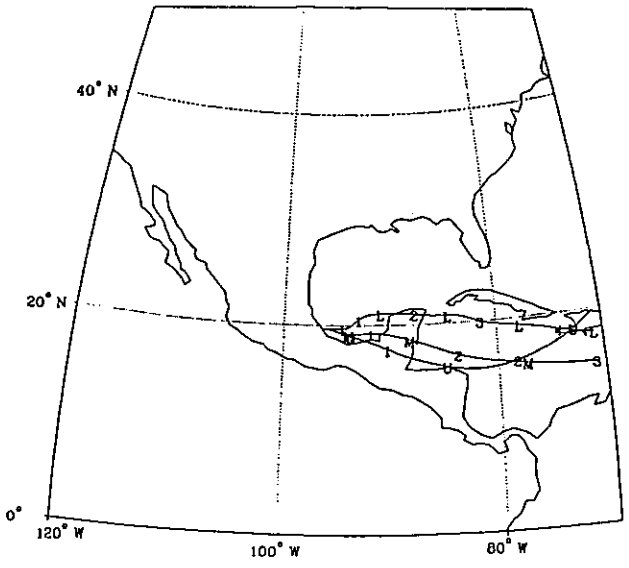

TRAJECTORIES TO FP9 (19.10N, 95.67W)
86211 – 7/30/86 AT 0Z
L: 1000 MB M: 850 MB U: 700 MB

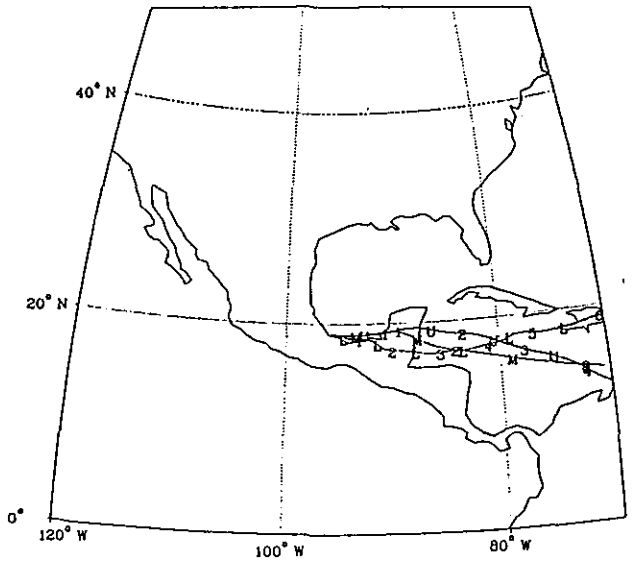

TRAJECTORIES TO F11 (18.22N, 94.33W)
86211 – 7/30/86 AT 12Z
L: 1000 MB M: 850 MB U: 700 MB

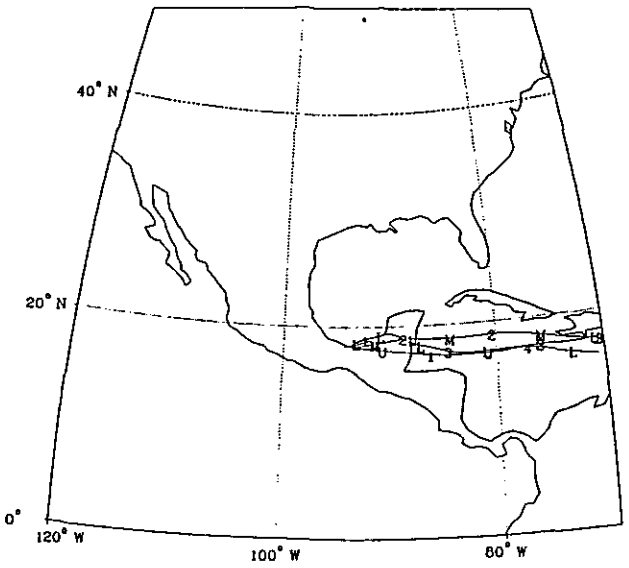

TRAJECTORIES TO F11 (18.55N, 93.13W)
86214 - 6/ 2/86 AT 0Z
L: 1000 MB M: 850 MB U: 700 MB

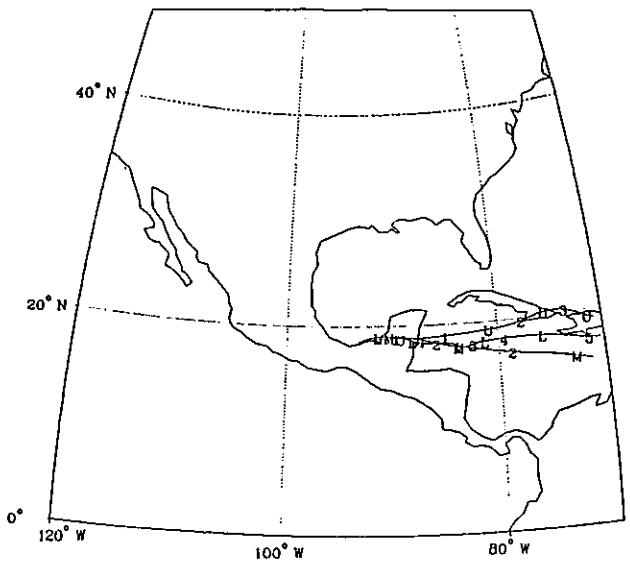

TRAJECTORIES TO F13 (19.57N, 92.00W)
86214 - 6/ 2/86 AT 12Z
L: 1000 MB M: 850 MB U: 700 MB

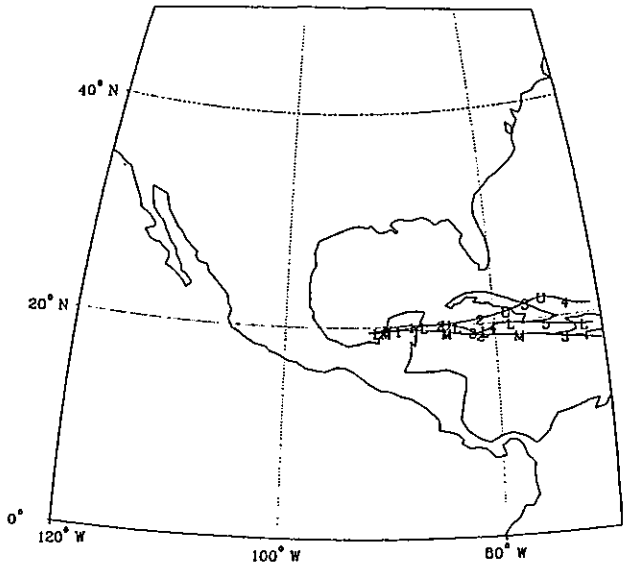

TRAJECTORIES TO F13 (20.58N, 90.97W)
86215 - 8/ 3/86 AT 0Z
L: 1000 MB M: 850 MB U: 700 MB

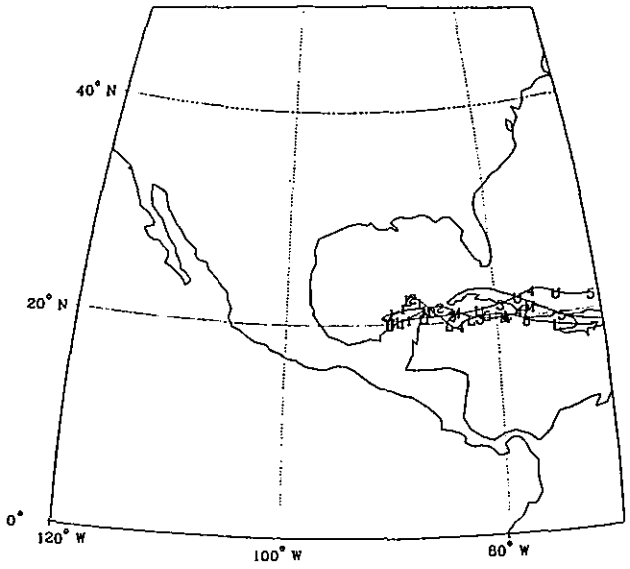

TRAJECTORIES TO F15 (21.33N, 89.73W)
86215 - 8/ 3/86 AT 12Z
L: 1000 MB M: 850 MB U: 700 MB

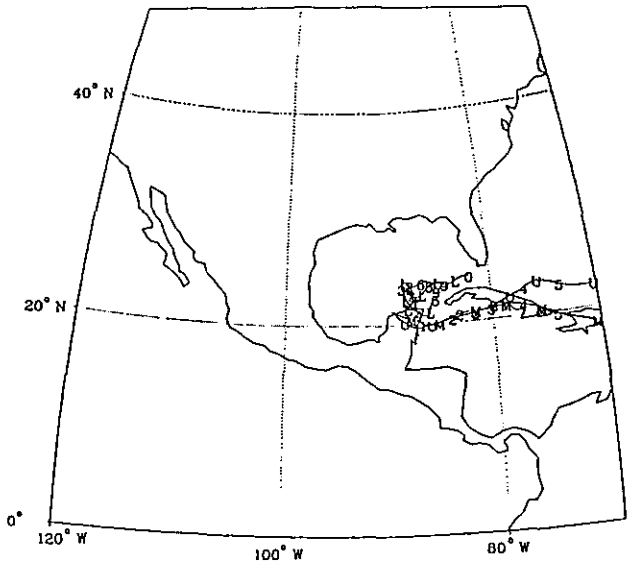

TRAJECTORIES TO FI5 (22.68N, 89.83W)
86218 - 6/ 6/86 AT 0Z
L: 1000 MB M: 850 MB U: 700 MB

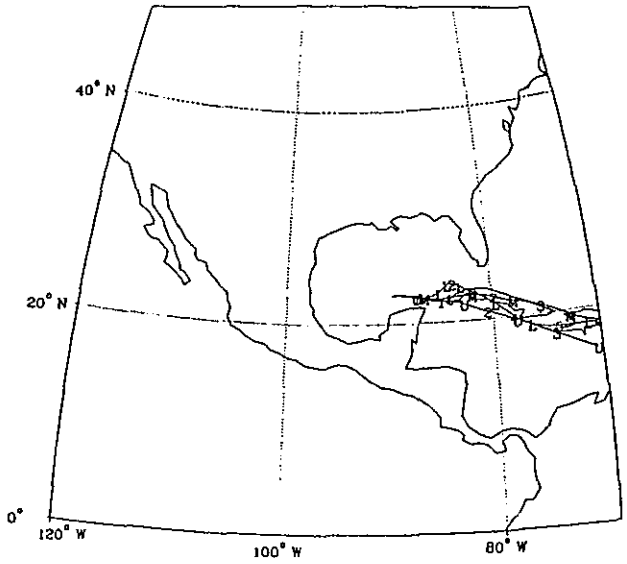

TRAJECTORIES TO FI7 (24.08N, 89.77W)
86218 - 6/ 6/86 AT 12Z
L: 1000 MB M: 850 MB U: 700 MB

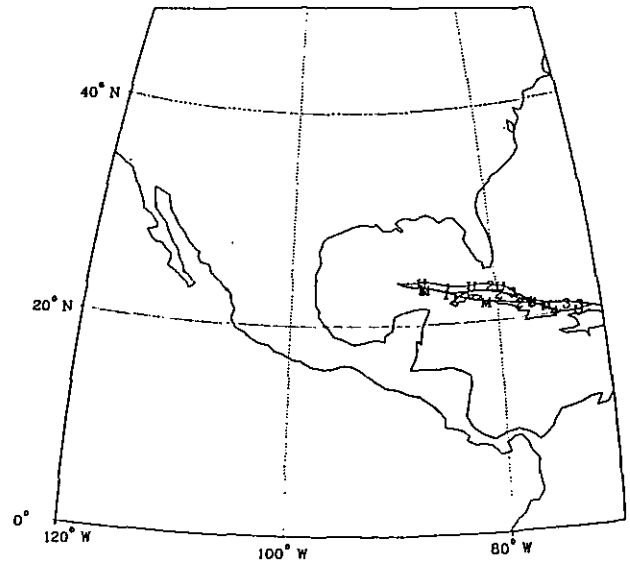

TRAJECTORIES TO F17 (25.68N, 89.67W)
86219 - 8/ 7/86 AT 0Z
L: 1000 MB M: 850 MB U: 700 MB

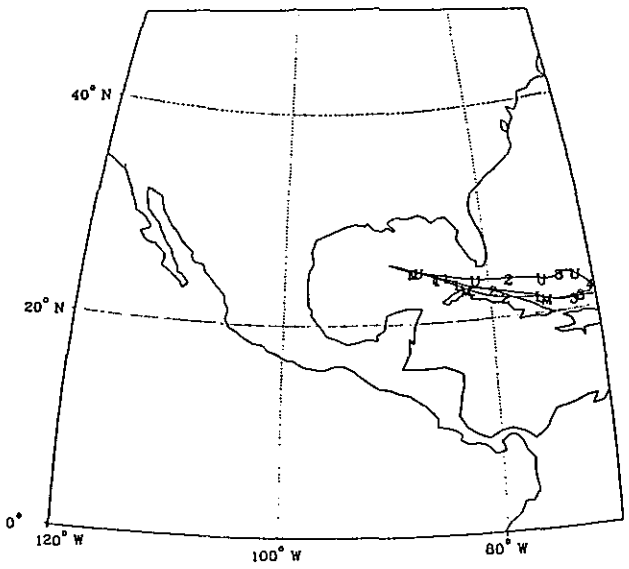

TRAJECTORIES TO F19 (27.42N, 89.57W)
86219 - 8/ 7/86 AT 12Z
L: 1000 MB M: 850 MB U: 700 MB

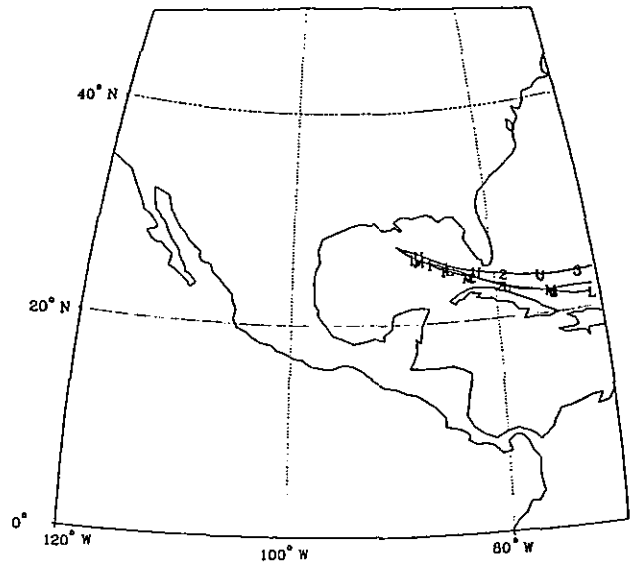

TRAJECTORIES TO F19 (28.93N, 90.00W)
86220 - 8/ 8/86 AT 0Z
L: 1000 MB M: 650 MB U: 700 MB

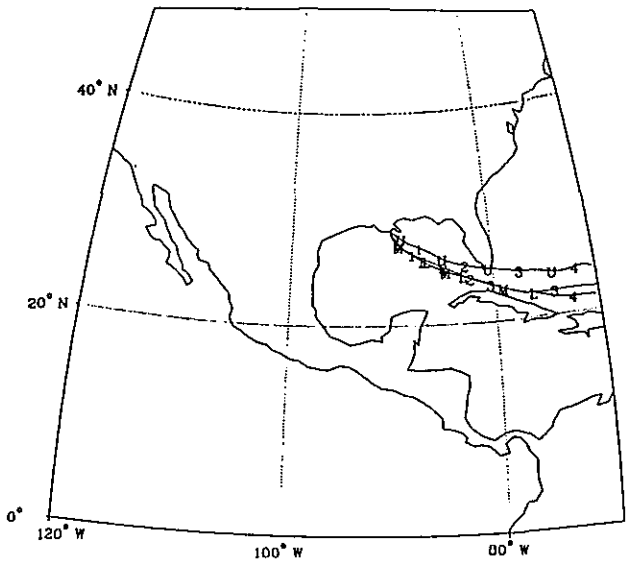

TRAJECTORIES TO F21 (28.52N, 91.72W)
86220 - 8/ 8/86 AT 12Z
L: 1000 MB M: 650 MB U: 700 MB

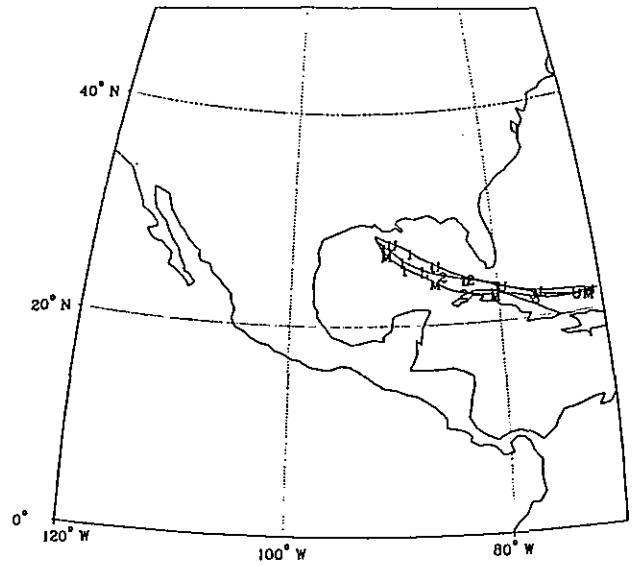

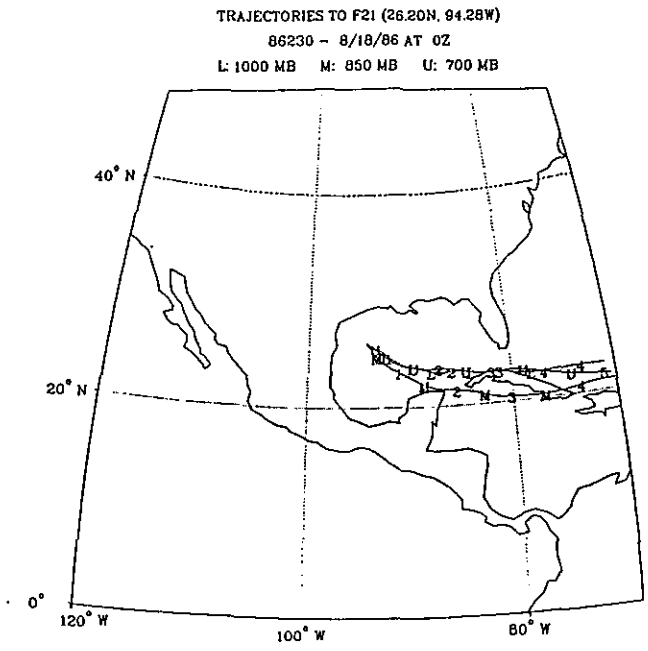
TRAJECTORIES TO F21 (26.20N, 94.28W)
86230 - 8/18/86 AT 0Z
L: 1000 MB M: 850 MB U: 700 MB
40° N
20° N
0°
120° W
100° W
80° W

TRAJECTORIES TO F22 (24.72N, 95.12W)
86232 - 8/20/86 AT 0Z
L: 1000 MB M: 850 MB U: 700 MB

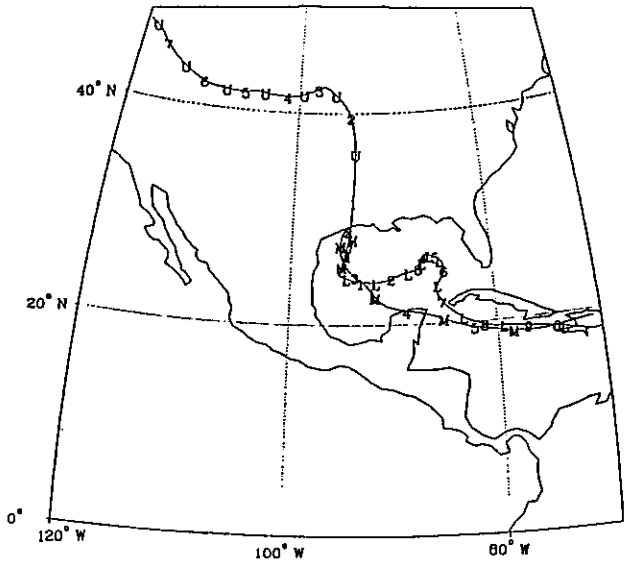

TRAJECTORIES TO F23 (23.27N, 95.83W)
86232 - 8/20/86 AT 12Z
L: 1000 MB M: 850 MB U: 700 MB

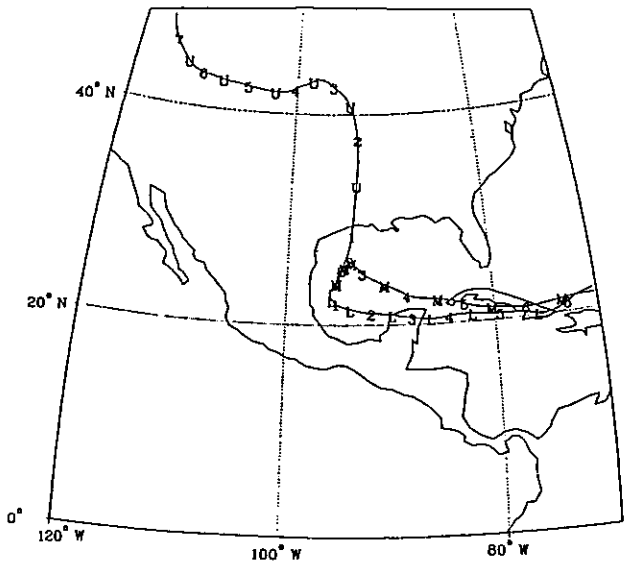

SOLAR MEASUREMENTS

Lois A. Stearns

Continuous global flux on a horizontal surface was measured in two spectral bands during the Gulf of Mexico project from 20 July through 8 August 1986. Eppley precision spectral pyranometers were used. The normalized filter functions of the two instruments are illustrated in Fig. 1. The spectral passbands of the instruments are 285-2800 nm (quartz dome) and 630-2800 nm (RG-2 filtered dome). The pyranometers were calibrated at the Solar Radiation Facility of NOAA's Geophysical Monitoring for Climatic Change both before and after the project. Calibration was based on the Absolute Radiation Scale at 25.0°C.

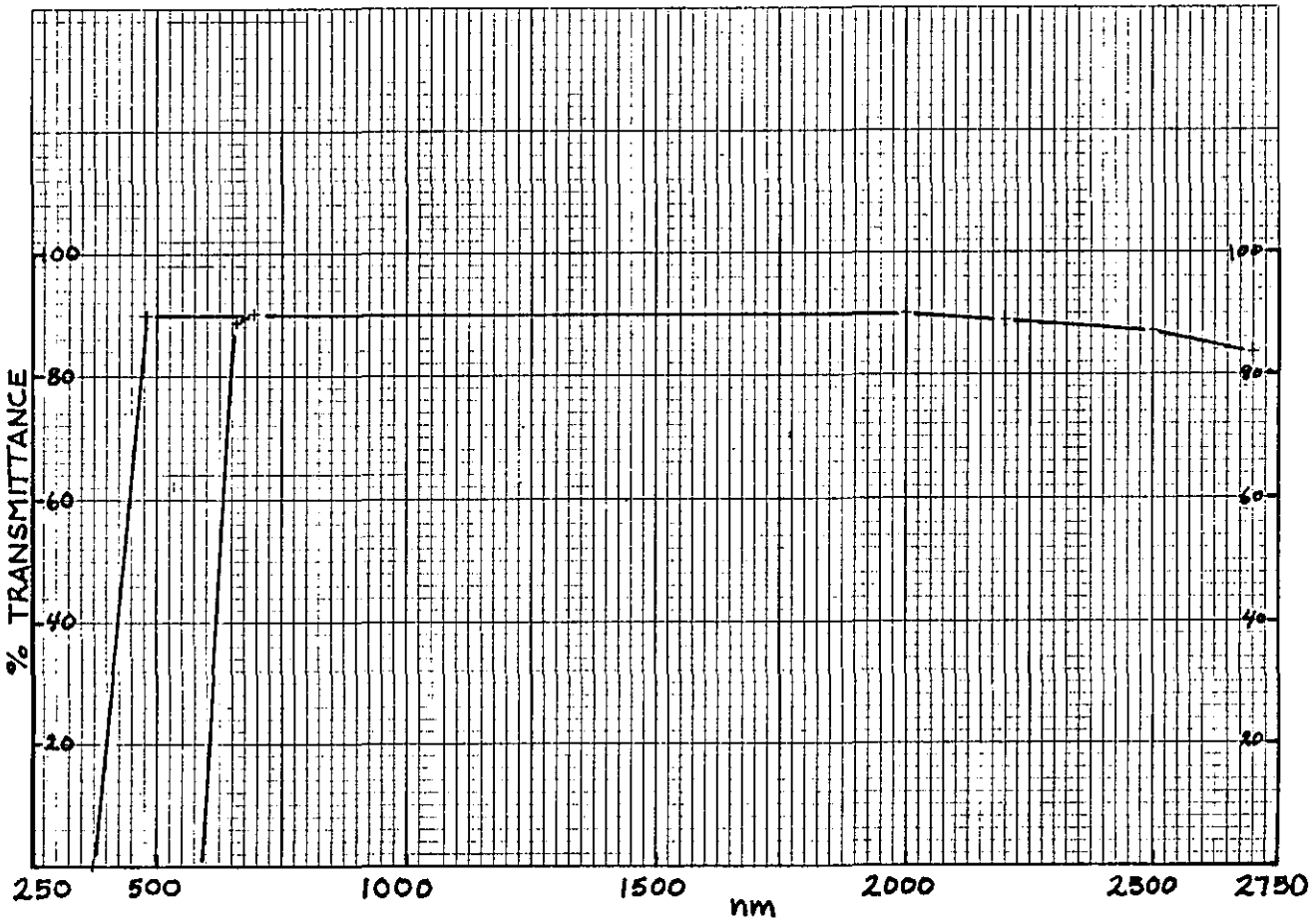

Figure 1. Filter functions of the quartz and RG-2 filter domes.

The instruments were mounted on gimbals at a high point on the ship, and thus away from salt spray. Nearby cables gave little interference to the solar power received by the pyranometers. The domes were cleaned daily. Voltage and zero checks were made daily on the strip chart recorder.

The e-folding response time of the pyranometer is 1 second. Flux variations on time scales of less than 5 seconds cannot be well resolved. Use of a strip chart recorder increases the time resolution to 1 minute. A small part of the time is due to the response of the recorder, which is state-of-the-art. The balance is due to random uncertainty in setting the time location on the charts.

Instrument errors have been thoroughly discussed by Dutton et al. (1985). Compensation for errors was made when applicable. The data reduction of strip chart recording introduces a possible error of 2.2 W m^{-2} to the total flux of 1.98 W m^{-2} to the narrower band flux. This is because the pen line thickness is about 0.2 ordinate on the chart.

The plots in the Appendix include three curves. The squares represent model data that were calculated for the noontime longitude and latitude position of the ship; the curve represents the total irradiance calculated for a clear, no-haze day. The triangles represent measured data for the 285 to 2800 nm, and the circles represent the narrower passband of 630 to 2800 nm. Linear interpolation was employed when data were missing because of problems with cables, masts, bars, and radar interference. The difference between the curves is the irradiance for the 285- to 630-nm wavelengths.

REFERENCES

Dutton, E.G., J.J. DeLuisi, and D.J. Endres, 1985: Solar radiation at the Barrow, AK, GMCC Baseline Observatory 1976-1983. NOAA Data Report ERL ARL-6, 112 pp.

APPENDIX

Day of year (DOY) irradiance

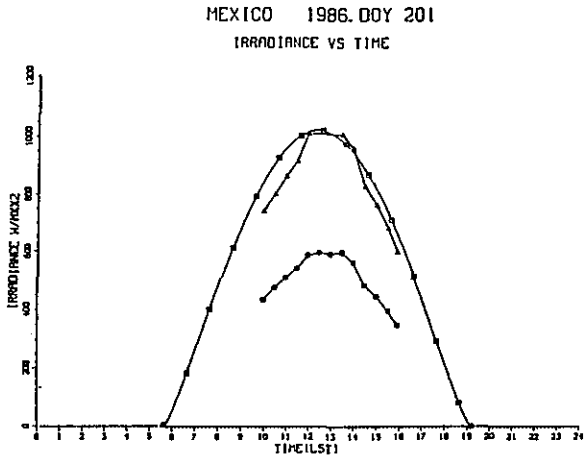
MEXICO 1986 DOY 201
IRRADIANCE VS TIME
IRRADIANCE W/MM2
TIME(LST)

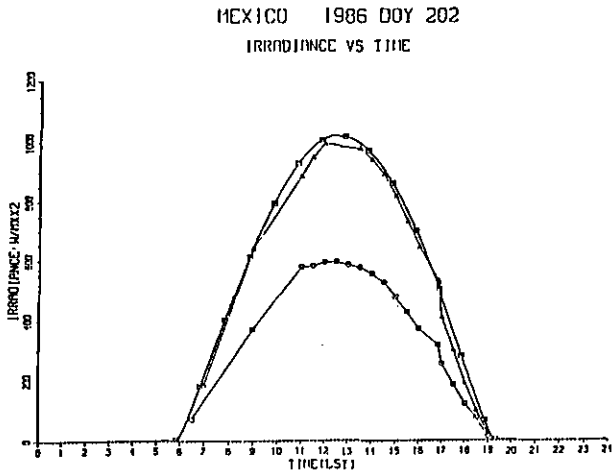
MEXICO 1986 DOY 202
IRRADIANCE VS TIME
IRRADIANCE W/MM2
TIME(LST)

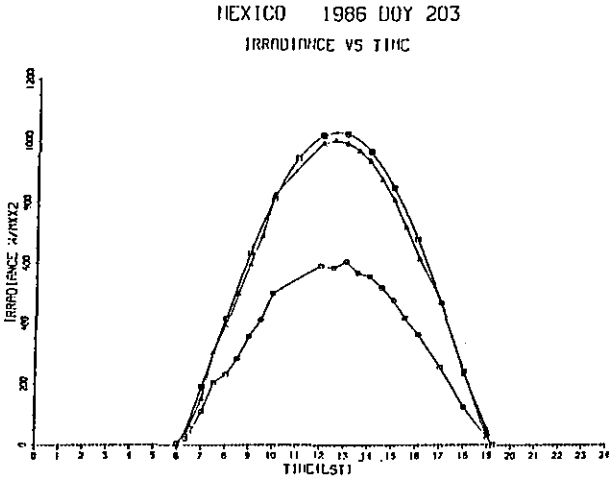
MEXICO 1986 DOY 203
IRRADIANCE VS TIME
IRRADIANCE W/MM2
TIME(LST)

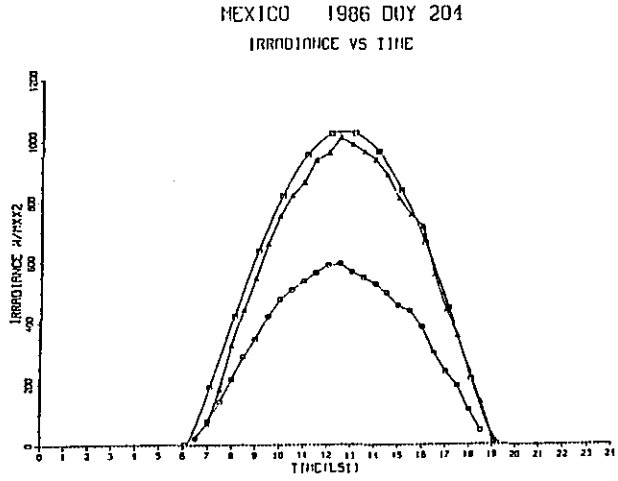
MEXICO 1986 DOY 204
IRRADIANCE VS TIME
IRRADIANCE W/MM2
TIME(LST)

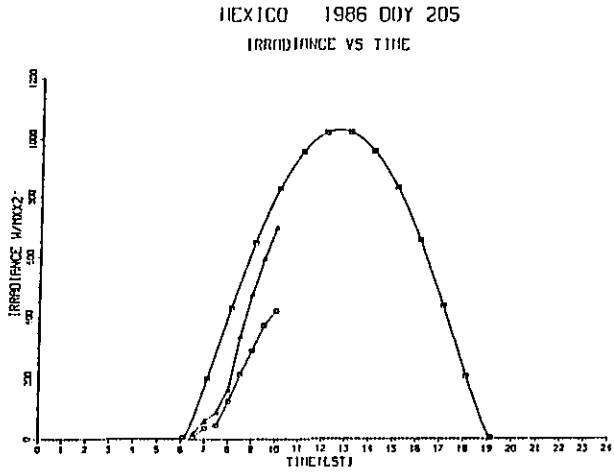
MEXICO 1986 DOY 205
IRRADIANCE VS TIME
IRRADIANCE W/MX2
TIME(LST)

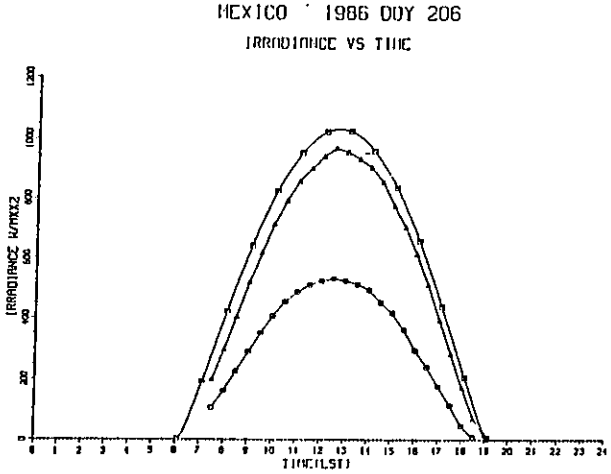
MEXICO 1986 DOY 206
IRRADIANCE VS TIME
IRRADIANCE W/MX2
TIME(LST)

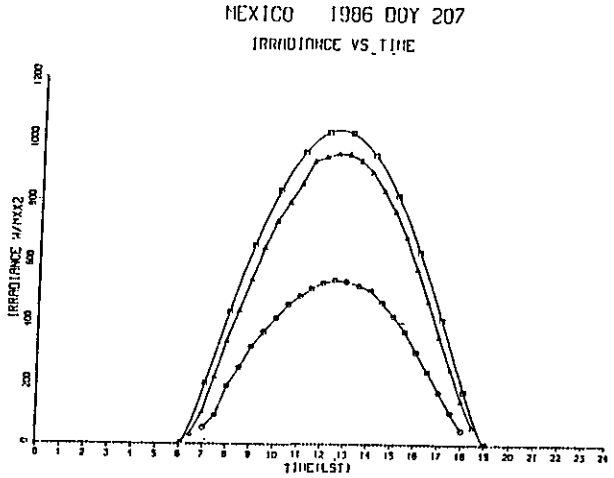
MEXICO 1986 DOY 207
IRRADIANCE VS TIME
IRRADIANCE W/MX2
TIME(LST)

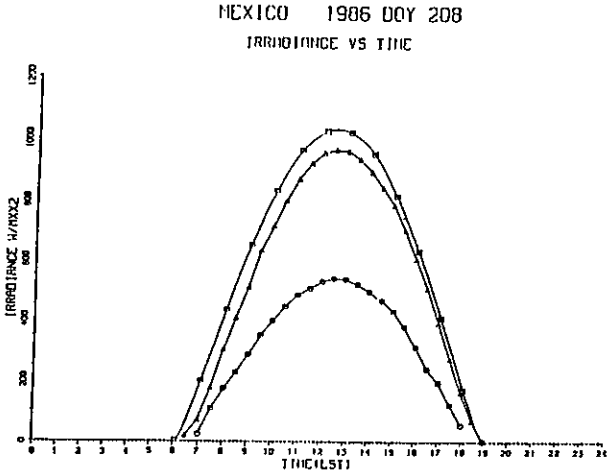
MEXICO 1986 DOY 208
IRRADIANCE VS TIME
IRRADIANCE W/MX2
TIME(LST)

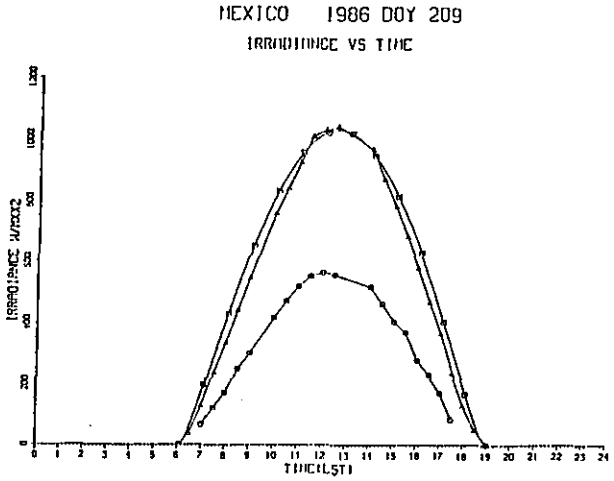
MEXICO 1986 DOY 209
IRRADIANCE VS TIME
IRRADIANCE W/MM2
TIME(LST)

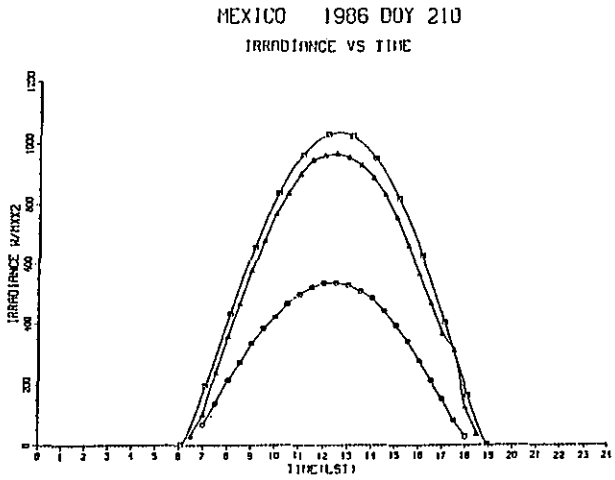
MEXICO 1986 DOY 210
IRRADIANCE VS TIME
IRRADIANCE W/MM2
TIME(LST)

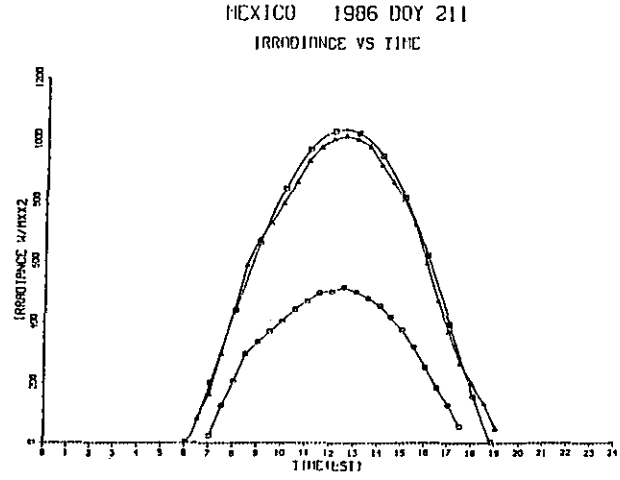
MEXICO 1986 DOY 211
IRRADIANCE VS TIME
IRRADIANCE W/MM2
TIME(LST)

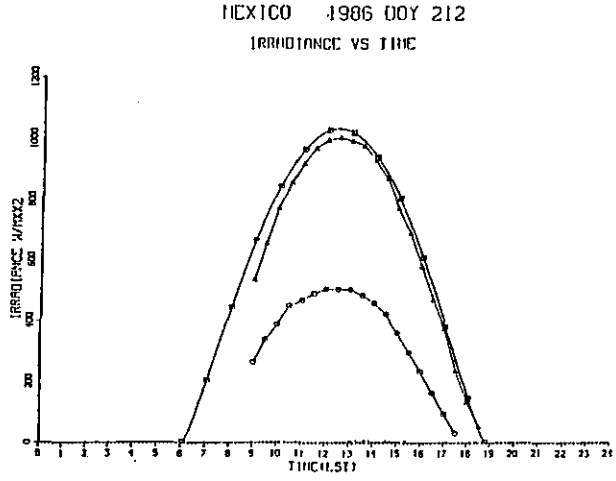
MEXICO 1986 DOY 212
IRRADIANCE VS TIME
IRRADIANCE W/MM2
TIME(LST)

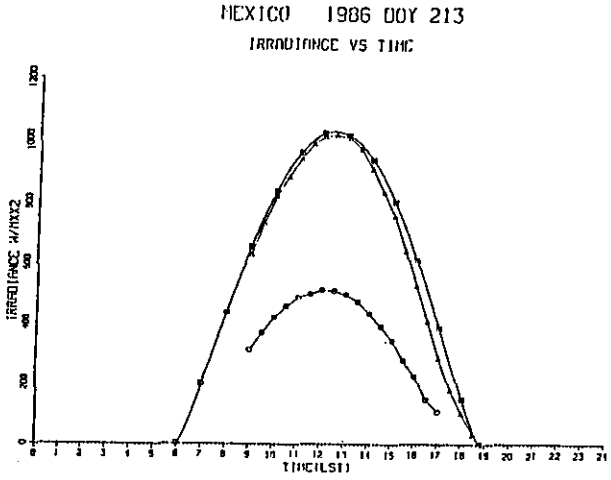
MEXICO 1986 DOY 213
IRRADIANCE VS TIME
IRRADIANCE W/MX2
TIME(LST)

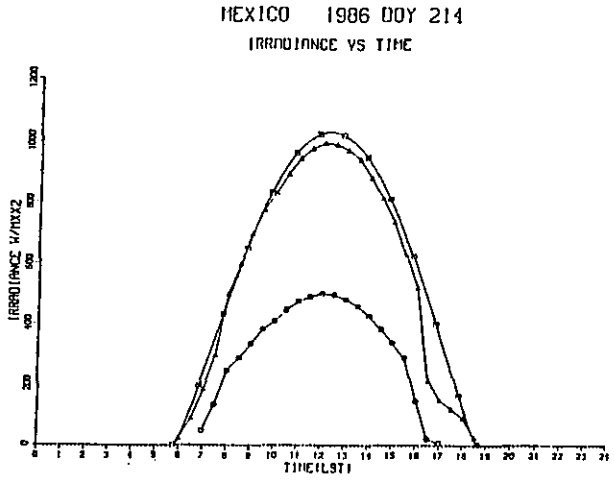
MEXICO 1986 DOY 214
IRRADIANCE VS TIME
IRRADIANCE W/MX2
TIME(LST)

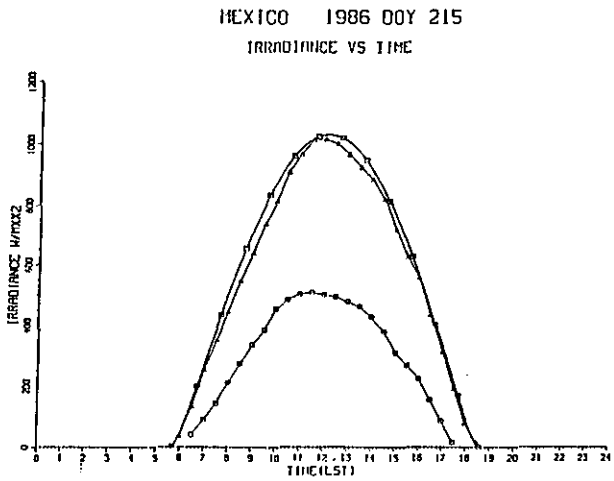
MEXICO 1986 DOY 215
IRRADIANCE VS TIME
IRRADIANCE W/MX2
TIME(LST)

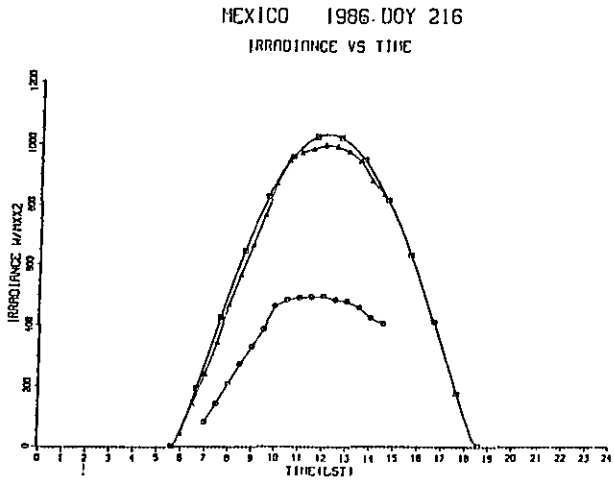
MEXICO 1986 DOY 216
IRRADIANCE VS TIME
IRRADIANCE W/MX2
TIME(LST)

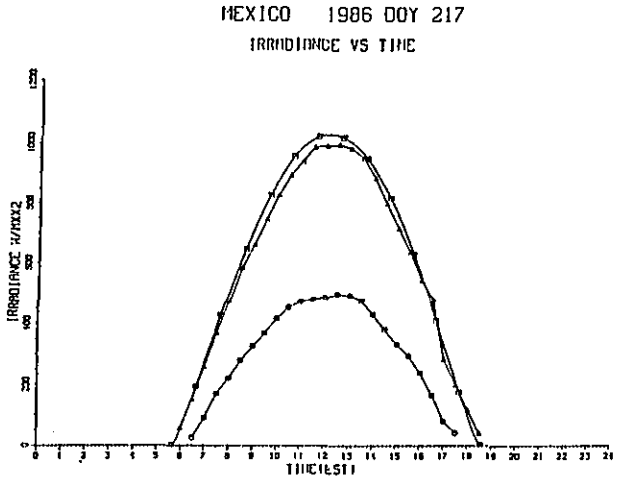
MEXICO 1986 DOY 217
IRRADIANCE VS TIME
IRRADIANCE W/MX2
TIME(LST)

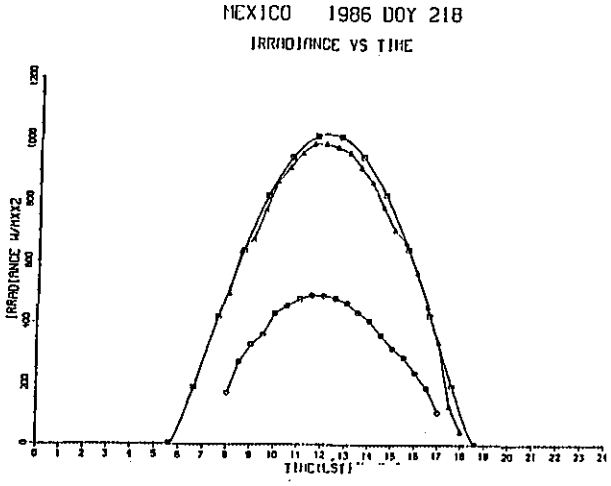
MEXICO 1986 DOY 218
IRRADIANCE VS TIME
IRRADIANCE W/MX2
TIME(LST)

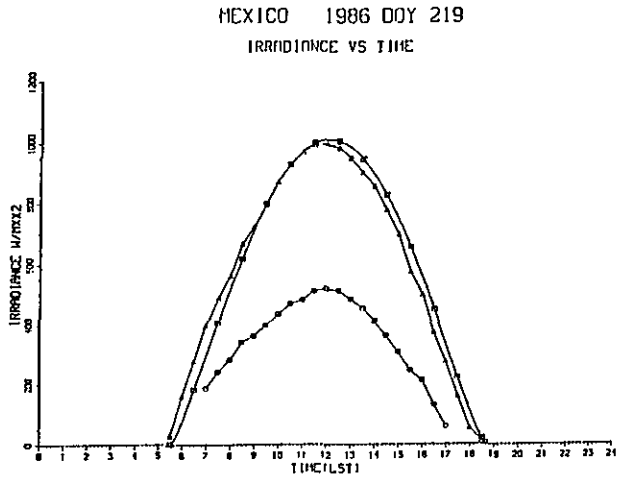
MEXICO 1986 DOY 219
IRRADIANCE VS TIME
IRRADIANCE W/MX2
TIME(LST)

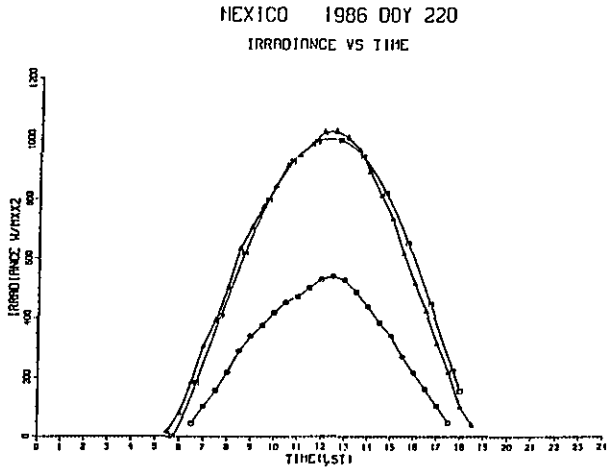
MEXICO 1986 DOY 220
IRRADIANCE VS TIME
IRRADIANCE W/MX2
TIME(LST)

LOCAL WINDS ALONG THE EASTERN COAST OF MEXICO

Everett C. Nickerson

1. INTRODUCTION

The normal diurnal variation in coastal winds can profoundly affect the transport and ultimate fate of pollutants that originate in those coastal regions. The differential heating and cooling of the land surface with respect to the water surface gives rise to vertical circulations of the normal land-sea breeze type, to variations in the depth of the mixed layer, to along-coast winds associated with the Coriolis force, and to the development of clouds and precipitation, given the right meteorological conditions.

2. RESULTS OF PREVIOUS STUDIES

An extensive set of surface meteorological measurements was obtained in the state of Veracruz in 1982-1983 and subsequently reported on (Jauregui-Ostos, 1984). Data were obtained from a network of five stations whose maximum distance from the coast was 13 km. Figure 1, taken from the report, shows the representative summertime diurnal variation at the coastal station of Laguna Verde. A northerly synoptic flow in the early morning hours gradually gives way to a sea breeze, which reaches its maximum intensity at approximately 1500 local time as the land surface heats up. The direction of that thermally driven flow is modified in response to the Coriolis force. The reader is referred to the report for a more complete description of the seasonal differences as well as the diurnal variation in temperature and precipitation.

3. TWO-DIMENSIONAL NUMERICAL SEA BREEZE CALCULATIONS

The 3-D mesoscale model of Nickerson et al. (1986) has been extended to include an improved representation of the planetary boundary layer, as well as soil temperature, soil moisture, and vegetation (Mahfouf et al., 1987). Two-dimensional calculations have been carried out to simulate the evolution of

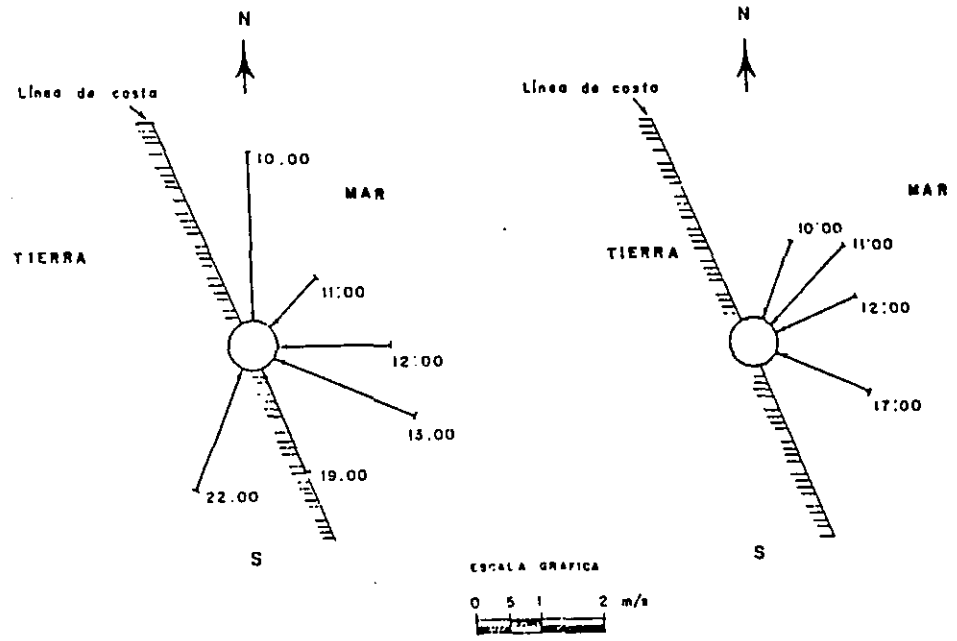

Figure 1. Diurnal variation of the surface wind during sea breeze conditions at Laguna Verde, Veracruz. (From Jauregui-Ostos, 1984.)

the sea breeze that develops in response to the differential heating of the land surface (here specified as the western boundary of the model. Figure 2 shows the horizontal component of the wind perpendicular to the shore at 1500 local time; Fig. 3 shows the corresponding vertical velocity. In agreement with the observations, the sea breeze reaches an intensity of approximately 5 m/s and extends some tens of kilometers inland. The vertical depth of the onshore flow is about 1 km, and the weaker return flow extends to 3 km. The land breeze that develops at night would be on the order of several meters per second.

4. CONCLUSIONS

A comprehensive numerical model could provide useful information on airflow, clouds, and precipitation, and hence have an important role in our understanding of the scavenging and removal of atmospheric contaminants in coastal regions. At present, we are attempting to merge the model of Mahfouf

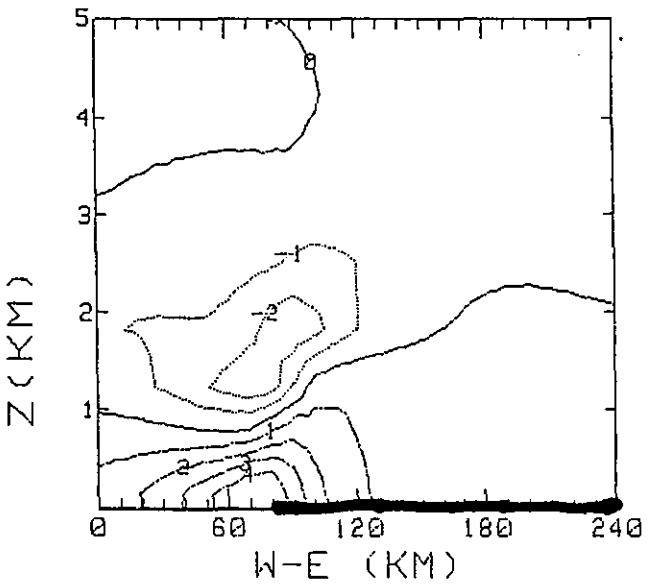

Figure 2. Horizontal wind speed (m/s). Positive values indicate flow from the sea to the land (denoted by the solid line at the bottom of the figure).

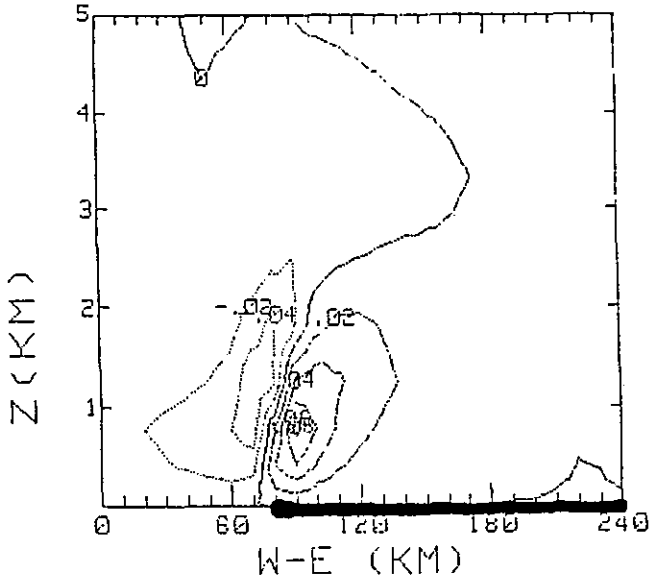

Figure 3. Vertical wind speed (m/s).

et al. (1987) with the treatment of aerosol and gas scavenging contained in the model of Chaumerliac et al. (1987). It should be noted that although 2-D simulations may be capable of elucidating the major features of the problem, it will probably be necessary to carry out 3-D simulations.

REFERENCES

Chaumerliac, N., E. Richard, J-P. Pinty, and E.C. Nickerson, 1987: J. Geophys. Res., 92, D3:3114-3126.

Jauregui-Ostos, E., 1984: Desarrollo de un modelo de difusion atmosferica para evitar la contaminacion ambiental en montana, valle y costa. Universidad Veracruzana.

Mahfouf, J-F., E. Richard, and P. Mascart, 1987: The influence of the soil and vegetation on the development of mesoscale circulations. J. Clim. Appl. Meteorol. (in press).

Nickerson, E. C., E. Richard, R. Rosset, and D.R. Smith, 1986: Mon. Wea. Rev., 114:398-414.

METEOROLOGICAL DESCRIPTION OF RAINWATER CASE DAYS

Cecilia Girz Griffith

1. INTRODUCTION

The six rainwater case days from the 1986 Gulf of Mexico cruise (Table 1) represent convection caused by several types of forcing. The meteorological setting on each of these days was determined by analyzing standard National Weather Service plots of surface and upper-air data, plots of thermodynamic sounding data, and loops of GOES (Geostationary Operational Environmental

Table 1. Satellite-derived parameters for the rainwater cases

Date	Time of rain sample (LT)†	Ship location	Type of convection	Max. size (km^2)	Cloud lifetime (UCT)	Min. temp. (°C)	Est. cloud top (km)
23 Jul	0530-0545	23°2.5'N 97°37.5'W	Isolated	2,612*	1100-1300	-54	12.20
28 Jul	0115-0130	18°0'N 95°50'W	Mesoscale	37,000E	0000F-1100	-75	16.64
30 Jul	0530 0630	18°19.9'N 94°34.3'W	Isolated	500E	1100-1130	unknown	NA
1 Aug	0628-0720	18°10'N 94°20'W	Convection w/meso.sys.	2,000E	1230	>-5G	5.92
10 Aug	0930-1025	29°20'N 94°50'W	Isolated	10,588*	1300-1500	-53	12.00
11 Aug	1440-1847	29°20'N 94°50'W	Prefrontal	410,002*	1700-0200	-72	25.00

† LT = local time
* Maximum size of cloud during its lifetime measured at -20°C
E Maximum size of cloud during its lifetime estimated from -32°C
F First available image; cloud initiated before this time
G Estimated from hard-copy gray scale

Satellite) thermal infrared (10-12 μm) imagery. Temporal frequency and spatial resolution of these data sets varied. The upper-air (radiosonde) data are taken twice daily, the surface data are archived at 3-h intervals, and the IR images are archived hourly. In the U.S.A., surface stations are about 100 km apart and stations of the radiosonde network are about 400 km apart; in Mexico these networks are much sparser, and over the Gulf of Mexico, of course, they are nonexistent. The satellite data are approximately 8 km × 8 km at the satellite subpoint (the Equator and 135°W), but pixel (satellite picture element) area increases away from the subpoint.

Archiving restrictions and the spatial or temporal resolution limit the usefulness of these data. For example, the land-based radiosonde data (Fig. 1) are often not representative of the atmosphere over the Gulf where convection can begin. The sounding network is also too sparse to capture meso-β-scale (20-200 km) features. The in-house archive of GOES hard copy and

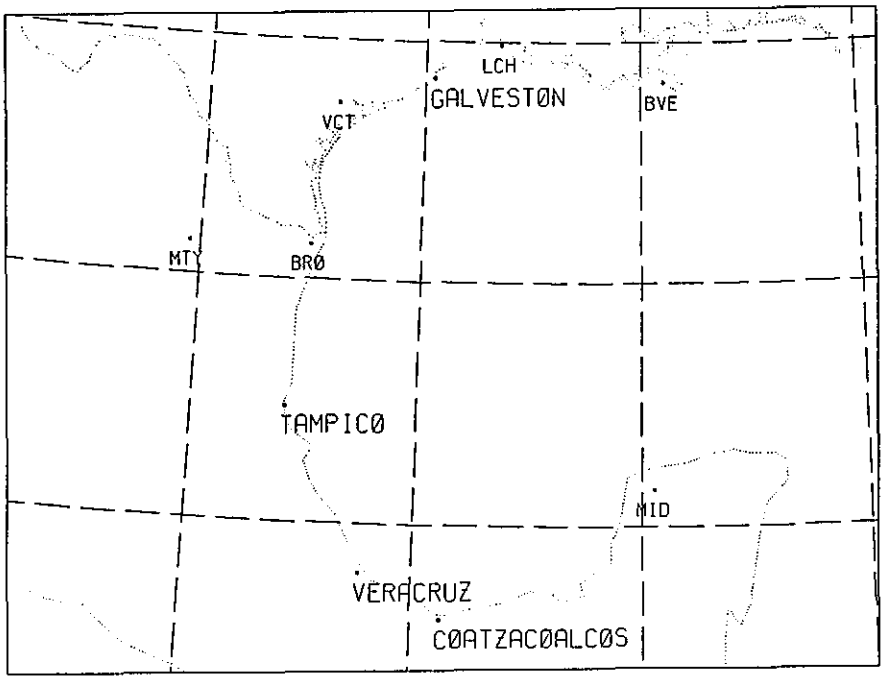

Figure 1. Locations of radiosonde stations in the Gulf of Mexico coastal region. The three-character station identifier is shown for Brownsville, Texas (BRO), Bootheville, Louisiana (BVE), Lake Charles, Louisiana (LCH), Merida, U.S.M. (MID), Monterrey, U.S.M. (MTY), and Victoria, Texas (VCT). Lake Charles did not operate on any day of interest.

digital data did not include data south of about 21.5°N. Hard copy images were borrowed from the National Hurricane Center (NHC) in Miami, Florida, to make satellite assessments for the 28 and 30 July cases in the vicinity of Veracruz, U.S.M., and the 1 August case near Coatzacoalcos, U.S.M. The in-house hard copy IR images are enhanced with the MB curve (Table 2), whereas the NHC hard-copy images are enhanced with the JF curve (Table 3). These two curves are identical for temperatures colder than -32°C (that is, the enhancement of cloud tops), but the JF curve has an additional enhancement at the warm end for the identification of ocean currents. The JF curve also has a demarcation for the freezing level (0°C), unlike the MB curve.

The surface and upper-air plots and the GOES loops can be used to locate warm and cold fronts, high- and low-pressure systems, cloud cover, and cloud type. The surface and satellite data can also be used to identify the existence and location of additional features, such as outflow boundaries from convective storms and land- or sea-breeze regimes. Winds are indicated in the surface and upper-air data. The GOES infrared data, viewed in loops of 16 images, show cloud motions, and levels (high, middle, or low) at which clouds occur, as well. Quantitative measurements from the GOES data include cloud area, cloud lifetime, the coldest temperature within a cloud, and volumetric rain estimates. Satellite-derived cloud areas are defined by the -20°C isotherm, the threshold temperature of raining clouds in a convective rain estimation technique based on GOES IR data (Griffith, 1987); a minimum size of 500 km^2 defines a cloud in the results shown here. Cloud areas are also measured at five colder thresholds (-31°, -42°, -48°, -52°, and -69°C). The coldest temperature in the cloud is converted to an estimated cloud top height with sounding data. For the three cases when only hard-copy data are available, cloud area is estimated (by eye) from the gray area at -32°C, and minimum cloud temperature is estimated from the gray scale. However, no rain estimates were made from the hard-copy data.

The sounding plots provide a graphic assessment of the convective potential of the sampled air mass, and parameters derived from the soundings include convective condensation level (CCL), and positive and negative buoyant energy. The CCL is used here as an estimate of cloud base. The positive buoyant energy is a measure of the maximum amount of energy liberated in cloud

Table 2. GOES MB enhancement for infrared images

Segment number	Temperature range (°C)	Comments	Gray shade
1	58.8 to 29.3	Little or no useful met. data	Black
2	28.2 to 6.8	Low-level/sea surface difference	Black to dark gray
3	6.3 to -31.2	Middle level	Dark gray to light gray
4	-32.2 to -42.2	First-level contour	Medium gray
5	-43.2 to -53.2	Thunderstorm	Light gray
6	-54.2 to -59.2	Thunderstorm	Dark gray
7	-60.2 to -63.2	Thunderstorm	Black
8	-64.2 to -80.2	Overshooting tops	Black to white
9	-81.2 to -110.2		White

Table 3. GOES JF enhancement for infrared images

Segment number	Temperature range (°C)	Comments	Gray shade
1	56.8 to 24.8	Warm water and land	Black
2	24.3 to 10.8	Water temperature gradient	Black to white
3	10.3 to -0.2	Buffer zone	White
4	-0.7 to -32.2	Middle-level clouds and freezing level	Med. gray to light gray
5	-32.2 to -42.2	First-level contour	Medium gray
6	-43.2 to -53.2	Thunderstorm	Light gray
7	-54.2 to -59.2	Thunderstorm	Dark gray
8	-60.2 to -63.2	Thunderstorm	Black
9	-64.2 to -80.2	Overshooting tops	Black to white
10	-81.2 to -110.2		White

condensation processes for a parcel of air rising moist adiabatically; no entrainment, precipitation drag, or other work is included in this calculation that would decrease the energy generated by a parcel undergoing moist adiabatic ascent. Negative buoyancy is the work that needs to be supplied by other processes to raise a parcel through the low-level environment, given the temperature and moisture structure of the lower atmosphere.

The recurrent synoptic-scale features during the period of this study are a low-pressure system over the Mexican land area and a high-pressure system in the Gulf of Mexico. This low-pressure/high-pressure couplet is due to differential heating of the land surface versus the water surface. Incoming solar radiation is absorbed by each surface but is reradiated more rapidly by land than by water (hours for the former, months for the latter). The reradiated energy heats the lower layers of the atmosphere, causing a general rising motion over the land and resulting in lower pressure there. The general, synoptic-scale, horizontal wind pattern is a clockwise circulation in the Gulf; winds are easterly at Merida and Coatzacoalcos, turning to winds with a southerly component at Veracruz and Tampico, and finally westerly winds along the Texas Gulf coast near Galveston. No tropical depression, tropical storm, or hurricane existed near the ship during the six rainwater case days.

On the mesoscale, differential heating between the land and sea surfaces causes the vertical circulation of land- or sea-breezes. Again, during the day the rising motion over the land results in a low-level horizontal flow from sea to land (sea breeze); the opposite flow occurs at night when the Gulf is warmer (land breeze). The formation of a line of cumulus along the coast is an indication of the presence of a sea breeze.

2. 23 JULY 1986 (DAY OF YEAR 204)

The synoptic setting at 1200 UTC (Universal Time Coordinated) (Fig. 2a) shows a 1010-mb surface low in western Mexico at 25°N, 106°W, and relative high pressure area over the Gulf of Mexico. There is a deep layer (from the surface to 500 mb) of 10-15 kn winds out of the southeast along the Mexican coast near Tampico and out of the east over the Gulf of Mexico (see Fig. 2b). The winds at Merida, Mexico (Fig. 3a) and Brownsville, Texas (Fig. 3b) are typical of this layer.

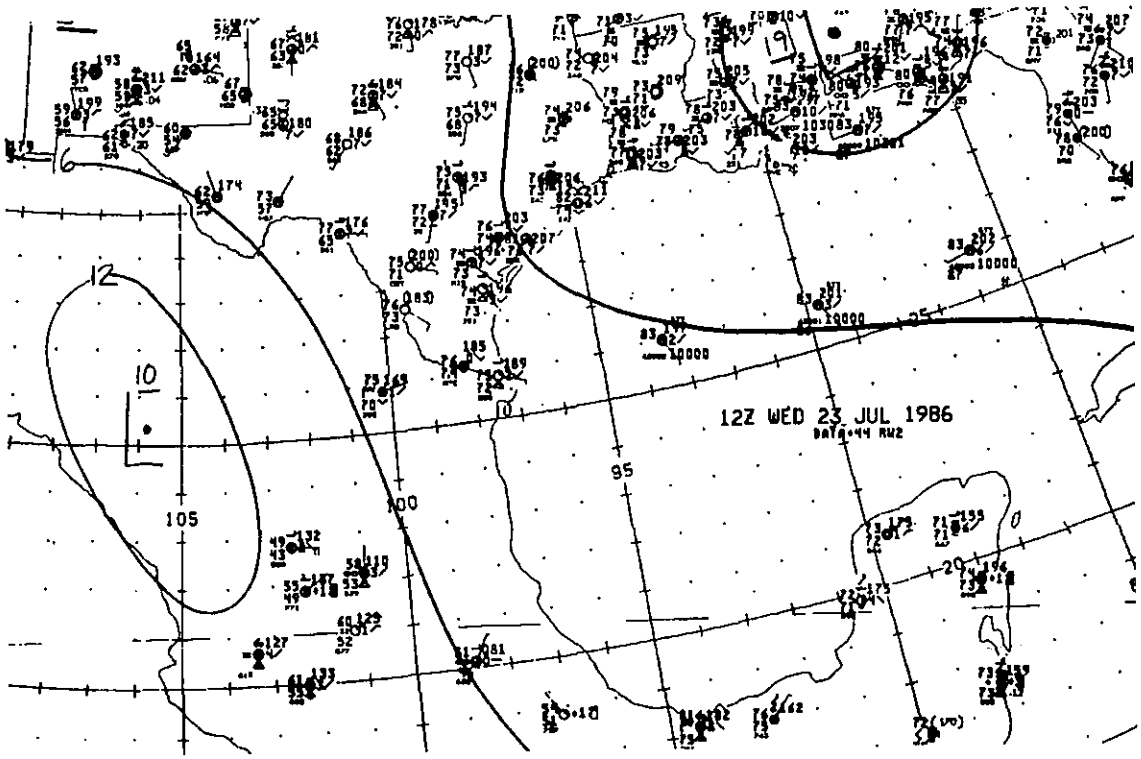

Figure 2a. Surface map for 1200 UTC on 23 July 1986.

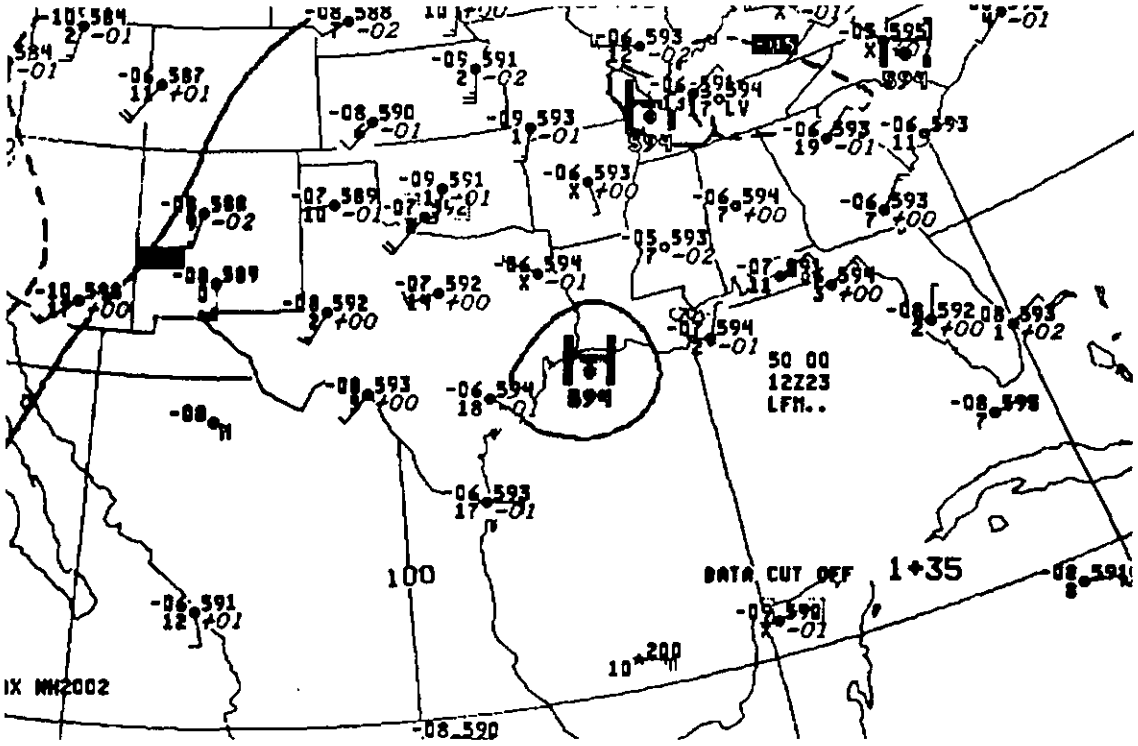

Figure 2b. 500-mb map for 1200 UTC on 23 July 1986.

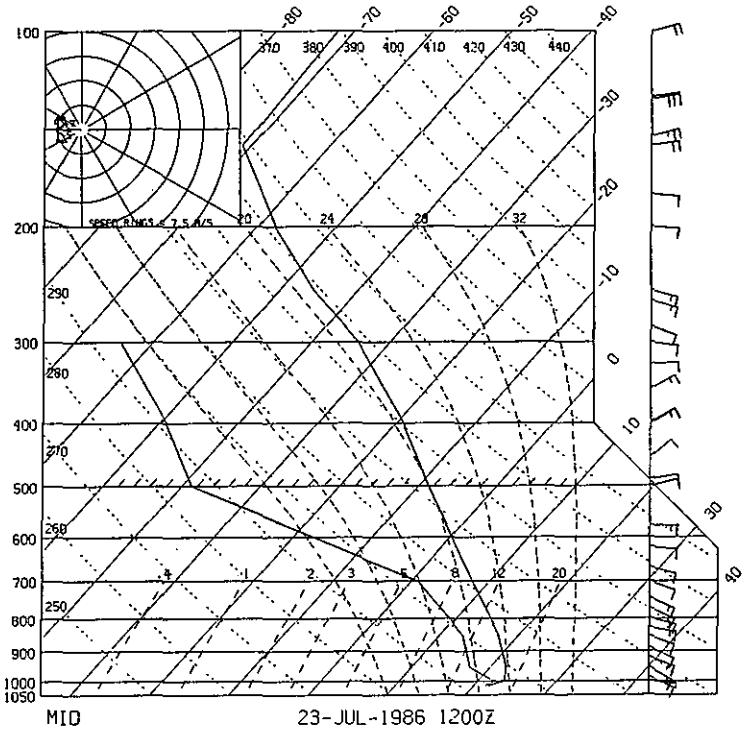

Figure 3a. Merida, Mexico (MID) sounding for 1200 UTC on 23 July 1986.

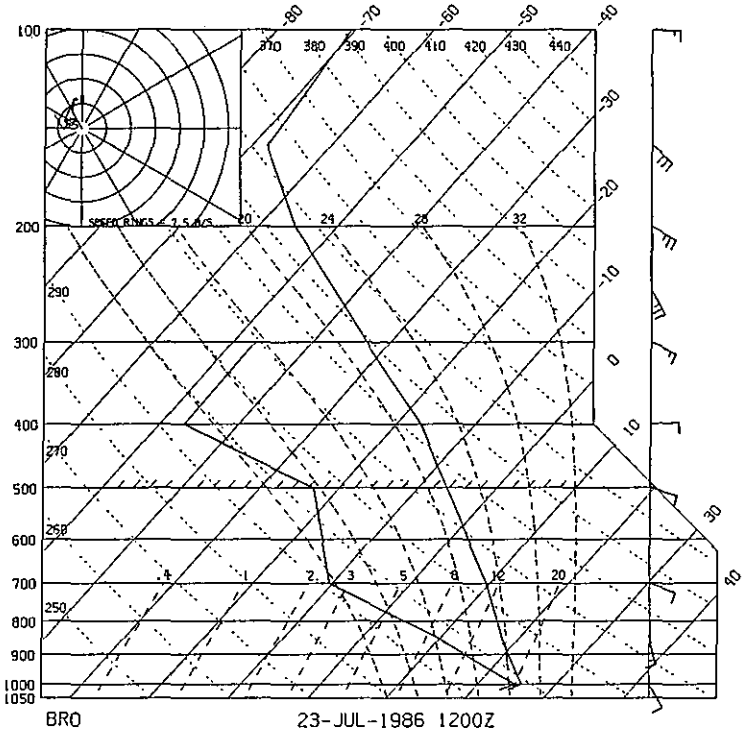

Figure 3b. Brownsville, Texas (BRO) sounding for 1200 UTC on 23 July 1986.

At the time of the rain event, the ship was north of Tampico at 23° 2.5'N, 97° 37.5'W, and sampled rain from what was apparently isolated convection that formed between 0900 and 0930 UTC in the Gulf, southeast of the ship, about 40 km from shore. This system is on the southern edge of the satellite images (Fig. 4), but there seems to be no evidence in the hemispheric surface map that it was spawned by a disturbance to the south. The system moves with the predominant wind toward the northwest, and is close to the coast at 1100 UTC (Fig. 4a). By 1300 UTC (Fig. 4b) it is entirely onshore where it dies out by 1500 UTC.

From the satellite, this convective cloud is seen to be small and short-lived (Table 1), but rather intense; a significant fraction of its top is colder than -40°C during its lifetime (Fig. 5a). Minimum temperatures (Fig. 5a) are 5°-10°C colder than this, and rain production (Fig. 5b) has a maximum hourly value of 3×10^9 m^3. Positive buoyant energy (Table 4) as determined from the morning sounding at Merida is modest (~900 J/kg), but is much larger at Brownsville (~2400 J/kg). With the long fetch over the Gulf for a parcel trajectory from Merida to Brownsville, the air can moisten. In this instance dew point temperatures are 3°C higher at Brownsville than at Merida. Consequently, at Brownsville the parcel has a higher positive buoyancy than at Merida. The buoyancy of an actual parcel at Tampico (~100 km south of Brownsville, and ~200 km northwest of Merida) probably lies somewhere between the Merida and Brownsville results.

28 JULY 1986 (DAY OF YEAR 209)

The 0000 UTC surface map (Fig. 6a) shows a 1007-mb low over the interior of Mexico (27°N,103°W), and a high in the central Gulf. The wind in the vicinity of Veracruz is from the south, backing to easterlies aloft between 850 (Fig. 6b) and 300 mb (Fig. 6c). No soundings from Mexican stations were available. The closest upper-air station is Brownsville, and it may not be representative of the atmosphere ~130 km to the south near Veracruz. The winds below 500 mb, for instance, do not correspond to the winds in Fig. 6. However, the sounding indicates (Table 4) a modest amount of positive buoyant energy, with substantial negative buoyancy due to an 80-mb inversion layer centered at 900 mb (Fig. 7). Cloud base, estimated from the CCL, is rather high at 2.3 km.

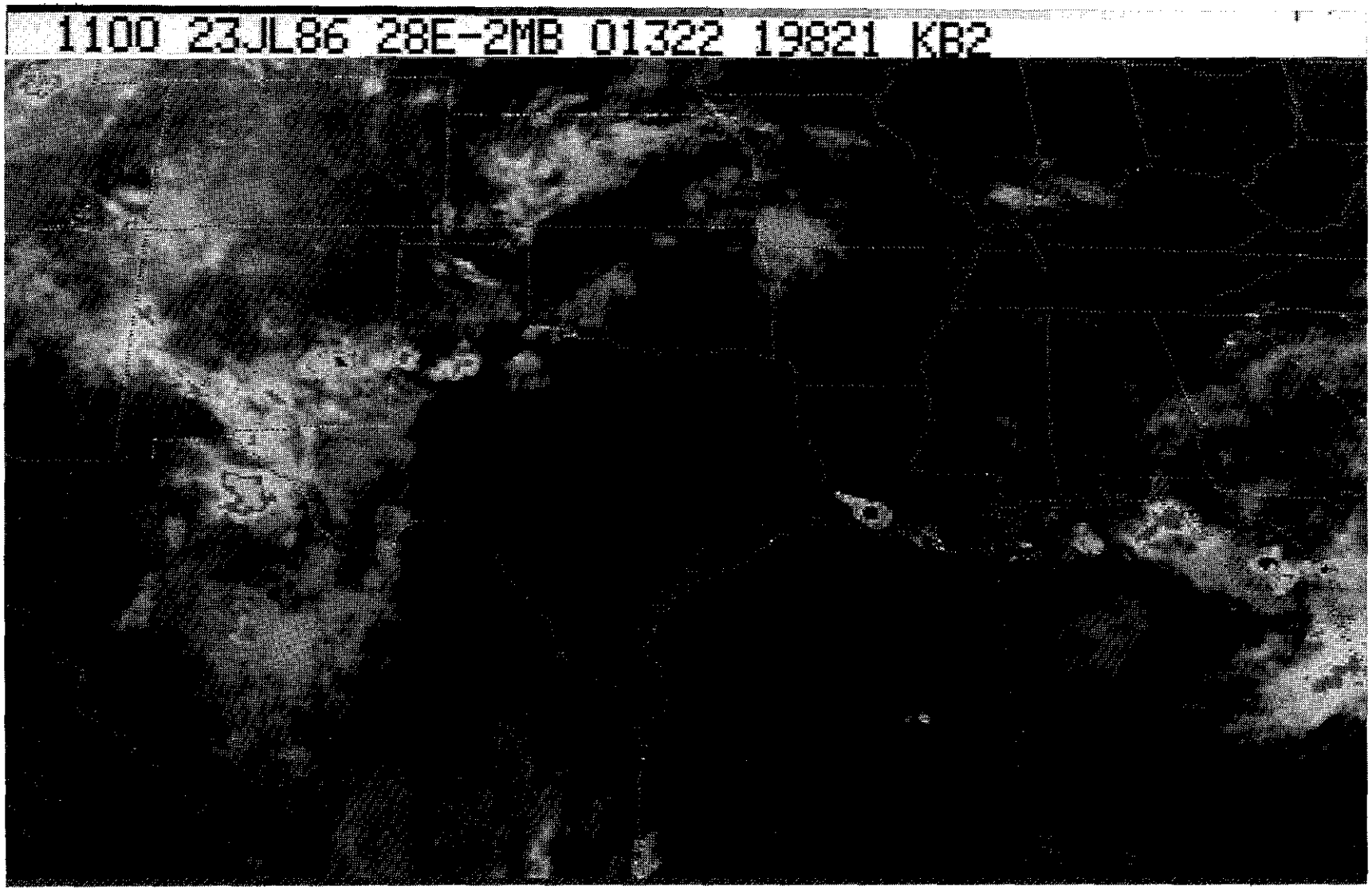

Figure 4a. GOES IR image (MB enhancement) for 1100 UTC on 23 July 1986.

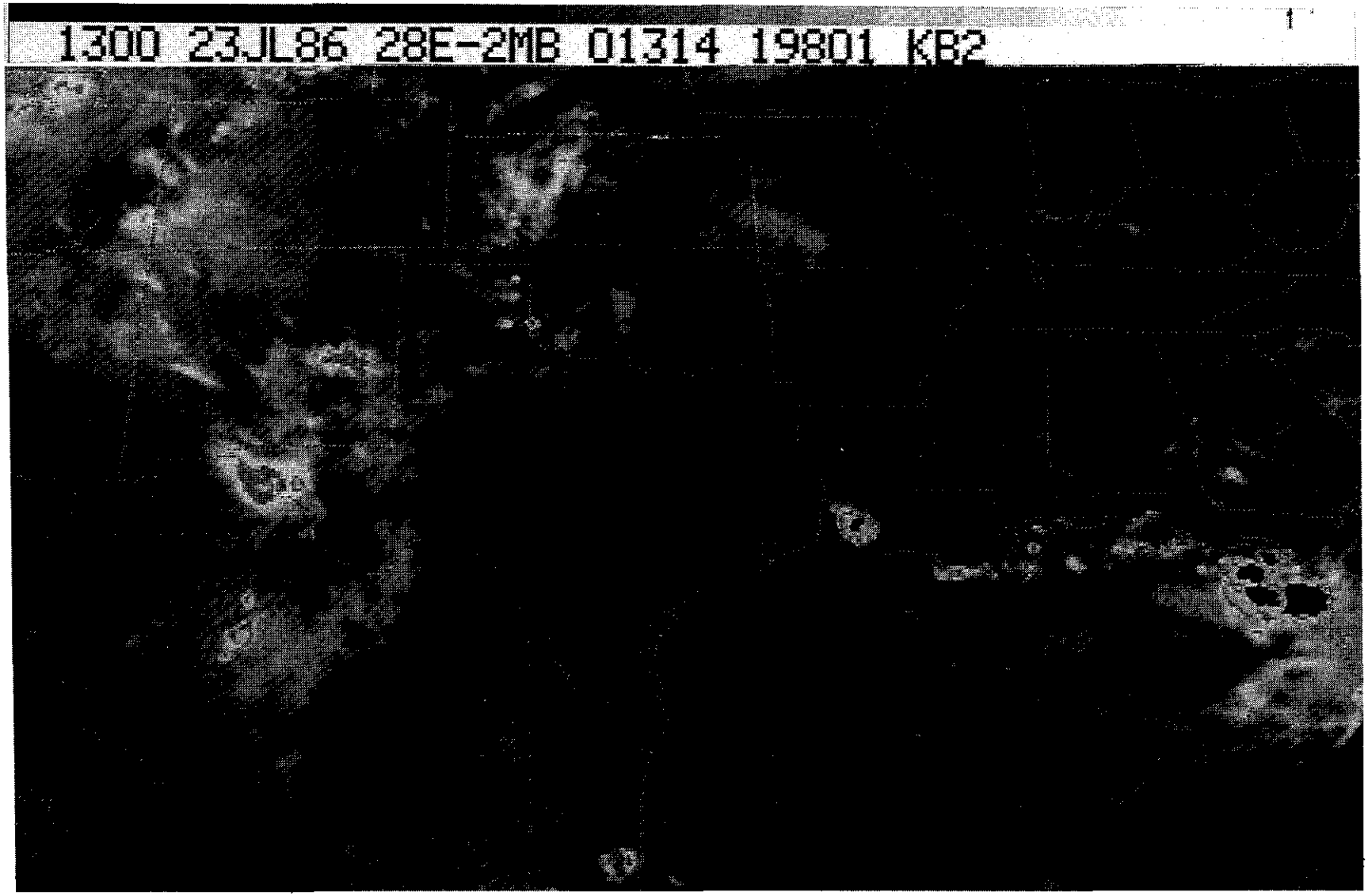

Figure 4b. GOES IR image (MB enhancement) for 1300 UTC on 23 July 1986.

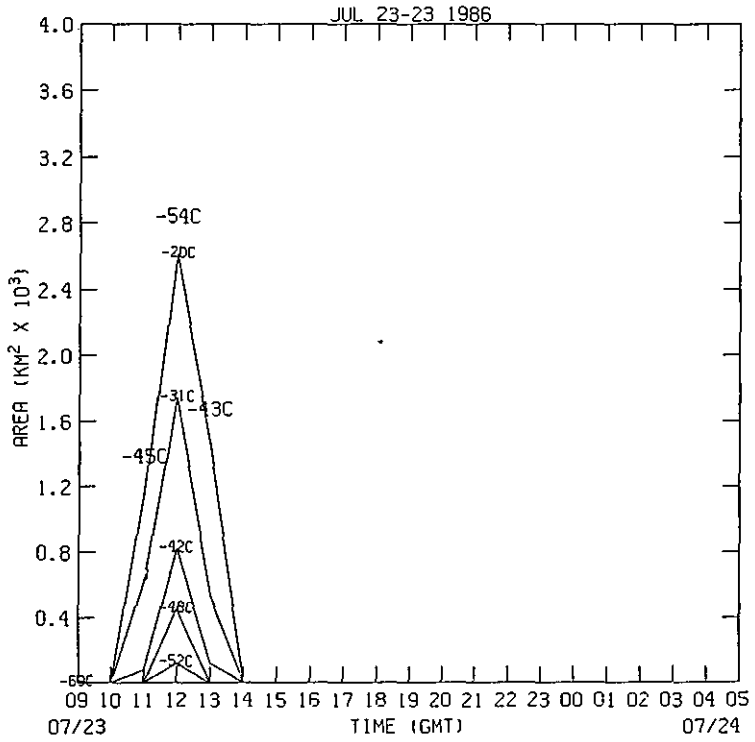

Figure 5a. GOES IR cloud area time series for 23 July 1986. Minimum temperatures (°C) in the cloud are the numbers above the warmest temperature curve.

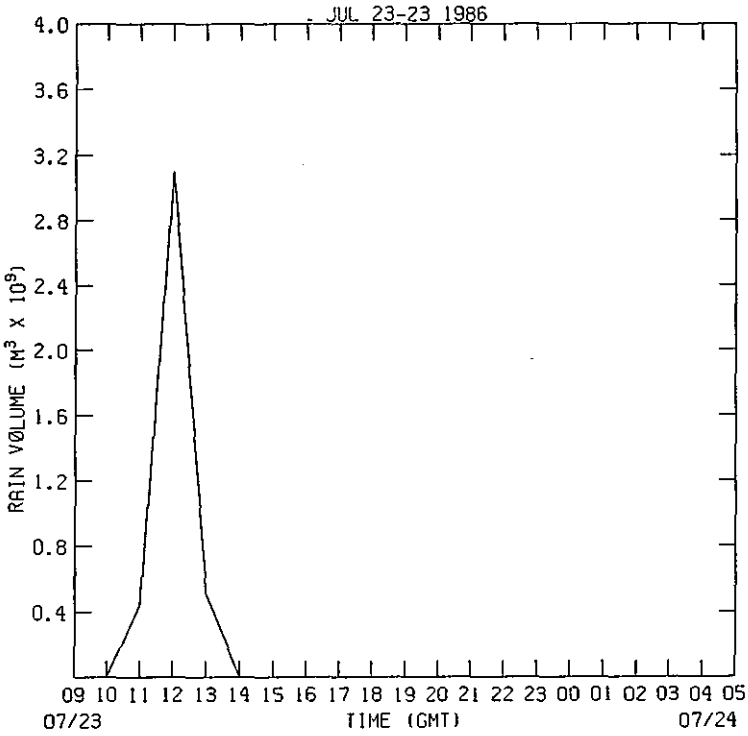

Figure 5b. Satellite-derived rainfall time series for 23 July 1986.

Table 4. Sounding-derived parameters for the rain water cases

Date	Time (UTC)	Station	Parcel T/TD (°C)	CCL (km)	Buoyant energy (J/kg) Pos.	Buoyant energy (J/kg) Neg.
23 Jul	1200	MID	22.8/20.7	1.15	887.3	-93.8
	1200	BRO	24.8/23.7	0.63	2370.8	-11.6
28 Jul	0000	BRO	27.9/20.9	2.30	909.9	-241.8
30 Jul	1200	BRO	25.1/24.1	0.01	2.9	-8.3
			28/26	0.01	3861.5	0.0
1 Aug	1200	BRO	24.9/24.2	0.45	0.7	-2.9
			28/24	0.45	1.6	-0.1
10 Aug	1200	VCT	24.3/23.8	0.37	2675.4	-0.5
11 Aug	1200	VCT	24.4/23.9	0.38	8.0	-0.7
12 Aug	0000	VCT	25.0/21.8	1.40	939.6	-60.7

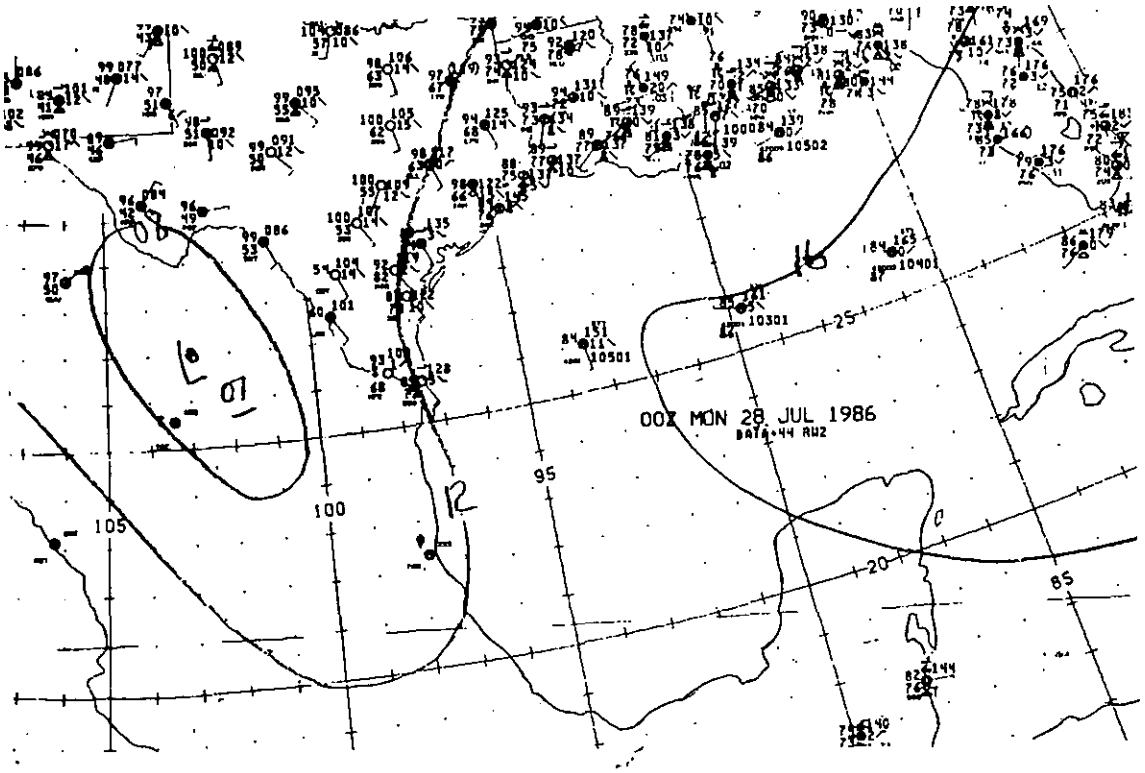

Figure 6a. Surface map for 0000 UTC on 28 July 1986.

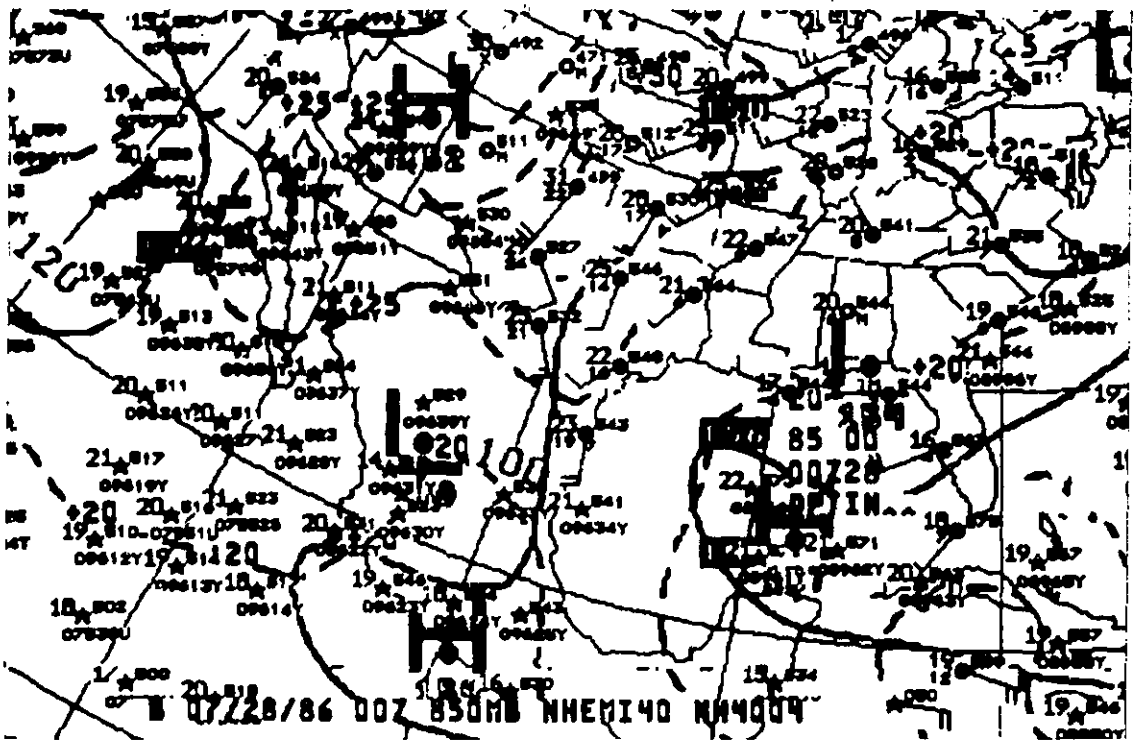

Figure 6b. 850-mb hemispheric analysis for 0000 UTC on 28 July 1986.

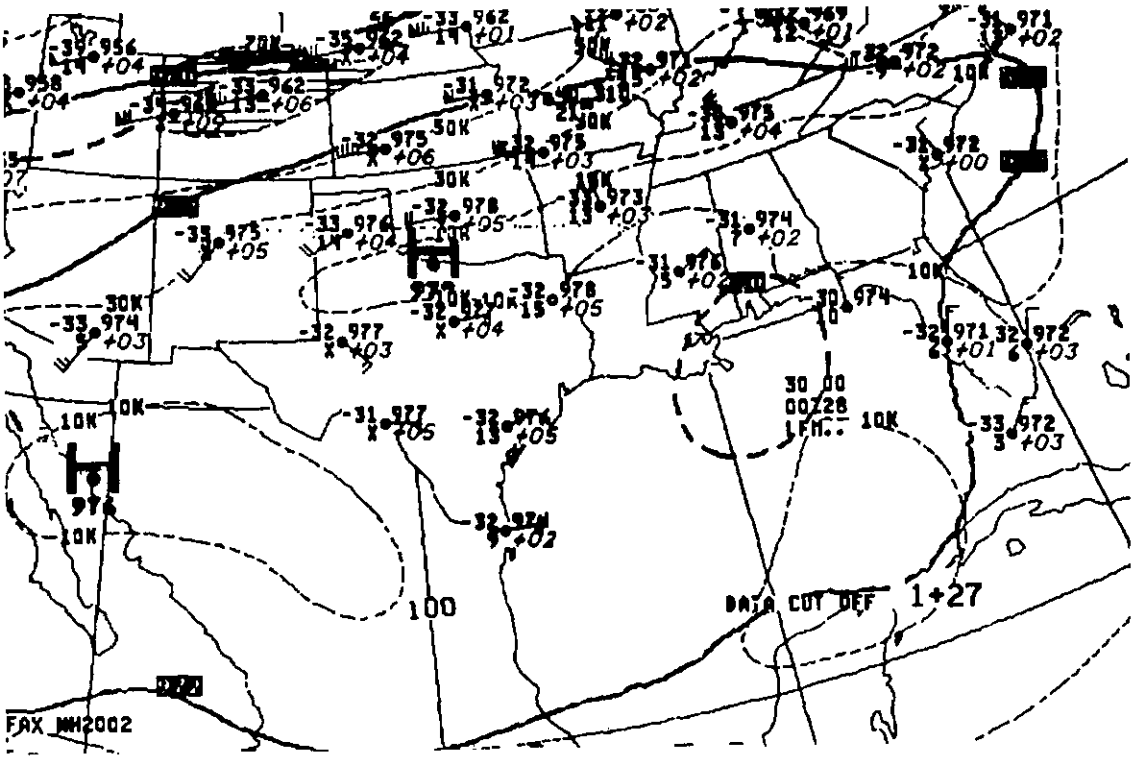

Figure 6c. 300-mb map for 0000 UTC on 28 July 1986.

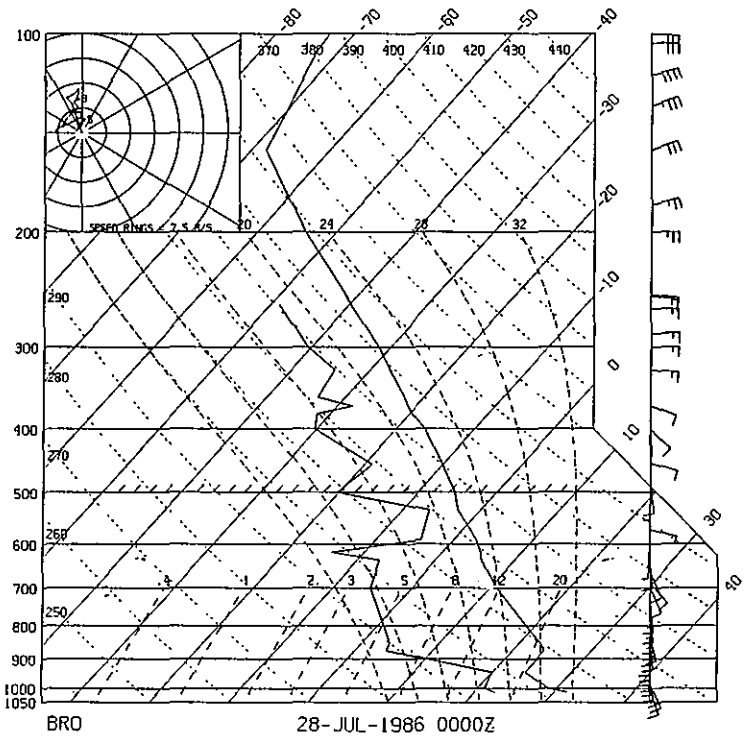

Figure 7. Brownsville, Texas (BRO) sounding for 0000 UTC on 28 July 1986.

An intense, mature mesoscale convective system already exists near Coatzacoalcos at 0000 UTC on 28 July 1986. This system hugs the coast as it moves westward and then northwestward toward Veracruz. At 0430 UTC (Fig. 8a) it can be seen to have tops colder than -75°C and to be very circular, indicating little shear in the winds aloft. The system probably has its maximum extent of 37,000 km^2 (estimated by eye) at this time (Table 1). The 0530 UTC image is missing, and in the 0630 UTC image (Fig. 8b) the system is starting to decay; it is less circular, and cloud tops have warmed by about 10°C. By 1100 UTC all cloud tops are approximately 0°C and the system is no longer easily identified.

4. 30 JULY 1986 (DAY OF YEAR 211)

A surface high is nestled at the Gulf coast in the vicinity of Veracruz at 0000 and 1200 UTC (Fig. 9). At 1200 UTC the 1017-mb high is north of the ship's location in the harbor of Coatzacoalcos. From the surface to 100 mb,

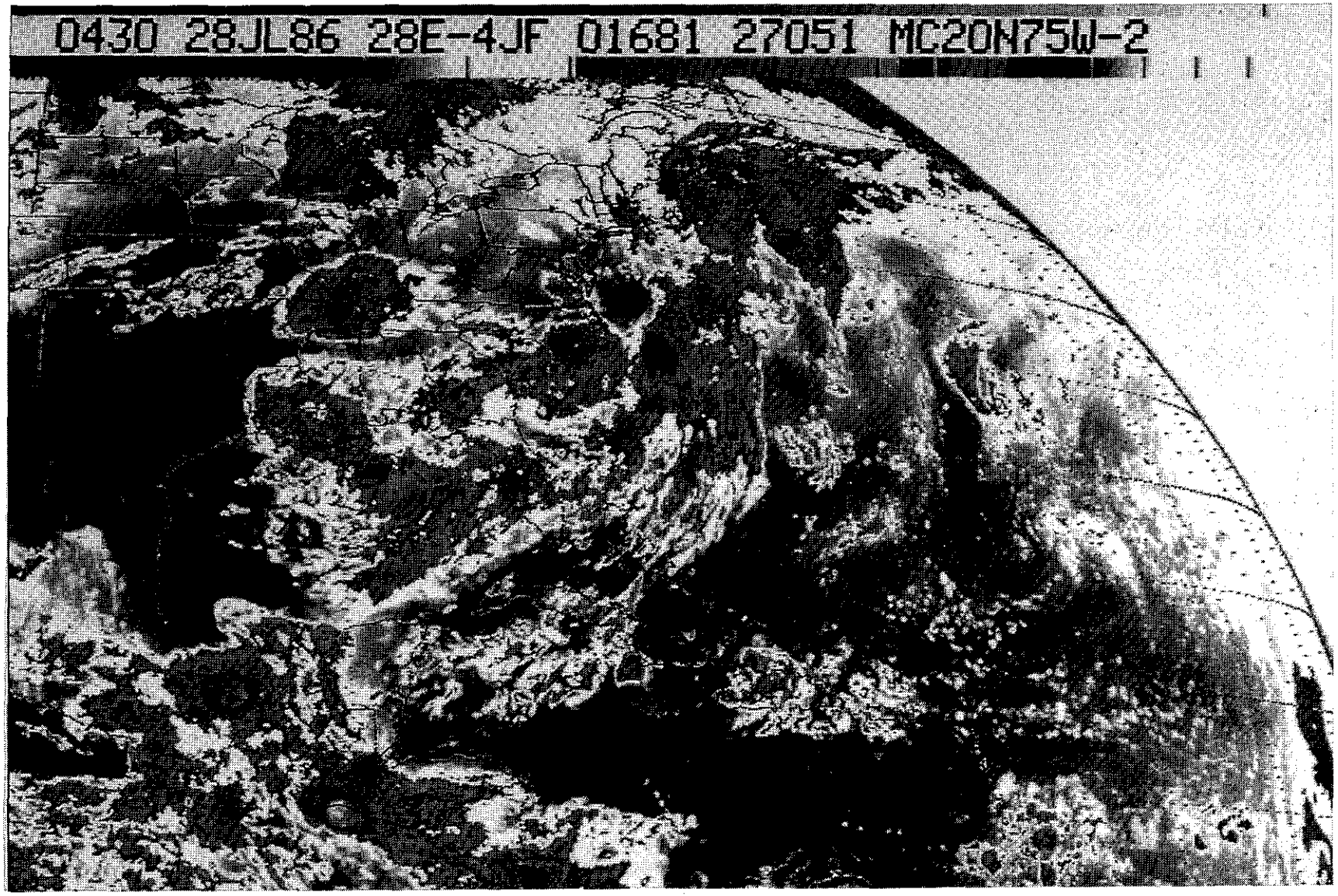

Figure 8a. GOES IR image (JF enhancement) for 0430 UTC on 28 July 1986.

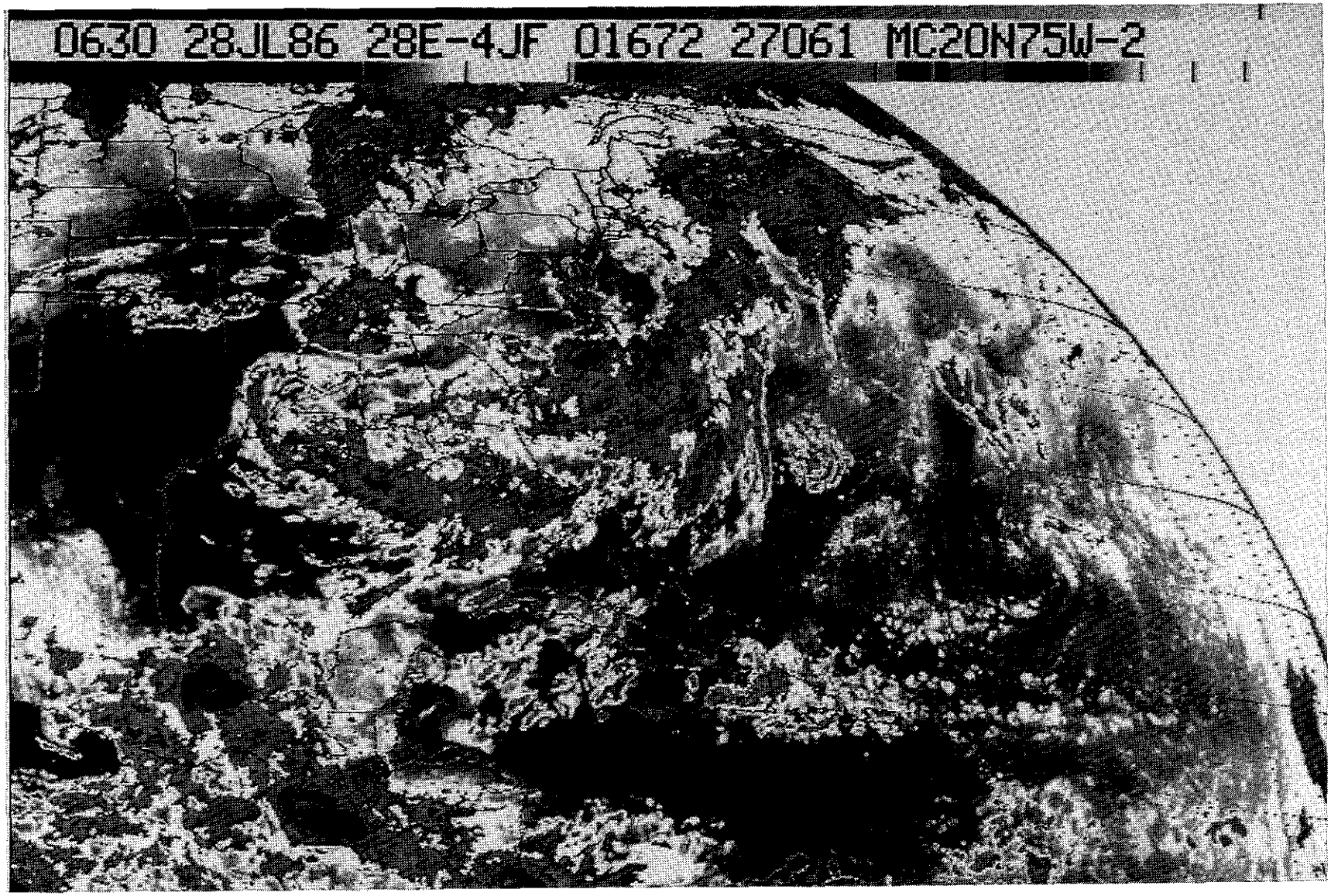

Figure 8b. GOES IR image (JF enhancement) for 0630 UTC on 28 July 1986.

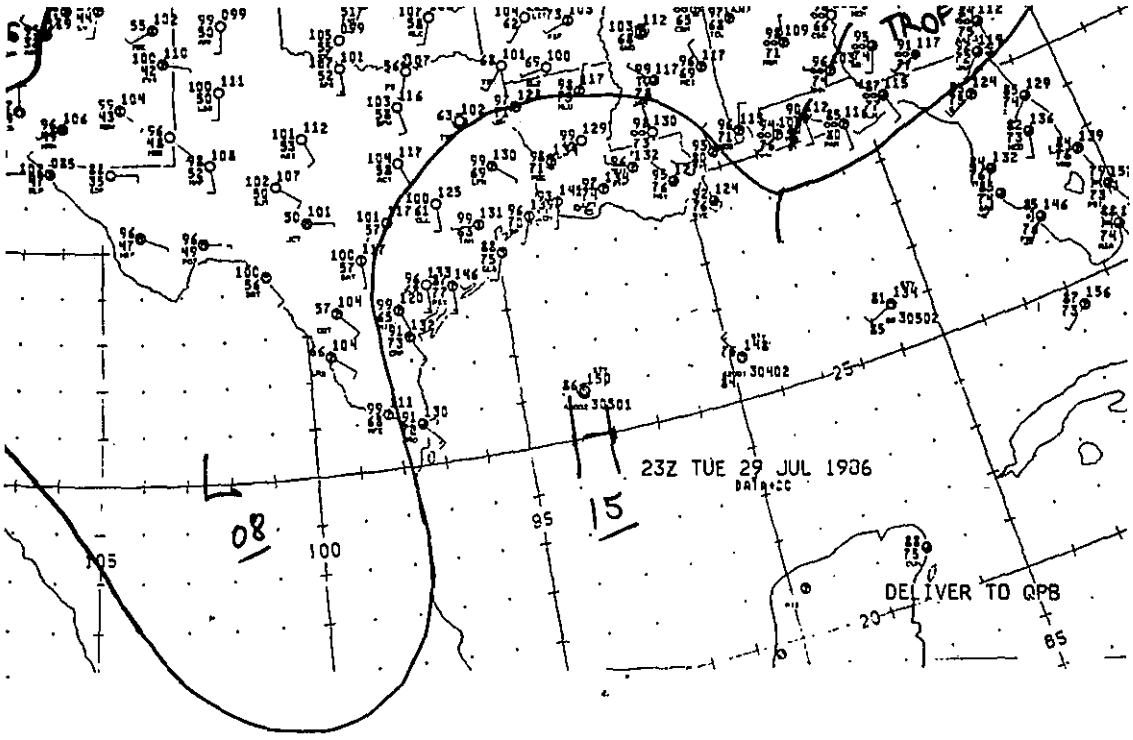

Figure 9a. Surface map for 2300 UTC on 29 July 1986.

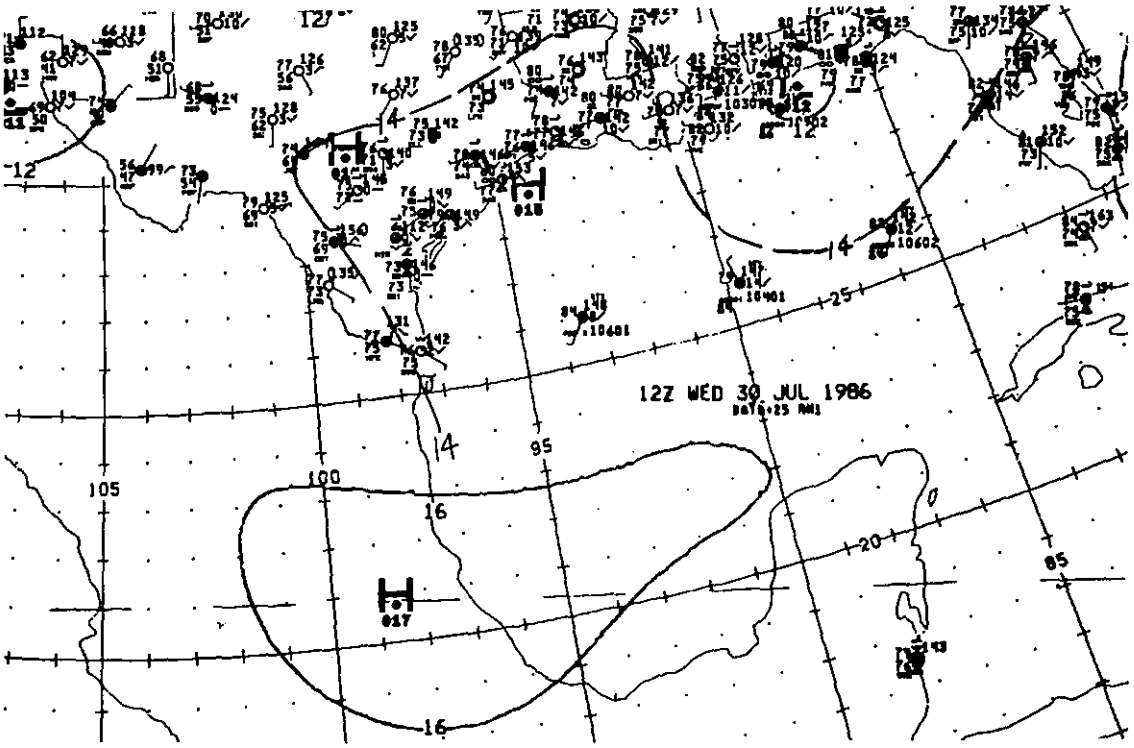

Figure 9b. Surfce map for 1200 UTC on 30 July 1986.

the winds in the vicinity of the ship have a westerly component. Again, no Mexican soundings are available. Brownsville, ~130 km to the north (Fig. 10), has a surface inversion that results in little buoyancy. However, if this is overcome by raising the parcel with a greater surface temperature and dew point (Table 4), the positive buoyancy increases to 3861 J/kg and the negative buoyancy is zero.

From the satellite images the convection at the ship's location near Veracruz appears to be small, isolated convection that forms on shore, moves south inland, and dissipates. No convection is evident in the 1030 UTC image at the ship's location. The 1100 UTC image suffered transmission difficulties in the scan lines through 18° to 19°N, so it is impossible to make anything but very gross estimates of cloud size and minimum top temperature (Table 1), but there is convection that forms at the coast. By 1230 UTC (Fig. 11), two small cloud remnants exist, one southeast and the other north of Veracruz.

5. 1 AUGUST 1986 (DAY OF YEAR 213)

The 0900 UTC surface map (Fig. 12a) indicates a 1016-mb high in the-northern Gulf of Mexico. Three hours later (Fig. 12b) Coatzacoalcos is reporting a 10-kn wind from the north and fair-weather cumulus. Above the surface the synoptic-scale flow in the vicinity of the ship has an easterly component (Fig. 13).

From the satellite data it appears that a long-lived (>10 h) mesoscale system initiates in Guatemala, moves toward the northwest, and produces the small, warm convection at the ship's location offshore from Coatzacoalcos. However, a crucial image (1130 UTC) is missing from the archive. The Guatemalan system is colder than -60°C, but the cloud that is sampled for rainwater is relatively warm, a little colder than freezing on the one image in which it can be seen (Table 1). At 1230 UTC the center of the Guatemalan mesoscale system has moved onto the southern Mexican coast, south of Coatzacoalcos, and this system appears to extend northward over Coatzacoalcos (Fig. 14a). At 1330 UTC (Fig. 14b) the inland portion of this piece begins to regenerate as a small but intense cloud (tops colder than -42°C) that moves toward the southwest and can still be tracked as late as

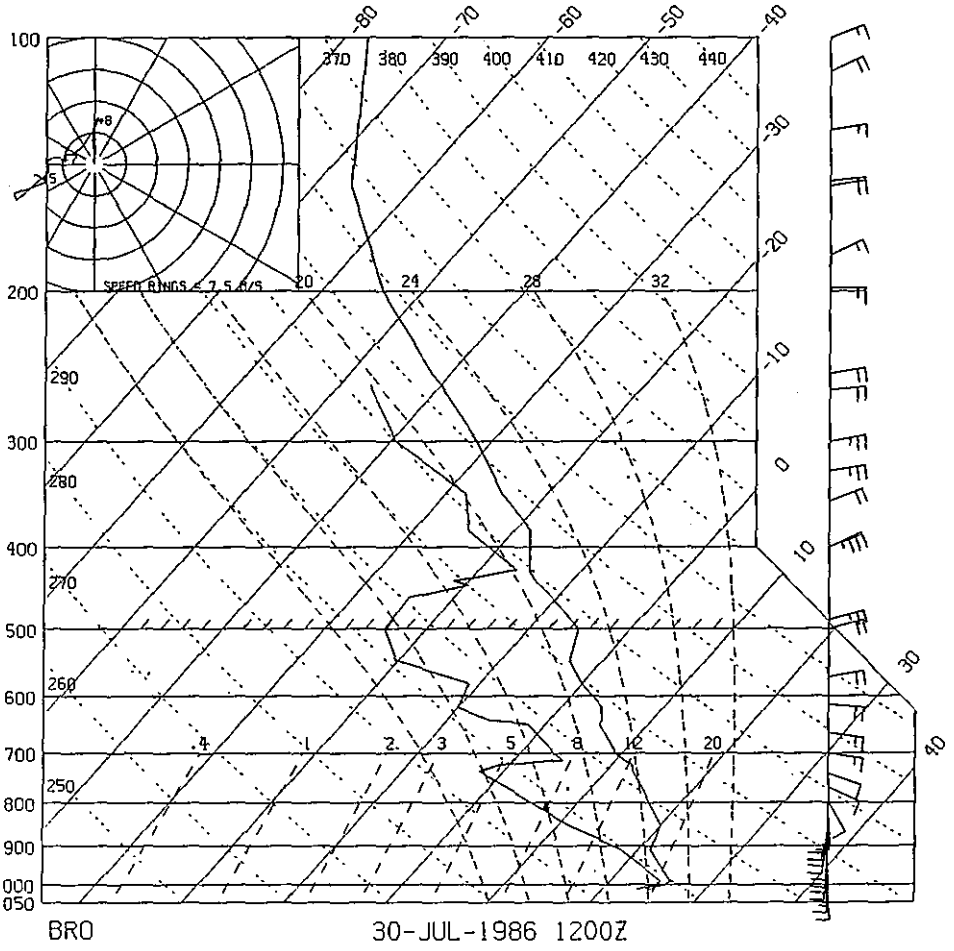

Figure 10. Brownsville, Texas (BRO) sounding for 1200 UTC on 30 July 1986.

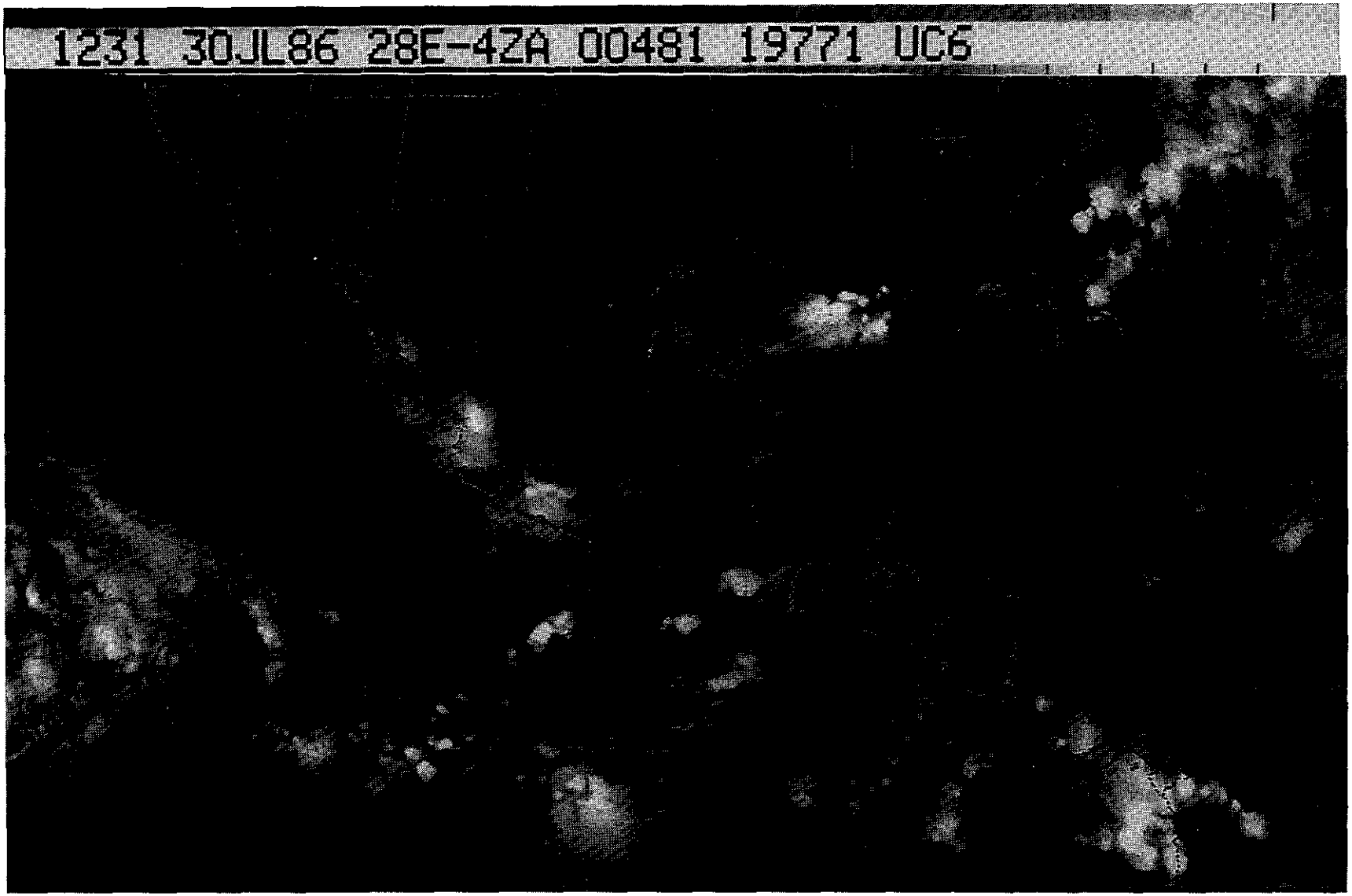

Figure 11. GOES IR image (linear enhancement) for 1230 UTC on 30 July 1986.

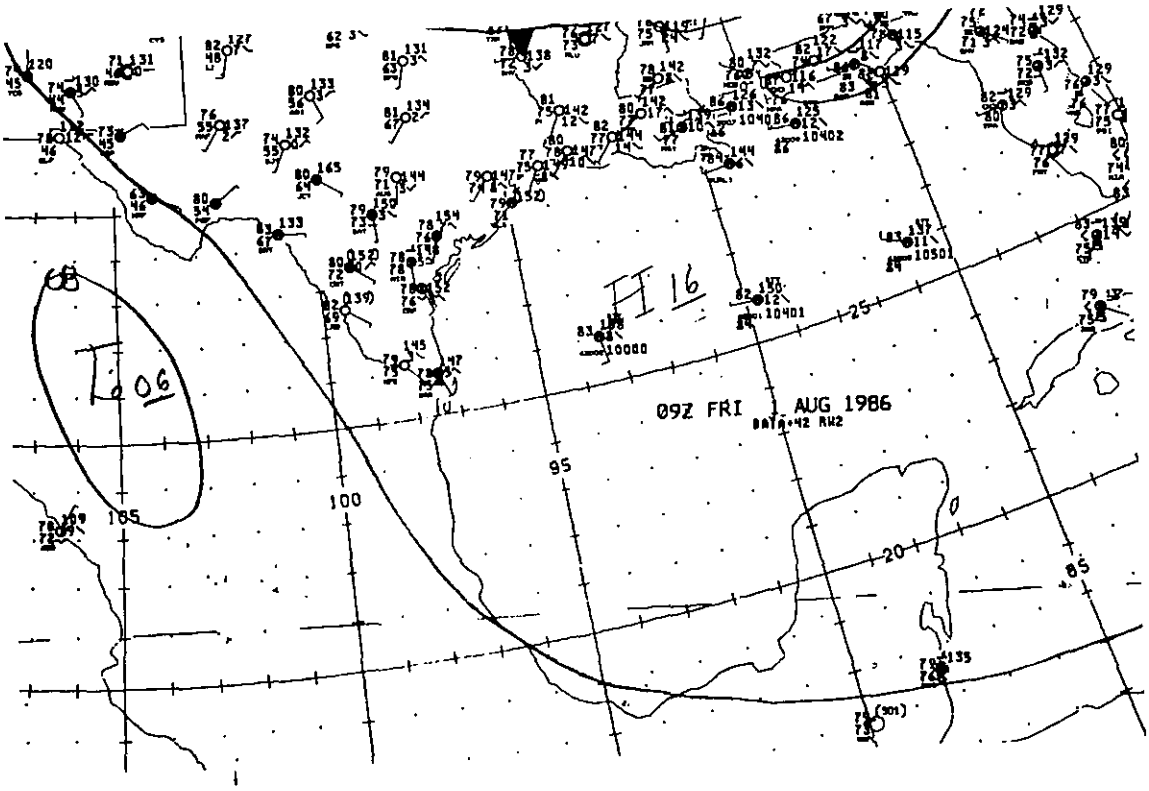

Figure 12a. Surface map for 0900 UTC on 1 August 1986.

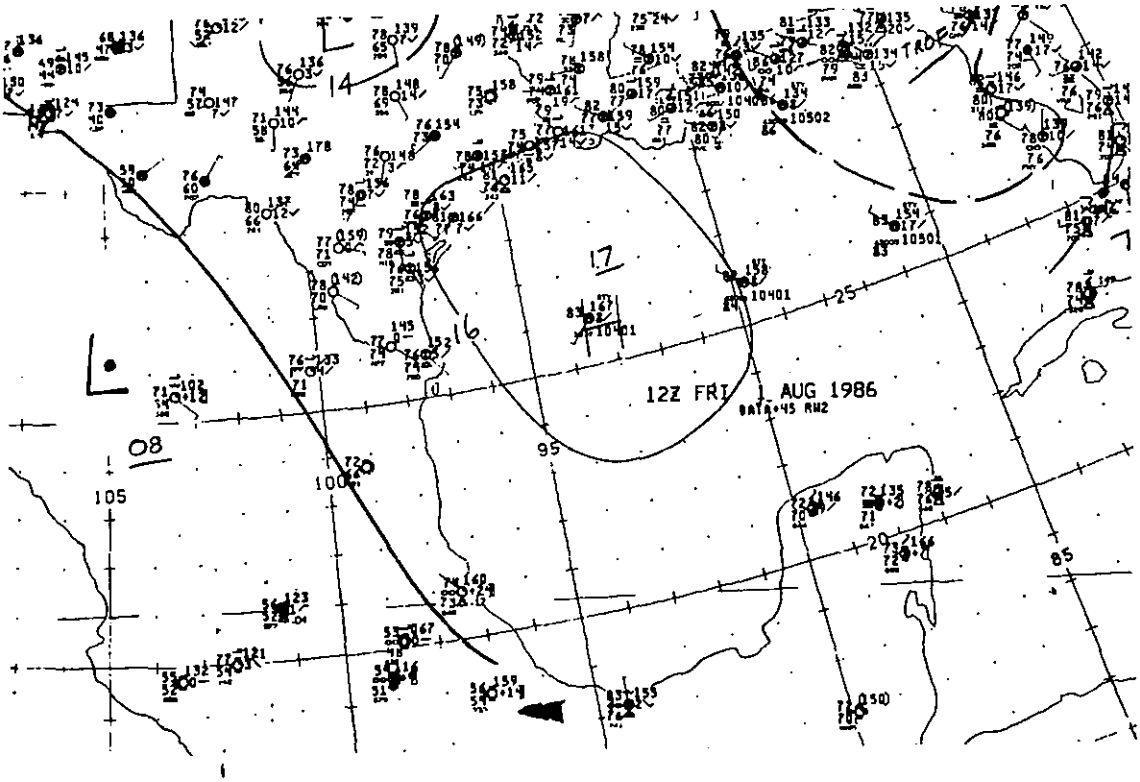

Figure 12b. Surface map for 1200 UTC on 1 August 1986.

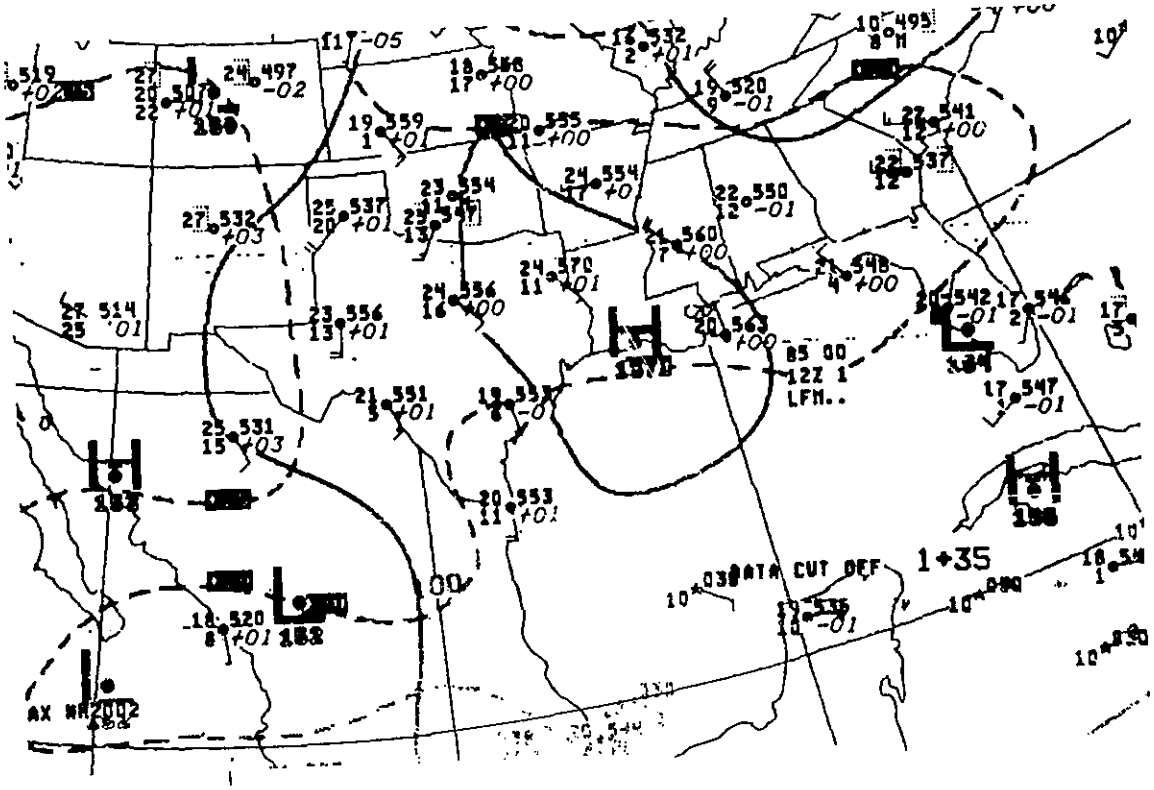

Figure 13. 850-mb map for 1200 UTC on 1 August 1986.

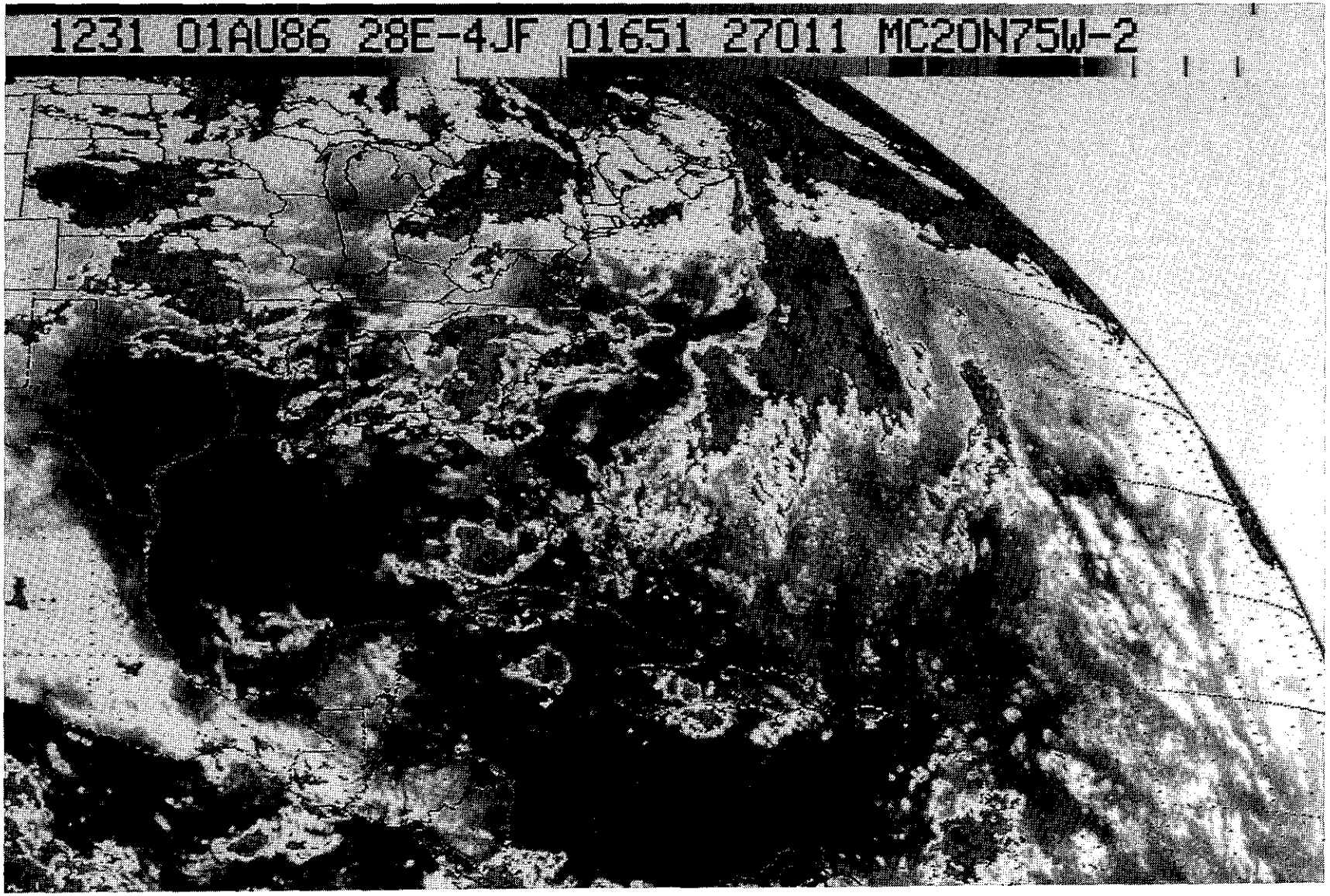

Figure 14a. GOES IR image (JF enhancement) for 1230 UTC on 1 August 1986.

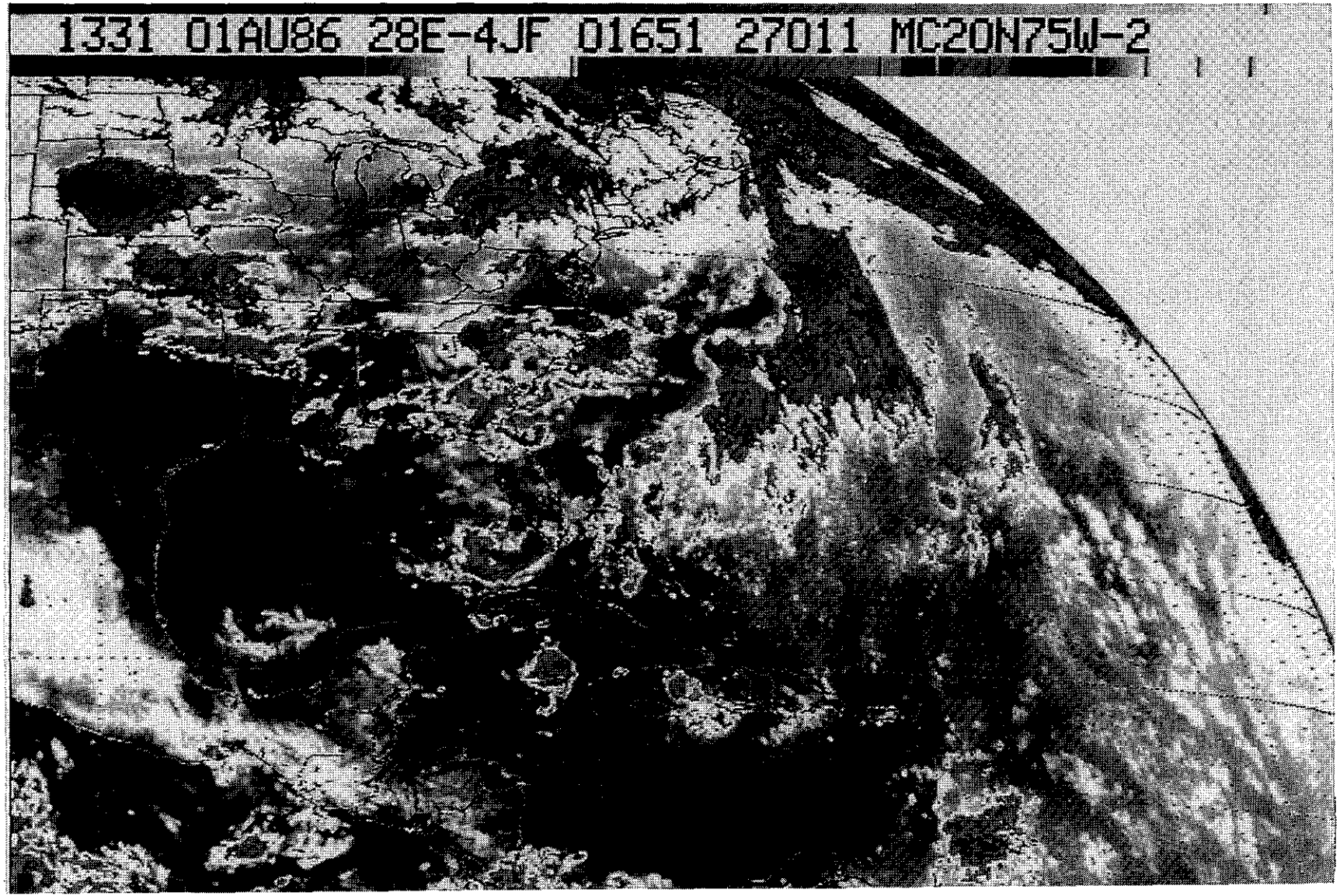

Figure 14b. GOES IR image (JF enhancement) for 1330 UTC on 1 August 1986.

2230 UTC. Because no looping capability exists with the hard copy imagery and because some images are missing, this interpretation may be incorrect. An alternate interpretation of the images is that a boundary of some sort (e.g., a gravity wave) moving over the Gulf from west to east interacted with the northern end of the mesoscale system to initiate convection at the location of the ship; this convection moved southward and exploded over land into a system that lasted several hours and was more vigorous over land than over the Gulf coastal waters.

The closest available 1200 UTC sounding (Fig. 15) on this date is ~160 km to the north-northwest at Brownsville, where the surface temperature and dew point temperature are 25° and 23.4°C, respectively; this surface temperature is cooler than at Coatzacoalcos, but the moisture is about the same. The temperature and dew point at Coatzacoalcos are 28° and 24°C, respectively. These values produce about the same, very small amount of buoyant energy as the Brownsville sounding, as noted in Table 4.

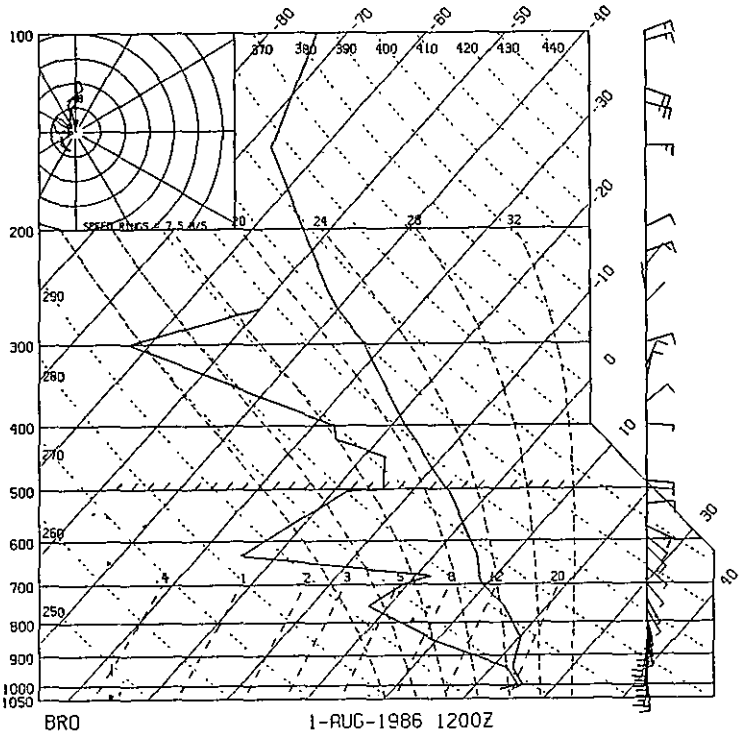

Figure 15. Brownsville, Texas (BRO) sounding for 1200 UTC on 1 August 1986.

6. 10 AUGUST 1986 (DAY OF YEAR 222)

The 1200 UTC synoptic setting (Fig. 16a) shows a 1004-mb surface low in western Mexico (at about 25°N,106°W) and a surface cold front (through southeast Colorado, northern Oklahoma, and southern Missouri) approaching Texas. From the surface to 700 mb (Fig. 16b), the winds are southeasterly to southerly in the Gulf and at the coastal stations, turning to southwesterly inland over Texas. Above 300 mb (Fig. 16c), there is a small closed low in the Gulf near the Texas coastline (26°N,97°W). By 1500 UTC the surface cold front (Fig. 17) is still in southeast Colorado and southern Missouri, but has sagged into central Oklahoma; it is too far from the coast, however, to have an effect on the convection sampled by the ship in Galveston harbor (29°20'N, 94°50'W).

From the satellite, the cloud producing the rainwater sample can be seen to form offshore over the Gulf waters as isolated convection rather than being part of a sea breeze. At 1200 UTC (Fig. 18) the cloud is colder than -20°C, but smaller than the 500-km^2 size threshold. No visible images are available until 1630 UTC (Fig. 19); the sea breeze can be seen at this time as the small cumulus onshore, much less developed than the convection at the ship. The convection at the ship grows and decays while it translates slowly toward the southwest. Maximum areal extent of 10,588 km^2 (Table 1) is reached at 1400 UTC, and the storm is below the size threshold by 1600 UTC (Fig. 20). During the two hours of its lifetime the convection is colder than -52°C, with minimum temperatures as shown in Fig. 20a. A moderate maximum rain volume of 18×10^9 m^3 is inferred from the GOES data (Fig. 20b).

The nearest sounding is at Victoria, Texas, about 190 km south-southwest of Galveston (Fig. 21). Positive buoyant energy at Victoria (Table 4) is very large (>2600 J/kg), and negative buoyant energy is very small. The convection that is sampled by the ship may not be tapping this same source of energy, because it formed over the water rather than over land, and because it dies out surprisingly quickly, given this much buoyant energy. Cloud base at Victoria is 0.37 km.

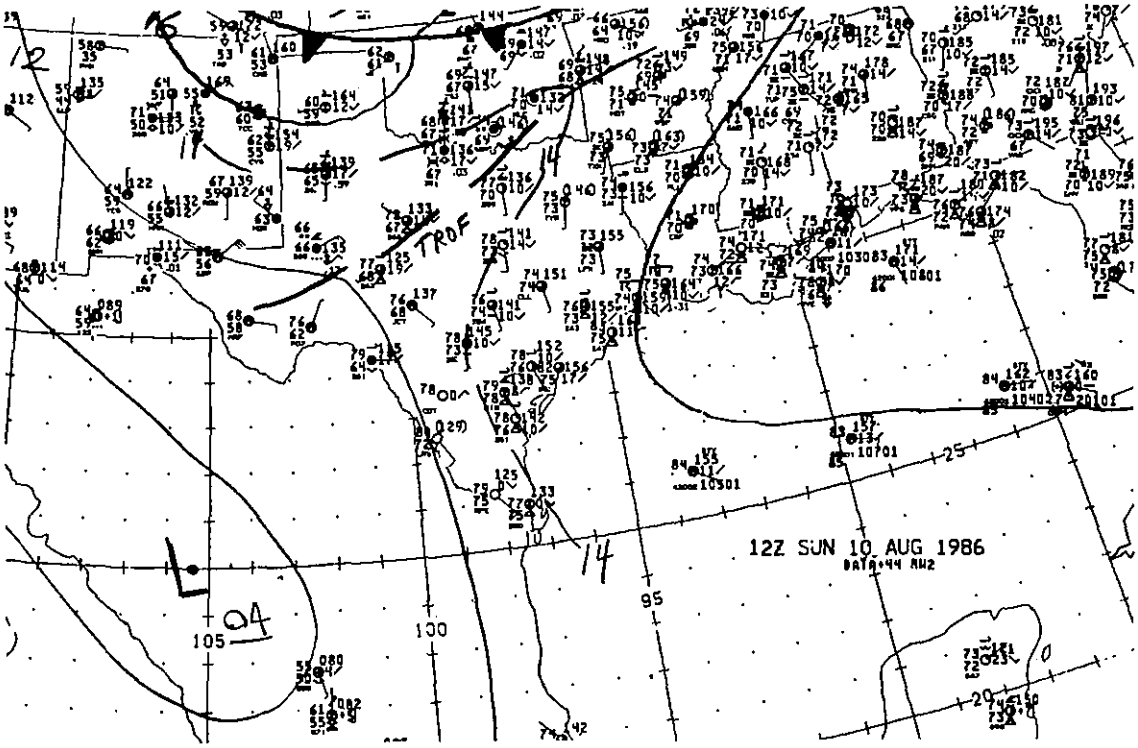

Figure 16a. Surface map for 1200 UTC on 10 August 1986.

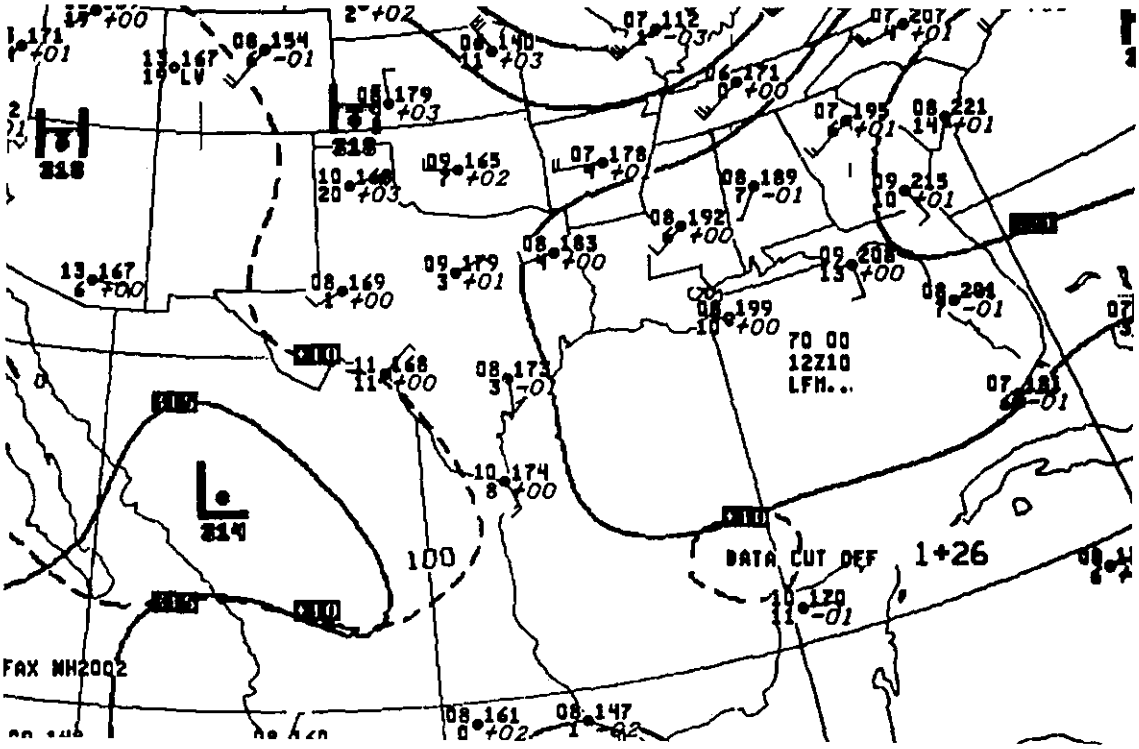

Figure 16b. 700-mb map for 1200 UTC on 10 August 1986.

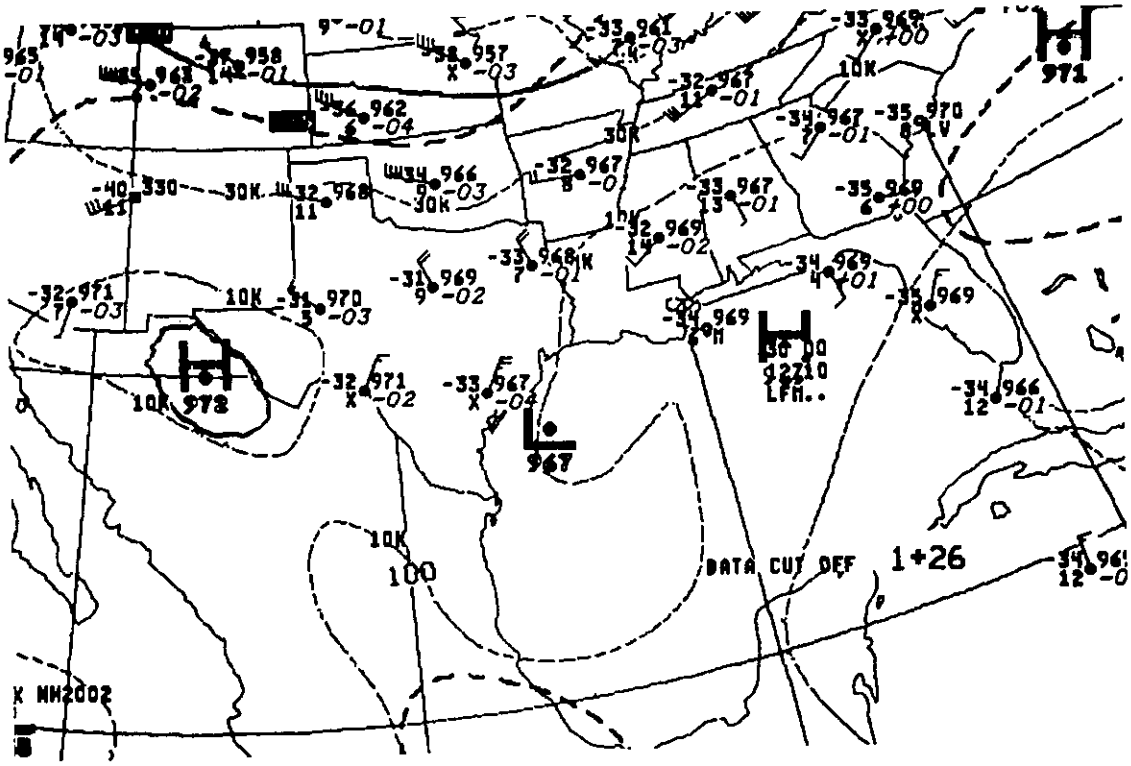

Figure 16c. 300-mb map for 1200 UTC on 10 August 1986.

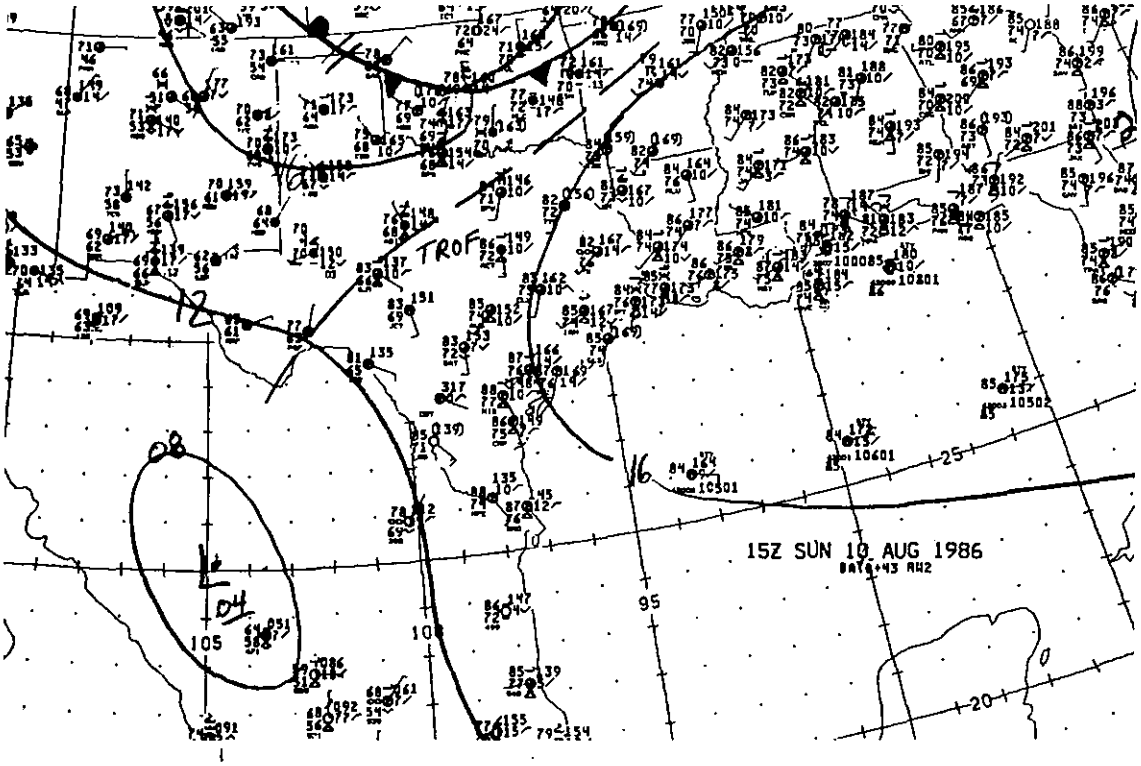

Figure 17. Surface map for 1500 UTC on 10 August 1986.

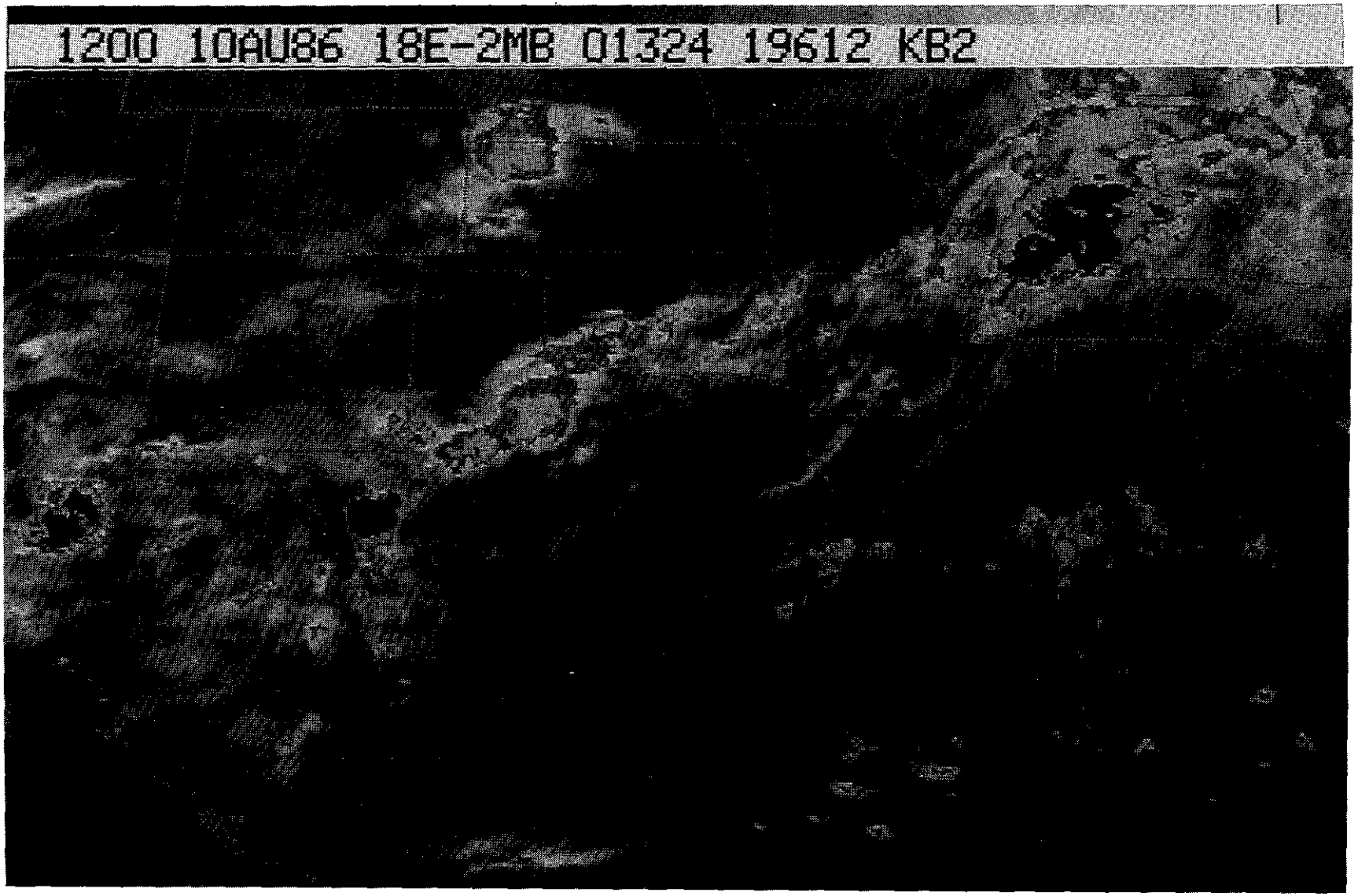

Figure 18. GOES IR image (MB enhancement) for 1200 UTC on 10 August 1986.

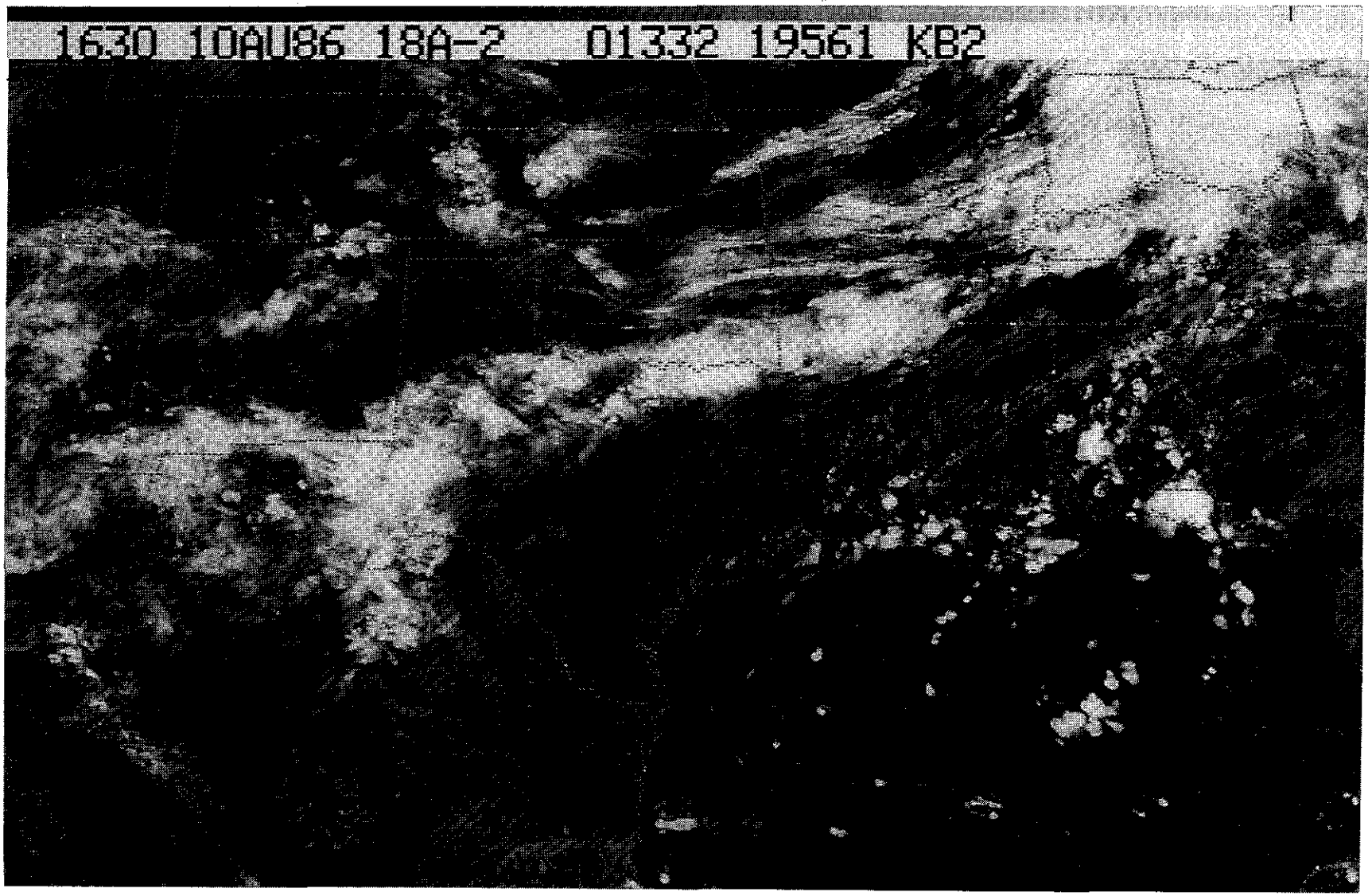

Figure 19. GOES visible image for 1630 UTC on 10 August 1986.

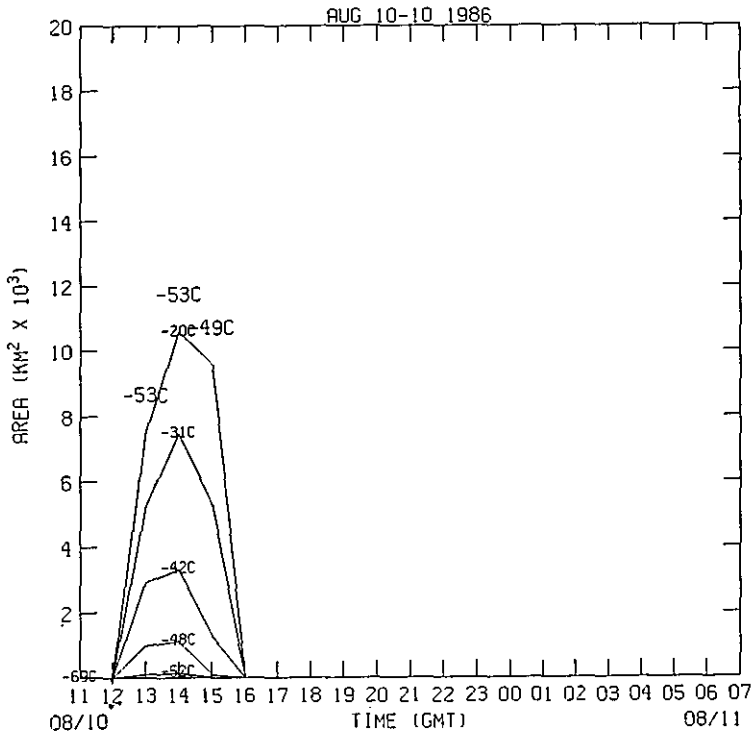

Figure 20a. GEOS IR cloud area time series for 10 August 1986. Minimum temperatures (°C) in the cloud are the numbers above the warmest temperature curve.

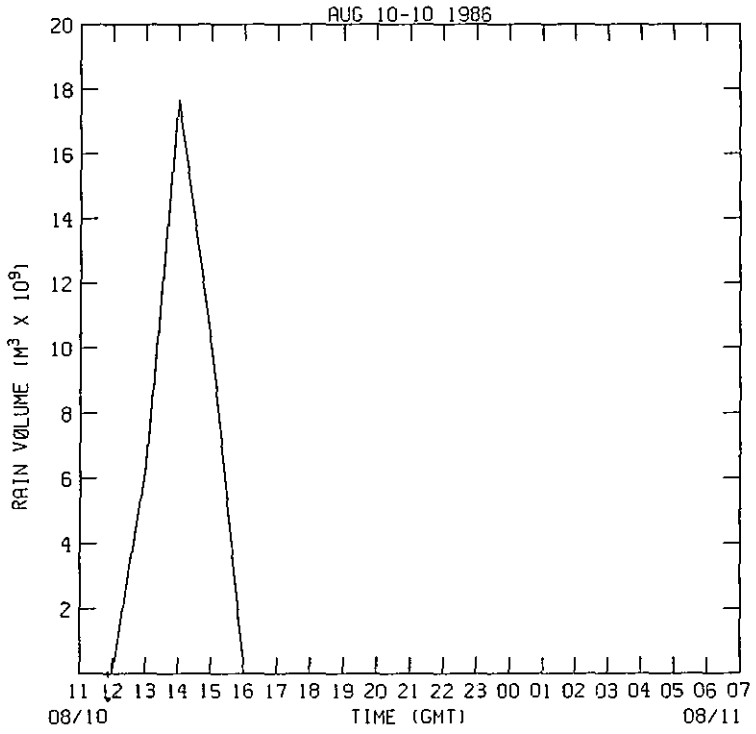

Figure 20b. Satellite-derived rainfall time series for 10 August 1986.

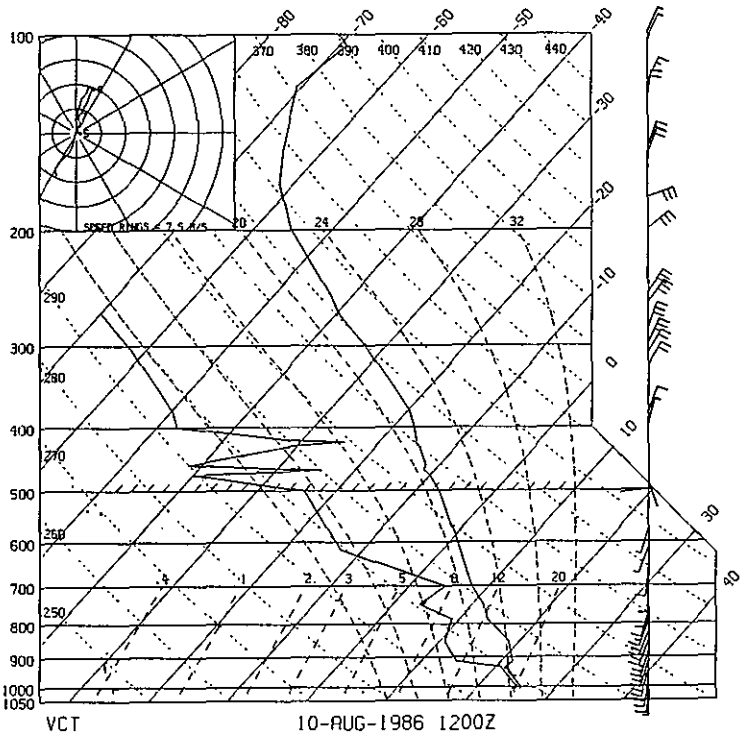

Figure 21. Victoria, Texas (VCT) sounding for 1200 UTC on 10 August 1986.

7. 11 AUGUST 1986 (DAY OF YEAR 223)

Still offshore from Galveston (29°20'N, 94°50'W), the ship encountered rain from convection forced ahead of the cold front that now lies through the Texas panhandle, northern Texas, and southern Arkansas (Fig. 22). The convective storms are in the vicinity of Galveston at 1700 UTC (Fig. 23a); the system is centered in Louisiana, and extends as a roughly east-west line well into Alabama and east Texas. As the front moves onto the Gulf coast, the prefrontal, convective line moves offshore (Fig. 23b) and the part of the system that passed over the ship dissipates and dies in the Gulf after 0200 UTC (Fig. 23c). However, the convection in Louisiana persists for many more hours. This is a large system with large areas of cold tops (Fig. 24a); minimum temperatures are also among the coldest in these six cases and the satellite-derived rain volumes (Fig. 24b) are the largest.

As with the previous case, the closest sounding (Fig. 25a) is 190 km away at Victoria where both the positive and negative buoyant energy are very small. Again, the 1200 UTC sounding may not be representative of the

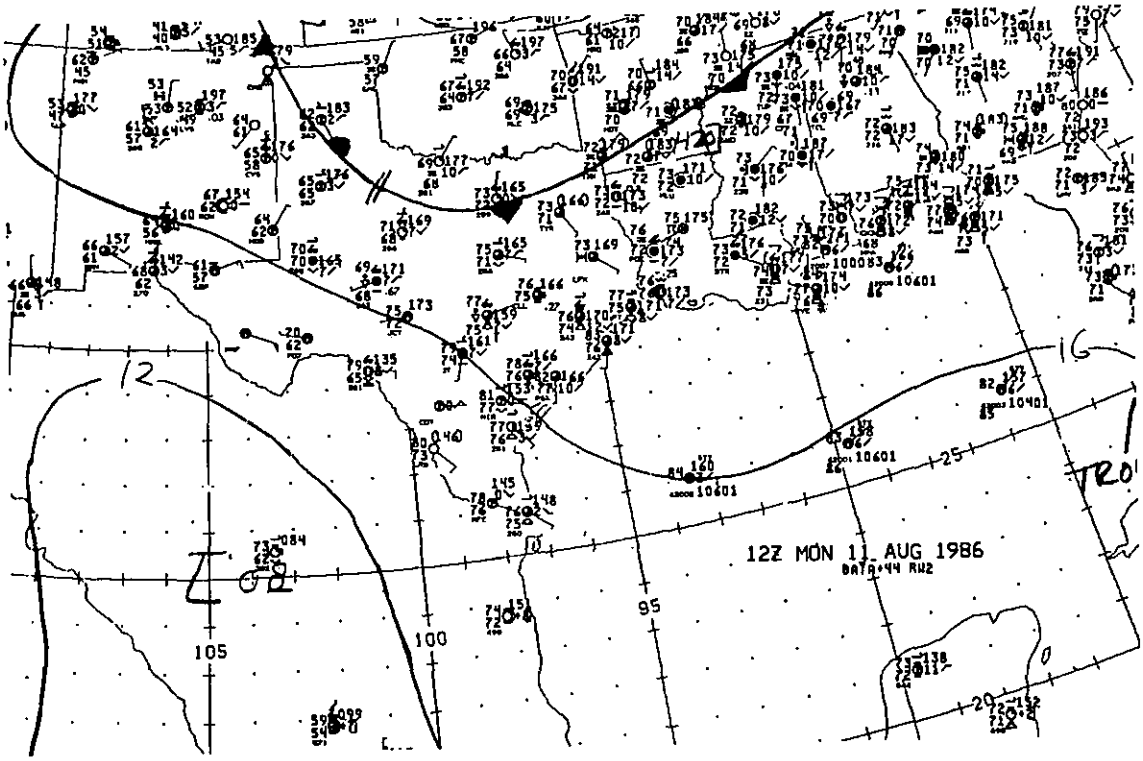

Figure 22. Surface map for 1200 UTC on 11 August 1986.

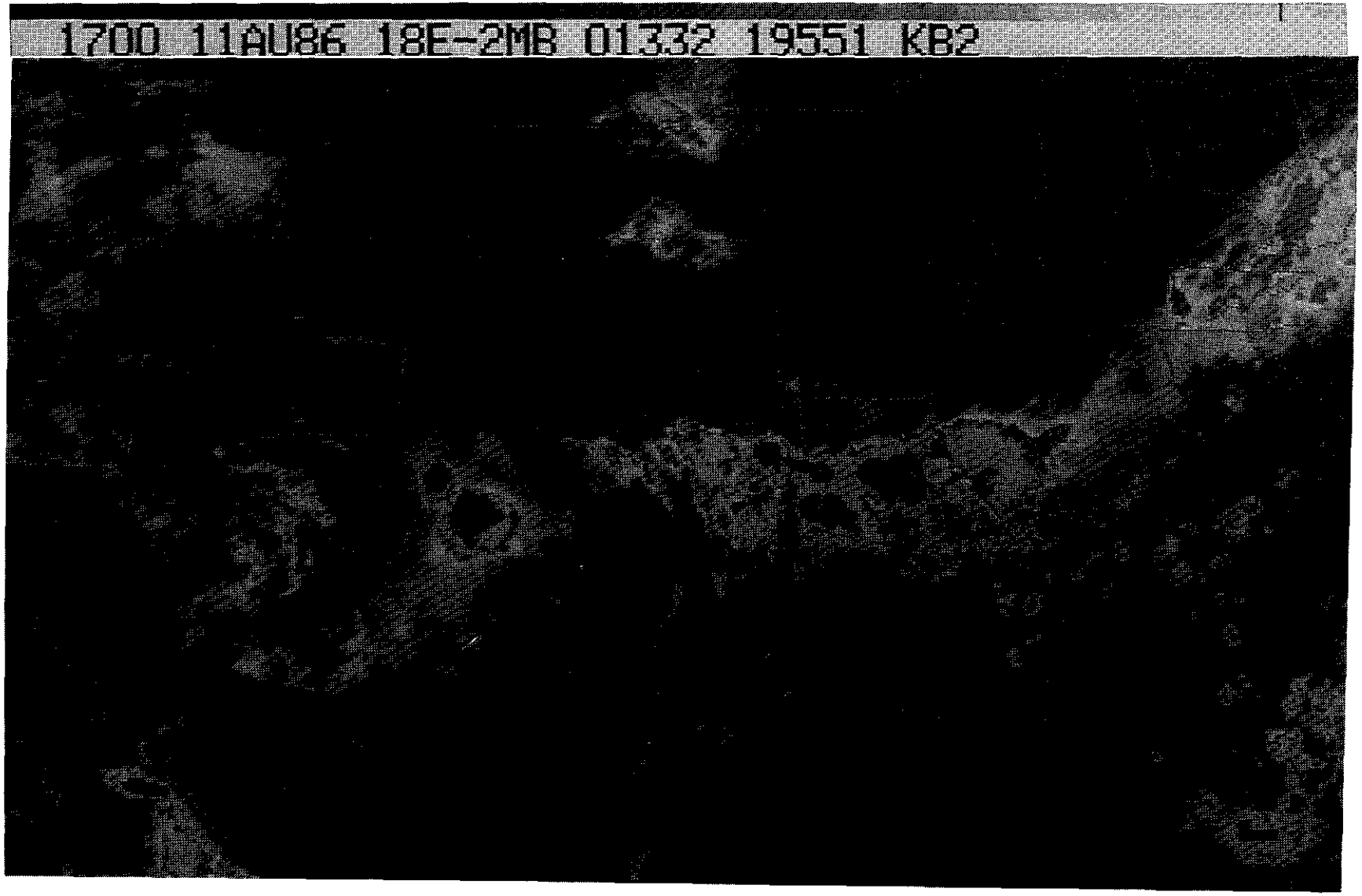

Figure 23a. GOES IR image (MB enhancement) for 1700 UTC on 11 August 1986.

Figure 23b. GOES IR image (MB enhancement) for 1900 UTC on 11 August 1986.

Figure 23c. GOES IR image (MB enhancement) for 0200 UTC on 12 August 1986.

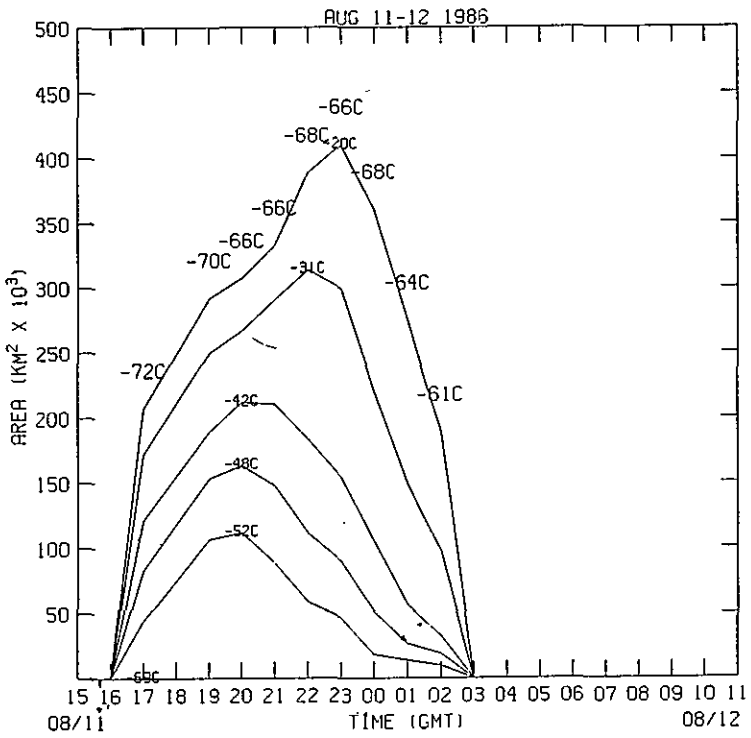

Figure 24a. GOES IR cloud area time series for 11-12 August 1986. Minimum temperatures (°C) in the cloud are the numbers above the warmest temperature curve.

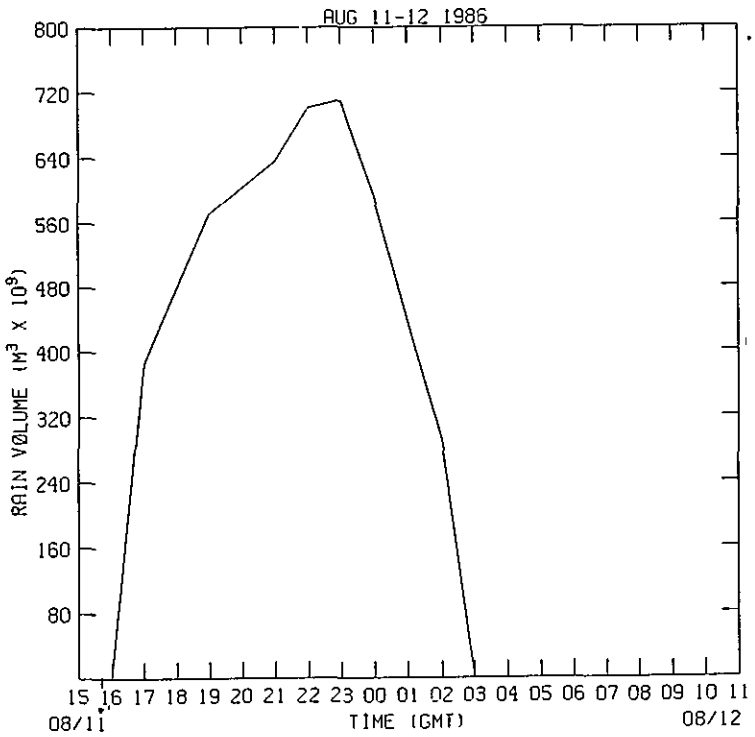

Figure 24b. Satellite-derived rainfall time series for 11-12 August 1986.

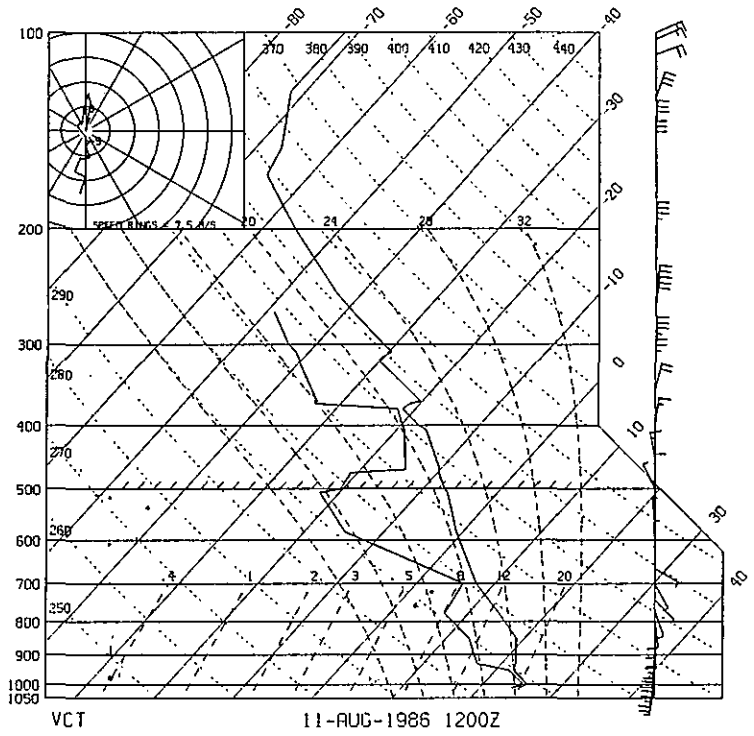

Figure 25a. Victoria, Texas (VCT) sounding for 1200 UTC on 11 August 1986.

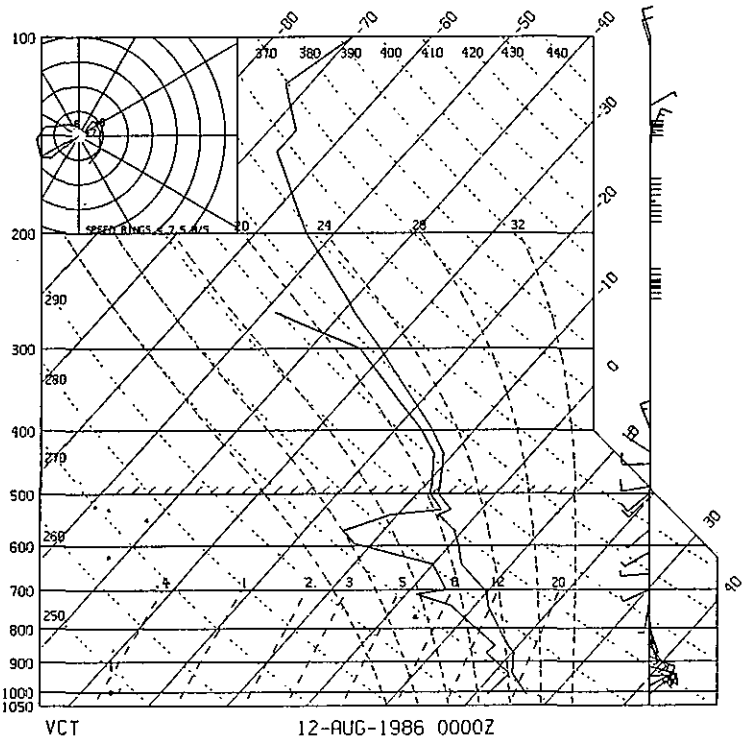

Figure 25b. Victoria, Texas (VCT) sounding for 0000 UTC on 12 August 1986.

atmosphere that produced the convection at the ship, for the cloud line does not reach Victoria until 2100 UTC. The 0000 UTC Victoria sounding on 12 August 1986 (Fig. 25b) results in more positive buoyant energy (Table 4) than 12 h earlier, because of a more unstable atmosphere at the later time. Cloud base is about 1 km higher than 12 h earlier because of a drier boundary layer at Victoria at 0000 UTC.

REFERENCE

Griffith, C.G., 1987: Comparisons of gauge and satellite rain estimates for the central United States during August 1979. J. Geo. Res., 92, 9551-9566.

PART VI. SUMMARY AND CONCLUSIONS

SUMMARY AND CONCLUSION

Farn P. Parungo

Numerous independent investigations of marine air chemistry over the Gulf of Mexico were conducted in July-August 1987 on U.S.M. Naval Oceanographic Research Ship H-02 by a group of scientists from the U.S.A. (Chief Scientist, Farn P. Parungo) and U.S.M. (Chief Scientists, Humberto Bravo A. and Luis D. Salastorrea). On 23-24 March 1987 the participating scientists held a workshop in Boulder, Colorado, to discuss their chemical, physical, and meteorological measurements and to exchange their knowledge and opinions. This report is the final product of the research cruise and the workshop. The activities and results are summarized as follows:

A. The cruise started at Galveston, Texas, U.S.A., and ended at Veracruz, U.S.M. The ship sailed along the western Gulf shelf where off-shore oil drills are operating; stopped at several large cities that are major sources of air pollution; passed regions where the oil refining industry is active; and crossed deep Campeche Bay, a site of thriving fisheries and oil exploration. It also crossed the open Gulf and abyssal water. Thus, the investigation covered the vastly diverse geography of the Gulf. The measurements in the cruise represent a wide geographic variety.

B. During the cruise (20 July to 22 August 1986), the atmospheric conditions were calm (no storms or hurricanes). Surface wind speeds ranged from 0 to 25 km with an average of 10 km. Wind directions measured onboard were variable and shifting, with little discernible pattern. The large-scale air trajectories analyzed by Harris demonstrated that the prevailing winds were easterly from the Caribbean sea at all three levels (except for a few intrusions of continental air mass). Nickerson's model indicated a clear oscillation of land breeze and sea breeze at the shoreline regions. The radiation measured by Stearns showed good agreement with the seasonal prediction in these latitudes. The air temperature was in the 30°-40°C range, and the relative humidity was 70-95%. It was typical summer weather in the Gulf. Thus our chemical measurements can be considered representative for the summer season.

C. For the first time, quantitative measurements documented amounts of various gases throughout the Gulf.

1. The in-situ measurements of O_3 (Sec. I, Bravo et al.) showed that the highest concentrations (>10 ppb) were along the coast of Tampico-Veracruz-Coalzacoalcos where oil drilling and petroleum refineries are most active. The lowest concentrations (<0.01 ppb) were found on at the open sea. The typical bell-shaped curve of diurnal variations of O_3 concentrations observed on the continent was not found in the Gulf. This is probably due to the fact that seawater is a vast sink for O_3; because O_3 can be rapidly adsorbed it fails to show any periodic variation in the atmosphere.

2. The concentrations of total hydrocarbons (THC) measured by Bravo et al. ranged from 4 ppm (near cities) to 0.07 ppm (at open Gulf), indicating that concentrated THC are anthropogenic. Flask air samples measured by Conway and Steele showed that CH_4 concentrations were at seasonal minimum with slight variation (1652-1733 ppb), and the lowest values fit in well with the GMCC baseline measurements at Key Biscayne, FL (KEY) and American Virgin Island (AVI). The CO_2 concentrations varied from 344-354 ppm. The lowest values agreed with the baseline measurements at KEY and AVI. The other values were higher and more variable.

3. The average concentration of H_2S over the Gulf was measured by Bravo et al. as 1 $\mu g/m^3$ (σ = 3 $\mu g/m^3$), which is higher than the concentration in ordinary marine environments (<0.5 $\mu g/m^3$). The highly concentrated H_2S may be oxidized and converted to sulfate particles and thus can be a natural source to the regional atmospheric sulfate budget.

4. Dimethyl sulfide (DMS), which is the predominant natural precursor for sulfate aerosols in marine environments, was measured by Hoyt onboard. DMS concentrations in surface water, affected by biological activities, varied with geography, ranging from 22 to 244 ng/L with an average of 130 ng/L. The values fit the data in oligotrophic areas (e.g., tropical N. Atlantic Ocean and Gulf of Mexico), but are less than half the values for the upwelling areas (e.g., the Equator and Peru shelf). The sea-to-air flux in the Gulf was calculated as ~300 $(\mu g/m^2)/D$. If no chemical reaction consumed DMS in the air, its atmospheric concentration would be in equilibrium with the concentration in surface seawater. Since the Henry's Law constant for DMS is 0.074, the DMS concentration in the air should be ~150 $nmol/m^3$ (~9 $\mu g/m^3$). However, Hoyt's measurements of DMS in the Gulf air were <20 ng/m^3, less than the calculated

value by a factor of 450. The results suggest that once DMS is emitted from sea to air, it is oxidized rapidly and converted to other sulfur gases or sulfate particles. The residence time of DMS is shorter in the Gulf (estimated ~1.6 h) than in the open ocean (5-20 h). This is probably due to the highly polluted environment where concentrated aerosols and gases may catalytically accelerate the DMS oxidation rate. Therefore, one should not underestimate the DMS contribution to the natural sulfur-compound budget in the Gulf, merely on the basis of its low concentration in the air. Nevertheless, it is difficult, with present data, to assess its importance to the total sulfur budget quantitatively.

D. Spatial and temporal variations of aerosol characteristics in the Gulf were investigated.

1. Aerosol number concentrations (C_n) were measured by Nagamoto and Parungo. The variability of C_n was understandably high. Near large cities and refineries, C_n was ~$10^5/cm^3$; in remote Gulf waters C_n dropped to $10^3/cm^3$, which is still an order of magnitude higher than the C_n in the South Pacific Ocean. Total particle mass concentrations (C_m) were measured by Bravo et al. Near the cities C_m was >90 $\mu g/m^3$; in the middle of the Gulf, C_m was 13 $\mu g/m^3$. The mean C_m was 32 $\mu g/m^3$ for night samples, 18 $\mu g/m^3$ for day samples. The results indicate that the Gulf is heavily polluted with aerosol particles.

Measurements of ion concentrations (C_i) of aerosols, by Madel and Parungo, showed that the C_i of Na^+ or Cl^- was affected by wind speed and direction. The C_i of non-seasalt sulfate and nitrate aerosols were higher near cities than over remote waters. The C_i ratios between non-seasalt sulfate and seasalt sulfate ranged from 0.6 (at the center of the Gulf) to 12 (near oil refineries). The results indicate that overall Gulf air was highly contaminated with sulfate and nitrate aerosols. The average of total C_i (10.5 $\mu g/m^3$), which represents the soluble aerosol mass, is only 42% of average C_m (25.25 $\mu g/m^3$), suggesting that the majority of aerosols were water-insoluble particles. X-ray energy spectrometry demonstrated that most particles contained crustal elements (e.g., Si, Al, Fe, K, Ca, S) probably of continental origin. Only <50% of the particles contained Na, Cl, and Mg as in seasalt. Near shore, total C_n, C_m, C_i showed higher concentration at night than in daytime. This is probably because the land-breeze carried pollutants to the Gulf and planetary boundary layers were lower at night, which may reduce convection and distribution of the pollutants. In the middle of the Gulf this diurnal variation was less significant.

3. Spot tests with $BaCl_2$ showed that 70-90% of total particles contained sulfate. The C_n of small sulfate particles ($d < 1$ μm) showed two modes per day along the coast region, a small peak in the afternoon when the particles were probably produced by photo-oxidation, and a greater peak in the early morning when particles were transported to the Gulf by the land breeze. Farther from the coast, only the small peak in the afternoon was observed. Nitrate particles detected by Nitron spot test were present more (>75%) in large particles ($d > 1$ μm) and less in smaller ones (<50%). The C_n of nitrate-containing particles had a diurnal variation similar to that of sulfate-containing particles. Both nitrate and non-seasalt sulfate appeared in electromicrographs to be a coating on seasalt particles and crustal dust.

4. During the cruise, an intensified anticyclonic ring was observed by Salastorrea and Veneroni in the western Gulf. Its position, maximum depth, orientation, growth, and decline were surveyed. The vortex could cause upwelling of deep water and sinking of surface water. Previously, a Russian-Cuban team located a great upwelling zone in Campeche Bay where Nagamoto and Parungo found high concentrations of biological particles ($9 \times 10^4/cm^3$) in the surface seawater, where Hoyt measured the highest DMS in water (244 ng/L), where Quintana and Parungo observed the highest biomass in the air, and where Rosinski et al. detected the highest ice nucleus activities. It appears that upwelling carries nutrient-rich deep water into the euphotic layer to support biological activities, which produce DMS, a precursor of sulfate particles. Ice nuclei, which were identified as small volatile particles (0.1-0.4 μm), had their highest activity at midday. They were probably products of photochemical reactions, and mixtures of hydrophobic organic materials and hydrophilic sulfate. Therefore, the particles acted best as a condensation-followed-by-freezing mechanism. Ice nuclei are triggers to initiate most precipitation. Without them, most clouds would not produce snow or rain.

E. Meteorological analysis by Griffith indicated that the rain events encountered during the cruise were convective in general although caused by several different types of dynamic forcing. The acidity of rain samples varied from event to event (pH ranged from 4.0 to 6.1) and sometimes changed with time in the same event. Most ion concentrations in rain decreased with increasing rainfall rates, indicating that dilution by liquid-water content in clouds is a

major influential factor. Case studies showed that concentration ratios Cl^-/Na^+ and Mg^{++}/Na^+ in rainwater remained consistent throughout an event, suggesting that Na^+, Cl^-, and Mg^{++} were probably incorporated in rain through a common mechanism (i.e., cloud-base condensation nucleation). Ratios H^+/Na^+, $SO_4^=/Na^+$, NO_3^-/Na^+, and NH_4^+/Na^+ showed lower values at the beginning of an event, increased to maximum 5-10 min later, and then decreased to a consistent value. In-cloud scavenging of gases and cloud microphysical processes are suggested to explain the variations. Comparisons of the chemistry of seawater, aerosols, and rainwater revealed that in this marine environment, >80% of $SO_4^=$ and NO_3^- was incorporated in rain through the aerosol phase and only <20% through the gas phase. The relative importance of these mechanisms is different over the continent, where gas-phase incorporation has been observed to dominate.

F. On the basis of chemical analyses of rainwater and aerosols, rainfall rate, and dry deposition velocities, dry and wet depositions of major ions were computed. In the Gulf, wet deposition is 4-20 times more important than dry deposition. Washout factors (ratios between concentrations in air and in rain) were the same for Na^+, Cl^-, and Mg^{++} (1.56×10^3); slightly higher for Ca^{++} (1.67×10^3) and K^+ (1.71×10^3), probably because of cloud-top entrainment of continental air; and highest for $SO_4^=$ (1.81×10^3) and NO_3^- (1.99×10^3), probably because of scavenging of gases. Calculations showed that both in-cloud scavenging and below-cloud scavenging are important processes for incorporating pollutants in rain.

G. This research was the first collaboration between U.S.A. and U.S.M. scientists to study air chemistry over the Gulf that the two nations share. We hope this pilot project will lead to a comprehensive cooperative program. For future operation we recommend the following:

1. Use of research aircraft to coordinate with surface surveys. Thus, 3-dimensional instead of 2-dimensional air chemistry data could be acquired, and cloud physics and chemistry could be investigated.

2. Up-grade of instrumentation onboard the research ship. SO_2, NO_x, CO_2, CH_3SCH_3, THC, H_2O_2, and O_3 should be monitored in situ continuously to observe temporal and spatial variations. Rainwater samples should be analyzed onboard immediately after collection.

3. More research cruises in diverse climates to investigate seasonal variations.

☆ U.S. GOVERNMENT PRINTING OFFICE: 1988—573-002/80,516 REGION NO. 8